Investigating the effect of tetracycline on gut microbiome metabolism and microbe-host interactions

Keerthisinghe, Rajapaksha Pathiranage Tharushi Prabha

2021

Keerthisinghe, R. P. T. P. (2021). Investigating the effect of tetracycline on gut microbiome metabolism and microbe-host interactions. Doctoral thesis, Nanyang Technological University, Singapore. https://hdl.handle.net/10356/152079

https://hdl.handle.net/10356/152079

https://doi.org/10.32657/10356/152079

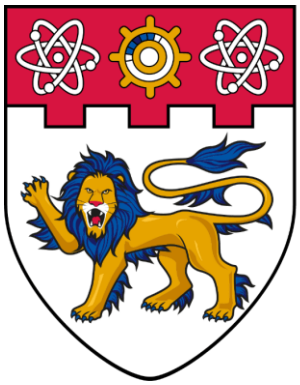

NANYANG TECHNOLOGICAL UNIVERSITY
SINGAPORE

INVESTIGATING THE EFFECT OF TETRACYCLINE ON GUT MICROBIOME METABOLISM AND MICROBE-HOST INTERACTIONS

RAJAPAKSHA PATHIRANAGE THARUSHI PRABHA KEERTHISINGHE

SCHOOL OF CIVIL AND ENVIRONMENTAL ENGINEERING

2021

INVESTIGATING THE EFFECT OF TETRACYCLINE ON GUT MICROBIOME METABOLISM AND MICROBE-HOST INTERACTIONS

RAJAPAKSHA PATHIRANAGE THARUSHI PRABHA KEERTHISINGHE

School of Civil and Environmental Engineering

A thesis submitted to the Nanyang Technological University in partial fulfilment of the requirement for the degree of Doctor of Philosophy

Statement of Originality

I hereby certify that the work embodied in this thesis is the result of original research, is free of plagiarised materials, and has not been submitted for a higher degree to any other University or Institution.

26/06/2021

. . . .

Date

. . . .

Rajapaksha Pathiranage
Tharushi Prabha Keerthisinghe

Supervisor Declaration Statement

I have reviewed the content and presentation style of this thesis and declare it is free of plagiarism and of sufficient grammatical clarity to be examined. To the best of my knowledge, the research and writing are those of the candidate except as acknowledged in the Author Attribution Statement. I confirm that the investigations were conducted in accord with the ethics policies and integrity standards of Nanyang Technological University and that the research data are presented honestly and without prejudice.

26/06/2021

. . . . . .

Date

. . . . . .

Fang Mingliang

Authorship Attribution Statement

*(B) This thesis contains material from [3] paper(s) published in the following peer-reviewed journal(s) / from papers accepted at conferences in which I am listed as an author.

Chapter 3 is published as **Keerthisinghe, T. P.,** Wang, F., Wang, M., Yang, Q., Li, J., Yang, J., Xi, L., Dong, W., and Fang, M. (2020). Long-term exposure to TET increases body weight of juvenile zebrafish as indicated in host metabolism and gut microbiome. *Environment International*, **139**: 105705. DOI: 10.1016/j.envint.2020.105705.

The contributions of the co-authors are as follows:

- Asst/Prof Fang Mingliang provided the initial project direction, guided the entire project, and edited the manuscript drafts.
- Prof Wu Dong provided substantial advice, guided the project, and edited the manuscript drafts.
- Prof. Lin Xi provided substantial advice and edited the manuscript drafts.
- I prepared the manuscript drafts. The manuscript was revised by Mr. Feng Wang, Mr. Mengjing Wang, Dr. Qin Yang, Ms. Jiawei Li, and Dr. Jingfeng Yang.
- I co-designed the study with Asst/Prof Fang Mingliang and performed part of the laboratory work, including metabolomics and lipidomics sample preparation and profiling in the School of Civil and Environmental Engineering and Nanyang Environment and Water Research Institute. I also analyzed the metabolomics, lipidomics, and microbial community data.
- Mr. Feng Wang conducted part of the laboratory work, including fish culture, sample collection, tissue staining, and RNA analysis at Inner Mongolia Key Laboratory of Toxicant Monitoring and Toxicology, College of Animal Science and Technology, Inner Mongolia University for the Nationalities.

- Ms. Jiawei Li and Dr. Jingfeng Yang assisted in the experiment on fish culture and sample collection.

Chapter 4 and one part of Chapter 6 are published as **Keerthisinghe, T. P**., Wang, M., Zhang, Y., Dong, W., and Fang, M. (2019). Low-dose tetracycline exposure alters gut bacterial metabolism and host-immune response: "Personalized" effect? *Environment International*, **131**: 104989. DOI: 10.1016/j.envint.2019.104989.

The contributions of the co-authors are as follows:

- Asst/Prof Fang Mingliang provided the initial project direction, guided the entire project, and edited the manuscript drafts.
- I prepared the manuscript drafts. The manuscript was revised by Mr. Mengjing Wang and Dr. Yingdan Zhang.
- I co-designed the study with Asst/Prof Fang and performed part of the laboratory work, including anaerobic bacteria culture and metabolomics sample preparation and profiling in the School of Civil and Environmental Engineering and Nanyang Environment and Water Research Institute. I also analyzed the metabolomics data.
- Mr. Mengjing Wang assisted in immune assays and data analysis.
- Prof Wu Dong provided substantial advice and edited the manuscript drafts.

Chapter 5 is published as **Keerthisinghe, T.P.,** Yang, Q., Chow, A., Fang, M., 2021. Feeding state greatly modulates the effect of xenobiotics on gut microbiome metabolism: A case study of tetracycline. *Journal of Hazardous Materials* 413. DOI: 10.1016/j.jhazmat.2021.125441.

The contributions of the co-authors are as follows:

- Asst/Prof Fang Mingliang provided the initial project direction, guided the entire project, and edited the manuscript drafts.
- I prepared the manuscript drafts. The manuscript was revised by Ms. Agnes Chow and Dr. Qin Yang.
- I co-designed the study with Asst/Prof Fang and performed part of the laboratory work, including culture and TET treatment of gut microbiome culture, metabolomics sample preparation, and profiling Nanyang Environment and Water Research Institute. I also analyzed the metabolomics data and contributed to maintain the reactor with gut microbiome reactor.
- Dr. Qin Yang assisted in maintaining the reactor with the gut microbiome community.

26/06/2021

. . . . . .

Date

. . . . . .

Rajapaksha Pathiranage
Tharushi Prabha Keerthisinghe

ACKNOWLEDGEMENTS

Foremost, I express my gratitude to my supervisor Prof. Fang Mingliang for his academic guidance and support throughout my PhD study. Since I was completely new to the field of metabolomics and mass spectrometry, without his continuous guidance and training, successful completion of my PhD study will never be possible.

I thank my first supervisor in NTU, Prof. Seungdae Oh, for admitting me as a PhD student in his group and providing academic guidance in the first year of my PhD study.

I extend my gratitude to Prof. Wu Dong and his lab members including Mr. Feng Wang, Ms. Jiawei Li, and Dr. Jingfeng Yang, for their help in the zebrafish study.

Sincere thanks also go to the technical staff in the Environmental Lab and AEBC, Mr. Ong Chee Yung, Mr. Tan Han Khiang, Mrs. Lim-Tay Chew Wang, Ms. Maria Chong Ai Shing, Ms. Emily Mar'atusalihat, and Ms. Ong Qian Mei for the kind help for my experiments. Special thanks go to NEWRY Analytical Cluster staff, Dr. Lv Yunbo, Dr. Han Yuan, Ms. Elvy Riani Wanjaya, and Ms. Koh Danyu for their professional assistance and kind support in method development and troubleshooting in analytical work.

Special thanks go to my group members for their continuous friendly support and encouragement during my study. I thank Dr. Zhang Yingdan and Dr. Yang Qin for kindly helping me learn microbiological and molecular techniques and especially for maintaining the reactor with the gut microbial community, which was a major part of my study. I also thank Dr. Jia Shenglan, Dr. Zhao Fangrong, Dr. Xu Tengfei, and Dr. Liu Min for continuously helping me in method development and troubleshooting in metabolomics and lipidomics experiments and Mr. Mengjing Wang for assisting me in immunological assays. I extend my thanks to Ms. Peng Bo, Mr. Yang Junjie, and all other groupmates for their kind support in my research work.

Lastly, I would like to express my sincere thanks to my parents, brother, husband, and friends for supporting and encouraging me throughout my PhD study.

TABLE OF CONTENTS

SUMMARY

Tetracycline (TET) is an extensively used antibiotic for human therapeutic purposes and veterinary medicine. Extensive use in a wide range of applications leads to the frequent occurrence of TET in aquatic environments. Thus, there is a higher possibility for the aquatic organisms inhabiting those environments to expose to TET. Effects of TET on aquatic organisms such as freshwater fish species have been studied, mostly focusing on the toxic effects at embryonic and larval stages. However, limited information is available on the possible long-term effect of TET exposure on aquatic fishes at the juvenile stage, especially at low or environmentally relevant levels. Moreover, studying the simultaneous impacts on aquatic organisms and their gut microbiome exposed to chemicals and their correlation is rare, even though it has been done for some rodent models.

This thesis first started by investigating the effects of long-term TET exposure on zebrafish (*Danio rerio*). The study exposed zebrafish at the juvenile stage to two different low levels of TET for a one-month period until their adulthood. Subsequently, the study analyzed growth (i.e., body weight and length) and liver characteristics (i.e., histology, gene expression, lipidome, and metabolome) of zebrafish. In addition, the study also examined the alterations in zebrafish gut microbial community. The results revealed an interesting observation of increased body weight gain and liver lipid accumulation in zebrafish upon TET exposure, along with substantial changes in the gut microbiome with an increase in known obesogenic microbial factors.

Hence, a hypothesis can be generated to link the observed host effects in zebrafish to the TET mediated gut microbiome dysbiosis. Thus, the next sections of the thesis have more focus on the gut microbiome. Accordingly, TET-induced gut microbiome changes that may possibly be associated with host weight gain were investigated using a few approaches: TET-induced metabolic change in a few representative pure gut bacterial strains; TET caused metabolic consequences in an *in vitro* gut microbiome secretome; and the contribution of TET affected metabolic and immunological gut microbiome-host interactions to obesity-related complications.

Thus, the second part of the thesis investigated the TET-induced metabolic alteration in model gut bacteria. This study used three model gut bacteria including *Bacteroides fragilis, Clostridium sporogenes,* and *Escherichia coli,* which represent several types of the most abundant bacterial genera in the gut. Subsequently, a global and targeted metabolomics approach was used to characterize the metabolomic disruption from TET exposure.

The third part of the thesis explored the metabolic consequences of TET exposed gut microbiome secretome that may possibly be linked with host effects such as increased body weight gain. First, an *in vitro* gut microbiome was established using the fecal matter from a single healthy donor as the inoculum and exposed to multiple doses of TET at two feeding states: fed and fasted. To understand more host relevant effects, this section of the thesis focused on the important gut microbial metabolites with known host health implications, incorporating a targeted approach along with the global metabolomics analysis.

This thesis also tentatively explored the contribution of TET altered microbe-host interactions mediated through gut microbial metabolites and immunoregulatory compounds on obesity-related complications. Particularly, the study investigated the obesity-related complications using an *in vitro* liver cell model (HepG2) by analyzing the cytotoxic effects and lipid dysregulations upon exposure to TET treated gut microbiome secretome. For the immune response, the study examined the lipopolysaccharides (LPS) levels in the secretome of TET exposed gut microbiome.

LIST OF PUBLICATIONS

- **Keerthisinghe, T.P.**, Nguyen, L.N., Kwon, E.E., Oh, S., 2019. Antiseptic chlorhexidine in activated sludge: Biosorption, antimicrobial susceptibility, and alteration of community structure. *Journal of Environmental Management*, 237, 629–635. DOI: 10.1016/j.jenvman.2019.02.043.

- **Keerthisinghe, T.P.,** Wang, F., Wang, M., Yang, Q., Li, J., Yang, J., Xi, L., Dong, W., Fang, M., 2020. Long-term exposure to TET increases body weight of juvenile zebra fish as indicated in host metabolism and gut microbiome. *Environment International*, 139: 105705. DOI: 10.1016/j.envint.2020.105705.

- **Keerthisinghe, T.P.,** Wang, M., Zhang, Y., Dong, W., Fang, M., 2019. Low-dose tetracycline exposure alters gut bacterial metabolism and host-immune response: "Personalized" effect? *Environment International*, 131: 104989. DOI: 10.1016/j.envint.2019.104989.

- **Keerthisinghe, T.P.,** Yang, Q., Chow, A., Fang, M., 2021. Feeding state greatly modulates the effect of xenobiotics on gut microbiome metabolism: A case study of tetracycline. *Journal of Hazardous Materials* 413. DOI: 10.1016/j.jhazmat.2021.125441

- Li, J., Dong, T., **Keerthisinghe, T.P.,** Chen, H., Li, M., Chu, W., Yang, J., Hu, Z., Allen, S., Dong, W., Fang, M., 2020. Long-term oxytetracycline exposure potentially alters brain thyroid hormone and serotonin homeostasis in zebrafish. *Journal of Hazardous Materials*, 399: 123061. DOI: 10.1016/j.jhazmat.2020.123061.

- Yang, Q., **Keerthisinghe, T.P.,** Tan, T.R.J., Cao, X., Setyawati, M.I., DeLoid, G., Ng, K.W., Loo, S.C.J., Demokritou, P., Fang, M., 2020. A high-throughput method to characterize the gut bacteria growth upon engineered nanomaterial treatment. *Environmental Science Nano*, 7, 3155–3166. DOI: 10.1039/d0en00568a.

- Zhang, Y., **Keerthisinghe, T.P.,** Han, Y., Liu, M., Wanjaya, E.R., Fang, M., 2018. "Cocktail" of xenobiotics at human relevant levels reshapes the gut bacterial metabolome in a species-specific manner. *Environmental Science and Technology*, 52(9), 11402–11410. DOI: 10.1021/acs.est.8b02629.

LIST OF TABLES

LIST OF FIGURES

LIST OF ABBREVIATIONS

Abbreviation	Description
TET	Tetracycline
GI	Gastrointestinal
SCFAs	Short chain fatty acids
BCAAs	Branched chain amino acids
MW	Molecular weight
LPS	Lipopolysaccharides
STAT	Subtherapeutic antibiotic treatment
BMI	Body mass index
CD14	Cluster of differentiation
TLR	Toll-like receptor
TAG	Triglyceride
FAs	Fatty acids
NASH	Nonalcoholic steatohepatitis
PAMPs	Pathogen-associated molecular patterns
IL	Interleukin
NLRP	Nod-like receptor protein
TNF	Tumor necrosis factor
AHR	Aryl hydrocarbon receptor
GPCR	G protein–coupled receptor
DCA	Deoxycholic acid
LCA	Lithocholic acid
UDCA	Ursodeoxycholic acid

TGR	Takeda G protein-coupled receptor
FXR	Farnesoid X receptor
PXR	Pregnane X receptor
GLP	Glucagon-like peptide
CaSR	Calcium-sensing receptor
NK	Natural killer
NMDAR	N-methyl-D-aspartate receptor
a7nAChR	A7 nicotinic acetylcholine receptor
HCA3	Hominids contain a third member
DRD2	Dopamine receptor D2
NADPH	Nicotinamide adenine dinucleotide phosphate
TAAR	Trace amine-associated receptors
PYY	Peptide YY
PPAR	Peroxisome proliferator-activated receptor
TMAO	Trimethylamine N-oxide
TMA	Trimethylamine
CLA	Conjugated linoleic acid
CLnA	Conjugate linolenic acid
PFA	Paraformaldehyde
H&E	Hematoxylin and eosin
LC-MS	Liquid chromatography-mass spectrometry
Q-TOF	Quadrupole time-of-flight
MTBE	Methyl tert-butyl ether
HPLC	High performance liquid chromatography

DDA	Data-dependent acquisition
OTUs	Operational taxonomic unit
NMDS	Non-metric multidimensional scaling
PICRUSt	Phylogenetic investigation of communities by reconstruction of unobserved states
SEM	Standard error of the mean
ANOVA	One-factor analysis of variance
PERMANOVA	Permutational multivariate analysis of variance
SM	Sphingomyelin
PC	Phos phatidylcholine
PE	Phosphatidylethanolamine
DAG	Diglyceride
Cer	Ceramide
FA	Fatty acids
FABP	Fatty acid binding protein
LDA	Linear discriminant analysis
LEfSe	Linear discriminant analysis effect size
COGs	Clusters of orthologs groups
RCM	Reinforced clostridial medium
OD	Optical density
IC	Inhibitory concentration
PBS	Phosphate buffered saline
PCA	Principal component analysis
PFBBr	2, 3, 4, 5, 6-penta-fluorobenzyl bromide
GC-MS	Gas chromatography- mass spectrometry

QA	Quality assurance
QC	Quality control
MSD	Mass selective detector
mGAM	Modified Gifu anaerobic broth
ESI	Electrospray ionization
COD	Chemical oxygen demand
ASV	Amplicon sequence variants
NOAEL	No-observed-adverse-effect level
DMEM	Dulbecco’s modified Eagle’s medium
FBS	Fetal bovine serum
DMSO	Dimethyl sulfoxide
LAL	Limulus amebocyte lysate
PMA	Phorbol 12-myristate 13-acetate
PMB	Polymyxin B
ELISA	Enzyme-linked immunosorbent assay

Chapter 1. Introduction

1.1. Background

Tetracycline (TET) is an extensively used antibiotic for human therapeutic purposes and veterinary and aquaculture medicine, with the largest domestic sales volume in the U.S., accounting for 70% of all antibiotics (Food and Drug Administration, 2017). The extensive use in a wide range of applications led to the frequent occurrence of TET in aquatic environments. Notably, up to 4.2 and 158 μg/L TET levels were reported in surface water and wastewater; respectively (Borghi and Palma, 2014; Bu et al., 2013; Pena et al., 2010). Thus, there is a higher possibility of exposing the aquatic organisms inhabiting those environments to TET. Toxic effects of TET on aquatic organisms such as zebrafish (*Danio rerio*) have been studied previously, mostly focusing on toxic effects at embryonic and larval stages. For example, TET has been reported to generate toxic effects such as decreased body length, delayed hatching, increased yolk sac area, and absence of a swim bladder in zebrafish embryos or larvae even under 20 μg/L exposure (Zhang et al., 2015). Enhanced oxidative stress and apoptosis in zebrafish embryos have also been observed (Yu et al., 2019; Zhang et al., 2015). However, limited information is available on the possible long-term effect of TET exposure on aquatic fishes at the juvenile stage, especially at low or environmentally relevant levels. In addition, the impact of TET on the zebrafish gut microbiome has rarely been studied.

Several recent reviews highlighted the importance of considering the gut microbiome alterations upon xenobiotic exposure, which is typically overlooked in existing approaches for toxicological studies and risk assessment (Claus et al., 2016; Licht and Bahl, 2019; Velmurugan, 2018). The gut microbiome, inhabiting the organisms' gastrointestinal tract (GI), is an essential organ that strongly interacts with its host, including nutrient synthesis and metabolism, epithelial development, and regulation of immune system responses (Bäckhed et al., 2005; Eckburg et al., 2010; Magnúsdóttir et al., 2015; Morowitz et al., 2011). Exposure to pharmaceuticals and environmental chemicals is typical external stress for the indigenous gut microbiota,

which directly alters its composition and functionality (Maier et al., 2018; Maurice et al., 2013; Modi et al., 2014).

A growing body of evidence suggests that TET can alter the gut microbiome composition in human (*in vitro*), mice, and swine (Jung et al., 2018; Looft et al., 2012; Roca-Saavedra et al., 2018). At the same time, one study reported TET's effect on the human gut microbiome metabolome *in vitro*, focusing on a few targeted metabolite groups (Carman et al., 2005). Furthermore, few other studies reported the effects of TET on the gut microbiome and subsequent host effects such as increased body weight gain (Marciano et al., 2017) and altered host metabolome (Behr et al., 2017) in rodent models. In addition to TET, gut microbiome dysbiosis mediated host effects, especially the increased body weight gain and related complications (i.e., dysregulated liver lipid metabolism), induced by different other antibiotics in rodents and human subjects have been frequently reported (Cho et al., 2012; Cox et al., 2014; Hernández et al., 2013; Jin et al., 2016; Thuny et al., 2010). However, investigations on simultaneous impacts on aquatic organisms and their gut microbiome exposed to chemicals and their correlation are rare. Thus, it is of great importance to assess the effects of TET on the aquatic organisms (i.e., body weight alterations and liver function dysregulations) and their gut microbiome simultaneously.

Gut microbiome dysbiosis mediated effects on the host upon xenobiotic exposure are highly related to the microbiome community composition. Specially, some key organisms in the gut microbiome play essential roles in modulating host health. For example, the Firmicutes/Bacteroidetes ratio has been described as higher in obese mice than in normal-weight mice (Cox and Blaser, 2013; Turnbaugh et al., 2006). Also, an increase in the Firmicutes' abundance is usually considered an obesogenic factor (Arumugam et al., 2011). In addition, some gut bacterial strains are specific to produce enzymes involved in producing metabolites crucial in host health modulation (Besten et al., 2013; Grill et al., 1995; Morrison and Preston, 2016; Takamine and Imamura, 1995; Wells et al., 2000; Wikoff et al., 2009). However, only limited studies on the response of pure gut bacterial strains to xenobiotics are available (Maier et al., 2018). To date, TET-induced metabolic alterations in pure gut bacterial strains, which represent the most abundant genera in the gut microbiome, have not been studied, especially employing a global metabolomics approach.

Furthermore, it is well known that the gut microbiome-host interactions are mostly mediated through the metabolites produced, transformed, and/or regulated by the gut microbiome (Wikoff et al., 2009; Zhang & Davies, 2016). The connection between dysregulated metabolite levels (i.e., short chain fatty acids (SCFAs) and branched chain amino acids (BCAAs) and host body weight changes has been revealed in previous studies (Cho et al., 2012; Cox and Blaser, 2013). Furthermore, nutrient status in the diet (i.e., high-fat, fiber-rich) is known to alter the antibiotic-induced effects on the gut microbiome (Fujisaka et al., 2016; Ng et al., 2019). Nevertheless, metabolic consequences of TET exposed gut microbiome, which may subsequently modulate the host functions, have not been fully investigated yet, except for a few targeted metabolomics studies (Carman et al., 2005). Besides, another major knowledge gap of those previous studies is how the nutrient status such as the fed and fasted conditions affect the impact of TET on the gut microbiome metabolome.

Lastly, liver abnormalities such as lipid accumulation are known obesity-related complications mediated through the gut microbiome. The link between gut microbiome and host obesity through gut microbial metabolites and immunoregulatory compounds such as LPS have been previously revealed (Cho et al., 2012; Cox & Blaser, 2013; Jin et al., 2016). A substantial amount of low molecular weight (MW) metabolites produced by the gut microbiome is absorbed by the colonic lumen. Consequently, those can be bioavailable for the host organs, especially livers, due to the portal circulation (Matsumoto et al., 2017). However, metabolic and immunological dysfunctions associated with host weight gain caused by TET affected gut microbiome have not yet been investigated. Notably, the contribution of TET altered gut bacterial metabolites, specifically at low MW, to the host weight gain has not been studied yet. Further, lipopolysaccharides (LPS) is an immunoregulatory compound that is engaged in the host immune response modulation, and infusion of LPS is known to contribute the increased weight gain (Cox and Blaser, 2013). Induced LPS release in *E. coli* with TET exposure has been reported (Evans and Pollack, 1993). However, the influence of TET on the LPS production by the gut microbiome and other primary gut bacteria that mainly contribute to the gut LPS pool remains unclear.

1.2. Purpose and Scope

The objectives of this PhD work are to

(i) Investigate the effect of long-term TET exposure at environmentally relevant levels on juvenile zebrafish in terms of growth (i.e., body weight and length), physical deformities, and liver functions, simultaneously focusing on the impact on zebrafish gut microbiome (i.e., microbial community composition and functions).

(ii) Ascertain the TET-induced metabolic alterations in model gut bacteria, which represent the several types of most abundant genera in the gut microbiome using a global and targeted metabolomics approach.

(iii) Characterize the metabolic consequences of TET exposed *in vitro* gut microbiome secretome that may possibly be linked with host effects such as increased body weight gain under the fed and fasted states focusing on important gut microbiome produced/ transformed metabolites including tryptophan and indole derivatives, tyrosine and phenol derivatives, BCAAs, SCFAs, bile acids, and vitamins.

(iv) Understand the contribution of TET affected low MW metabolites and immunoregulatory compounds (i.e., LPS) in the gut microbiome secretome to the host weight gain and related complications using *in vitro* liver cell model (HepG2) and *in vitro* host immune responses.

1.3. Dissertation Overview

This dissertation includes seven chapters. Chapter 1 and 2 are the introduction and literature review. Chapter 7 is the conclusions and recommendations.

Chapter 3 investigated the toxic effects of TET exposure on aquatic organisms at low or environmentally relevant levels using an *in vivo* zebrafish model. The study exposed zebrafish at the juvenile stage to two different low or environmentally relevant levels of TET for a one-month period until their adulthood. And the study analyzed the growth (i.e., body weight and length) and liver characteristics such as

histology, gene expression, lipidome, and metabolome of zebrafish. Lastly, the study further evaluated the alterations in zebrafish gut microbial community composition and functions upon TET exposure.

Chapter 4 investigated the TET-induced metabolic alterations in three model gut bacteria including *Bacteroides fragilis*, *Clostridium sporogenes*, and *Escherichia coli*, which represent several types of the most abundant bacterial genera in the gut. The study incorporated global and targeted metabolomics approaches to characterize the metabolomic disruption from TET exposure at multiple dose levels.

Chapter 5 characterized the metabolic consequences of TET exposed *in vitro* gut microbiome. First, an *in vitro* gut microbiome was established using the fecal matter from a single healthy donor as the inoculum. The *in vitro* gut microbiome was then exposed to three different doses of TET under the fed and fasted states. To understand more host relevant effects, this section analyzed the important gut microbial metabolites in the gut microbiome secretome upon TET exposure using a targeted approach along with the global metabolomics analysis.

Chapter 6 explored the contribution of low MW metabolites and immunoregulatory compounds (i.e., LPS) in the secretome of TET affected gut microbiome to the host weight gain and related complications using *in vitro* models. For the study of *in vitro* liver effects, the pre-treated gut microbiome secretome by filtering with MW cut-off filters were dosed to human liver cancer cells (HepG2), and the cytotoxic effects and lipid dysregulations were investigated. The study next analyzed the LPS levels in the TET exposed gut microbiome secretome. Furthermore, TET-induced alterations in LPS release and immune response modulation by two main Gram-negative strains (i.e., *B. fragilis and E. coli*), which represent the main bacterial orders that contribute to the gut LPS pool, were investigated.

Chapter 2. Literature Review

2.1. TET Structure and Mode of Action

TET, initially known as Achromycin, was first discovered from *Streptornyces aureofaciens, Streptornyces. rimosus,* and *Streptornyces. viridofaciens* in 1953 after discovering two other TET family antibiotics, chlortetracycline and oxytetracycline in 1948 (Borghi and Palma, 2014; Chopra and Roberts, 2001; Finlay et al., 1950; Young and Tuttle, 1952). Later, more derivatives of the TET family antibiotics such as demeclocycline, rolitetracycline, methacycline, doxycycline, and minocycline were developed. TETs are all composed of a four-ring core to which the various functional groups and substituents are attached. The absolute configuration of the natural carbon atom (C-4) and the presence of the amide group (C-2) are some of the structural features necessary for the action of TET family antibiotics (**Figure 2.1**).

The primary mode of action of TET is the inhibition of protein synthesis. TET binds to the 30S fraction of the bacterial ribosome, preventing the binding of aminoacyl-tRNA to the A site of the bacterial ribosome and thereby interfere with the supply and connecting of the amino acids forming proteins (Borghi and Palma, 2014; Hasan et al., 1985). In addition to the primary target, TET can also inhibit a few other processes in bacteria, such as cell division and synthesis of nucleic acid, folic acid, and vitamin B_{12} (Eagle and Saz, 1954; Hash et al., 1964). Furthermore, vitamin K metabolism and cell wall synthesis are also reported as the targets of TET (Hash et al., 1964).

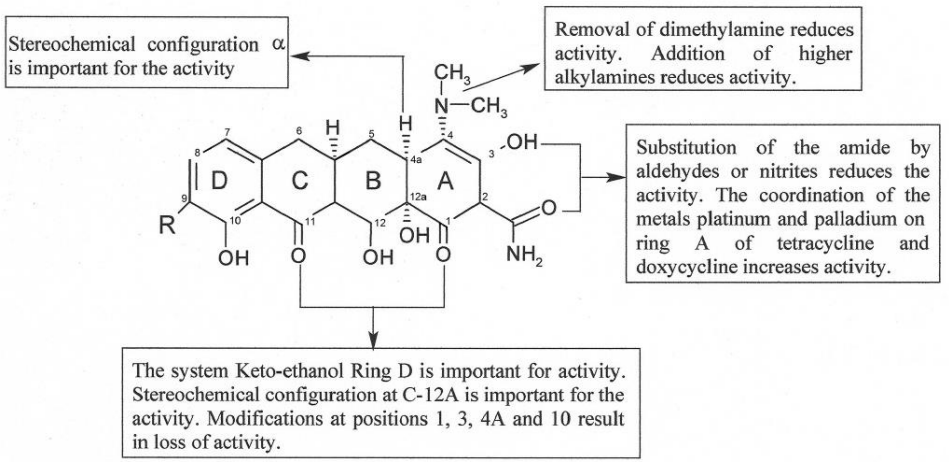

Figure 2.1. Structure and activity of TET family antibiotics
Adapted from (Borghi and Palma, 2014)

2.2. Production and Applications of TET

TET represents one of the most successful classes of antibiotics used in the past 50 years. It is also considered the second most produced and consumed antibiotic in the world (Borghi and Palma, 2014). TET sales represent the largest volume of domestic sales in USA, which is 5,866,588 kg in 2016, corresponds to 70% of all antibiotics (Food and Drug Administration, 2017).

TET is a broad-spectrum antibiotic effective against Gram-positive and Gram-negative bacteria as well as protozoan parasites (Nelson and Levy, 2011). TET is typically administered as an oral antibacterial agent to treat respiratory infections caused by *Mycoplasma pneumoniae, Chlamydia pneumoniae,* and *Chlamydia psittaci,* bowel infections such as cholera, and genital infections (Chopra and Roberts, 2001; Nelson and Levy, 2011). In addition, TET is used as a topical treatment for periodontal infection and acne vulgaris. Furthermore, anti-inflammation, immunosuppression, inhibition of lipase and collagenase activity, and wound healing are some of the nonantibacterial roles of TET family antibiotics (Nelson and Levy, 2011; Roberts, 2003).

Instead of its primary use as a human therapeutic drug, TET also plays an important role in veterinary medicine. One such popular use is as a growth promoter for cattle, pigs, sheep, and poultry (Sarmah et al., 2006). TET family antibiotics are also used

in aquaculture to control infections in salmon, catfish, and lobsters. Moreover, infections in plants such as fruit and palm trees are also treated with TETs (Chopra and Roberts, 2001; Nelson and Levy, 2011). A summary of widespread applications of TET is shown in **Figure 2.2.**

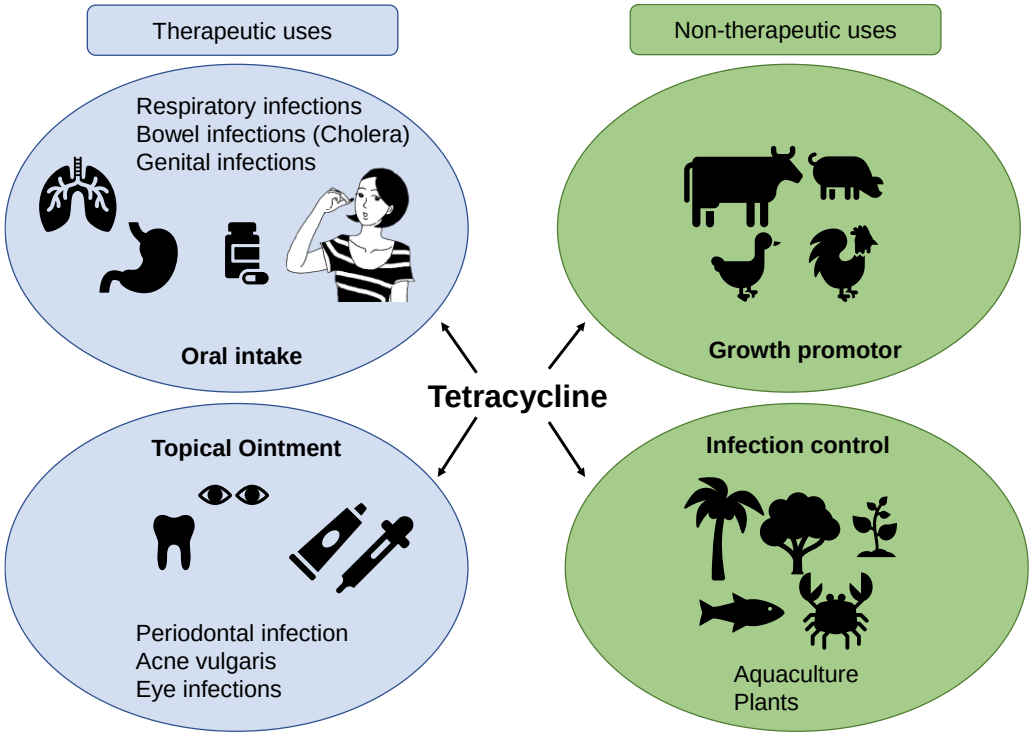

Figure 2.2. Widespread applications of TET

2.3. Bioavailability of TET

The estimated bioavailability of TET in the human body upon oral administration is approximately 77-88%, and the urinary and fecal eliminations are 30% and 20-60%; respectively (Agwuh and MacGowan, 2006). One study reported TET levels ranged from 10 to 97 µg/g feces in the feces of 10 volunteers given 1 g TET/day (Carman et al., 2005). On the contrary, poor absorption of TET, which is between 25-30% was also reported (Borghi and Palma, 2014). Furthermore, TET takes 15-30 and 4.5-9 days for 50% degradation in water and pig manure; respectively (Kühne et al., 2001). Another study reported 50-70 days for 50% degradation of TET in pig manure (Winckler and Grafe, 2000).

2.4. The Occurrence of TET Residues in Food and Environment

Extensive use of TET in a wide range of applications, especially in livestock applications and aquaculture, leads to the frequent occurrence of TET residues in aquatic environments. **Figure 2.3** shows the possible exposure pathways for veterinary antibiotics in the environments. TET levels vary from 0.005-0.008 µg/L were found in surface and groundwater nearby animal farms in Tehran, Iran (Javid et al., 2016). Moreover, <0.005 -4.2 µg/L levels in surface water (Arikan et al., 2008; Borghi and Palma, 2014; Bu et al., 2013; Deng et al., 2018; Javid et al., 2016; Kolpin et al., 2002; Tong et al., 2014) and a maximum of 158 µg/L in wastewater streams were reported (Pena et al., 2010) (**Table 2.1**).

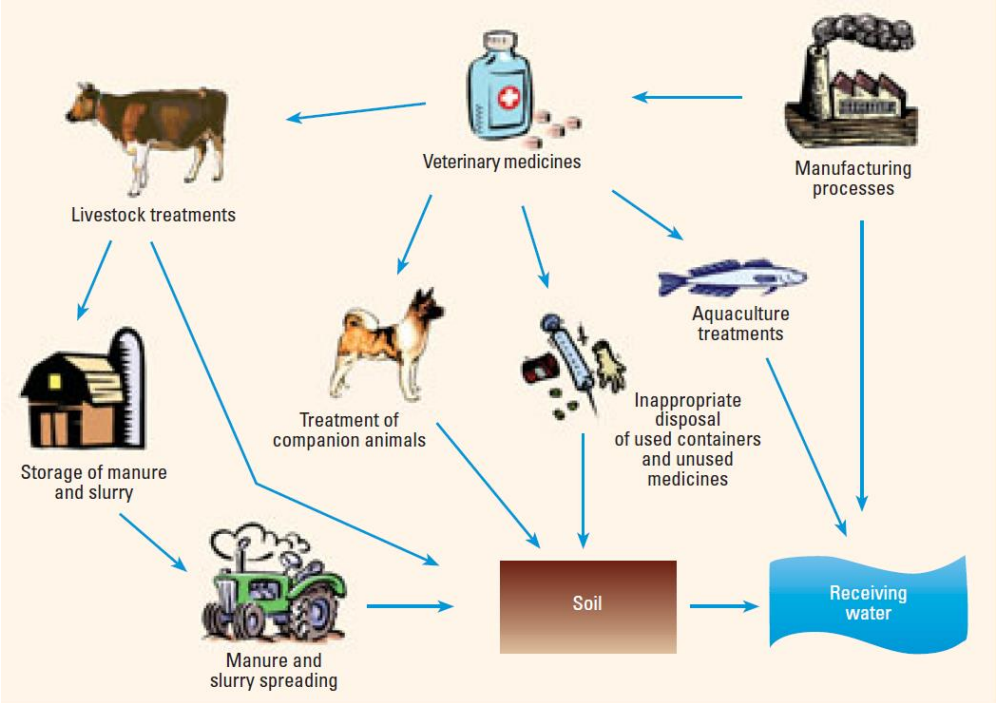

Figure 2.3. Exposure pathways of veterinary antibiotics in the environment
Adapted from (Boxall et al., 2003)

Table 2.1. Occurrence of TET in aquatic environments

Environment	TET concentration (µg/L)	Reference
Surface and ground water (Iran)	0.005-0.008	(Javid et al., 2016)
Surface water (USA)	up to 0.11	(Kolpin et al., 2002)
Surface water (China)	up to 0.137	(Tong et al., 2014)
Ground water (China)	up to 0.115	(Tong et al., 2014)
Surface water (China)	up to 0.32	(Bu et al., 2013)
Surface water (USA)	up to 0.005	(Arikan et al., 2008)
River water (Hong Kong)	up to 0.031	(Deng et al., 2018)
Wastewater effluent (Hong Kong)	up to 1.3	(Gulkowska et al., 2008)
Hospital effluent (Portugal)	up to 158	(Pena et al., 2010)
Surface water (Germany)	1.2-4.2	(Borghi and Palma, 2014)
Natural water (USA)	0.11	(Borghi and Palma, 2014)
Water (UK)	0.1	(Borghi and Palma, 2014)
Surface water (UK)	up to 0.11	(Borghi and Palma, 2014)

Table 2.2. Occurrence of TET in food

Food/ milk samples	TET concentration (µg/kg)	Reference
Commercial milk (Iran)	241.45	(Aalipour et al., 2015)
Meat (Croatia)	0-5.35	(Vragović et al., 2011)
Fish (Greece and Spain)	11.1-13.1	(Cháfer-Pericás et al., 2011)
Milk (Croatia)	0-4.26	(Vragović et al., 2011)

Furthermore, due to its widespread use as a growth promoter for farm animals and antimicrobial agent in animal husbandry and aquaculture, TET residues are detected in various animal-based food products including milk, meat, and fish (**Table 2.2**). A study on commercial milk samples in Iran has reported TET levels ranging up to 241.45 µg/kg (Aalipour et al., 2015), while another study reported 0-4.26 µg/kg TET in milk samples collected in Croatia (Bilandžić et al., 2011; Vragović et al., 2011). A range of 11.1-13.1 µg /kg of TET was reported in fish from the marine farms in Greece and Spain (Cháfer-Pericás et al., 2011), while 0-5.35 µg/kg was reported in meat samples from Croatia (Vragović et al., 2011).

2.5. Toxic Effects of TET on Aquatic Organisms

Due to the frequent and abundant occurrence of TET in aquatic environments, inhabiting organisms have a higher possibility of being exposed to TET. Toxic effects of TET on aquatic organisms have been studied previously, mostly focusing on the effects at embryonic and larval stages. For example, TET has been reported to generate toxic effects such as decreased body length, delayed hatching, increased yolk sac area, and absence of a swim bladder on zebrafish embryos or larvae even under 20 µg/L exposure levels (Zhang et al., 2015). Enhanced oxidative stress and apoptosis in zebrafish embryos upon TET exposure have also been reported (Yu et al., 2019; Zhang et al., 2015). Furthermore, another study reported histological alterations in gills of a freshwater fish species, *Gambusia holbrooki*, upon TET exposure (Nunes et al., 2015).

In addition to embryonic and larval toxicity studies, few studies reported the effects of TET on the gut microbiome of aquatic fishes. In a recent study, altered gut microbial community structure with increased abundance of antibiotic resistance bacteria in goldfish, *Carassius auratus Linnaeu*s, was reported upon TET treatment at 0.285 and 2.85 µg/L (Jia et al., 2020). Another study reported the effects of oxytetracycline, a TET family antibiotic, on zebrafish gut microbiome (Almeida et al., 2019). Yet, no reports on TET mediated toxic effects on zebrafish and its gut microbiome.

2.6. Gut Microbiome in Toxicological Studies

Several recent reviews highlighted the importance of considering gut microbiome alterations upon xenobiotic exposure, which is typically overlooked in existing approaches for toxicological studies and risk assessment (Claus et al., 2016; Licht and Bahl, 2019; Velmurugan, 2018). The organisms' gastrointestinal (GI) tract, especially the colon, is colonized with a diverse community of microbial flora, which consists of ~100 trillion bacterial cells belong to ~800–1000 different bacterial species (Bäckhed et al., 2005). Firmicutes and Bacteroidetes are the two most abundant phyla in the gut, which is around 90%, followed by Proteobacteria and Actinobacteria (De Filippo et al., 2010; Eckburg et al., 2010; The Human Microbiome Project Consortium, 2012).

The intestinal microflora is considered an essential organ that carries out a number of crucial functions related to host health. Evidence from earlier studies suggested the strong interaction between the gut microbiome and its host, and the relationship is considered a commensal or mutualistic relationship (Bäckhed et al., 2005). The key functions carried out by the gut microbiome includes digestion of polysaccharides (i.e., plant-derived pectins, cellulose, hemicellulose, and resistant starches) that cannot be digested directly by the host, metabolism of glycans, amino acids, and xenobiotics, biosynthesis of vitamins and isoprenoids, regulation of immune system responses, epithelial development, protection against epithelial cell injury, regulation of host fat storage, and stimulation of intestinal angiogenesis (Eckburg et al., 2010; Gill et al., 2006).

Besides, the gut microbiome contributes to the progression of diseases and adverse health effects in the host, including inflammatory bowel disease, obesity, diabetes, metabolic syndrome, colorectal cancer, cardiovascular diseases, and mental health disorders (Chen and Devaraj, 2018; Cox and Blaser, 2013; Halfvarson et al., 2017; Kostic et al., 2015; Pedersen et al., 2016; Scheperjans et al., 2015; Wang et al., 2011; Zhang and Davies, 2016). All these beneficial and adverse effects of the gut microbiome on its host are summarised in **Figure 2.4**. Collectively, there are numerous known and unknown impacts of the gut microbiome on the host's functions, metabolism, and diseases.

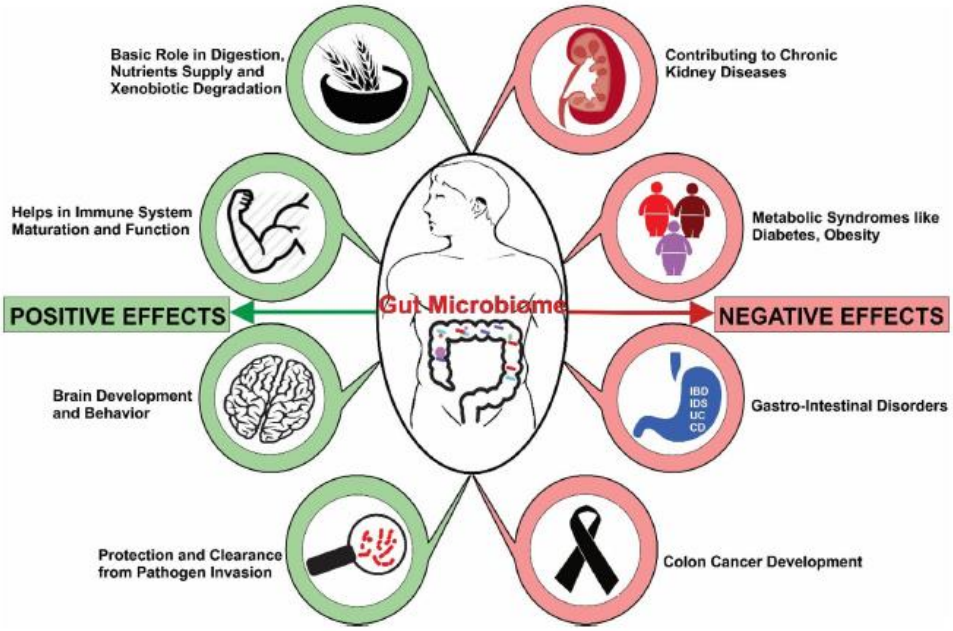

Figure 2.4. Gut microbiome-associated host health and diseases
Adapted from (Dekaboruah et al., 2020)

2.7. Xenobiotic Exposure of Gut Microbiome

Many prior studies reveal the adverse effects of xenobiotic exposure on the gut microbiome (Francino, 2016; Modi et al., 2014; Pérez-cobas et al., 2013). For example, in one study, exposure to 14 xenobiotics, including host-targeted drugs and antibiotics, resulted in community composition change, inducing the genes responsible for drug metabolism, drug resistance, and stress response (Maurice et al., 2013). Besides the prevalent interest in gut microbial community composition and its functional alterations, only limited studies focused on the response of pure gut bacterial strains towards xenobiotics. In one study, a screen of >1,000 marketed drugs against 40 representative gut bacterial strains from 38 bacterial species and 21 genera showed that 24% of the human targeted drugs inhibited the growth of at least one strain *in vitro* (Maier et al., 2018). The study showed the significant susceptibility of species with higher relative abundance across individuals towards human targeted drugs.

Furthermore, mounting evidence shows the toxic effects of xenobiotic exposure on the host, mediated through gut microbiome dysbiosis. Altered host metabolism (Behr

et al., 2017; Pi et al., 2019), obesity (Cho et al., 2012; Cox et al., 2014; Hernández et al., 2013; Marciano et al., 2017; Thuny et al., 2010), liver abnormalities (Jin et al., 2016), and modulation of immune system responses (Jin et al., 2016) are few of those. These pieces of evidence suggest the importance of considering the gut microbiome in toxicological studies.

2.8. TET Mediated Gut Microbiome Dysbiosis and Altered Microbe-Host Interactions

A growing body of evidence suggests that TET can alter the gut microbial community in human (*in vitro*), mice, and swine (Jung et al., 2018; Looft et al., 2012; Roca-Saavedra et al., 2018). One *in vitro* study exposed the fecal matter from three individuals to 0.15, 1.5, 15, and 150 mg/ml of TET for 24 hours and 40 days and evaluated the bacterial community changes. Results revealed an increase in the relative abundance of *Bacteroides* in two individuals under TET exposure above 0.15 mg/L at both time points and an increase in *Clostridium* family XI for the other individual after 40 days exposure. In addition, the study also showed a slight increase in the copy number of TET resistance genes (Jung et al., 2018). In another study, TET's effect at multiple dose levels, including therapeutic oral dose and acceptable daily intake level, was investigated using *in vitro* human colonic microflora. The study claimed that none of the investigated parameters (i.e., few targeted metabolites such as SCFAs and bile acids, bacterial counts, sulfur reduction, and few bacterial enzyme levels) were responsive towards TET (Carman et al., 2005).

Studies on host effects associated with TET exposed gut microbiome are limited. One study showed achieving a higher body mass index (BMI) and body fat accumulation upon treating rats with 75 mg/ kg/day TET for two weeks (Marciano et al., 2017). Contradictory, mice fed with 100 µg/kg of TET for 16 weeks showed no change in weight upon treatment. However, gut microbiome alterations such as the increased abundance of the phylum Bacteroidetes compared to control were observed (Roca-Saavedra et al., 2018). Another study treated mice with clinically relevant doses of TET showed a decrease in fecal leukotriene B4 (LTB4), indicating the disturb on eicosanoid homeostasis (Antunes et al., 2011). Moreover, altered plasma metabolite

levels in the mice treated with approx. 5,000 mg/kg body weight of TET for 7, 14, and 28 days were reported. For instance, the relative abundance of some metabolites such as hippuric acid, 3-indoxyl sulfate was significantly affected (Behr et al., 2017).

2.9. Gut Microbiome-Associated Host Obesity

Association between antibiotic-induced gut microbiome dysbiosis and host obesity has been found in many previous studies (Cho et al., 2012; Cox et al., 2014; Hernández et al., 2013; Marciano et al., 2017; Thuny et al., 2010). The majority of these studies focused on the alterations in the gut microbial community composition linked with obesity or obesity-related complications (i.e., liver lipid alterations). Yet, only a few investigated the mechanism underlying microbiome-induced obesity.

2.9.1. Gut microbial changes associated with host body weight changes

Major gut microbial changes associated with host body weight were reported in a few previous studies. For example, the Firmicutes/Bacteroidetes ratio has been described as higher in obese mice than in normal-weight mice (Cox and Blaser, 2013; Turnbaugh et al., 2006). Also, an increase in the abundance of Firmicutes is usually considered an obesogenic factor (Arumugam et al., 2011). Conversely, an increased abundance of *Gammaproteobacteria (Escherichia)* and *Verrucomicrobia (Akkermansia)*was shown to be linked with host weight loss (Liou et al., 2013). Also, the contribution of two genera *Lactobacillus* and *Allobaculum*, family *Rikenellaceae*, and *Candidatus Arthromitus* in protection against weight gain has been reported (Cox et al., 2014). Collectively, these alterations in gut microbiome composition appear to be associated with host body weight changes, even though their role in modulating host weight gain is not elucidated.

2.9.2. Pathways in gut microbiome-induced obesity

Moreover, few mechanistic pathways explain the altered gut microbiome's contribution to inducing obesity by altering energy extraction from food or altering inflammation and immunity (**Figure 2.5**). Gut microbiome produced SCFAs are

known to be involved in microbe-induced obesity by slowing transit time, increasing energy extraction from food, or protecting against obesity by increasing satiety (Cox and Blaser, 2013). Early life subtherapeutic antibiotic treatment (STAT) increased the abundance of microbial genes involved in SCFA production, increasing the intestinal SCFA level. Subsequently, it also altered the hepatic expression of genes involved in lipid, cholesterol, and triglyceride (TAG) metabolism (Cho et al., 2012).

LPS produced by gut bacteria are also known to involve in microbe-induced obesity and related complications. LPS can involve in obesity as an inflammatory mediator that signals in a (cluster of differentiation) CD14/ (toll-like receptor) TLR4-dependent manner and/or by infusion of LPS alone can increase body weight gain, adiposity, insulin resistance, and liver TAG levels (Cox and Blaser, 2013). While there are many Gram-negative species within the gut microbiome, *Bacteroidetes is* the main phylum that contributes to LPS biosynthesis in the gut, while *proteobacteria* is a minor contributor to LPS biosynthesis (d'Hennezel et al., 2017). One study speculated the contribution of altered LPS levels resulted from antibiotic (i.e., Penicillin G, erythromycin, and their mix) altered gut microbiome to increased expression levels of key genes involved in liver fatty acid (FA) and TAG metabolism in mice (Jin et al., 2016).

Furthermore, sensing of bacterial flagellin through innate immunity receptor TLR5 is also known to cause hyperphagia-dependent weight gain, insulin resistance, increased adiposity, blood pressure, and cholesterolemia (Cox and Blaser, 2013; Vijay-kumar et al., 2010). Also, the mucosal intestinal microbiota can control the lymphotoxin, secreted by Th1 lymphocytes, which are known to be involved in obesity (Cox and Blaser, 2013; Upadhyay et al., 2013). Inflammasomes have also been known to involve in obesity-associated complications like nonalcoholic steatohepatitis (NASH). Inflammasomes are multiprotein complexes that sense pathogen-associated molecular patterns (PAMPs), which aid in mucosal defenses by activating the inflammatory cytokine precursors pro- interleukin (IL)-1β and pro-IL-18. Dysfunctions in inflammasomes such as lacking components (i.e., *Asc,* caspase, Nod-like receptor protein (NLRP)3) in inflammasome complex or signaling (*IL-18*) lead to increased hepatic tumor necrosis factor (TNF)-α expression leading to NASH.

Furthermore, the Aryl hydrocarbon receptor (AHR) is known to play a broad role in disrupting fat metabolism and contribute to NASH in obesity and associated complications such as liver fat accumulation (He et al., 2013; Krishnan et al., 2018; Xu et al., 2016). Since the gut microbiome produced tryptophan and indole derivatives are known AHR ligands (Bittinger et al., 2003; Hendrikx and Schnabl, 2019; Hubbard et al., 2015; Jin et al., 2014; Zelante et al., 2013), gut microbiome metabolite-mediated obesity complications through AHR can be speculated.

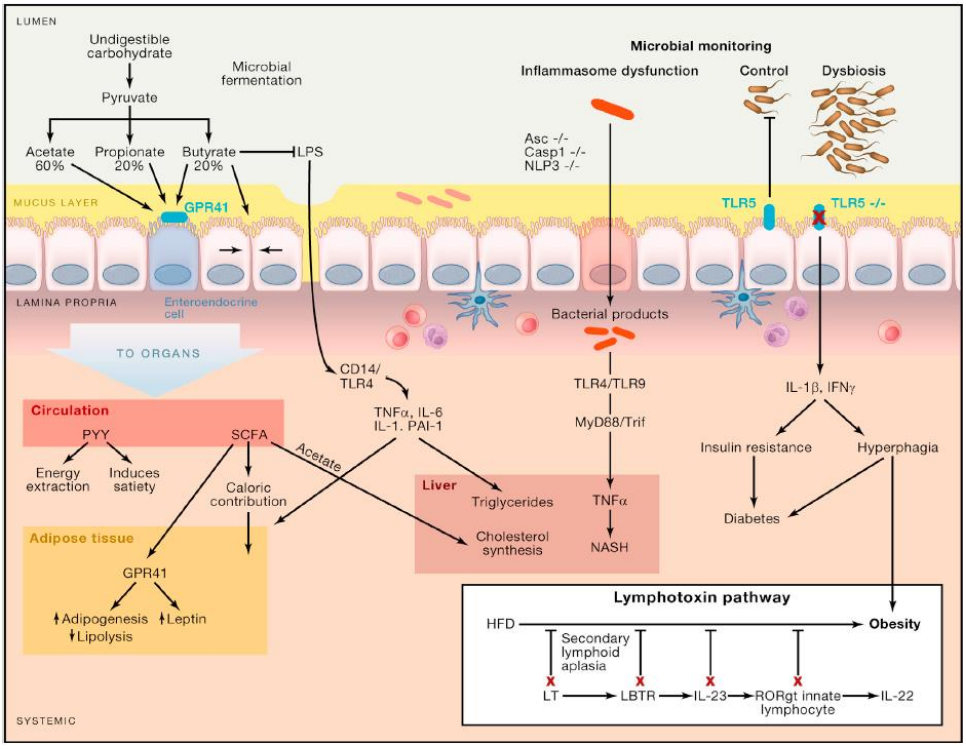

Figure 2.5. Pathways involving microbe-induced obesity
Adapted from (Cox and Blaser, 2013)

2.10. Gut Microbiome Metabolites and Host Health Modulation

In addition to the increased body weight gain in the host through metabolic and immunological interactions between the host and microbiota, gut microbiome is responsible for producing, transforming and/or regulating many other metabolites with known and unknown functions related to host health (Donia and Fischbach, 2016; Wikoff et al., 2009; Wilmanski et al., 2019; Zhang and Davies, 2016). The important gut microbiome metabolites can be categorized into few major representative groups:

tryptophan and indole derivatives, tyrosine and phenyl derivatives, other amino acid related metabolites, SCFAs, bile acids, FAs, BCAAs, and vitamins. Conversion pathways, biological mechanisms, and host-related functions of these metabolites are detailed in **Table 2.3** and **Section 2.10.1-2.10.6**.

2.10.1. Tryptophan and indole derivatives

Gut microbiome is metabolizing dietary tryptophan in few main pathways: the kynurenine pathway and to indole derivatives. For instance, tryptophan is converted to indoles by tryptophanase, which is available in microorganisms (Meyer and Hostetter, 2012), while *C. sporogenes* is known to involve in indole-3-propionic acid synthesis (Wikoff et al., 2009). For the kynurenine pathway, kynurenine is produced via enzymes, tryptophan 2, 3 Dioxygenase and kynurenine formamidase, known to present in bacterial species such as *Ralstonia metallidurans*. Subsequently, kynurenic acid is formed by trans- amination of kynurenine (Cervenka et al., 2017; Kaur et al., 2019).

Kynurenic acid modulates local inflammation, most likely through the activation of G protein–coupled receptor (GPCR), which is highly expressed in the GI tract immune cells (Cervenka et al., 2017). Furthermore, tryptamine, indole-3-aldehyde, kynurenic acid, and xanthurenic acid are agonists for transcriptional aryl hydrocarbon receptor (Hubbard et al., 2015; Jin et al., 2014; Zelante et al., 2013). AHR and its ligands play an important role in gut homeostasis and various intestinal diseases, including colitis and colon cancer, except for the obesity-related complications described in **Section 2.9.2** (Zelante et al., 2013; Zhang and Davies, 2016). Furthermore, the implication of kynurenines and other tryptophan metabolites in numerous neurological disorders that affect mental health has been reported (Cervenka et al., 2017; Dehhaghi et al., 2019).

2.10.2. Tyrosine and phenyl derivatives

Tyrosine is microbially converted to *p*-cresol through an intermediate, 4-hydroxy phenylacetic acid (Meyer and Hostetter, 2012). Also, *C. sporogenes* involved conversion of tyrosine to 4-hydroxy -phenylacetic acid, 4-hydroxy -phenyllactic acid, and their derivatives through aminotransferase reaction has been suggested (Dodd et

al., 2017). *P*-Cresol has been reported to induce genotoxic effects on colonocytes while *p*-cresol sulfate suppresses Th1-type cellular immune responses in mice (Saito et al., 2018; Shiba et al., 2014). Also, hydrocinnamic acid is a known inhibitor of branched-chain α -keto acid dehydrogenase kinase, which regulates the breakdown of BCAAs, while its level in the blood has been reported to positively correlate with gut microbial diversity (Pallister et al., 2017; Pedersen et al., 2016; Tso et al., 2013). In addition, the interaction of phenyllactic acid and the human host through GPCR has also been reported (Peters et al., 2019).

2.10.3. SCFAs

SCFAs include acetic acid, propionic acid, and butyric acid, which are produced by fermentation of fiber and proteins by the gut microbiome and considered as the most abundant microbial metabolites in the gut. Pentose-phosphate pathway for five-carbon sugars and Embden Meyerhof- Parnas pathway (glycolysis, for six-carbon sugars) are the two major pathways involved in anaerobic SCFA production from carbohydrates (Besten et al., 2013). The phylum Firmicutes produces butyrate as its primary metabolic end product, while Bacteroidetes is the main producer of acetate and propionate (Besten et al., 2013). Gut microbial community members such as *Akkermansia municiphilla* have been identified as key propionate producers, whereas *Ruminococcus bromii*, *Faecalibacterium prausnitzii*, *Eubacterium rectale*, and *Eubacterium hallii* are responsible for the production of significant fraction of butyrate (Morrison and Preston, 2016). In addition to modulating host obesity (as described in **Section 2.9.2**), providing energy for colorectal tissues and bacteria and promoting cellular mechanisms that maintain tissue integrity are the primary functions of SCFAs in the GI tract (Besten et al., 2013; Conlon and Bird, 2015; Topping and Clifton, 2001).

2.10.4. Bile acids

Deoxycholic acid (DCA) and lithocholic acid (LCA) are the common secondary bile acids transformed by gut bacteria through deconjugation and dihydroxylation of primary bile acid conjugates (Ridlon et al., 2006). In addition, ursodeoxycholic acid (UDCA) is also a secondary bile acid found in humans (Wahlström et al., 2016).

Bacterial genera *Eubacterium* and *clostridium* are known to carry out the a7-hydroxylation process, an important step in forming secondary bile acids (Takamine and Imamura, 1995; Wells et al., 2000). Also, the bacterial strains *B. fragilis* and *Bifidobacterium longum* are known to involve in bile acid deconjugation by enzymatic hydrolysis of the C-24 N-acyl amide bond linking bile acids to their amino acid conjugates (Grill et al., 1995; Stellwag and Hylemon, 1976).

Bile acids are ligands for the Takeda G protein-coupled receptor (TGR5), a bile acid-specific GPCR, and for the farnesoid X receptor (FXR) (Jia et al., 2018; Sayin et al., 2013). High levels of DCA in blood and faces are associated with increased risks of cholesterol gallstone disease, colon cancer, and liver cancer (Ridlon et al., 2014), while LCA is known to associate with colon cancer (Mcgarr et al., 2005).

2.10.5. BCAAs

Leucine, isoleucine, and valine are the main BCAAs involved with the gut microbiome. *Prevotella copri* and *Bacteroides vulgatusare* have been identified as the main species involved in the biosynthesis of BCAAs (Pedersen et al., 2016). It has been shown that the gut microbiome can influence the serum BCAA level, which is associated with insulin resistance and, thereby, induce type ii diabetes (Pedersen et al., 2016).

2.10.6. Vitamins

Furthermore, vitamin synthesis is an essential function by human gut microbiota, while specific B vitamins are among the key metabolites supplied to the host by gut bacteria (Magnúsdóttir et al., 2015; Morowitz et al., 2011). In addition, vitamin B_9 and B_{12} are known biomarkers linked to adult brain volume (Hooshmand et al., 2016)

Additionally, more gut microbiome produced or transformed metabolites and their relationship with host physiological functions and disease progression are detailed in **Table 2.3**.

Table 2.3. Gut microbial metabolites and host health implications

Category	Subcategory	Metabolite	Molecular functions	Host health implications
Amino acid-related	Tryptophan and indole derivatives	Indolepropionic acid	Pregnane X receptor (PXR) Agonist (Liu et al., 2020) AHR agonist (Liu et al., 2020)	Immunomodulatory (Donia and Fischbach, 2016) Promotes intestinal epithelial barrier function ((Liu et al., 2020) Neuroprotective (Liu et al., 2020) Antioxidant (Liu et al., 2020)
		Indole	AHR antagonist (Jin et al., 2014) Modulates Glucagon-like peptide (GLP)-1 secretion (Zhang and Davies, 2016)	Maintains host-microbe homeostasis at mucosal surface (Zhang and Davies, 2016)
		Indole-3-aldehyde	AHR agonist (Zhang and Davies, 2016)	Maintains host-microbe homeostasis at mucosal surface (Zhang and Davies, 2016)
		Skatole	AHR agonist (Liu et al., 2020)	Na
		Tryptamine	AHR agonist (Hubbard et al., 2015)	Neurotransmitter (Donia and Fischbach, 2016)

		Indole-3-acetic acid	AHR agonist (Liu et al., 2020) Inhibits microglial activation (Liu et al., 2020)	Anti-inflammatory effects in nonalcoholic fatty liver disease (Liu et al., 2020) Renal toxicity (Liu et al., 2020)
		Tryptophan	Regulates Ca2+-sensing receptor (CaSR) signaling pathway (Tan et al., 2017)	Inflammatory bowel diseases (Tan et al., 2017) Major depression, chronic brain injury, amyotrophic lateral sclerosis (Dehhaghi et al., 2019)
		Serotonin /5-hydroxytryptamine	Regulation of adipose tissue energy storage and expenditure (Cervenka et al., 2017) Brain-mediated appetite control (Cervenka et al., 2017)	Diabetes (Cervenka et al., 2017) Fat accumulation in adipose tissues (Cervenka et al., 2017) Depression, fatigue, and impaired cognitive function (Kaur et al., 2019) Neurotransmitter (Kaur et al., 2019)
		5-Hydroxy-L-tryptophan	AHR agonist (Bittinger et al., 2003)	NA
		Xanthurenic acid	AHR agonist (Hubbard et al., 2015)	NA

		Melatonin	Stimulation of IL-2, IL-6, and IL-12 production (Srinivasan et al., 2005) Decrease the activity of natural killer (NK) cells, granulocytes, and macrophages (Srinivasan et al., 2005)	Immunomodulatory (Srinivasan et al., 2005)
		Formylkynurenine	NA	NA
		Kynurenine	AHR agonist (Cervenka et al., 2017)	Alzheimer disease, anxiety, amyotrophic lateral sclerosis, Schizophrenia (Dehhaghi et al., 2019)
		Kynurenic acid	N-methyl-D-aspartate receptor (NMDAR) (Cervenka et al., 2017) a7 nicotinic acetylcholine receptor (a7nAChR) antagonist (Cervenka et al., 2017) GPR35 agonist (Cervenka et al.,	Modulate local inflammation (Cervenka et al., 2017) Alzheimer disease, anxiety, amyotrophic lateral sclerosis, Schizophrenia (Dehhaghi et al., 2019)

			2017) AHR agonist (Cervenka et al., 2017)	
		3-Hydroxy-L-kynurenine	NA	NA
		Quinolinic acid/ Pyridinedicarboxylic acid	NMDAR agonist (Cervenka et al., 2017) TH1 target cells' apoptosis (Dehhaghi et al., 2019) Selectively suppress the proliferation of killer cells, and CD4+ and CD8+ T lymphocytes (Dehhaghi et al., 2019)	Alzheimer disease, dementia complex, Huntington disease, and multiple sclerosis (Dehhaghi et al., 2019)
		Indole-3-acetaldehyde	NA	NA
		Indole-3-acetaldoxime	NA	NA
		Indole-3-acetonitrile	NA	NA
		Indole-3-pyruvic acid	NA	NA

		Indolelactic acid	NA	Ameliorates salt-sensitive hypertension (Liu et al., 2020)
		Indoleacetyl glutamine	NA	NA
	Tyrosine and phenyl derivatives	Phenyllactic acid	Highly potent activation of hominids contain a third member (HCA3) (Peters et al., 2019)	NA
		Phenethylamine	Agonist of dopamine receptor D2 (DRD2)/4 (Liu et al., 2020)	Neurotransmitter (Donia and Fischbach, 2016)
		Phenylacetic acid	NA	Toxic to colonocytes (Liu et al., 2020) Triggers steatosis (Liu et al., 2020)
		4-ethylphenyl sulfate	NA	Autistic spectrum disorder (Zhang and Davies, 2016)
		P-cresol	NA	Induce genotoxic effects on colonocytes (Saito et al., 2018)

		P-cresol sulfate	Activates nicotinamide adenine dinucleotide phosphate (NADPH) oxidase (Zhang and Davies, 2016) Th1-type cellular immune responses (Shiba et al., 2014)	Damages cell membranes (Zhang and Davies, 2016) Induces apoptosis (Zhang and Davies, 2016)
		Hippuric acid	NA	Metabolic syndrome (Pallister et al., 2017)
		3-phenylpropionate /Hydrocinnamate	Inhibitor of branched-chain α -keto acid dehydrogenase (Tso et al., 2013)	Positively correlate with gut microbial diversity (Pallister et al., 2017)
		Phenylacetylglutamine	NA	Cardiovascular disease (Wilmanski et al., 2019)
		Cinnamoylglycine	NA	Obesity (Wilmanski et al., 2019)
		Phenylpropionylglycine	NA	
		Phenylacetylglycine	NA	

		4-Hydroxyphenylacetic acid	NA	Genotoxic effects on human enterocytes (Liu et al., 2020)
		Tyramine	Agonist of trace amine-associated receptors (TAAR)1 (Liu et al., 2020)	Neuromodulators (Liu et al., 2020) Vasodilation (Liu et al., 2020)
		Trans-Cinnamate/Cinnamic acid		Regulates glucose transport (Liu et al., 2020) Antitumor (Liu et al., 2020)
		Tyrosine	Regulates CaSR signaling pathway (Tan et al., 2017)	Inflammatory bowel diseases (Tan et al., 2017)
		Coumaric acid/4-Hydroxycinnamate	NA	NA
		Phenylalanine	Regulates CaSR signaling pathway (Tan et al., 2017)	Inflammatory bowel diseases (Tan et al., 2017)
	BCAAs	L-leucine	NA	Insulin resistance (Pedersen et al., 2016) Type ii diabetes (Pedersen et al., 2016)

		Isoleusine	NA	Insulin resistance (Pedersen et al., 2016) Type ii diabetes (Pedersen et al., 2016)
		L-valine	NA	Insulin resistance (Pedersen et al., 2016) Type ii diabetes (Pedersen et al., 2016)
	Others	5-aminovaleric acid	NA	
		γ-aminobutyric acid (GABA)	NA	Neurotransmitter (Bhat et al., 2010)
		3-aminoisobutyric acid	NA	
		Imidazole propionate	NA	Insulin resistance (Koh et al., 2018)
Lipids and fatty acids (FAs)	SCFAs	Acetate	Activates GPCR41 and GPCR43 (Zhang and Davies, 2016)	Anti-inflammatory (Besten et al., 2013) Improves insulin sensitivity (Besten et al., 2013) Anti-lipogenic (Besten et al., 2013) Increases energy expenditure (Besten et al., 2013)
		Propionate	Activates GPCR41 and GPCR43 (Zhang and Davies, 2016) Upregulates GLP-1, Peptide YY (PYY), leptin (Zhang and Davies, 2016)	

		Butyrate	Activates GPCR41 and GPCR43 (Zhang and Davies, 2016) Activates GPCR109A (Zhang and Davies, 2016) Modulates peroxisome proliferator-activated receptor (PPAR)-γ (Zhang and Davies, 2016)	
	Trimethylamine N-oxide (TMAO) related	Trimethylamine (TMA)	NA	NA
		TMAO	NA	Cardiovascular disease (Wang et al., 2011)
	FAs	Conjugated linoleic acid (CLA)	NA	Body weight gain (Mensink, 2005) Cardiovascular disease (Mensink, 2005) Insulin resistance (Risérus et al., 2004)
		Conjugate linolenic acids (CLnAs)	NA	

		10-hydroxy-cis-12-octadecenoate	NA	
	Bile acids	Deoxycholic acid (DCA)	TGR5 agonist (Wahlström et al., 2016) FXR agonist (Jia et al., 2018)	Cholesterol gallstone disease (Ridlon et al., 2014) Colon cancer (Ridlon et al., 2014) Obesity-associated hepatocellular carcinoma (Ridlon et al., 2014)
		Lithocholic acid (LCA)	FXR agonist (Jia et al., 2018)	Colon cancer (Mcgarr et al., 2005)
		Ursodeoxycholic acid (UDCA)	Farnesoid X receptor (FXR) antagonist (Wahlström et al., 2016)	NA
		Glyco-cholic acid	FXR agonist (Wahlström et al., 2016)	NA
		Tauro-cholic acid	FXR agonist (Wahlström et al., 2016)	NA

		Glyco-chenodeoxycholic acid	FXR agonist (Wahlström et al., 2016)	NA
		Tauro-chenodeoxycholic acid	FXR agonist (Wahlström et al., 2016)	NA
Vitamins	B vitamins	Thiamine (B_1)	NA	Cellular metabolism (Vernocchi et al., 2016)
		Biotin (B_7)	NA	Cellular metabolism (Vernocchi et al., 2016)
		Riboflavin (B_2)	NA	Cellular metabolism (Vernocchi et al., 2016)
		Pantothenic acid (B_5)	NA	Cellular metabolism (Vernocchi et al., 2016)
		Folate (B_9)	NA	Adult brain volume biomarker (Hooshmand et al., 2016) Cellular metabolism (Vernocchi et al., 2016)
		Nicotinic acid(B_3)	NA	Cellular metabolism (Vernocchi et al., 2016)
		Pyridoxine (B_6)	NA	Cellular metabolism (Vernocchi et al., 2016)

		Cyanocobalamin (B_{12})	NA	Adult brain volume biomarker (Hooshmand et al., 2016) Cellular metabolism (Vernocchi et al., 2016)
	Others	Menadione (K_3)	NA	Cellular metabolism (Vernocchi et al., 2016)

2.11. Summary of Literature Review

From the literature review, the following knowledge gaps are identified:

To date, there are no investigations on the long-term toxic effects of TET on juvenile zebrafish during its development into adult fish. More importantly, TET mediated changes in zebrafish gut microbiome have not been studied along with the effects on zebrafish host. Furthermore, gut microbiome-associated increased host weight gain induced by antibiotic exposure has been reported for some rodent models. However, this phenomenon has rarely been investigated in aquatic organisms. Therefore, long-term effects of TET exposure on zebrafish host focusing on body weight changes and gut microbiome alterations are yet to be studied.

Furthermore, it is known that certain pure gut bacterial strains play a critical role in maintaining a healthy gut microbiome and host-related functions. For instance, some marked changes in the gut microbiome composition have been known to associate with changes in host body weight. Furthermore, certain bacterial strains are specifically known to possess enzymes involved in producing important metabolites. Yet, there is a knowledge gap for understanding the metabolic alterations induced by TET exposure in pure gut bacterial strains.

Also, the gut microbiome-host interactions are mostly mediated through the metabolites produced, transformed, and regulated by the gut microbiome. Some of the gut bacterial metabolites contribute to the host body weight changes, as revealed in previous studies. Nevertheless, the metabolic consequences of TET exposed gut microbiome, which may subsequently modulate host functions, have not been fully investigated yet, except for a few targeted metabolomics studies. Besides, another major knowledge gap of those previous studies is how the nutrient status such as fed and fasted conditions affect the impact of TET on the gut microbiome.

Liver abnormalities, such as lipid accumulation, are known obesity-related complications mediated through the gut microbiome. The link between gut microbiome and host obesity and related complications through gut microbial metabolites and immunoregulatory compounds such as LPS has been previously revealed. However, metabolic and immunological dysfunctions associated with host

weight gain caused by TET affected gut microbiome have not yet been investigated. Furthermore, the influence of TET on the LPS production of primary gut bacterial orders contribute to the gut LPS pool, and thereby the effects on the host remain unclear.

Chapter 3. Long-term Exposure to TET Increases Body Weight of Juvenile Zebrafish as Indicated in Host Metabolism and Gut Microbiome

3.1. Overview

Chapter 3 investigated the toxic effects of TET exposure on aquatic organisms at low or environmentally relevant levels using an *in vivo* zebrafish model. The study exposed zebrafish at the juvenile stage to two different low or environmentally relevant levels of TET for a one-month period until their adulthood. And the study analyzed the growth (i.e., body weight and length) and liver characteristics such as histology, gene expression, lipidome, and metabolome of zebrafish. Lastly, the study further evaluated the alterations in zebrafish gut microbial community composition and functions upon TET exposure. This chapter has been published as **Keerthisinghe, T. P.,** Wang, F., Wang, M., Yang, Q., Li, J., Yang, J., Xi, L., Dong, W., and Fang, M. (2020). Long-term exposure to TET increases body weight of juvenile zebrafish as indicated in host metabolism and gut microbiome. *Environment International*, **139**: 105705. DOI: 10.1016/j.envint.2020.105705.

3.2. Introduction

TET is an extensively used antibiotic for human therapeutic purposes, veterinary medicine, and aquaculture and most frequently detected in aquatic environments up to 158 μg/L (Bu et al., 2013; Food and Drug Administration, 2017; Pena et al., 2010). Thus, there is a higher possibility of exposing the aquatic organisms inhabiting those environments to TET. Toxic effects of TET on aquatic organisms such as zebrafish (*Danio rerio*) have been studied previously, especially for embryonic and larval toxicity. For example, TET has been reported to generate toxic effects such as decreased body length, delayed hatching, increased yolk sac area, and absence of a swim bladder on zebrafish embryos or larvae even under 20 μg/L exposure levels (Zhang et al., 2015). Enhanced oxidative stress and apoptosis in zebrafish embryos

have also been observed (Yu et al., 2019; Zhang et al., 2015). However, very little information is available on the long-term toxic effect of TET on juvenile zebrafish during its development into adult fish, which is a critical window for the growth.

The effect of antibiotics on the gut microbiome and its subsequent host effect has been a hot-spot in many recent studies. For example, exposure to antibiotic penicillin can induce obesity in rodent model during a critical development period by altering gut microbiome (Cox et al., 2014). TET has been shown to cause dysbiosis in the gut microbiome of mice (Roca-Saavedra et al., 2018), swine (Looft et al., 2012), and human (*in vitro*) (Jung et al., 2018). However, very little information is available for TET's effect on the zebrafish gut microbiome.

In this study, we have exposed offspring juvenile zebrafish to TET for one-month until the adult stage. Interestingly, we have observed increased body weight gain, but not the body length in TET exposed fish, with liver histological abnormalities and significant metabolic dysregulations, especially the enrichment of liver lipids. Furthermore, gut microbial community analysis reveals that TET could alter the gut microbial community composition and increase bacterial diversity.

3.3. Methodology

3.3.1. Fish culture, TET exposure, and sample collection

Zebrafish at offspring were maintained at 28℃ in a recirculating AHAB system (Aquatic Habitats) under a 14:10-h light/dark cycle and were fed with brine shrimp and a mix of Ziegler's Adult Zebrafish Complete Diet (Aquatic Habitats). Adult care and reproductive techniques were noninvasive and approved by the Inner Mongolia University for the Nationalities Institutional Animal Care and Use Committee.

TET hydrochloride was purchased from Sigma-Aldrich, St. Louis, MO. The stock solutions were prepared in Milli-Q® H_2O and diluted in above-mentioned system medium to prepare the exposure solutions. The exposure concentrations were selected to represent TET levels detected in aquatic environments including wastewater/farming water (non-detection (n.d.) - 158 μg/L) and surface water (n.d. -

320 ng/L) as detailed in **Table B1**. Thus, 1 and 100 μg/L were selected to represent low and high environmental concentrations; respectively.

For the TET exposure, fish at offspring stage were maintained in the system until 60 days post-fertilization (i.e., 60 dpf, juvenile stage) and 120 fish were randomly selected and divided into three sets of 4 tanks (10 fish per tank). Two sets (n=4 tanks for each) were dosed with TET at 1 and 100 μg/L, and the remaining 4 tanks were maintained as the control without TET exposure. The fish were exposed to TET dissolved culture medium or culture medium without TET (control) under a semi-static flow condition, and the tanks were replenished with the fresh medium every five days. After 30 days of development in control and TET dosed tanks, fish were sacrificed and measured for body weight and length. The liver samples and the intestinal parts were dissected, snap-frozen, and stored in − 80 °C until further processing.

3.3.2. Histopathological analysis of the liver tissues

After sacrification, part of zebrafish liver samples was dissected and fixed in 4% paraformaldehyde (PFA). Liver samples of one fish from each tank were used for the analysis, resulting four replicates per treatment. Paraffin sections of livers in parasagittal plane were prepared according to our previous method (Dong et al., 2014), which were further stained with hematoxylin and eosin (H&E) to observe the histomorphological changes.

3.3.3. Hepatic gene expression profiling

The liver tissues of three zebrafish from each tank were pooled together as one sample (n=4 for each treatment), and the total RNA was extracted by TRIzol™ Plus RNA Purification kit (Thermo Fisher Scientific), according to the manufacturer's instructions. Total RNA was reverse transcribed to cDNA using High Capacity cDNA Reverse Transcription Kits (Applied Biosystems Inc., Grand Island, NY, USA; Thermo Fisher Scientific; 4368814). To quantify mRNA expression, real-time PCR was performed using an ABI PRISM 7000 Sequence Detection System (Applied Biosystems). Hepatic gene primers (**Table B2**) were synthesized using PrimerQuest

(Integrated DNA Technologies, Coralville, IA, USA). 18s rRNA was used as the housekeeping gene to normalize target gene expression.

3.3.4. Metabolite and lipid extraction

Similar to RNA extract, the liver tissues of three zebrafish from each tank were pooled together as one replicate (n=4 for each treatment). The extraction was carried out according to our previous studies (Ivanisevic et al., 2016; Montenegro-Burke et al., 2019). Briefly, 1 mL of cold methanol:H_2O (4:1, v/v) was added to each tissue sample, homogenized with metal beads in a homogenizer, and sonicated in an ice bath for 10 min. The mixture was then transferred to a new 1.5 mL Eppendorf vial and the sample was rinsed with additional 200 µL extraction solvent. The combined ~1.2 mL extraction solution in each sample was splitted into two fractions at a ratio of 5:1 (v/v) to analyze metabolites and lipids; respectively. For the metabolites, the samples were incubated for 1 h at − 20 °C, followed by 15-min centrifugation at 13,000 rpm at 4 °C to precipitate proteins. The resulting supernatants were evaporated to dryness by speed-vacuum evaporation (CentriVap Benchtop Centrifugal Vacuum Concentrator, Labconco, U.S.A.), while the settled proteins were quantified for future normalization. The dry extracts were then reconstituted in acetonitrile:H_2O (1:1, v/v), normalized by protein content, sonicated for 10 min, and centrifuged to remove insoluble debris. The supernatants were transferred to vials and stored at − 80 °C prior to analysis.

For the lipids, liquid-liquid methyl tert-butyl ether (MTBE) lipid extraction method was used, which was modified according to a previous study (Chen et al., 2013). Briefly, MTBE was added to the samples to achieve a ratio of MTBE:methanol (20:6, v/v). Then samples were sonicated for 30 min and the phase separation was induced by adding high performance liquid chromatography (HPLC) grade water to achieve a ratio of MTBE:methanol:H_2O (20:6:7, v/v/v), which was followed by centrifugation for 15 min at 4 °C. The upper phase was then collected, dried, and dissolved in $CHCl_3$:methanol (2:1, v/v) to the protein-content normalized volume.

3.3.5. Metabolite profiling, identification, and pathway analysis

The profiling of metabolites was conducted using an HPLC system (Agilent Technologies, Singapore) coupled to a 6550 quadrupole time-of-flight (Q-TOF) (Agilent Technologies, Singapore), in accordance with our previous studies (Beyer et al., 2018; Fang et al., 2015). The metabolite profiling and quality control are detailed in **Section 3.3.8** and **Text A1**. A pooled mixture of treated and control samples was run with data-dependent acquisition (DDA) auto-MS/MS and targeted MS/MS of selected precursors. The processing of metabolome data was carried out using XCMS online web platform (http://xcmsonline.scripps.edu) (detailed in **Text A1**). First screening was based on the significant features, with p-value ≤ 0.05, |fold change| > 1.2, and intensity > 10,000 ion counts. All those features were manually checked to minimize the false positive hits. MS/MS fragment match, accurate mass match, and in-house retention time match were the methods used for metabolite identification. Open source platforms KEGG (http://www.genome.jp/kegg/) and Metaboanalyst (http://www.metaboanalyst.ca) were incorporated for further pathway analysis. The heatmap analysis was conducted using R software (http://www.R-project.org, V. 3.5.1).

3.3.6. Lipid profiling and identification

Lipid profiling was performed in accordance with a previous study (Pizarro et al., 2013). Briefly, the profiling of lipids was conducted using a reversed-phase HPLC system coupled to the same 6550 Q-TOF. The lipid profiling method is detailed in **Text A1**. The data processing was carried out in a similar way to metabolomics analysis (see **Section 3.3.5**) using XCMS online web platform. In addition, MS-DIAL (V. 2.84) software program with built-in LipidBlast database was incorporated for the lipid annotation (Kind et al., 2013; Tsugawa et al., 2015).

3.3.7. DNA extraction and Illumina MiSeq platform sequencing

Similarly, the intestinal content of three fish in each tank was pooled as one sample and samples from three tanks per treatment (n=3) were used to extract DNA using FastDNA® SPIN Kit (MP Biomedicals, CA, USA) according to the manufacturer's protocol. The V3-V4 variable region of the 16S rRNA was amplified for each sample

using the primer set 338F 5'-ACTCCTACGGGAGGCAGCAG-3' and 806R 5'-GGACTACHVGGGTWTCTAAT-3' (Mao et al., 2018). The analysis of raw sequence data was carried out at the Centre for Genomic Research, Shanghai Majorbio Biotechnology Co. Ltd, China, with the Illumina MiSeq paired-end 300 bp protocol (Illumina, Inc., San Diego, CA, USA). The raw sequence data were processed using QIIME 1.7.0 followed by clustering into operational taxonomic units (OTUs) according to criteria of 97% sequence similarity by QIIME (Metcalf et al., 2016). The normalized sequences were aligned against SILVA database and clustered into different taxonomic levels (including phylum, class, order, family, and genus) at 70% threshold. The comparison of TET treated and control zebrafish gut microbial communities including non-metric multidimensional scaling (NMDS) analysis and Bray-Curtis index calculation were conducted by PAST (https://folk.uio.no/ohammer/past/). A predictive metagenomic approach using 16s rRNA gene sequence functional prediction, where the Phylogenetic Investigation of Communities by Reconstruction of Unobserved States (PICRUSt) was used to predict the KEGG category and functional enzyme was incorporated to investigate functional changes in the microbial community (Langille et al., 2013).

3.3.8. Quality assurance (QA)/ quality control (QC) and statistical analysis

For the QA/QC of liver metabolome and lipidome analysis, a pooled mix sample of metabolites/lipids prepared by pooling all treated and control samples were analyzed after every six injections of biological samples to correct the mass, retention time and response drift. All the data were expressed as mean ± standard error of the mean (SEM). Differences between groups or treatments for phenotype, metabolites, lipids, gene expression, and microbial community characteristics (e.g., alpha diversity indices and community composition) were examined for statistical significance using Student's t-test or one-factor analysis of variance (*ANOVA*) with Duncan's post-hoc test, with the significance level set at p-value ≤ 0.05. In addition, for the microbial community analysis, permutational multivariate analysis of variance (*PERMANOVA*) test (Bonferroni-corrected p-value ≤ 0.05) was employed to compare the difference in phylogenetic structure among the three groups (Anderson, 2001).

3.4. Results and Discussion

3.4.1. Body weight increase and liver microstructural changes in TET treated juvenile zebrafish

We kept monitoring the growth of juvenile zebrafish after dosing TET at 1 and 100 µg/L. We did not observe any significant deformity in the TET treated groups compared to the control. Interestingly, we observed significantly increased body weights in both 1 and 100 µg/L TET treated fish compared to control (**Figure 3.1a and C1**). However, there was no change in the body length (**Figure 3.1b**), suggesting an increased BMI. Specifically, the average daily weight gain was 0.2 ± 0.07 mg for the control group, and it was increased to 0.8 ± 0.09 and 0.6 ± 0.1 mg for 1 and 100 µg/L; respectively, while the body length was ~3 cm for all three groups after one-month period.

Because the antibiotic exposure and the increased body weight gain can potentially alter the liver functions, we next performed a histopathological analysis for zebrafish liver tissues. The representative microscopic images of H&E-stained liver histological sections showed nuclear chromatin condensation and lipid vacuoles generation in TET exposed fish (**Figure 3.1c**). The observed effects in the livers of zebrafish may be linked with the body weight gain, especially the vacuoles observed in the livers is a sign of lipid accumulation which directly can be linked with the increased weight gain (Goodman, 2014).

All those pieces of evidence showed that TET exposure at environmentally relevant levels is likely to induce weight gain in adult fish if the exposure starts from juvenile period. This observation is consistent with several recent studies on weight gain induced by early-life antibiotic exposure in rodent animals (Cho et al., 2012; Cox et al., 2014; Marciano et al., 2017). Treatment of rats with 75 mg/kg/day TET has caused higher BMI and a lower body water percentage than the control group, indicating a greater accumulation of body fat compared to control groups (Marciano et al., 2017). In contrast to the observation at the juvenile stage, TET exposure at early stages of life including embryonic and larval stages caused inhibitory effects on zebrafish growth such as decreased body length, delayed hatching, increased yolk sac

area, and absence of a swim bladder (Zhang et al., 2015). Major physical transformations during such early stages compared to that in the juvenile stage may be made the zebrafish more vulnerable to TET. Overall, to the best of our knowledge, this is the first time to report increased body weight in a fish model under TET exposure.

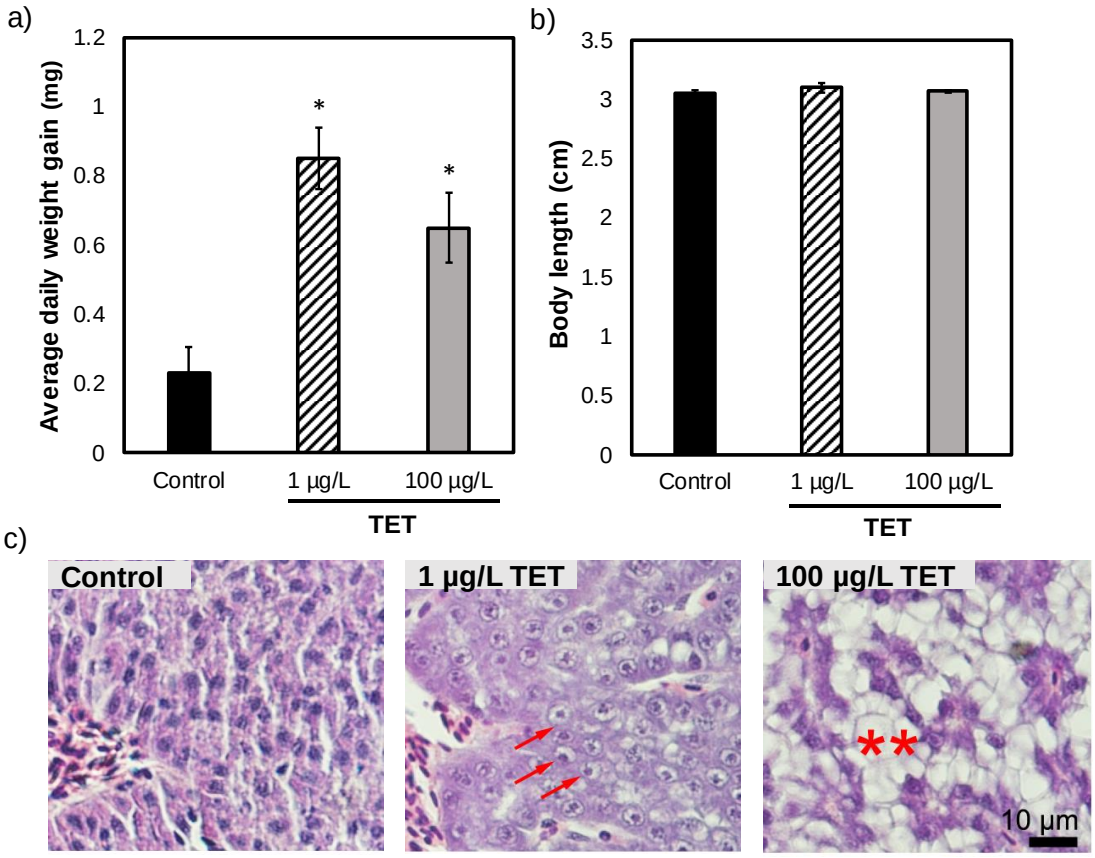

Figure 3.1. Effect of TET exposure on zebrafish growth and liver microstructure a) Average daily weight gain; b) Average body length; and c) Representative microscopic images of H&E stained liver sections (at the scale of 10 µm), showing nuclear chromatin condensation (red arrow) and vacuoles (red asterisks) of juvenile zebrafish exposed to TET at 0 (control), 1, and 100 µg/L. Data presented as the mean ± SEM of four replicates and "*" indicates the statistical significance (p-value ≤0.05) between TET treated and control groups.

3.4.2. Lipid dysregulations in the livers from TET exposed zebrafish

Knowing that the increased body weight gain with liver lipid vacuoles formation can be linked with hepatic lipid accumulation (Jin et al., 2016), we conducted the lipidomics analysis to compare the composition of liver lipidome between control

and TET treated zebrafish. The results showed higher responsive lipid features upon exposure to higher dose of TET. For instance, dysregulated lipid features under 100 µg/L TET exposure was 1.2 folds higher than those under 1 µg/L TET exposure (**Figure 3.2a**). For the lipid identification, 99, 119, and 106 lipids belonging to glycerophospholipid, glycerolipid, and sphingolipid lipid classes were annotated; respectively (detailed in **Figure 3.2b and Table B3-B5**). Interestingly, only triglyceride (TAG) levels were increased significantly in the livers from 100 µg/L TET treated zebrafish with a fold change of 1.5, while sphingomyelin (SM) levels only showed a slight increase. Some representative TAGs are shown in **Figure 3.2c and Table B3**. For instance, TAG (52:5) and TAG (53:6) were significantly increased in 1.7 and 1.9 folds; respectively, in response to TET.

Upregulation of TAG synthesis pathway has been observed in response to early life subtherapeutic antibiotic treatment in mice, which is consistent with our observation (Cho et al., 2012). Another study reported increased hepatic TAG levels upon exposure of mice to erythromycin with increased body weight (Jin et al., 2016). It is interesting that we observed a similar hepatic TAG accumulation in zebrafish upon treatment with environmentally relevant levels of TET, though the exposure routes for rodents and fishes are distinct.

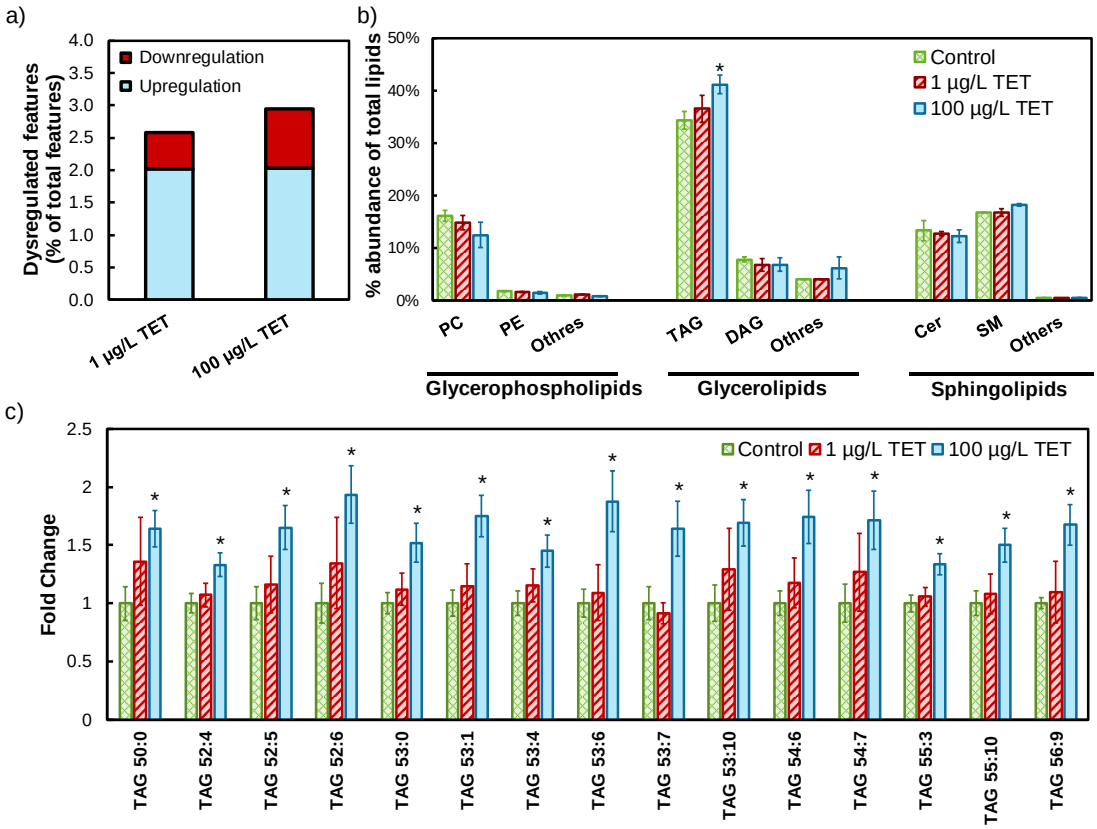

Figure 3.2. Lipid alterations in the livers from zebrafish exposed to 1 and 100 µg/L of TET

a) Up and down regulated significant features detected by global lipid profiling (|fold change| > 1.2, *p*-value ≤ 0.05, abundance > 10,000, percentage was calculated based on total detected feature numbers for each condition); b) bar graph representation of lipid classes as percentage of total identified lipids; and c) fold change of representative significant TAGs relative to controls. Data presented as the mean ± SEM of four replicates and "*" indicates the statistical significance (*p*-value ≤0.05) between TET treated and control groups. PC, phosphatidylcholine; PE, phosphatidylethanolamine; DAG, diglyceride; Cer, ceramide.

3.4.3. Metabolic alterations in the livers from TET exposed zebrafish

To characterize the metabolic changes that might be associated with TET-induced obesity and liver abnormalities, we further performed untargeted metabolomic profiling. In general, the higher TET dose level induced more responsive metabolite features in the livers of zebrafish. For instance, significantly dysregulated metabolic features observed under 100 µg/L of TET exposure were 1.4 and 1.3 times higher than that in the 1 µg/L under ESI (+) and ESI (-) modes; respectively (**Figure 3.3a**).

A total of 35 metabolites were identified and confirmed by MS/MS data and retention time matching, which were significantly dysregulated in the livers of zebrafish exposed to at least one of the two doses of TET (**Figure 3.3b and Table B6**). Among them, linoleic acid, oleic acid, and phenylalanine showed the fold change of 1.9, 1.9, and 1.3; respectively, for the low dose and stearic acid, s-adenosylmethionine, and serine showed the fold change of 4.1, 4.1, and 1.4; respectively for the high dose. For the pathway analysis, enrichment analysis of metabolic pathways highlighted the altered alpha linolenic acid and linoleic acid metabolism and phenylalanine and tyrosine metabolism pathways under 1 µg/L of TET and methyl histidine metabolism and methionine metabolism pathways under 100 µg/L of TET exposure (**Figure 3.3c and C2**).

Interestingly, some of the metabolic changes have been previously reported to be associated with obesity and hepatic fat accumulation. Increased TAG levels observed in lipidomics analysis (**Figure 3.2b and c**) may be resulted from the dysregulated levels of fatty acids (FAs). It has been shown that the free FA, especially palmitic acid in the liver, is linked with increased TAG levels in mice (Kohout et al., 1971). FAs are in the upstream of the TAG synthesis, which can regulate the TAG accumulation and known to be linked with obesity-associated liver abnormalities (Fabbrini et al., 2010; Tong et al., 2019). Further, methionine related metabolites including s-adenosylmethionine, highly upregulated in the livers of TET treated zebrafish (**Figure 3.3b**), were known to correlate with BMI (Elshorbagy et al., 2013). The dysregulated methionine metabolism has also shown to be associated with hepatic steatosis in zebrafish that explains the possible association between methionine metabolism and hepatic lipid accumulation (Elshorbagy et al., 2013). Furthermore, some of the responsive metabolites such as tyrosine, 4-hydroxycinnamic acid, and α-linolenic acid are well known to be produced/transformed by the gut microbiome (Wikoff et al., 2009). Therefore, the metabolic alterations in the host may possibly be incurred from the altered composition and functional capabilities of the gut microbiome upon TET exposure.

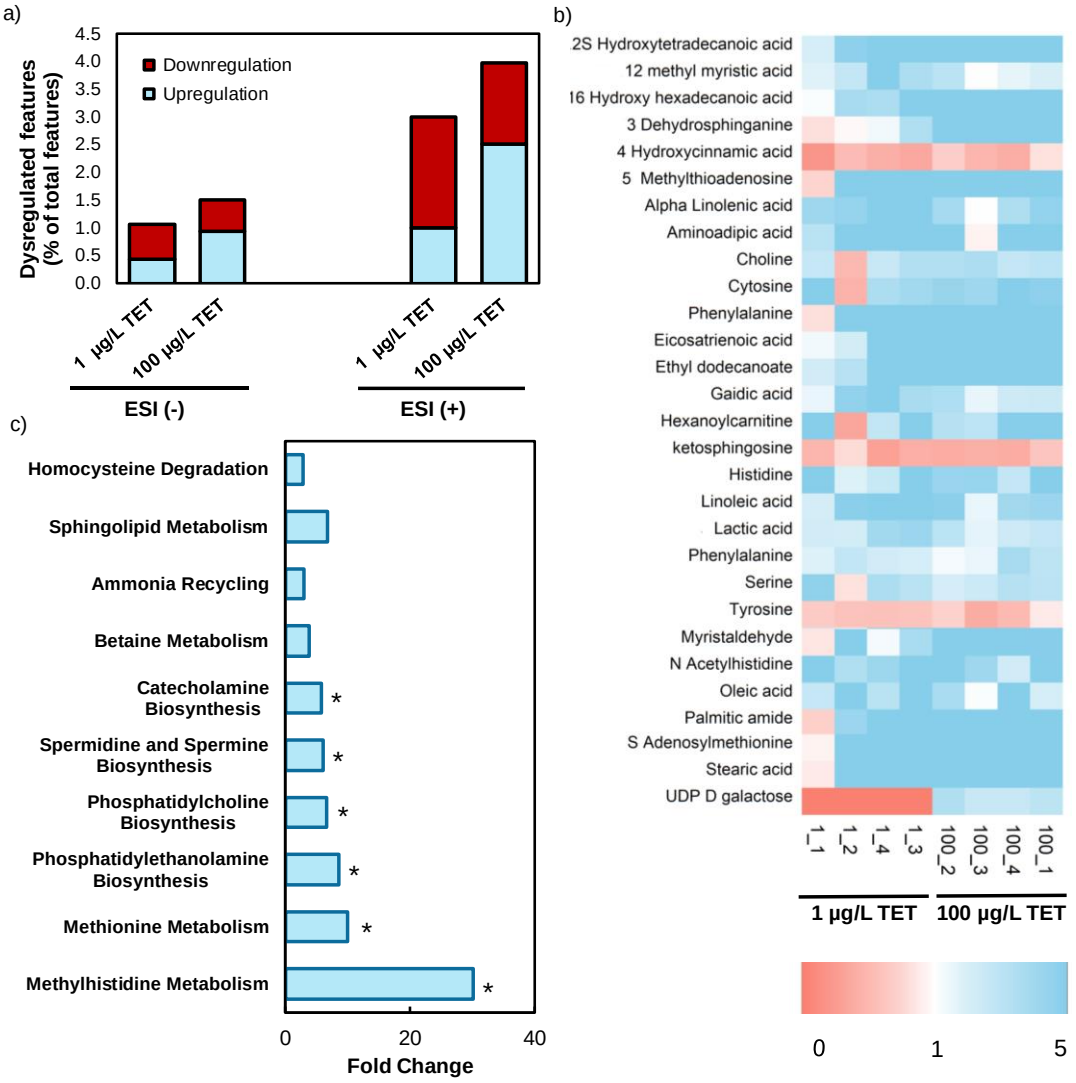

Figure 3.3. Metabolic alterations in the livers of zebrafish exposed to 1 and 100 µg/L of TET

a) Up and down regulated significant features detected by global metabolomic profiling (|fold change| > 1.2, *p*-value ≤ 0.05, abundance>10,000, percentage was calculated based on total detected feature numbers for each condition); b) heatmap analysis of significant metabolites (the heatmap values represent the abundance ratios of metabolites in each replicate to control; the blue color represents the upregulation relative to the control and the red are the downregulated metabolites); and c) enrichment analysis of significant metabolic pathways at 100 µg/L. "*" indicates the statistical significance (*p*-value ≤0.05) between TET treated and control groups.

3.4.4. Alterations in the expression of genes involved in hepatic lipid metabolism in response to TET exposure

We next analyzed the expression of a few targeted genes that are highly related with lipid transport and formation in the livers of zebrafish. Specifically, the changes in gene expression involved in lipid transport (i.e., *apoa4*, *fabp2*, and *fabp11*) and lipogenic factor (i.e., *pparαb*, *pparγ*, and *c/ebpα*) are shown in **Figure 3.4**. Generally, the genes involved were all upregulated in the livers from zebrafish under TET exposure with a clear dose dependence. For example, *apoa4* was increased by 3 and 5 folds in 1 and 100 μg/L of TET; respectively.

Fabp2 and *fabp11* are two genes in the zebrafish genome encoding fatty acid binding proteins (FABPs) that bind with saturated, unsaturated, and long-chain FAs and thereby serve as their carriers (Esteves et al., 2016; Laprairie et al., 2017). It has been shown that certain FABPs have the potential to channel dietary fatty acids into enterocyte nuclei in zebrafish, which possibly explains the increased FAs in TET treated zebrafish liver tissues. Peroxisome proliferator-activated receptor (PPAR) transcription factors which respond to changing levels of lipids in the cell and in turn regulate the expression of genes for lipid storage and metabolism (Esteves et al., 2016). PPARα increases the expression of genes that facilitate the uptake and utilization of FAs in tissues, including liver tissues, while PPARγ activation increases the FA uptake and adipogenesis in adipocytes and other tissues (Laprairie et al., 2017). Hepatic expression of PPARγ, especially that of PPARγ2 is functionally enhanced in a number of obesity models (Uno et al., 2006). Furthermore, over-expression of *apoa4* in mice results in increased plasma concentrations of TAGs (Qu et al., 2019). Collectively, the alterations in the gene expression agree with the metabolomics and lipidomic observations, suggesting the metabolism of FAs to TAGs in the liver might be an underlying mechanism in weight gain.

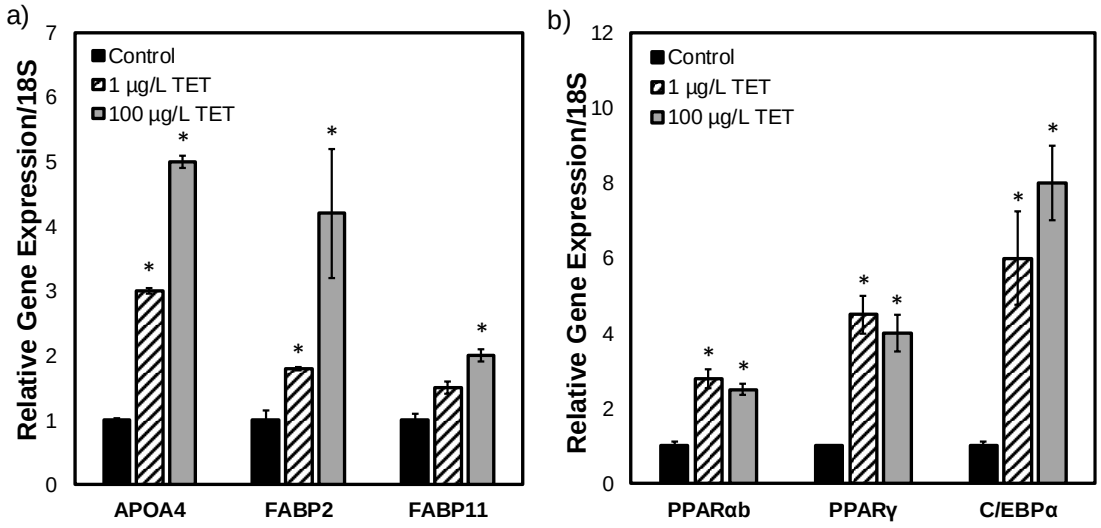

Figure 3.4. Expression of genes involved in lipid metabolism in livers of zebrafish exposed to 1 and 100 µg/L of TET
Relative gene expression involved in a) lipid transport (*apoa4*, *fabp2*, and *fabp11*) and b) lipogenic factor (*pparαb*, *pparγ*, and *c/ebpα*). Data presented as the mean ± SEM of four replicates and "*" indicates the statistical significance (*p*-value ≤ 0.05) between TET treated and control groups.

3.4.5. Dysbiosis of gut microbial community under TET exposure

Dysbiosis of gut microbiota induced by antibiotic exposure has been observed in mice (Cho et al., 2012; Cox et al., 2014) and pigs (Looft et al., 2012); the obesity linked with antibiotic caused gut microbiota dysbiosis has been suggested in previous studies (Cho et al., 2012; Cox et al., 2014; Dethlefsen and Relman, 2011; Francino, 2016; Marciano et al., 2017). Thus, we intended to observe the changes in zebrafish gut microbial community upon TET exposure. We have collected a total of 515,052 sequences and after clustering and alignment and found 105 OTUs based on a 0.97 threshold across all samples. Among the 105 OTUs, most of OTUs (n=67, 64%) were shared by 1 and 100 µg/L TET treated samples (**Figure C3**).

The rarefaction curves of sequenced intestinal content samples indicated that the sequencing depth was enough for all the samples by their saturated trend (**Figure C4**). Simultaneously, the rarefaction curves revealed that the community richness of TET exposed samples was higher than that of control samples, especially at 1 µg/L. We further confirmed this observation by alpha diversity indices including Chao index, Sobs index, and Shannon index, showing significantly higher diversity in the gut

microbiome of TET exposed zebrafish compared to control (**Figure 3.5a**). The OTU level community composition across the datasets was used for NMDS analysis and the plot showed that communities were closely clustered within each group (**Figure C5**). The Bray-Curtis index was calculated for all pairwise sample combinations and the *PERMANOVA* test indicated a significant difference in phylogenetic structure among the three groups (Bonferroni-corrected $p < 0.05$), even the pairwise differences between three groups were not significant (Anderson, 2001). In sum, we have observed one interesting fact that the low dose of antibiotic TET exposure could actually increase the gut microbial community diversity, though the high dose of those drugs is designed to inhibit the bacteria growth. This result was consistent with some previous studies. For example, treating mice with low-dose penicillin has also shown increased phylogenic diversity (Cox et al., 2014). For another, TET at low dose can trigger the growth of *Escherichia coli* (Migliore et al., 2013), which may be a reason for increased community diversity where the growth of certain bacterial species may be triggered by exposure to TET at low dose.

According to the phylum level analysis of microbial community composition, Fusobacteria was presented in the highest percentage among the three treatments, followed by Firmicutes and Bacteroidetes (**Figure 3.5b**). We observed slight changes in most of the phyla across both levels of TET. However, significant changes were found in three phyla, where the phylum Firmicutes was depleted in 6.2 folds under 100 µg/L TET exposure. Bacteroidetes and Proteobacteria was depleted in 2.4 folds and enriched in 2.0 folds; respectively, under 1 µg/L TET exposure. Interestingly, the ratio between Bacteroidetes and Firmicutes was increased to 2.9 and reduced to 0.19 under 1 and 100 µg/L of TET exposure; respectively, which may explain the higher weight gain under 1 µg/L exposure compared to 100 µg/L. The ratio has been described as higher in obese mice than in normal-weight mice (Roca-Saavedra et al., 2018; Turnbaugh et al., 2006). In addition, the increase in the abundance of Firmicutes is usually considered as an obesogenic factor (Roca-Saavedra et al., 2018); however, we only observed a slight increase in the relative abundance of Firmicutes under 1 µg/L TET exposure.

To determine the classified bacterial taxa with significant differences in abundance among the TET treated and control groups, we performed a biomarker analysis using

the linear discriminant analysis (LDA) effect size (LEfSe) method. As shown in **Figure 3.5c and d**, 15 bacterial clades presented in statistically significant differences with an LDA threshold of 3.5. Eight bacteria were significantly enriched in 1 μg/L TET samples, while 7 clades showed abundance advantage in 100 μg/L TET samples. Specifically, Firmicutes (phylum), *Ersipelotrichia* (class), *Erysipelotrichales* (order), *Erysipelotrichaceae* (family), and *Erysipelotrichaceae_g_norank* (genus) were enriched in 1 μg/L TET group samples (all $p < 0.05$). Furthermore, the members belonging to *Ersipelotrichia* accounted for 16.3% of the population in the 1 μg/L TET groups, but only 14.3% of that in control group, and 2.3% in 100 μg/L TET groups (**Figure C6**). Interestingly, the *Ersipelotrichia* bacteria have been reported to be increased in obese animal due to high-fat diet (Barouei et al., 2017), which can be considered as a potential biomarker for increased weight gain in zebrafish.

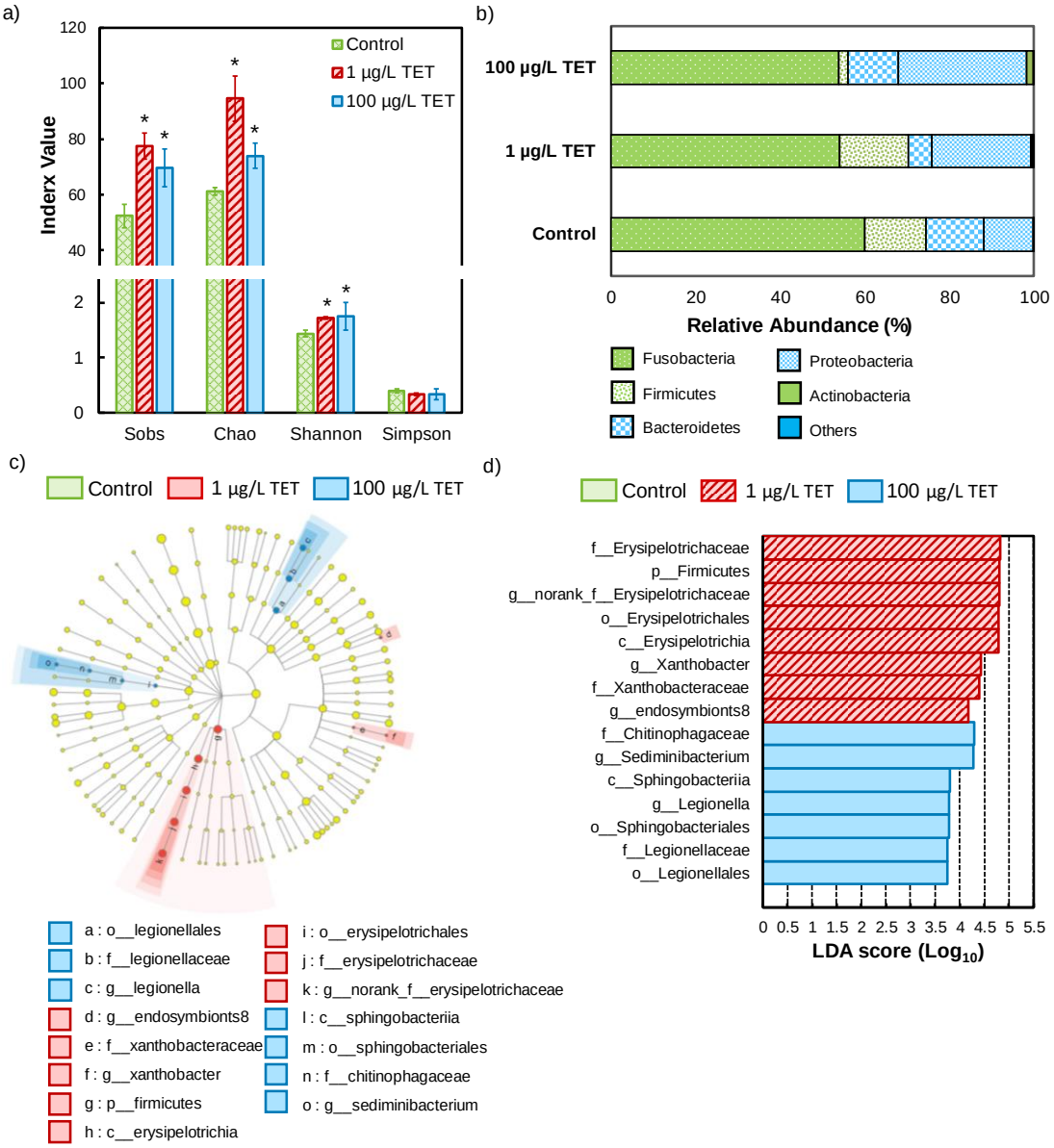

Figure 3.5. Microbial community shift in the gut microbiomes of zebrafish exposed to 1 and 100 µg/L of TET

a) Microbial diversity indices; b) Bar graph representation of phylum level relative abundance; c) LEfSe analysis of microbial abundance, the cladogram of microbial communities; and d) LDA score identified the size of differentiation between TET treated and control groups with a threshold value of 3.5. Data presented as the mean ± SEM of three replicates and "*" indicates the statistical significance (p-value ≤ 0.05) between TET treated and control groups.

3.4.6. Changes in the predicted functional capabilities of zebrafish gut microbiome under TET exposure

Considering the fact that the functional capabilities of gut microbial community may lead to alter the host physiology, we investigated the changes in the functional capabilities of the zebrafish gut microbiome induced by TET. Here we incorporated a predictive metagenomic approach using 16s rRNA gene sequence functional prediction where the PICRUSt was used to predict the KEGG category and functional enzyme (Langille et al., 2013). The prediction generated 129 KEGG functions and 207 clusters of orthologs groups (COGs) above 0.1% relative abundance in at least one group of samples. Membrane transport, carbohydrate metabolism, and amino acid metabolism were among highly abundant KEGG metabolic pathways (**Figure C7**), while amino acid transport and metabolism, carbohydrate transport and metabolism, and energy production and conversion were among highly abundant COG functional categories in the zebrafish gut microbiome (**Figure 3.6a**). Interestingly, the COG abundance for lipid transport and metabolism pathways were significantly higher in TET exposed communities compared to that in control (**Figure 3.6b**). Even though the exact mechanism was not clear at this stage, resulted dysregulations in metabolite levels from the upregulated pathways may possibly be the cause of lipid accumulation in the zebrafish hosts and thereby induce weight gain. Number of such mechanisms explaining the gut microbiome dysbiosis linked weight gain have previously been suggested. For example, the immune system regulation by immunoregulatory compounds excreted by gut microbiome including lipopolysaccharide (LPS) are known to be involved in host obesity (Cox and Blaser, 2013).

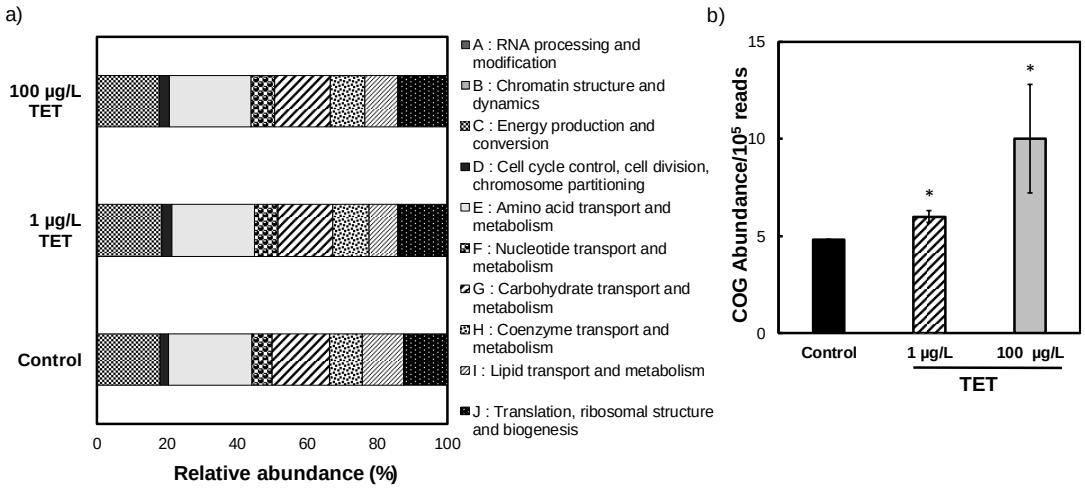

Figure 3.6. Altered predicted functional capabilities in the gut microbiomes of zebrafish exposed to 1 and 100 µg/L of TET
a) COG function classification and b) COG abundance of lipid transport and metabolism. Data presented as the mean ± SEM of four replicates and "*" indicates the statistical significance (p-value ≤ 0.05) between TET treated and control groups.

3.5. Short Summary

This study showed that low or environmentally relevant levels of TET could increase the zebrafish body weight with hepatic lipid accumulation when the exposure starts from the juvenile period. To the best of our knowledge, this is the first time to study the effect of TET on the zebrafish at the juvenile stage and to observe an increased body weight gain in response to a relatively low concentration of TET. In addition, a few metabolites and metabolic pathways such as fatty acid and methionine metabolism that could be linked with the body weight gain through hepatic lipid accumulation were discovered. Further, alteration and increased diversity of gut microbiota were observed with increased obesogenic factors such as the ratio between Bacteroidetes and Firmicutes, and possible biomarkers for obesity were identified. In sum, the possible link between increased body weight and the dysbiosis of gut microbiota can be speculated. However, further *in vivo* studies such as fecal transplantation need to be conducted to validate this link and elucidate the mechanism behind the induced weight gain in zebrafish. Furthermore, more doses of TET treatment to figure out the dose-response relationship can also be considered in future studies.

Chapter 4. Tetracycline Exposure Alters Gut Bacterial Metabolism in a Species-Specific Pattern

4.1. Overview

Chapter 4 investigated the TET-induced metabolic alterations in three model gut bacteria including *Bacteroides fragilis*, *Clostridium sporogenes*, and *Escherichia coli*, which represent several types of the most abundant bacterial genera in the gut. The study incorporated global and targeted metabolomics approaches to characterize the metabolomic disruption from TET exposure at multiple dose levels. This chapter has been published as a part of **Keerthisinghe, T. P**., Wang, M., Zhang, Y., Dong, W., and Fang, M. (2019). Low-dose tetracycline exposure alters gut bacterial metabolism and host-immune response: "Personalized" effect? *Environment International*, **131**: 104989. DOI: 10.1016/j.envint.2019.104989.

4.2. Introduction

A growing body of evidence suggests the disruption of human microbiota by therapeutic levels of TET (Carman et al., 2005; Jung et al., 2018), those studies only reported the altered community composition and emergence of TET resistance. Those previous studies mostly focused on the pharmaceutical levels, and the effect of low dose exposure (i.e., sub-therapeutic levels and dietary exposure) on TET on the gut microbiome remains unknown. More importantly, very limited information is available on the effect of TET on the gut microbiome metabolome, although several studies have shown the effect of TET and TET family antibiotics on the bacterial metabolome, focusing mainly on understanding their mechanism of action through metabolomics (Hoerr et al., 2016; Jones-Dias et al., 2017; Lin et al., 2014). Overall, due to the high complexity of the gut microbiome composition, there is no indicator on how the metabolome changes in the ecosystem can be reflected in pure strains. It is of great scientific value to investigate the response of the primary strains to the TET exposure and enable the possible system-wide metabolome prediction based on the community structure.

In this study, we selected three model gut bacteria, including *Bacteriodes fragilis, Clostridium sporogenes,* and *Escherichia coli,* which represent several types of the most abundant bacterial genera in the gut (Eckburg et al., 2010; Zhang et al., 2018). Subsequently, a global and targeted metabolomics approach was used to characterize the metabolomic disruption from three different doses of TET, including sub-pharmaceutical and dietary exposure levels.

4.3. Methodology

4.3.1. Bacterial strains and cultivation

Three model bacteria were applied in this study, including *Bacteroides fragilis* ATCC25285, *Clostridium sporogenes* ATCC15579, and *Escherichia coli* K12-MG1655. The rationale was fully described in our previous study (Zhang et al., 2018). The bacterial cultures were stored at -80^{o}C in a reinforced clostridial medium (RCM) (Oxide, Thermo Scientific Microbiology, Singapore), containing 25% glycerol. All bacteria were revived in RCM in an anaerobic growth incubator at 37^{o}C overnight before the following experiment.

4.3.2. TET treatment of model bacteria

TET hydrochloride was purchased from Sigma-Aldrich, Singapore. The inhibition of TET on model bacteria was tested by dose-response assay, and the growth was monitored by reading the optical density at 600 nm with a spectrophotometer (DR1900, HACH, Southeast Asia). The fitting of the four-parameter logistic curve is used to predict the inhibitory concentration (IC) (Huang et al., 2012). The detailed methods are mentioned in the supplementary material **Text A2**.

For the metabolomics, each model bacterium was treated with TET at three different dose concentrations (**Table B7**). Sub-pharmaceutical levels of IC_{90} and IC_{50} for each bacterium were selected as the high and middle dose levels of TET; respectively. The human relevant dietary exposure concentration of TET in the gut was roughly predicted with a previously used model (Zhang et al., 2018). As a result, the low dose at 0.01 mg/L was selected to simulate the TET concentrations occurring in the gut

via the consumption of poultry and dairy products containing TET residues (Aalipour et al., 2015; Cháfer-Pericás et al., 2011).

The bacterial cultivation and TET treatment followed our previous study (Zhang et al., 2018). Briefly, 1% (v/v) of overnight revived bacterial culture was inoculated and allowed to grow to the late exponential phase before the TET treatment. All bacterial cultures and controls were prepared in triplicates and were cultivated in an incubating shaker, under anaerobic conditions at 37°C, for 24 hours. After incubation, the cell pellets and the secretome were separated via centrifugation at 8,000 rpm for 3 minutes for metabolomics and immunological studies; respectively. The cell pellets were then rapidly washed in ice-cooled phosphate-buffered saline (PBS) to remove the growth medium residues. Thereafter, the cell pellets immediately proceeded to metabolite extraction, and the secretome was stored at -40°C until analysis. Optical density measurements were also conducted upon harvest for normalization.

4.3.3. Metabolite extraction and profiling

Metabolite extraction and profiling were conducted according to our previous study (Zhang et al., 2018). Briefly, the metabolites were extracted from cell pellets via a pre-chilled extraction buffer (acetonitrile/methanol/water, 2/2/1, v/v/v) by glass bead assisted homogenization and freeze-thaw cycles. The extract was dried by speed-vacuum evaporation (CentriVap Benchtop Centrifugal Vacuum Concentrator, Labconco, U.S.A.) at 10°C, which was followed by reconstitution in acetonitrile/water (1/1, v/v) with a normalized volume by the bacteria culture optical density.

The profiling of metabolites was conducted using a high performance liquid chromatography (HPLC) system (Agilent Technologies) coupled to a 6550 quadrupole time-of-flight (Q-TOF) (Agilent Technologies, Singapore), in accordance with our previous study (Zhang et al., 2018). The metabolite profiling and quality control methods are detailed in **Section 4.3.6** and **Text A2**. A pooled mixture of treated and control samples of each bacteria was run with data-dependent acquisition (DDA) auto-MS/MS and targeted MS/MS of selected precursors (Zhang et al., 2018).

4.3.4. Metabolites identification and metabolic pathway analysis

The metabolome data processing was carried out using an XCMS online web platform (http://xcmsonline.scripps.edu) (detailed in **Text A2**). The first screening was based on the significant features, with *p*-value ≤ 0.05, |fold change| > 1.5, and intensity >10,000 ion counts. All those features were manually checked to minimize the false positive hits. MS/MS fragment, accurate mass, and in-house retention time match were the methods used for metabolite identification. Open source platforms KEGG (http://www.genome.jp/kegg/) and Metaboanalyst (http://www.metaboanalyst.ca) were incorporated for further pathway analysis. Statistical analysis, including principal component analysis (PCA) and heatmap analysis, was conducted by PAST (https://folk.uio.no/ohammer/past/) and R software (http://www.R-project.org); respectively.

4.3.5. Derivatization and GC-MS analysis of SCFAs

The analysis method of SCFA was modified from a previous study (L. He et al., 2018). Briefly, the bacterial extract was derivatized with 2, 3, 4, 5, 6-penta-fluorobenzyl bromide (PFBBr) purchased from Sigma-Aldrich, Singapore, prior to gas chromatography- mass spectrometry (GC-MS) analysis. The internal standard ^{13}C-sodium acetate was purchased from Cambridge Isotope Laboratories. Briefly, 100 mM PFBBr in acetone, 0.5 M phosphate buffer (pH 7), and sample were mixed at a ratio of 14:2:5 (v/v/v) with the spiked internal standard in a glass tube, vortexed, and incubated in a water bath at 60°C for 1.5 hours. The derivatized products were then extracted with hexane, followed by drying, reconstituting in toluene, and analyzed using a GC system (Agilent technologies), coupled with 5977A mass selective detector (MSD). The detailed GC method is mentioned in **Text A2**.

4.3.6. QA/QC and statistical analysis

For the QA/QC of bacterial metabolome analysis, a pooled mix sample of metabolites prepared by pooling all treated and control samples were analyzed after every six injections of biological samples to correct the mass, retention time, and response drift. The bacterial metabolome experiment was conducted twice and the relative standard deviation (RSD) was less than 15% from replicates in intra and inter-batches. Error

bars represent the standard deviation (SD) of triplicate assessments. Differences between groups or treatments were examined for statistical significance using *Student's t*-test or a one-factor analysis of variance (*ANOVA*), with Duncan's post-hoc test, with significance level set at p-value ≤ 0.05.

4.4. Results and Discussion

4.4.1. Bacterial growth under low dose TET exposure

We first evaluated the susceptibility of three model bacteria, *B. fragilis, C. sporogenes,* and *E. coli* to TET. The growth of the model bacteria under different dose levels of TET is shown in **Figure C8**. *B. fragilis*, and *C. sporogenes* showed lower IC_{90} (0.16 and 0.13 mg/L; respectively) compared to that of *E. coli* (7.4 mg/L). The possible dietary level exposure concentration of the gut microbiome to TET was approximately 0.015 mg/L (**Text A2**), which can induce subtle effects on the growth of *B. fragilis,* where its IC_{10} was 0.008 mg/L. Accordingly, to investigate the effect of low dose TET exposure on the metabolome and the immune response, we selected sub-pharmaceutical level of IC_{90} and IC_{50} for each strain as the high and middle levels of exposure, respectively, and 0.01 mg/L as the low exposure concentration of the possible dietary level of exposure.

4.4.2. Global profiling of the metabolome

We profiled the global metabolome of three model bacteria to observe their response to three different doses of TET. In general, higher levels of TET-induced more responsive metabolite features in each bacterium. For instance, significantly dysregulated features observed in *B. fragilis* under high and middle doses of TET exposure were 5.5 and 4.4 times higher than that in the low; respectively (**Figure 4.1a and Figure C9**). However, the responsive feature numbers were highly varying among the three bacteria under the high dose of TET, which was 16.5%, 3.2%, and 5.5% of the total detected feature numbers for *B. fragilis, C. sporogenes,* and *E. coli*, respectively, where *B. fragilis* showed comparatively higher sensitivity towards TET.

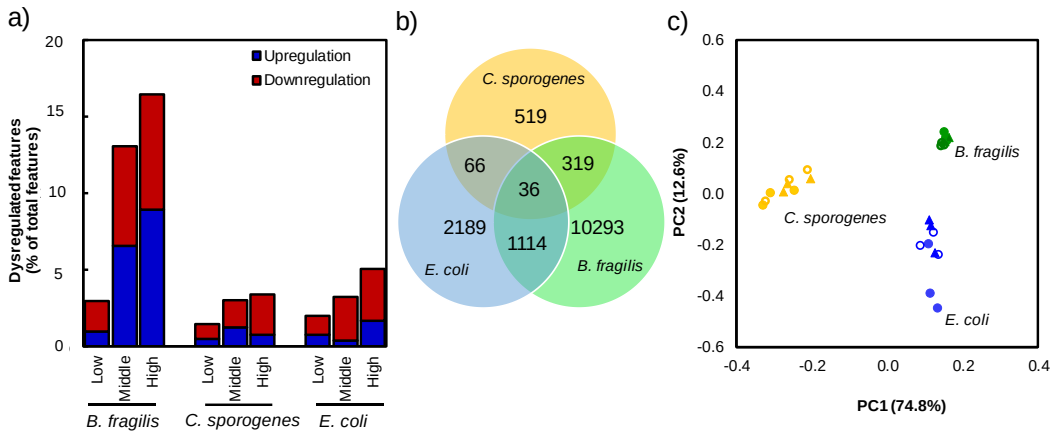

Figure 4.1. Global metabolite profiling of the three model bacteria under three different levels of TET exposure
(a) Up and down regulated significant features detected by global profiling (|fold change| > 1.5, *p*-value ≤0.05, abundance >10,000, percentage was calculated based on total detected feature numbers for each condition); (b) Classic Venn diagram summarizing the number of shared and distinct features in each model bacteria under the high level of TET exposure; and (c) Principal component analysis (PCA) of significant metabolite features in three model bacteria under TET exposure. The dark circle, triangle, and open circle represent the high, middle, and low dose; respectively.

To get a further comparison on metabolic responses of the three model bacteria to TET, we have conducted meta-analysis of the responsive features at the high dose. In general, most of the features were not shared across the three model organisms. Only 36 significantly dysregulated features were found to be shared among three model bacterial strains, which was less than 5% of the total significant features in each bacterium, while this pattern was consistent among all dose levels (**Figure 4.1b and Figure C10**). Further principle component analysis of responsive features among three model bacteria showed a separation among three bacteria (**Figure 4.1c**). Collectively, our results suggest the species-specific and concentration-dependent metabolic response of model gut bacteria to TET.

The above findings revealed a difference in sensitivities of the metabolome of each bacterium towards TET, although the IC_{90} was quite similar for *B. fragilis and C. sporogenes*. The response of metabolite features may non-growth-associated, as we dosed TET at the late exponential phase. The target sites, resistance capabilities, and uptake mechanisms specific to a bacterium may lead to the difference in their responses towards the same antibiotic. For instance, TET exposure can inhibit the

cell wall synthesis of *E. coli* (Cheng and Snell, 1961); but not, however, in *Staphylococcus aureus* (Hash et al., 1964). Moreover, *B. fragilis* and *E. coli* have shown efficient uptake of TET through outer membrane porin channels (Fayolle et al., 1980; McMurry and Levy, 1978; Schnappinger and Hillen, 1996), Higher and fast enrichment of *Bacteroides* compared to *Firmicutes* in the gut microbial community treated with TET further reveals that the genera *Bacteroides* are more competitive under TET exposure (Jung et al., 2018).

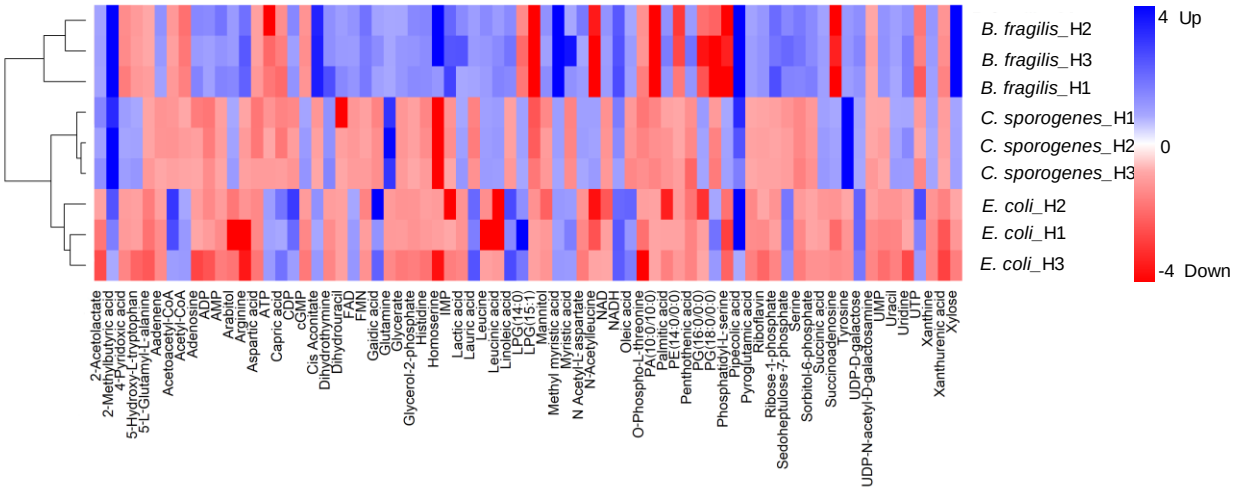

Figure 4.2. Heatmap and hierarchical analysis of significant metabolites in three model bacteria under the high level of TET exposure
The heatmap values represent the abundance ratios of metabolites in each replicate to control; the blue color represents the upregulation relative to the control and the red are the downregulated metabolites.

4.4.3. Metabolite identification and dose-response relationship

Metabolite identification

We further identify the significantly dysregulated features in model bacteria treated with the high dose of TET by MS/MS data and retention time matching. A total of 116 metabolites were identified across three model bacteria, and 98 of them were significantly dysregulated in at least one bacterium (**Table B8**). The responsive metabolites across different model bacteria were compared, as shown by the heatmap analysis in **Figure 4.2**. The majority of the metabolites in *B. fragilis* were up-regulated at the high level of TET exposure, which contrasted with that in *C. sporogenes* and *E. coli*, where more features were down-regulated. The two Gram-

negative bacteria, *B. fragilis,* and *E. coli* showed more shared features among them in meta-analysis; however, they did not show a close relationship according to the hierarchical clustering of identified metabolites.

Dose-response relationship of responsive metabolites

To understand the response of metabolites under different doses of TET, we searched the identified metabolites against the middle and low dose levels of TET. Most of these metabolites were not significantly dysregulated under the low and middle levels of exposure. For example, among the 60 significantly dysregulated metabolites in *B. fragilis* under the high level of TET, only 38 and 20 were found to have significant dysregulation under middle and low levels of TET; respectively (**Table B8**). Further, part of the identified metabolites showed a dose-response relationship (**Figure 4.3**). For instance, the fold change of serine is in *B. fragilis* exposed to high, middle, and low levels of TET were 2.1 ± 0.2, 1.2 ± 0.2, and 1.1 ± 0.3; respectively (**Figure 4.3a and Table B8**).

The higher fold change in the high dose may result due to the higher availability of TET to act on the target sites; however, the low dose still can induce alterations in some metabolites such as aspartic acid and pyroglutamic acid (**Figure 4.3a**), which emphasize the possible effect of TET intake on gut microbiome metabolism through the consumption of food products containing TET residues. There are a number of other targets of TET, such as fermentation and oxidation process (Hash et al., 1964), cell wall synthesis (Miller, 1969), and vitamin metabolism (Hash et al., 1964), in addition to its primary target of inhibiting the protein synthesis. Therefore, the resulting metabolic changes could be from direct pathway targeting by TET or due to the inhibition of the synthesis of proteins involved in these pathways (Hash et al., 1964). Dysregulations in metabolites related to vitamin metabolism, nucleotide, and amino acid biosynthesis have been reported in previous bacterial metabolomics studies, which also include antibiotics with a similar mode of action (Belenky et al., 2015; Zampieri et al., 2017).

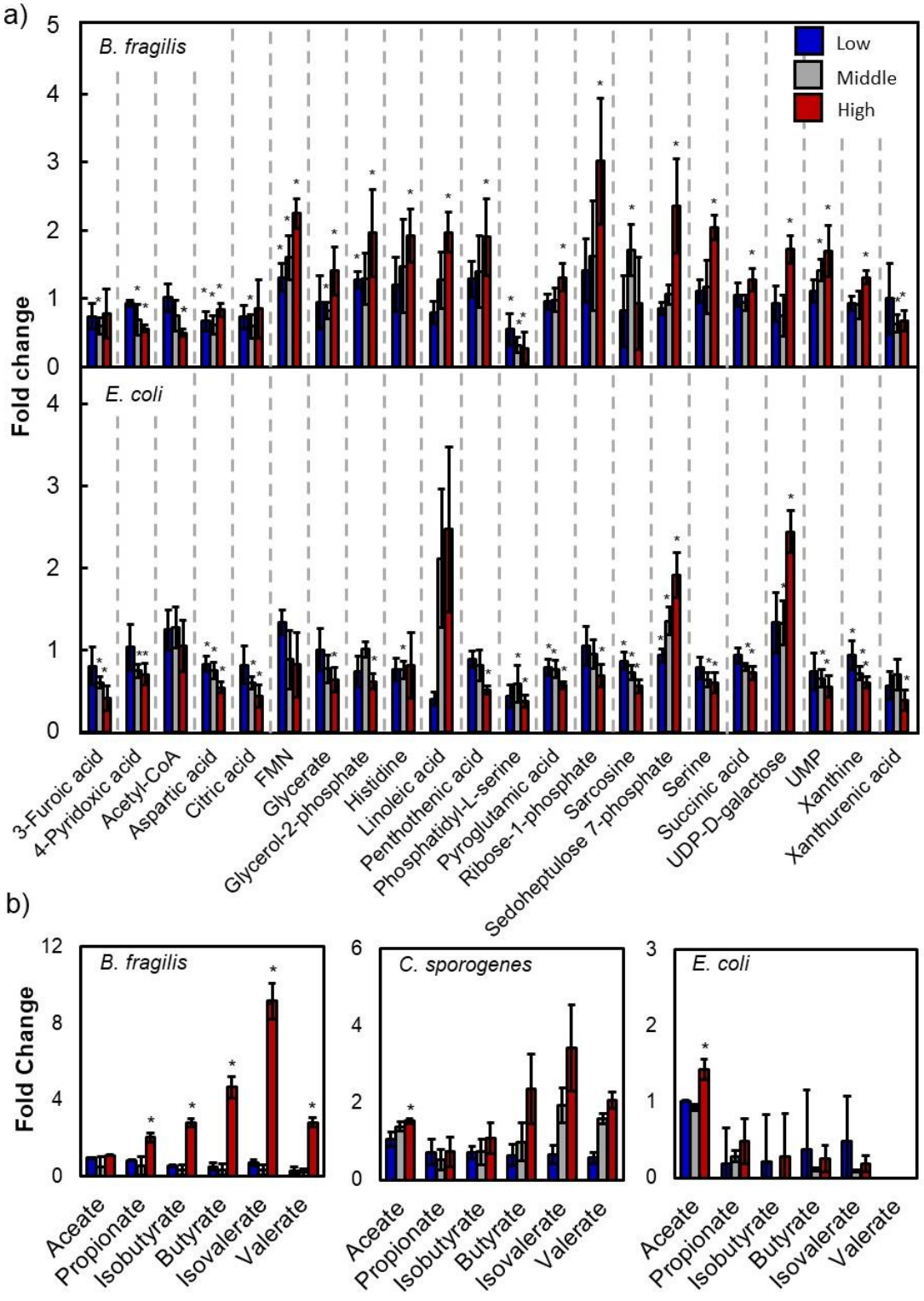

Figure 4.3. The metabolite examples with clear dose-response towards three different levels of TET

Fold change of (a) representatives from the identified metabolites in *B. fragilis* and *E. coli* and (b) fold change of SCFAs relative to controls in three model bacteria. Data

presented as the mean ± SD of four replicates and "*" indicates the statistical significance (p-value ≤ 0.05) between TET treated and control groups.

4.4.4. Metabolic pathway analysis

We next performed a pathway impact analysis to examine the pathways highly affected by the TET. In general, the riboflavin (vitamin B_2) metabolism was among one of the highly affected pathways in *B. fragilis* and *C. sporogenes* while nucleotides (i.e., purine and pyrimidine), amino acids (i.e., alanine, aspartate, and glutamate), and the butanoate metabolism were significantly affected in *B. fragilis* and *E. coli* under the exposure to the high dose of TET (**Figure 4.4**). Further, the nucleotide, amino acid, vitamin, and FA metabolism are among the significantly affected pathways under the middle and low doses of TET (**Figure C11 and C12**).

Effect of TET on vitamin metabolism

Vitamin synthesis and metabolism were highly affected under TET exposure, as reflected in the global pathway analysis and metabolite identification. For instance, metabolites involved in the riboflavin metabolism, such as riboflavin and D-ribose 5-phosphate, were significantly dysregulated in *B. fragilis* in 1.6 ± 0.2 and 3.1 ± 0.9 folds; respectively at the high level of TET exposure (**Figure C13**); while other vitamin B related metabolites, such as pyridoxic acid, were significantly dysregulated, even at the middle level of exposure (**Figure 4.3a and Table B8**). The genera to which the three model bacteria belong are known vitamin producers in the gut microbiome, while certain B vitamins were among the key metabolites supplied to the host by gut bacteria (Magnúsdóttir et al., 2015; Morowitz et al., 2011). In addition, vitamin B is also known as a biomarker linked to adult brain volume (Hooshmand et al., 2016). Thus, the effect on vitamin metabolism by TET may affect the host metabolic requirements and health conditions.

Effect of TET on lipid and FA metabolism

Metabolites related to lipids and fatty acid metabolism in *B. fragilis* and *C. sporogenes* were affected under TET exposure, with a fold change ranging from 0.07 to 2.7 and 0.4 to 1.2; respectively, under high dose of TET exposure (**Figure 4.2, 4.3, and Table B8**). Interestingly, metabolites, such as linoleic acid in *B. fragilis*, showed

a dose-response relationship to TET (**Figure 4.3a**), while some glycerophospholipids and ceramides were significantly changed in *B. fragilis*, even at the low dose of TET exposure (**Figure 4.3a and Table B8**). A high effect on plasma lipid metabolites of mice treated with TET has been observed, which may be mediated through the effect of TET on the gut microbiome (Behr et al., 2017). Further, linoleic acid related gut microbiome produced metabolites such as conjugated linoleic acids (CLA) are known to be involved in body weight gain, cardiovascular disease, insulin resistance, and lipid peroxidation, which further emphasized the possible metabolically driven effects of TET on host health (Devillard et al., 2007; Mensink, 2005; Risérus et al., 2004).

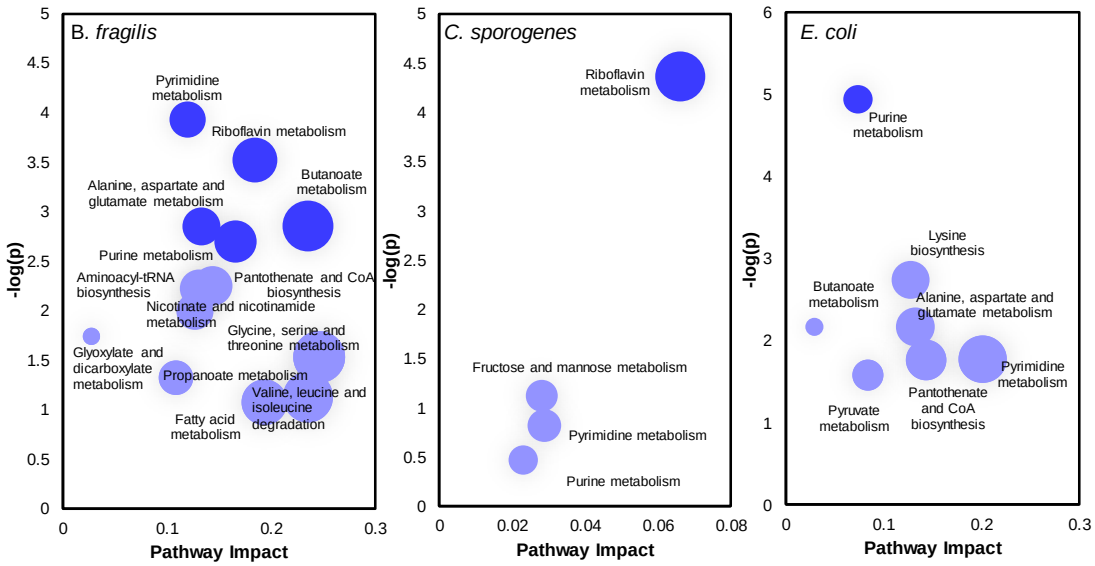

Figure 4.4. Pathway impact analysis of significant metabolic pathways in model bacteria under the high level of TET exposure
The data analysis was conducted by the open-source platform MetaboAnalyst. The size of the bubble implies the pathway impact and the color intensity indicates the significance of the impact (p-value ≤ 0.05).

Effect of TET on SCFAs

We incorporated a GC-MS based approach to analyze the SCFAs, which cannot be detected in our global metabolomic method. The SCFA production in *B. fragilis* showed a higher sensitivity to TET exposure (**Figure 4.3b**), with a significantly high fold change of propionic, butyric, and valeric acid from 2 to 9.2 to the control, at the high dose of TET exposure. However, this was not observed on the other two bacteria.

The increased cecal SCFA levels, with an increase in percentage body fat was previously reported under the exposure of TET family antibiotics (Cho et al., 2012). The SCFAs have been the focus of gut microbiome studies in the past, and the increased SCFAs have been shown to have connections to obesity and numerous other metabolic diseases (Turnbaugh et al., 2006; Zhang and Davies, 2016). Collectively, our results and the literature suggest that the TET-induced alteration in gut microbial SCFA metabolism and thereby can induce adverse effects on the host's health. The sensitivity difference among the three primary bacteria suggested that the overall effect of TET in the gut microbiome will be highly dependent on the gut microbiome composition.

4.5. Short Summary

This metabolome study of the three model bacteria, *B. fragilis*, *C.sporogenes,* and *E. coli* showed a species-specific, concentration-dependent metabolic response towards TET. Notably, *B. fragilis* was highly sensitive to TET exposure, while TET generated the lowest metabolic response in *C. sporogenes*. Overall, this finding suggests the possible incidence of metabolic consequences by altred Firmicutes to Bacteroides ratio, which can be linked with increased host body weight gain. Furthermore, TET exposure resulted in dysregulations in several metabolic pathways, known to be related to several host diseases, such as weight gain and diabetes in model bacterial strains. More importantly, dysregulation of nucleotide, amino acid, vitamin, and fatty acid metabolism at dietary dose emphasizes the risk of facing alterations in the gut microbiome of non-antibiotic users. Collectively, it is likely that the risk of TET exposure from either sub-pharmaceutical or dietary exposure depends on the gut bacterial composition, leading to a "personalized" response of TET to the metabolome of the host. However, the interaction between chemicals, bacteria, and the effect on the host is very complex, and future study is warranted. The chemical can affect the ratio of bacteria, and the later will pre- or post-determine the effect of the former on the possible effect on the host.

Chapter 5. Tetracycline Alters Gut Microbiome Secretome Metabolism *In vitro* under the Fed and Fasted States

5.1. Overview

Chapter 5 characterized the metabolic consequences of TET exposed in vitro gut microbiome. First, an in vitro gut microbiome was established using the fecal matter from a single healthy donor as the inoculum. The in vitro gut microbiome was then exposed to three different doses of TET under the fed and fasted states. To understand more host relevant effects, this section analyzed the important gut microbial metabolites in the gut microbiome secretome upon TET exposure using a targeted approach along with the global metabolomics analysis. This chapter has been published as **Keerthisinghe, T.P.**, Yang, Q., Chow, A., Fang, M., 2021. Feeding state greatly modulates the effect of xenobiotics on gut microbiome metabolism: A case study of tetracycline. *Journal of Hazardous Materials* 413. DOI: 10.1016/j.jhazmat.2021.125441.

5.2. Introduction

Exposure to pharmaceuticals and environmental chemicals is typical external stress for the indigenous human gut microbiota, which directly alter its composition and functionality, inducing genes responsible for drug metabolism, drug resistance, and stress response (Maier et al., 2018; Maurice et al., 2013; Zhang et al., 2018). There are multiple possible ways of exposing the human gut microbiome to TET, particularly through therapeutic use and indirectly through the consumption of food with TET residues.

A growing body of evidence suggests that TET can alter the gut microbiome in *in vitro* human gut microbiome, mice, and swine (Jung et al., 2018; Looft et al., 2012; Roca-Saavedra et al., 2018). However, only a limited information is available on its effect on the gut microbiome metabolome, except for a few *in vitro* studies. In one study, the effect of TET at multiple dose levels including therapeutic oral dose and

acceptable daily intake level on few targeted metabolites such as SCFAs and bile acids was studied along with bacterial counts, sulfur reduction, and a few bacterial enzyme levels using *in vitro* human colonic microflora, and claimed that none of those were responsive towards TET (Carman et al., 2005). Furthermore, several other studies reported the effect of TET family antibiotics on gut microbiome and subsequent host effects such as increased body weight gain and altered host metabolome in zebrafish and rodent models (Behr et al., 2017;; Li et al., 2020; Marciano et al., 2017). However, to date, no study has investigated the effect of TET on the global metabolome of the gut microbiome focusing on host-related metabolites. Besides, another major knowledge gap of those previous studies is, how the nutrient status such as fed and fasted conditions affect the impact of TET on the gut microbiome. Since the fed and fasted states create different nutrient levels in the colon, incoming drugs may affect the colonic microbiome distinctly. This is an under-studied area, even though a few studies investigated how a diet of high fat or fiber-rich affects the gut microbiome and host health under antibiotic exposure (Fujisaka et al., 2016; Ng et al., 2019). The result revealed that the fiber-deficient diet aggravates microbiota collapse and delays the recovery upon treatment of rats with ciprofloxacin and streptomycin.

To address these gaps, we aimed to understand the effect of TET on the overall composition of the gut microbiome secretome *in vitro*, under the fed (nutrient-rich) and fasted (nutrient-deficient) states, mainly focusing on the colonic nutrient levels and bacteria generated metabolites with known link to modulate host health. We first established an *in vitro* gut microbiome culture representing the human colonic microbiota and exposed it to three different doses of TET including therapeutic and dietary dose levels under the two different feeding states. The bacterial secretome under each treatment was then characterized by performing a global metabolomic analysis as well as a targeted analysis of some key bacterial metabolites such as SCFAs.

5.3. Methodology

5.3.1. Establishment of in vitro gut microbial community

In vitro gut microbiome was established and maintained in a compact chemostat system (Winpact model FS-05) under controlled conditions. Detailed information on reactor startup, inoculation procedure, and reactor maintenance is included in **Text A3**. Briefly, modified Gifu anaerobic broth (mGAM) purchased from HyServe GmbH & Co.KG, Germany was used as the growth media and the fecal matter from one healthy donor who had not been received antibiotics for more than 8 months prior to sampling was used as the reactor inoculum in accordance with a few previous studies (Liu et al., 2018; Maier et al., 2018; Taylor et al., 2015). The collection and use of human feces samples was approved by Institutional Review Board (IRB) at Nanyang Technological University, Singapore (IRB-2017-02-023). The chemostat was run with a working volume of 2 liters and a residence time of 2.8 days with controlled temperature (at 37 °C), dissolved oxygen, flow rate, and pH (7.0). The system reached a relative steady state after 20 days of operation in terms of biomass concentration, chemical oxygen demand (COD) removal, and the SCFA levels (**Figure C14**).

5.3.2. DNA extraction and 16S rRNA gene sequence analysis

DNA was extracted for microbial community analysis from the fecal inoculum, stable reactor culture, and the reactor culture incubated under the fed and fasted states using the QIAamp® Fast DNA stool mini kit (QIAGEN), according to the manufacturer's protocol. The sequencing and analysis were carried out at NovogeneAIT Genomics, Singapore. The methods for sequence data processing and analysis are detailed in **Text A3**. Briefly, the sequencing of 16S rRNA genes was conducted using the IonS5TMXL sequencing platform and the raw sequence data was processed using QIIME2 (V2019.4.0). Sequence analysis was performed by DADA2 package (V2019.04.1) to identify amplicon sequence variants (ASV). Species annotation at each taxonomic rank was conducted using pre-Trained Naive Bayes classifier by aligning each representative sequence against the SSUrRNA database of the SILVA database (https://www.arb-silva.de/no_cache/download/archive/release_132/).

Further filtration, rarefaction, and normalization were performed using the online platform, MicrobiomeAnalyst (https://www.microbiomeanalyst.ca/) (Chong et al., 2020).

5.3.3. TET exposure of in vitro gut microbiome

TET hydrochloride was purchased from Sigma-Aldrich, Singapore. The stock solution of TET was prepared in Milli-Q® H_2O and diluted in sterile mGAM to prepare the exposure solutions. For TET exposure, the stable gut microbial culture taken from the above-mentioned reactor was immediately transferred to the anaerobic chamber and divided into 15 mL Falcon tubes. All the subsequent dilutions (for nutrient supply) and TET dosing were performed inside the anaerobic chamber.

TET exposure experiment was conducted under two different feeding states: fed and fasted. TET dose levels and the feeding state for all treatments are summarized in **Table B9** and the rationale for the dose selection is detailed in **Text A3**. The fed state condition was achieved by supplying extra nutrients through the addition of fresh mGAM to the aliquoted microbial culture in the 15 mL Falcon tube in a ratio of 1:1 (v:v). For the fasted state, microbial culture from the *in vitro* reactor was directly used without any extra nutrient supply. Subsequently, the microbial cultures under both fed and fasted states were dosed with the designed TET concentrations (10, 1, 0.01, and 0 mg/L). Each TET dose/control was prepared in five replicates for both feeding states. The prepared cultures were incubated in a shaking incubator under anaerobic conditions at 37 °C for 24 h. In addition to the above treatments for the microbial culture, blank media was also incubated alongside as a negative control to check for contamination and the result showed that there was no bacterial growth.

5.3.4. Secretome sample preparation

After TET exposure of 24 h, the optical density (OD_{600}) measurements were immediately conducted for each replicate upon harvest for future normalization. Subsequently, bacterial cell pellets and secretome were separated via centrifugation at 10,000 rpm for 5 min. The preparation method of bacterial supernatant for the metabolomics analysis was modified from a previous study (Zampieri et al., 2018). Briefly, 100 µL bacterial supernatant was transferred into a 500 µL Eppendorf

microcentrifuge tube and 100 µL of ice-cold extraction buffer (acetonitrile: methanol, 1:1, v:v) was added to each tube immediately. The samples were then vortex mixed and incubated for 1 h at −20 °C, followed by 15 min centrifugation at 13,000 rpm at 4 °C to precipitate proteins and insoluble debris according to our previous study (Zhang et al., 2018). The supernatants were then transferred to vials and stored at −80 °C prior to analysis. The blank media was also processed alongside the microbial cultures for metabolomic analysis to identify the nutrients in culture media.

5.3.5. Metabolite profiling, identification, and pathways analysis

The profiling of metabolites was conducted using an HPLC system (Agilent Technologies, Singapore) coupled to a 6550 Q-TOF (Agilent Technologies, Singapore), in accordance with our previous studies (Beyer et al., 2018; Fang et al., 2015; Keerthisinghe et al., 2019). The metabolite profiling and quality control methods are detailed in **Section 5.3.7** and **Text A3**. Briefly, to achieve better metabolite coverage, two different separation methods were used. A Waters ACQUITY UPLC BEH Amide (3 µm, 2.1×100 mm) in negative electrospray ionization (ESI) mode (HILIC-ESI (-)) was used for better separation of polar metabolites and an Atlantis T3 column (3 µm, 2.1 × 100 mm) in both ESI (+) and ESI (-) modes (RP-ESI (±)) was used for hydrophobic metabolites. Both profiling methods were slightly modified from a previous study (Wang et al., 2019). Furthermore, a pooled mixture of treated and control samples was run with data-dependent acquisition (DDA) auto-MS/MS and targeted MS/MS of selected precursors. The processing of metabolome data was carried out using the XCMS online web platform (http://xcmsonline.scripps.edu). First, the pairwise analyses of 10 mg/L TET treated group and the control for both fed and fasted states were conducted. The first screening for the pairwise analysis was based on the significant features, with p-value ≤ 0.05, |fold change| > 1.2, and intensity > 10,000 ion counts. All those features were manually checked to minimize the false positive hits. MS/MS fragment match, accurate mass match, and in-house retention time match were the methods used for metabolite identification. In addition to global identification, global metabolic data sets were searched against an in-house library covering ~105 important gut microbial metabolites, which was established after an extensive

literature search (Donia and Fischbach, 2016; Wikoff et al., 2009; Zelante et al., 2013; Zhang and Davies, 2016). Overlapped metabolic features across different dose levels at both feeding states were then aligned by m/z and retention time. The Open source platform, KEGG (http://www.genome.jp/kegg/) and a few publications were referred for targeted pathway analysis (Meyer and Hostetter, 2012; Wikoff et al., 2009; Zelante et al., 2013). The heatmap was generated using GraphPad Prism 8.0 (GraphPad Software Inc., San Diego, CA) and the multivariate analysis was performed with PAST (https://folk.uio.no/ohammer/past/).

5.3.6. SCFA analysis

SCFAs, which cannot be detected in the global metabolomics analysis, were analyzed in accordance with a previous study (Chen et al., 2017). A gas chromatograph (GC7890A, Agilent, USA) of DB-FFAP fused-silica capillary column equipped with a flame ionization detector was utilized to analyze the composition of SCFAs. The centrifuged gut microbiome supernatant was diluted 10 times and acidified with 10% (v/v) formic acid before the analysis. The column operating temperature profiles were 80 °C for 1 min, increased to 120 °C at 20 °C /min, then to 205 °C at 10 °C /min, and held for 2 min at 205 °C. The injector and detector temperatures were 260 °C. The sample injection volume was 0.5 µL.

5.3.7. QA/QC and statistical analysis

For the QA/QC of bacterial metabolome analysis, a pooled mix sample of metabolites prepared by pooling all treated and control samples were analyzed after every six injections of biological samples to correct the mass, retention time, and response drift. For the SCFA analysis, a pooled mixture of treated/control samples prepared for SCFA analysis was analyzed after every six injections to correct the response drift. All the data were expressed as mean ± standard deviation of the mean (SD). Differences between groups or treatments were examined for statistical significance using Student's *t*-test or a one-factor analysis of variance (*ANOVA*), with Duncan's post-hoc test, with the significance level set at p-value ≤ 0.05.

5.4. Results and Discussion

5.4.1. Growth and community composition of in vitro gut microbiome under the fed and fasted states

The OD_{600} readings after 24 h incubation revealed a growth in bacterial culture from the *in vitro* reactor at the fed state but not in the fasted state (**Figure C15**). Furthermore, significant inhibition of bacterial growth was observed at 10 and 1 mg/L TET with a reduction of ~20 and ~5% (i.e., 80 and 95% OD_{600} in relation to control); respectively at the fed state, while 0.01 mg/L was below no-observed-adverse-effect level (NOAEL). In contrast, at the fasted state, TET was not able to induce inhibitory effects on bacterial growth at any of the dose levels. At the fed state, the reactor culture with bacteria was diluted 50% in mGAM; thus, there were sufficient nutrients for the bacteria to enter the growth state. On the contrary, at the fasted state, the bacterial culture was maintained at stable conditions without entering the growth phase due to lack of external nutrients. Overall, this result is consistent with the fact that TET is designed to inhibit the growth of bacteria, and the growth inhibitory effects were only observed at the fed state where the bacteria was in growth phase (Chopra and Roberts, 2001; Schnappinger and Hillen, 1996).

To validate our *in vitro* gut microbiome as an appropriate representation of the human colonic microbiome and to compare the difference in microbial community composition under the fed and fasted states, we have performed 16S rRNA gene sequence-based microbial community analysis. As shown in **Figure C16**, Bacteroides and Firmicutes were the two most abundant phyla with a relative abundance of 42% and 28%; respectively, at the fed state *in vitro* gut microbiome. This observation was in line with previously published data on human gut microbiome composition where Bacteroides and Firmicutes comprised the major portion of human gut flora (De Filippo et al., 2010; Eckburg et al., 2010; The Human Microbiome Project Consortium, 2012). The abundance pattern was quite consistent for the fasted state with values of 47% and 43%; respectively, where Bacteroides and Firmicutes were yet the two most abundant phyla, though an increase in Firmicutes was observed. Moreover, the composition of our *in vitro* gut microbial community was comparable with the human colonic/fecal microbiota composition in lower

taxonomic levels including class and genes levels as well (**Figure C17, C18 and C18**) (De Filippo et al., 2010; Liu et al., 2018). Furthermore, the microbial community composition of the *in vitro* system is comparable with the previously reported *in vitro* systems. For instance, the class level community composition revealed that the *Bacteroidia* (52%) and *Clostridia* (18%) were the two most abundant classes in our *in vitro* system, as shown in Fig. S4. In comparison, a previous study reported a similar observation where *Bacteroidia* (41-54%) and *Clostridia* (28-40%) were the two most dominant classes (Liu et al., 2018).

In addition, a reduction in the relative abundance of genera *Fusobacterium* from 25% in the fed state to 6% in the fasted state was observed, which was consistent with the observation of reduced relative abundance of *Fusobacterium* after fasting in four participants who harbored higher *Fusobacterium* prior to fasting (He et al., 2019). Also, a slight increase in phyla Bacteroidetes in the fasted state compared to the fed state is consistent with literature where an increase in Bacteroidetes was observed after the fasted period, which makes it the dominant phyla (Mesnage et al., 2019). However, our observation of increased abundance of Firmicutes in the fasted state gut microbiome was contrasted with the observation of reduced relative abundance of Firmicutes after the fasting period (Mesnage et al., 2019). The difference in the *in vitro* and *in vivo* conditions and the difference in fasted period may be the main reasons for the observed differences. Thus, our *in vitro* system can be considered as a reasonable representation of the human gut microbiota, though the culturing of extreme oxygen-sensitive genera such as *Faecalibacterium* was challenging (Duncan et al., 2002).

5.4.2. Global metabolomic profiling of the gut microbiome secretome under different treatments

We first performed the global metabolomics analysis for the gut microbiome secretome to understand how the TET treatment at three different dose levels under the fed and fasted states affects the secretome composition in relative to their TET free controls. In general, overall dysregulations followed a dose-response relationship as shown in **Figure 5.1a**. For example, significantly dysregulated features observed in the HILIC-ESI (-) profiling method under 10 and 1 mg/L of TET exposure were

~16.8 and ~11.8 folds higher than that in the 0.01 mg/L; respectively. Furthermore, the fed state profoundly affected the secretome composition compared to the fasted state where the dysregulated features at 10 mg/L TET was 5.3, 6.5, and 8.7 folds higher in the fed state compared to the fasted state in HILIC-ESI (-), RP-ESI (+), and RP-ESI (-) profiling methods; respectively. To get a further comparison of gut bacterial metabolic response to TET under the fed and fasted states, we conducted a meta-analysis of the responsive features at each dose. In general, fewer features were shared between two feeding states, and the fed state had more unique features with significant changes. Specifically, 588 features were shared between the two feeding states under the HILIC-ESI (-) profiling method, which corresponds to ~46% of the total significant features in the fasted state and <10% of the significant features in the fed state under TET exposure at 10 mg/L (**Figure 5.1b**). For the RP-ESI (+) profiling method, 361 significant features were shared between the two feeding states corresponding to ~44% of the total significant features in the fasted state and <7% in the fed state. This pattern was nearly consistent among all the dose levels and profiling methods (**Figure C19**). Collectively, the results showed a unique metabolic response of gut microbiome secretome composition towards TET under the two different feeding states. Furthermore, principal component analysis (PCA) and hierarchical clustering of metabolic features detected under the RP-ESI (+) profiling method revealed that the 10 and 1 mg/L TET treated groups at the fed state and 10 mg/L TET treated group at the fasted state were clearly separated from each other and other groups. In contrast, the clusters of the other treatment groups overlap with each other (**Figure C21**).

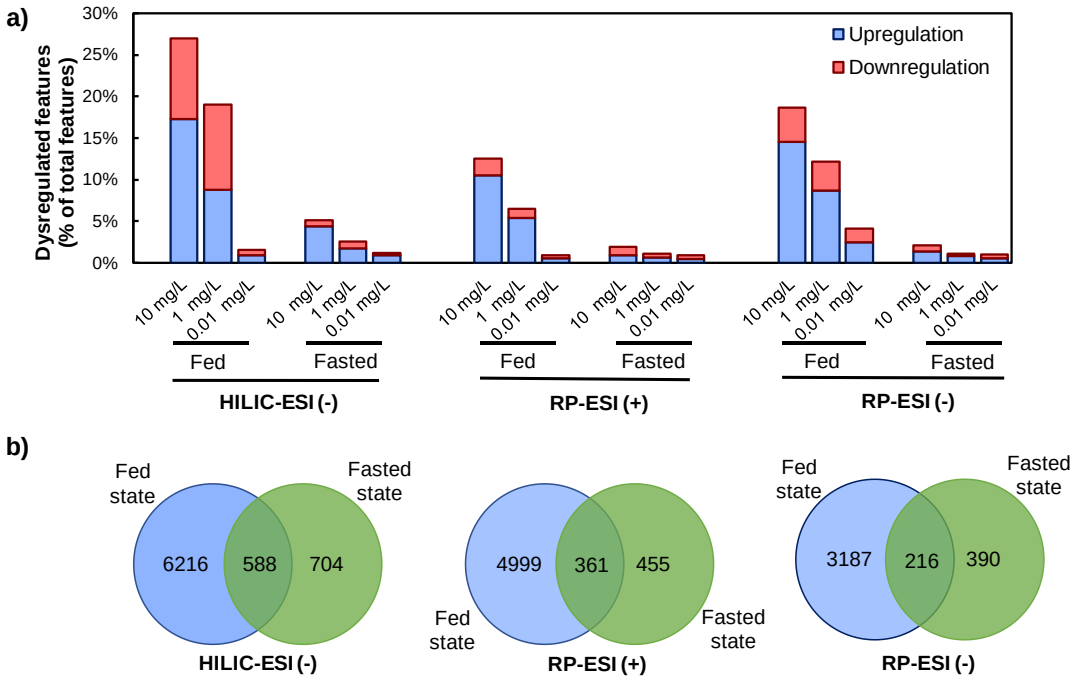

Figure 5.1. Global metabolite profiling of the gut microbiome secretome under TET exposure at the fed and fasted states

a) Up and downregulated significant features detected by global profiling (|fold change| > 1.2, *p*-value ⩽ 0.05, abundance >10,000 ion counts and the percentage was calculated based on total detected feature numbers for each condition) and b) classic Venn diagram summarizing the number of shared and distinct features under the fed and fasted states observed in the HILIC-ESI (-), RP-ESI (+), and RP-ESI (-) profiling methods at 10 mg/L TET exposure.

5.4.3. Metabolite identification under different treatments

The global metabolomics approach further facilitated us to detect and identify a range of metabolic features in the gut microbiome secretome. In addition, we extended our identification with the in-house targeted list of important gut microbial metabolites. Accordingly, we were able to identify 110 metabolic features and 62 of them were significantly altered under 10 mg/L TET at the fed state. In contrast, only 14 of the identified metabolites were significantly dysregulated under the fasted state. In comparison, 43 and 10 metabolic features were significantly altered at 1 mg/L TET under the fed and fasted states; respectively, while only 7 and 1 were altered at 0.01 mg/L TET under the fed and fasted states; respectively. Knowing that mGAM is a nutrient-rich media with essential nutrients for the growth and survival of the gut microbiome, we were interested in differentiating the nutrients supplied by mGAM

from gut microbiome produced metabolites that were present in the bacterial secretome. The metabolites with significantly high levels in the blank medium compared to gut microbiome secretome were considered as supplied nutrients. Meanwhile, metabolic features were considered as gut microbiome products for those with a significantly higher level in the gut bacterial secretome than the blank media (**Text A3 and Table B10**). Accordingly, we have identified 50 metabolic features as nutrients while the other 60 were gut microbiome produced metabolites. Consumption of 30 nutrients was significantly affected under 10 mg/L TET at the fed state, while there were only 6 nutrients under the fasted state (**Figure 5.2 and Table B11**). Similarly, more alterations were observed for the gut microbial metabolites under the fed state compared to the fasted state. As shown in **Figure 5.3** and detailed in **Table B11**, ~32 of the metabolites were dysregulated under the fed state at 10 mg/L TET exposure. In contrast, only 8 metabolites were dysregulated under the fasted state. The detailed result and discussion are shown below.

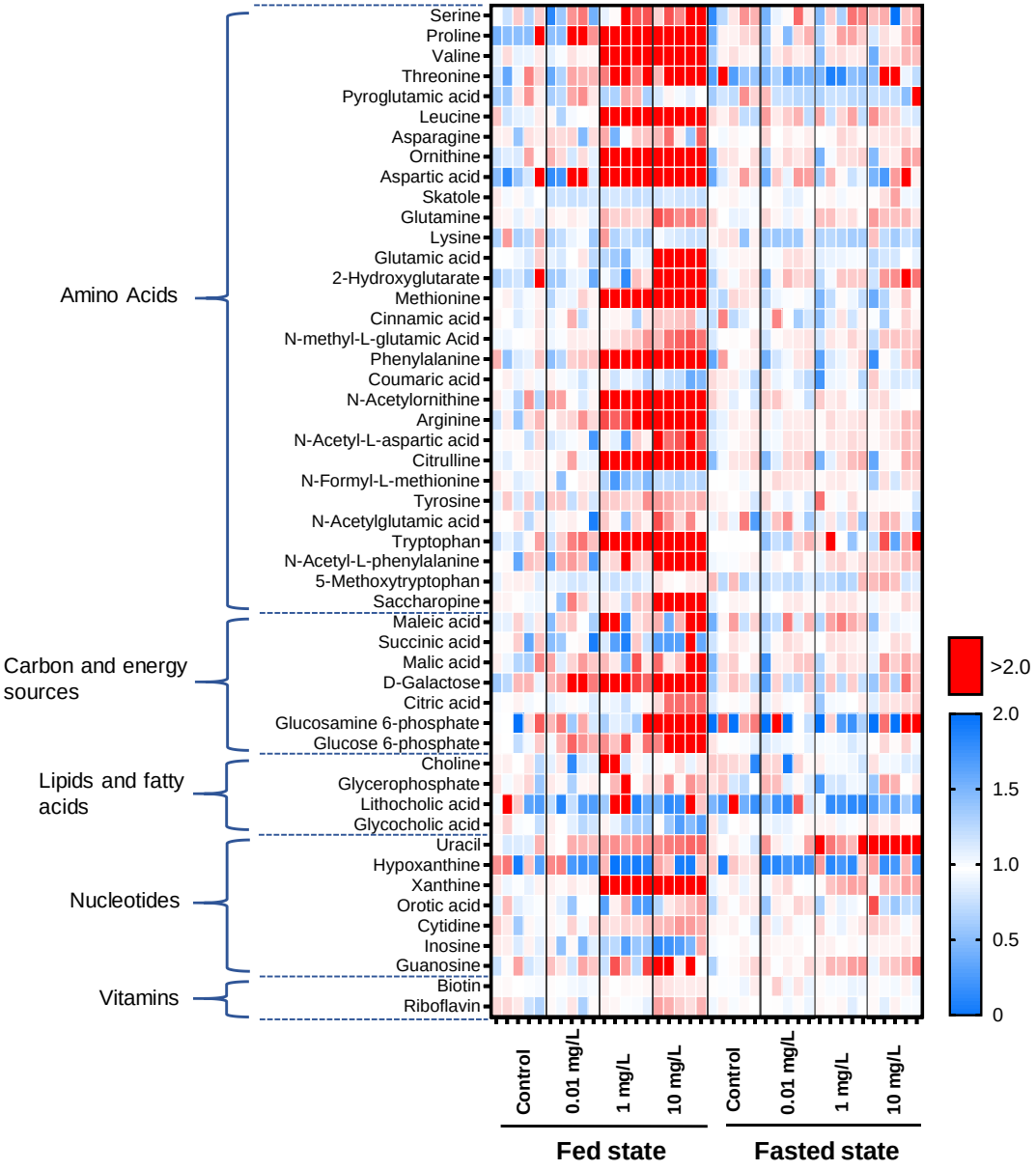

Figure 5.2. Heatmap analysis representing the nutrient levels in the gut microbiome secretome under TET exposure at the fed and fasted states

The heatmap values represent the abundance ratios of nutrients in the bacterial secretome from each TET treatment to their respective control. The red and blue colors represent the upregulated and downregulated metabolites relative to the control; respectively. White represents missed values or values with no difference from the control.

5.4.4. Alteration of nutrient levels in gut microbiome secretome under TET exposure

Consumption of the majority of nutrients was significantly inhibited under TET exposure at the fed state and amino acids comprised the major portion of those. For example, amino acids such as glutamate, leucine, valine, and ornithine were >10 fold higher in the secretome from 10 mg/L TET treatment compared to TET free control at the fed state. In addition, carbon and energy sources including galactose and citrate were increased by 10.6 and 1.7 folds; respectively. On the other hand, comparatively lower changes were observed in amino acids and nucleotide related nutrients at the fasted state (**Figure 5.2 and Table B11**). Furthermore, inhibition in consumption of most of the nutrients also showed a clear dose-response relationship at the fed state where the increase in leucine level at 10 and 1 mg/L TET were 16 and 10 times higher compared to that in 0.01 mg/L; respectively. This nutrient accumulation in the secretome was expected due to the inhibitory effect of TET on bacterial growth, especially at the fed state (**Figure C15**). Notably, the inhibition of protein synthesis, which is the primary mechanism of action of TET for bacterial growth inhibition, may lead to significant accumulation of amino acids in the bacterial secretome (Chopra and Roberts, 2001; Schnappinger and Hillen, 1996). The observation was also consistent with previous reports on the elevated amino acid levels observed in the feces of vancomycin, streptomycin, and roxithromycin treated rats (Behr et al., 2018).

Though the inhibited nutrient consumption was expected, its health implication is still worthy of being investigated in the future. For example, valine and leucine are BCAAs which are known to be linked with insulin resistance (IR) and metabolic syndrome (Pedersen et al., 2016). In addition, leucine and its derivations may enhance intestinal inflammation (F. He et al., 2018), while aromatic amino acids including tryptophan and phenylalanine have been shown to reduce intestinal inflammation through activating calcium-sensing receptor (CaSR) (Tan et al., 2017). However, the fate of elevated nutrient levels needs to be further investigated to understand whether they can be absorbed by the host and affect host physiology or excreted through the feces.

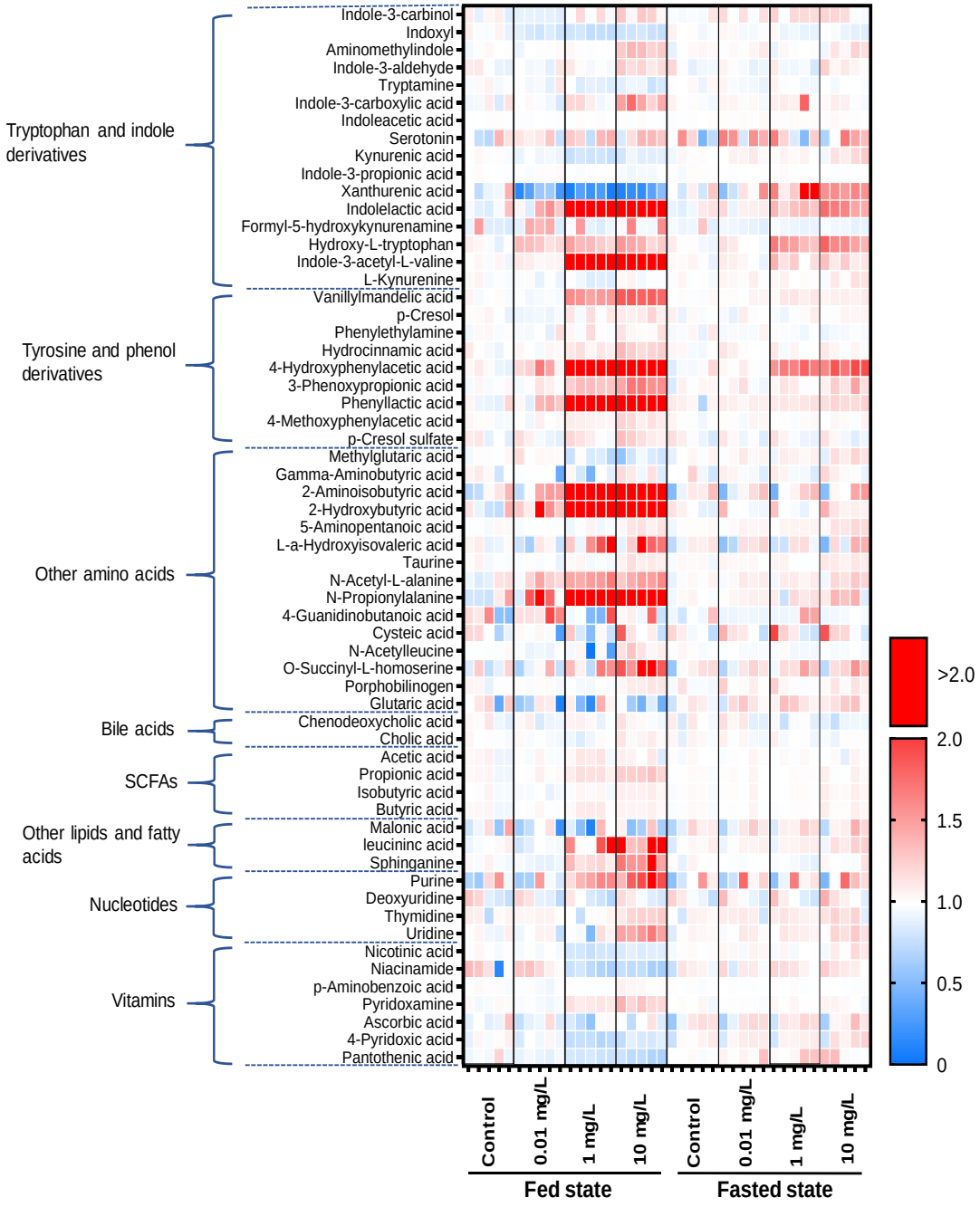

Figure 5.3. Heatmap analysis representing the metabolites produced by the gut microbiome under TET exposure at the fed and fasted states

The heatmap values represent the abundance ratios of metabolites in the bacterial secretome from each TET treatment to their respective control. The red and blue colors represent the upregulated and downregulated metabolites relative to the control; respectively. White represents missed values or values with no difference from the control.

5.4.5. Alteration of gut microbiome produced metabolite levels under TET exposure

A majority of the gut bacterial metabolites we identified in this study were previously known as typical gut microbial metabolites (Donia and Fischbach, 2016; Wikoff et al., 2009), which further validated our *in vitro* system as a close representation of the human colonic microbiota. The synthesis of the majority of these metabolites was significantly altered depending on the feeding state; however, no specific patterns in the alterations were observed. Some metabolites were higher in abundance under the fed state (e.g., kynurenine and phenethylamine). In comparison, some metabolites were lower (e.g., indoxyl and tryptamine) or have similar levels (e.g., indole-3-aldehyde and *p*-cresol) compared to those in the fasted state (**Figure C22**).

Upon TET treatment, more dysregulations were observed in the categories such as tryptophan and indole derivatives, tyrosine and phenyl derivatives, and vitamins at the fed state, while fewer were significantly altered at the fasted state. For example, tryptophan and indole derivatives that were significantly altered at the fed state under 10 mg/L TET exposure included indole-3-carbinol, indole-3-acetyl-L-valine, indole-3-aldehyde, indolelactic acid, and hydroxy-L-tryptophan, which were upregulated by 1.2-5.4 folds and tryptamine, indoxyl, kynurenic acid, and xanthurenic acid which were downregulated in 0.3-0.9 folds (**Figure 5.3 and Table B11**). Metabolizing tryptophan through the kynurenine pathway was believed to be affected by TET according to our targeted pathway analysis, as the kynurenic acid and xanthurenic acid in the kynurenine pathway were significantly downregulated (**Figure 5.4**). The kynurenine pathway and metabolizing to other indole derivatives are two major ways of metabolizing dietary tryptophan in the colon by microorganisms (Cervenka et al., 2017). For the tyrosine and phenyl related metabolites, 3-phenylpropionate (hydrocinnamic acid), phenyllactic acid, p-hydroxyphenylacetic acid, *p*-cresol, and its transformation product *p*-cresol sulfate were significantly upregulated in 1.3, 3, 45.6, 1.1, and 1.2 folds; respectively under 10 mg/L TET treatment at the fed state (**Figure 5.3 and Table B11**). Tyrosine is microbially converted to *p*-cresol through an intermediate; 4-hydroxy phenylacetic acid (Meyer and Hostetter, 2012). This pathway was observed to be slightly upregulated under TET exposure due to the observed higher levels of 4-hydroxyphenylacetic acid and the slight yet significant

upregulation of *p*-cresol and *p*-cresol sulfate (**Figure 5.5**). In addition, vitamin Bs such as nicotinate, pantothenic acid, and 4-pyridoxic acid, which were identified as microbiome produced vitamins in this study were inhibited significantly by 0.9, 0.7, and 0.8 folds; respectively (**Figure 5.3 and Table B11**). Furthermore, some of the dysregulated metabolites were altered in a TET dose-dependent manner. For instance, the increase in phenyllactic acid under 10 and 1 mg/L was 2.5 and 1.8 times higher compared to that in 0.01 mg/L; respectively. Interestingly, some of the metabolites were slightly responsive even at 0.01 mg/L TET, the dietary dose. For example, xanthurenic acid and indoxyl were changed in 0.4 and 0.8 folds; respectively.

Even though most of the responsive metabolites at the fed state were not dysregulated at the fasted state, some metabolites were responsive to TET at the fasted state as well. For example, tryptophan and indole derivatives such as indole-3-acetyl-L-valine, hydroxy-L-tryptophan, indole-3-aldehyde, and indoxyl, that were altered in the fed state were changed in comparatively lower, yet significant fold changes of 1.2, 1.6, 1.1, and 0.9; respectively at the fasted state under 10 mg/L TET exposure. Similarly, tyrosine and phenyl derivatives such as 3-phenoxypropionic acid and 4-hydroxyphenylacetic acid were found to be upregulated by 1.8 and 1.2 folds; respectively, which were also upregulated at the fed state. In addition, it was very interesting to observe that some metabolites showed opposite responses towards TET under the two feeding states. For instance, xanthurenic acid was significantly downregulated at the fed state (i.e., 0.3 folds at 10 mg/L TET) while it was upregulated in the fasted states (i.e., 1.6 folds at 10 mg/L TET) under TET exposure while its levels were quite similar for both feeding states in TET free controls (**Figure C22**).

5.4.6. Host health implications of TET altered gut microbiome metabolome

The majority of the responsive gut microbial metabolites, especially at the fed state, have been recognized to play an important role in host health modulation. Kynurenic acid is a gut microbiome produced metabolite by trans- amination of kynurenine and known to modulate local inflammation most likely through the activation of G protein–coupled receptor (GPCR), which is highly expressed in the immune cells of the GI tract (Cervenka et al., 2017). Furthermore, tryptamine, indole-3-aldehyde,

kynurenic acid, and xanthurenic acid are agonists for transcriptional aryl hydrocarbon receptor (AHR). On the other hand, indole, upstream to the indoxyl is known for its antagonist activity (Hubbard et al., 2015; Jin et al., 2014; Zelante et al., 2013). AHR and its ligands play an important role in gut homeostasis and various intestinal diseases, including colitis and colon cancer (Zelante et al., 2013; Zhang and Davies, 2016). Hydrocinnamic acid is a known inhibitor of branched-chain α -keto acid dehydrogenase kinase, which regulates the breakdown of BCAAs while its level in the blood has been reported to positively correlate with gut microbial diversity (Pallister et al., 2017; Pedersen et al., 2016; Tso et al., 2013). *p*-Cresol has been reported to induce genotoxic effects on colonocytes while *p*-cresol sulfate suppresses Th1-type cellular immune responses in mice (Saito et al., 2018; Shiba et al., 2014). Also, the interaction of phenyllactic acid and the human host through GPCR has also been reported (Peters et al., 2019). Furthermore, vitamin synthesis is one of the important functions of human gut microbiota while certain B vitamins are among the key metabolites supplied to the host by gut bacteria (Magnúsdóttir et al., 2015; Morowitz et al., 2011). Thus, TET exposure could affect the host nutrient supply mediated through the gut microbiome. Collectively, TET exposure of the human gut microbiome, especially at the fed state, can impose a great impact on the host physiology through dysregulating metabolites.

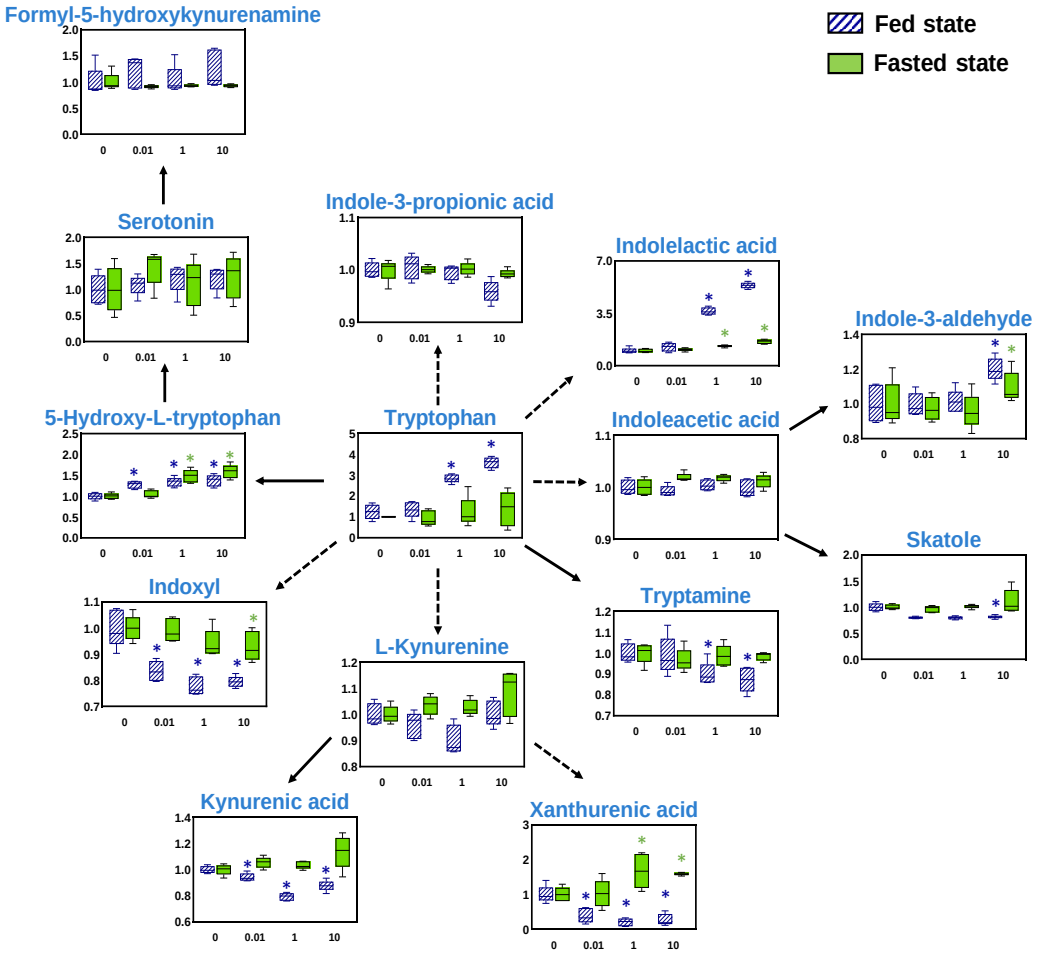

Figure 5.4. Tryptophan and indole metabolism pathways under TET exposure at the fed and fasted states

Y-axis indicates the fold changes of each metabolite compared to the control at the same feeding state and the X-axis indicates the TET concentration in mg/L. Arrows in solid lines indicate directly linked metabolites and dashed lines stand for metabolic pathways with intermediates that were not identified in our analysis. Data presented as the mean ± SD of five replicates and "*" indicates the statistical significance (*p*-value ≤0.05) between TET treated and respective control groups.

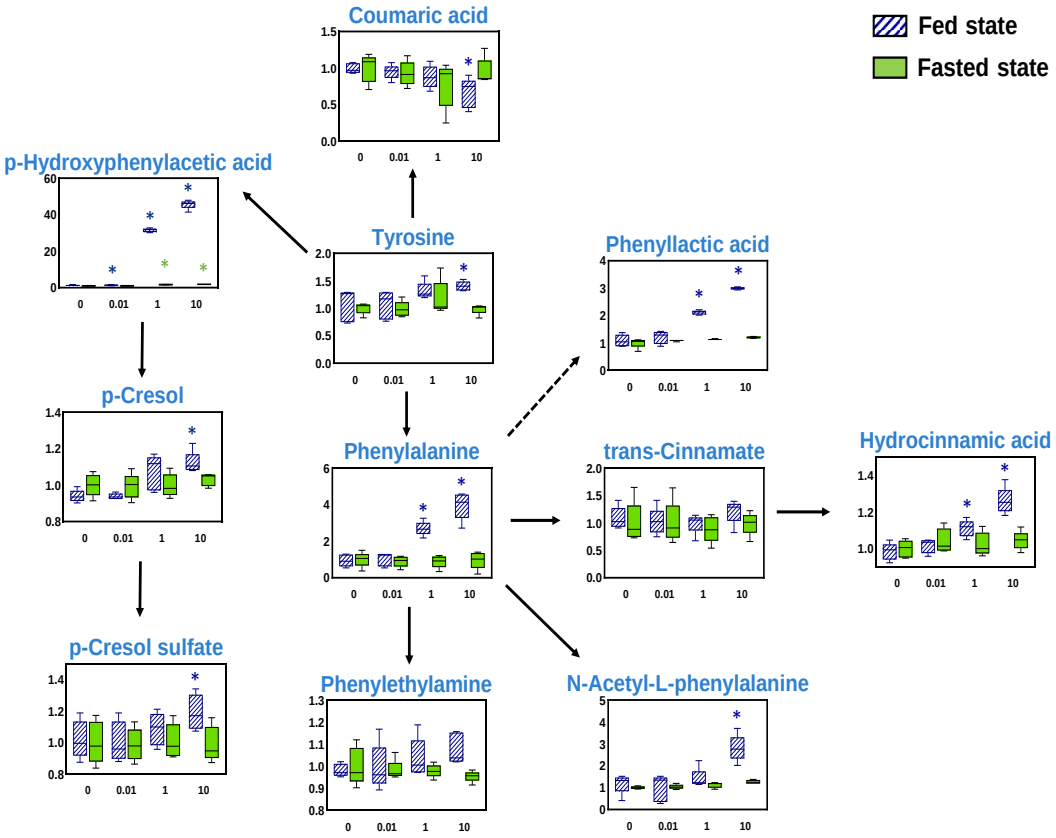

Figure 5.5. Tyrosine and phenyl related metabolism pathways under TET exposure at the fed and fasted states
Y-axis indicates the fold changes of each metabolite compared to the control at the same feeding state and the X-axis indicates the TET concentration in mg/L. Arrows in solid lines indicate directly linked metabolites and dashed lines stand for metabolic pathways with intermediates that were not identified in our analysis. Data presented as the mean ± SD of five replicates and "*" indicates the statistical significance (*p*-value ≤0.05) between TET treated and respective control groups.

5.5. Short Summary

This *in vitro* study aimed to understand the response of the gut microbiome at the fed and fasted states towards TET exposure revealed a significant alteration in the gut microbiome metabolome at the fed state in a TET dose-dependent manner. The changes mainly resulted from significantly inhibited nutrient consumption and dysregulated synthesis/transformation of metabolites by the gut microbiome, especially at the fed state. More importantly, nutrients, mainly the amino acids, were

highly accumulated in the gut microbiome secretome while higher levels of carbon and energy-related nutrients were also observed. Furthermore, gut microbial metabolites including tryptophan and indole derivatives, tyrosine and phenyl derivatives, and vitamins were significantly altered at the fed state under the clinical dose of TET. Interestingly, some of these metabolites were still responsive under the dietary dose of TET. In contrast, both nutrients as well as the gut microbial metabolites were less responsive at the fasted state compared to the significant, apparent alterations at the fed state. However, some of the tryptophan and indole derivatives and tyrosine and phenyl derivatives were responsive to TET exposure at clinical dose, under the fasted state. The majority of responsive nutrients and metabolites have been known to modulate host health, and thus a great impact of TET exposure on the host health can be expected. However, the gut microbiome metabolite-host interactions are highly complex due to numerous factors such as absorption capabilities of metabolites through colonic barriers and flow characteristics of colonic contents. Therefore, future studies are warranted to further confirm the link between TET exposure and host health mediated through gut microbial metabolites. Furthermore, the effect of more specific nutrition statuses such as high fat, high protein, or fiber-rich conditions on the impact of TET on gut microbiota can be further investigated.

Chapter 6. *In vitro* Host Effects Induced by Tetracycline Altered Metabolic and Immunologic Interactions between the Gut Microbiome and Host

6.1. Overview

Chapter 6 explored the contribution of low MW metabolites and immunoregulatory compounds (i.e., LPS) in the secretome of TET affected gut microbiome to the host weight gain and related complications using *in vitro* models. For the study of *in vitro* liver effects, the pre-treated gut microbiome secretome by filtering with MW cut-off filters were dosed to human liver cancer cells (HepG2), and the cytotoxic effects and lipid dysregulations were investigated. The study next analyzed the LPS levels in the TET exposed gut microbiome secretome. Furthermore, TET-induced alterations in LPS release and immune response modulation by two main Gram-negative strains (i.e., *B. fragilis and E. coli*), which represent the main bacterial orders that contribute to the gut LPS pool, were investigated.

6.2. Introduction

The effect of TET family antibiotics on the gut microbiome and subsequent host effects has been rarely studied. For example, increased body weight gain in a rodent model (Marciano et al., 2017), altered host metabolome in a rodent model (Behr et al., 2017), and altered brain functions in a zebrafish model (Li et al., 2020) upon exposure to TET family antibiotics has been documented. In addition to TET, gut microbiome dysbiosis-mediated host effects induced by different other antibiotics have been reported (Cho et al., 2012; Cox et al., 2014; Thuny et al., 2010). Specially, early life antibiotic exposure-associated host obesity is one of the highly studied areas in the recent decade, and some of the mechanisms involved in gut microbiome dysbiosis mediated host obesity have been elucidated (Cox and Blaser, 2013). However, the mechanistic pathways of inducing obesity by TET affected gut microbiome have not been explicated.

Furthermore, it is well known that gut microbiome-host interactions are mostly mediated through gut microbiome produced metabolites. A considerable portion of low molecular weight (MW) metabolites produced by gut microbiome are absorbed by the colonic lumen. Therefore, those can be bioavailable for the host organs such as livers, especially due to the portal circulation (Matsumoto et al., 2017). However, metabolic and immunological dysfunctions associated with host weight gain caused by TET affected gut microbiome have not yet been investigated. Particularly, the contribution of absorbed TET altered gut bacterial metabolites, specifically at low MW, to the host weight gain has not been studied yet. Further, LPS is an immunoregulatory compound that can be engaged in the host immune response modulation, and infusion of LPS alone can contribute to increased weight gain (Cox and Blaser, 2013). Induced LPS release in *E. coli* with TET exposure has been reported. However, the influence of TET on LPS production by the gut microbiome and other primary gut bacterial orders contribute to the gut LPS pool, and thereby the effects on the host remain unclear.

Accordingly, this study aimed to understand the contribution of TET affected low MW metabolites and immunoregulatory compounds (i.e., LPS) from gut microbiome to the host weight gain and related complications *in vitro*. First, an *in vitro* liver cell model (HepG2) was incorporated to study the cytotoxic effect caused by the gut bacterial secretome, and then the contribution of low molecular weight (MW) weight metabolites on liver lipid dysregulations was analyzed. Furthermore, high-throughput immune bioassays were used to determine TET's effect on gut microbiome LPS release and possible interactions between LPS subtypes from *B. fragilis* and *E. coli*; representatives of major bacterial orders that contribute to the gut LPS pool. In addition, we also used additional experiments to examine and predict the host effect (i.e., immune response modulation) of TET on different gut microbiome compositions.

6.3. Methodology

6.3.1. Establishment of in vitro gut microbial community, TET exposure of in vitro gut microbiome, and secretome preparation

The details on the establishment of *in vitro* gut microbial community and TET exposure experiments are detailed in **Section 5.3.1**. The gut microbiome secretome resulted from the fed state clinical level TET exposure (10 mg/L) and no TET control were used to assess the host effects of TET altered gut microbiome secretome since the clinical level TET treated gut microbiome under the fed sate showed the higher metabolic response. In addition, modified Gifu anaerobic broth (mGAM) was also used as a negative control for comparison purposes.

For secretome preparation, the secretomes resulted from each treatment were pooled together and centrifugally filtered through 10 and 30-kDa MW cutoff filters (Ultrafree-MC (Millipore)). Then each secretome/mGAM fractions (< 10 kDa and <30 kDa, and unfiltered secretome) were filtered through 0.22 sterile filters for sterilization. The resulted samples were then characterized by analyzing metabolite recovery according to the metabolite profiling method described in **Section 5.3.5** and secretome LPS levels (see **Section 6.3.6** for detailed methods).

6.3.2. TET exposure of model bacteria

For the immunological study, two model bacteria including *Bacteroides fragilis* ATCC25285 and *Escherichia coli* K12-MG1655 were applied. The model gut bacteria culturing method was detailed in **Section 4.3.1**. Briefly, both model bacteria were treated with three different doses of TET, inhibitory concentration $(IC)_{90}$, IC_{50}, and dietary level exposure concentration, which denotes by high, mid, and low; respectively. Details of the used concentrations are mentioned in **Table B7**.

6.3.3. HepG2 cell culture and cytotoxicity tests

As a widely used cell line, HepG2 (ATCC HB-8065, Rockville, MD, USA) was chosen as the experimental model. The cells were stored in a liquid nitrogen vapor phase and cultured in a humidified 37 °C atmosphere containing 5% CO_2. Dulbecco's

modified Eagle's medium (DMEM; with 4.5 g/L glucose, 10% fetal bovine serum (FBS), and L-glutamine) (Gibco, Thermo Fisher Scientific, Singapore) was applied as a growth medium following our previous studies (Peng et al., 2019; Zhang et al., 2020)

The cytotoxicity of gut bacterial secretome/mGAM on HepG2 cells was evaluated by the resazurin assay (Peng et al., 2019; Zhang et al., 2020). Briefly, the cells were seeded in 96-well flat-bottomed plates (Thermo Fisher Scientific, Singapore) with a density of 30,000 cells/well in 100 μL DMEM for ~7 h. Subsequently, the dose substances (i.e., TET 10 mg/L treated, control (TET 10 mg/L post-spiked), control (TET_0) gut microbiome secretome/mGAM in 10, 20, 30, 40, and 50-times dilutions and <10 kDa, <30 kDa, and unfiltered gut microbiome secretome/mGAM in 10, 20, 30 -times dilutions) were added into each well. Control (TET 10 mg/L post-spiked) group was prepared by adding the appropriate amount of TET to the control (TET_0) gut microbiome secretome to achieve 10 mg/L TET concentration. A dimethyl sulfoxide (DMSO) control (DMSO: 0.1%) was also prepared alongside the treatments. All treatments were conducted with three replicates. After 48 h treatment, resazurin (Sigma-Aldrich, Singapore) at a working concentration of 0.05 mg/mL was added into cells and further incubated for 10 h. The cytotoxicity was assessed by measuring the transformation product of resazurin using a microplate reader at fluorescence 570. The cell viability was calculated by setting the control cells as 100%.

6.3.4. HepG2 cell exposure experiment and lipid extraction

The exposure of HepG2 cells to gut microbiome secretome was performed in 6-well plates. The cells were first seeded on the plates with a density of 300,000 cells/well for ~7 h and then treated with DMSO control or substrates for another 48 h. The extraction method of intracellular metabolites was modified from our previous study (Peng et al., 2019). Briefly, cells were rapidly washed with 1 mL of ice-cold PBS and then harvested with a cell scraper in a 1.2 mL ice-cold quenching mixture solution of methanol and HPLC grade water (4:1, v/v) and finally transferred into a 2 mL Eppendorf vial. After that, the samples were vortexed, followed by three cycles of shock−freezing−thawing and sonication at 4 °C for 10 min.

For the lipid extraction, liquid-liquid methyl tert-butyl ether (MTBE) extraction method was used, which was modified according to a previous study (Chen et al., 2013). Briefly, MTBE was added to the samples to achieve a ratio of MTBE: methanol (20:6, v/v). Then samples were sonicated for 30 min and the phase separation was induced by adding HPLC grade water to achieve a ratio of MTBE:methanol:H_2O (20:6:7, v/v/v), which was followed by centrifugation for 15 min at 4 °C. The upper phase was then collected, dried, and dissolved in 0.1 ml of $CHCl_3$/methanol/IPA (2:1, v/v).

6.3.5. Lipid profiling and identification

Lipidomics profiling was performed in accordance with a previous study (Pizarro et al., 2013). Briefly, the profiling of lipids was conducted using a reversed-phase HPLC system coupled to the same 6550 Q-TOF. The lipid profiling method is detailed in **Text A1**. A pooled mixture of treated and control samples was run with data-dependent acquisition (DDA) auto-MS/MS and targeted MS/MS of selected precursors. The processing of global lipid data was carried out using XCMS online web platform (http://xcmsonline.scripps.edu) (detailed in **Text A1**). First screening was based on the significant features, with p-value ≤ 0.05, |fold change| > 1.2, and intensity > 10,000 ion counts. In addition, MS-DIAL (V. 2.84) software program with built-in LipidBlast database and Lipid maps online database were incorporated for the lipid annotation (Kind et al., 2013; Tsugawa et al., 2015).

6.3.6. Determination of LPS

LPS concentration in each TET treated/control bacterial secretome and filtered fractions were determined. Briefly, LPS-free tubes and vials were utilized as well as non-pyrogenic filters. The samples were kept on ice, diluted in pyrogen-free water plus 0.05% Tween 20 (Sigma-Aldrich Singapore), centrifuged at 2,500 g for 10 minutes, and the secretome was frozen at -20°C, pending analysis. Analyses of LPS were performed with a limulus amebocyte lysate (LAL) assay (Charles River, UK) according to the kit instructions (Townsend et al., 2007). The kit reagents enzymatically reacted with LPS and subsequently resulted in a color change, which

can be measured spectrophotometrically. The LPS concentration was then normalized based on the final OD_{600} of the bacterial culture.

6.3.7. Human cell immune stimulation assays

THP-1 cells (ATCC TIB-202) were cultured with RPMI1640 supplemented with 10% FBS and 2 mM L-glutamine under a humidified 5% CO_2 atmosphere at 37°C in an incubator. The THP-1 monocytes were maturated by exposure to THP-1 cells in 100 ng/mL phorbol 12-myristate 13-acetate (PMA) for 48 hours. After maturation, THP-1 macrophages were cultured with the normal medium for further analysis. The THP-1-derived macrophages were then exposed to TET treated/control bacterial secretome for 24 hours. A blank control group and a vehicle control group (0.1% DMSO in a culture medium) were prepared in parallel with these experiments. Further, 100 ng/ml LPS was used as the positive control and 100 μg/mL polymyxin B (PMB) was used to dissociate the LPS, which was used as the negative control for the samples with the highest LPS concentration. The concentrations of tumor necrosis factor (TNF)-alpha, interleukin (IL)-6, and (IL)-1β in culture supernatants were determined using enzyme-linked immunosorbent assay (ELISA) kits from Wuhan Biotech Co, Ltd, PR China.

6.3.8. QA/QC and statistical analysis

For the QA/QC of metabolome and lipidome analysis, a pooled mix sample of metabolites/lipids prepared by pooling all treated and control samples were analyzed after every six injections of biological samples to correct the mass, retention time and response drift. All the data were expressed as mean ± standard error of the mean (SEM). Differences between groups or treatments were examined for statistical significance using Student's t-test or one-factor analysis of variance (*ANOVA*) with Duncan's post-hoc test, with the significance level set at p-value ≤ 0.05.

6.4. Results and Discussion

6.4.1. Secretome pretreatment and characterization

The filtrates from 30 and 10 kDa MW cut-off filters were first characterized by analyzing LPS concentration to observe whether those were successfully removed by the MW cut-off filtration. The results showed both 30 and 10 kDa filters could eliminate the LPS where its levels were similar to that in mGAM, the bacterial growth media (**Figure 6.1a**). For example, the LPS level in the unfiltered gut microbiome secretome was ~16791 eu/ml, while it was <15 eu/ml for both <30 and <10 kDa fractions. In addition, metabolites levels in the filtered and unfiltered secretome were analyzed to check whether the filters could retain the metabolites. According to our observations, the majority of the key metabolites were not significantly different from those in the unfiltered secretome, while only a few metabolites showed lower recovery upon filtration (**Figure 6.1b**). For instance, phenylalanine levels were significantly reduced in 27 and 23 % in <10 kDa and <30 kDa fractions; respectively, compared to unfiltered control, probably due to the retaining of those metabolites by the membrane. On the other hand, metabolites such as indolelactic acid, kynurenic acid, and *p*-cresol sulfate were slightly increased in 20, 16, and 28 % upon filtration through 10 kDa MW cut-off filters. Collectively, the results indicated that the MW cut-off filtration method used for the pre-treatment of the gut microbiome secretome could successfully remove large molecules such as LPS while keeping the levels of majority of the metabolites unaffected.

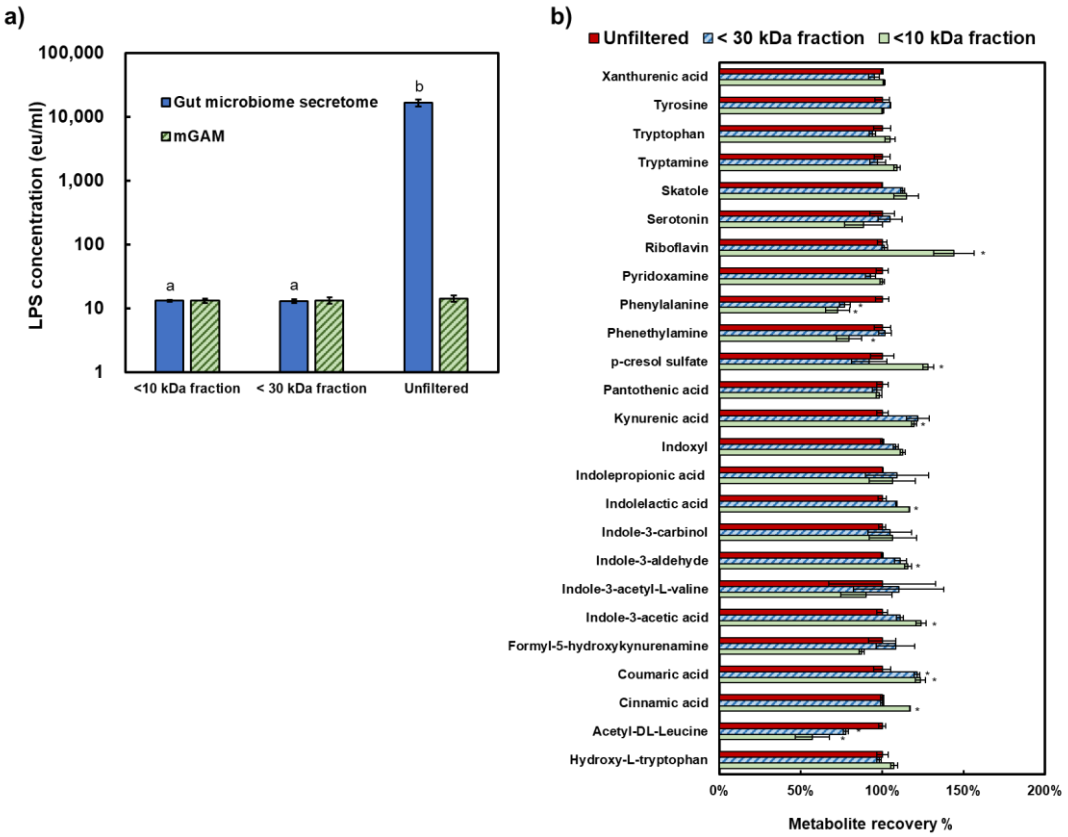

Figure 6.1. Characterization of the pretreated gut microbiome secretome
a) LPS concentration in the secretome. ("a" and "b" indicate the statistical significance ($p < 0.05$) with the filtered mGAM fraction at the same MW range and the unfiltered control from the same sample group; respectively) and b) metabolite recovery as the percentage of unfiltered control ("*" indicates the statistical significance (p-value ≤ 0.05) with the unfiltered control). All data presented as the mean ± SEM of three replicates.

6.4.2. Cell viability exposed to TET treated and pretreated gut microbiome secretome.

The HepG2 cells were first incubated with TET treated, non-treated gut microbiome secretome, and mGAM at different dilutions (i.e., 10, 20, 30, 40, and 50-times dilution) in the HepG2 growth media. The results showed that gut microbiome secretome (no TET) diluted 10, 20, and 30 times in the cell culture media could significantly affect the cell viability in ~52, 80, and 92 %; respectively, compared to DMSO control **(Figure 6.2a)**. Also, mGAM did not induce toxic effects on the HepG2 cells at any of the concentrations, suggesting that the metabolites produced by gut bacteria may induce toxic effects on the HepG2 cells. Furthermore, the effect

of TET treated gut microbiome secretome on cell viability was quite consistent with that in control (TET_0) secretome, where no significant difference between TET treated and control secretome treated groups was observed.

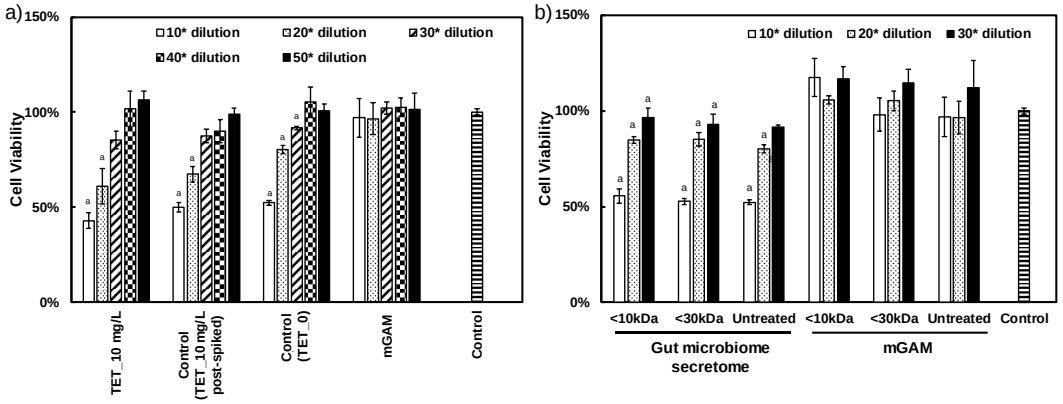

Figure 6.2. Viability of HepG2 cells exposed to TET treated and pretreated gut microbiome secretome
a) Exposure to TET 10 mg/L treated, control (TET 10 mg/L post-spiked), control (TET_0) gut microbiome secretome, and mGAM at different dilutions and b) Exposure to 10 and 30 kDa MW cut off filtered and unfiltered gut microbiome secretome and mGAM. "a" indicates the statistical significance (p-value ≤ 0.05) compared to the 0.1% DMSO control. Data presented as the mean ± SEM of three replicates.

We next assessed the cytotoxic effects of the gut microbiome secretome filtered using MW cut-off filters. There was no significant difference between the MW cut-off filtered and unfiltered secretome on the cell viability (**Figure 6.2b**). The results suggest that the toxic effects induced on HepG2 cells may be mediated by low MW metabolites. Cytotoxicity of fecal water on colonic epithelial cells has previously been reported (Federici et al., 2017) even though there is no direct evidence for cytotoxic effects on liver cells. In addition, some fecal metabolites such as *p*-cresol are known to show toxicity on human cancer cells (Andriamihaja et al., 2015).

6.4.3. Lipid dysregulations in the HepG2 cells induced by TET treated low MW fraction of the gut microbiome secretome

A substantial amount of the low MW metabolites produced by the gut microbiome are detected in portal blood, and therefore, those can be available in the hepatocytes (Matsumoto et al., 2017). Thus, the next target was to understand the lipid changes

solely caused by TET altered low MW (<10 kDa) metabolites. Accordingly, the composition of the lipidome between HepG2 cells treated with TET 10 mg/L treated and control (TET 10 mg/L post-spiked) gut microbiome secretome was compared. For the lipid identification, 118, 167, and 66 lipids belonging to glycerophospholipid, glycerolipid, and sphingolipid lipid classes were annotated; respectively, which was the three most abundant lipid classes (**Figure 6.3a and Table B12–B14**). None of these lipid classes significantly were differed between the two groups; however, a slight increase in phosphoethanolamines (PE) was observed. The analysis of total lipid features detected by pairwise lipidomics analysis between TET 10 mg/L dosed and control (TET 10 mg/L post-spiked) gut microbiome secretome revealed the HepG2 cells treated with TET 10 mg/L dosed secretome had more upregulated features than the downregulated features. Particularly, the majority of the significant features (|fold change| > 1.2, *p*-value ≤0.05, abundance>10,000) were upregulated, which is ~1.8 folds higher compared to downregulated features (**Figure 6.3b).** The observation was consistent for the identified significant lipid features as well. As shown in **Figure 6.3c**, among the 116 identified significant lipid features 79 were significantly upregulated while only 37 were downregulated. For example, lipids belong to DAG subclass were upregulated in 1.2-3.6 folds. Collectively, the low MW metabolic dysregulation in the gut microbiome secretome caused by TET exposure may contribute to the liver lipid accumulation even though a significant change in the lipids belongs to a particular lipid class was not observed. Accumulation of liver lipids upon antibiotic treatment has been shown using rodent models (Cho et al., 2012; Jin et al., 2016). However, this is the first time to use an *in vitro* experimental setup to observe the liver lipid accumulation, an obesity-related complication, mediated solely through small molecules in the gut microbiome secretome altered by TET exposure. Interestingly, this observation was also consistent with liver lipid accumulation and increased body weight gain in zebrafish upon TET exposure, as revealed in the first part of the thesis (see **Chapter 3**).

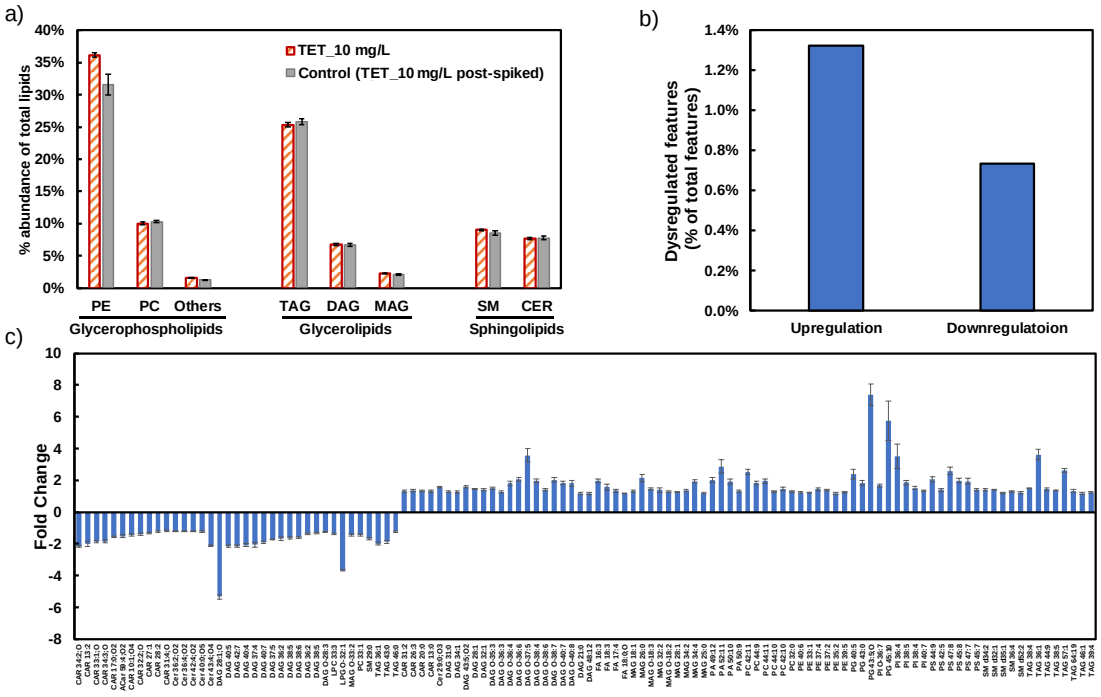

Figure 6.3. Lipid alterations in the HepG2 cells exposed to TET treated low MW fraction of the gut microbiome secretome

Bar graph representation of lipid classes as a percentage of total identified lipids ("*" indicates the statistical significance (p-value < 0.05) between TET 10 mg/L treated and control (TET 10 mg/L post-spiked) gut microbiome secretome dosed groups); (b) Up and down regulated significant features detected by pairwise comparison of global lipid profiling (|fold change| > 1.2, p-value ≤ 0.05, abundance>10,000, percentage was calculated based on total detected feature numbers for each condition); and (c) fold change of identified significant lipids ((|fold change| > 1.2, p-value ≤ 0.05) relative to control (TET 10 mg/L post-spiked) group. Data presented as the mean ± SEM of five replicates. PC, phosphatidylcholine; PE, phosphatidylethanolamine; DAG, diglyceride; TAG, triglyceride: MAG, monoglyceride; SM, sphingomyelins; Cer, ceramide.

6.4.4. Liver lipid accumulation and gut bacterial metabolites

There are many mechanistic pathways in which the disrupted microbiome can contribute to obesity and obesity-related complications by altering energy extraction from food or altering inflammation and immunity (Cox and Blaser, 2013). However, there are limited possible mechanisms mediated through the direct action of low MW metabolites (<10 kDa), which can be involved in obesity-related complications such as liver fat accumulation. One such possible mechanism is obesity and hepatic steatosis induced by activation of aryl hydrocarbon receptor (AHR). AHR is known to

play a broad role in disrupting fat metabolism and contribute to non-alcoholic steatohepatitis in obesity and associated complications such as liver fat accumulation (He et al., 2013; Krishnan et al., 2018; Xu et al., 2016). Metabolomics analysis of the gut microbiome secretome (**Section 5.4.5**) used to treat HepG2 cells showed altered levels of AHR agonists such as tryptamine (0.9 folds), indole-3-aldehyde (1.2 folds), indolelactic acid (5.4 folds), kynurenic acid (0.9 folds), hydroxy-L-tryptophan (1.4 folds), and xanthurenic acid (0.3 folds) upon TET treatment at the fed state (Bittinger et al., 2003; Hendrikx and Schnabl, 2019; Hubbard et al., 2015; Jin et al., 2014; Zelante et al., 2013). Reduced gut microbiome produced tryptamine levels related to liver lipid accumulation has also been reported (Krishnan et al., 2018). However, concluding their overall action on AHR is challenging as the metabolic dysregulations in the TET treated gut microbiome secretome may induce contradictory effects on AHR activation. Moreover, this may be the reason for not observing apparent changes in lipid subclasses. In addition, elevated BCAAs that occurred in the gut microbiome secretome upon TET treatment may also contribute to accumulated liver lipid levels. Highly upregulated levels of BCAAs (i.e., leucine 15.6 in folds and valine in 13 folds) were observed in the TET 10 mg/L treated gut microbiome secretome (**Section 5.4.4**). A positive association between elevated plasma BCAA levels and the elevated fatty liver index has been shown before (van den Berg et al., 2019). Collectively, TET-induced alterations in the gut microbiome metabolites at the low MW range have the possibility to contribute the liver lipid accumulation through different possible mechanisms.

6.4.5. Effect of TET exposure on LPS mediated host immune response

LPS excreted from bacteria is an immunoregulatory compound that facilitates the host immune system-gut microbiome interactions (Raetz and Whitfield, 2002; Round and Mazmanian, 2009; Yoo and Lee, 2016). Notably, LPS is known to link with increased host body weight gain through several mechanisms (Cox and Blaser, 2013). Knowing the antibiotics can affect the LPS release from bacteria, we were next interested in observing the effect of TET exposure on the LPS release by the gut microbiome. LPS level in the gut microbiome secretome measured by LAL assay did not showsignificant change upon TET treatment at 10 mg/L, compared to the control

(TET 10 mg/L post-spiked) (**Figure 6.4**). This observation indicates that the TET at the clinically relevant dose may not affect the LPS release by gut microbiome and may not involve in the modulation of immune system responses mediated through LPS.

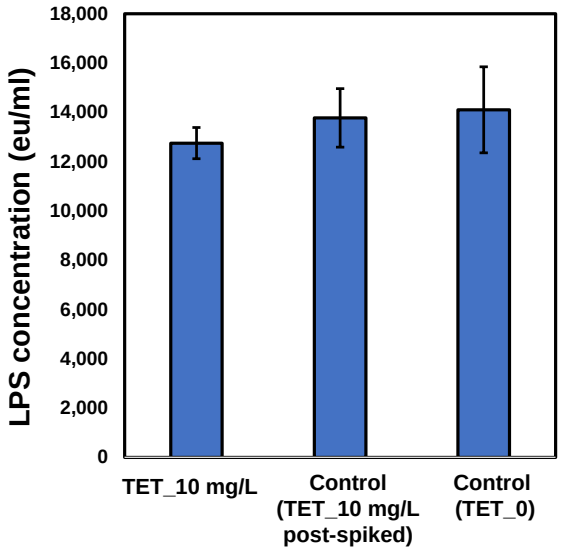

Figure 6.4. LPS concentration in the TET treated gut microbiome secretome
The data presented as the mean ± SEM of five replicates. "a" and "b" indicate the statistical significance (*p*-value ≤ 0.05) compared to the control (TET_0) and the control (TET 10 mg/L post-spiked); respectively.

We were next interested to understand the contribution of bacterial strains in the gut microbiome, which contribute to the total LPS pool in the gut. Gut LPS is primarily derived from dominant Gram-negative bacterial order *Bacteroidales,* and LPS of *E. coli* origin also substantially contribute to the gut LPS pool (d'Hennezel et al., 2017; Vatanen et al., 2016). Thus, we first determined the impact of TET on the LPS concentration in the secretome two model Gram-negative bacteria: *B. fragilis* from the order *Bacteroidales* and *E. coli*. Both model bacteria were treated with three different doses of TET, IC_{90}, IC_{50}, and dietary level exposure concentration, which denotes by high, mid, and low; respectively. As shown in **Figure 6.5a**, the LPS concentration measured by LAL assay was significantly higher in the *E. coli* treated with TET, with a fold change of 1.8, 1.6, and 1.2 for high, medium, and low dose exposure; respectively. In contrast, *B. fragilis* showed a slightly decreasing trend, with increasing TET levels.

We further confirmed the secretome-induced immune response by the inflammatory cytokine production of THP-1 macrophages cells dosed with the bacterial secretome. Generally, the cytokine (i.e. (TNF)-alpha, (IL)-6, and (IL)-1β) release with *E. coli* secretome was comparatively higher than that in *B. fragilis* (**Figure 6.5b**). A clear dose-response relationship with TET was observed for *E. coli*, where there was a lack of or slight increase with the *B. fragilis* secretome. Besides LPS, many other gut microbiota-derived metabolites, such as SCFAs and indoles, have been reported to modulate the immune response (Corrêa-Oliveira et al., 2016; Gao et al., 2018). To estimate the contribution of LPS in the cytokine production, we applied PMB to dissociate the LPS and observed a significant reduction of cytokine production in PMB treated *E. coli* secretome at the high level of TET, suggesting the primary involvement of *E. coli* LPS on the immune response modulation (**Figure 6.5b**).

Due to the difference in the effects of TET on *B. fragilis* and *E. coli* LPS activity, we were interested in observing the LPS activity in a bacteria mixture. Furthermore, a recent study reported the inhibition of immune response induced by *E. coli* by the LPS of *Bacteroides* species (Vatanen et al., 2016). Thus, we further expanded our study to observe the combined effect of the secretome of two bacteria under TET exposure. Generally, the dosing of increasing amount of *B. fragilis* secretome to the constant volume of *E. coli* secretome inhibited the total LPS activity in the mixture, regardless of the TET level (**Figure 6.5c**), reconfirming the neutralization effect of *B. fragilis* derived LPS on *E. coli* derived LPS. More interestingly, we have observed the effect of TET on the increase of LPS activity was highly dependent on the ratio of *B. fragilis* to *E. coli* LPS. For instance, at 0.01:1 to 1:1 ratios of *B. fragilis*:*E. coli* LPS, the fold change of LPS activity compared to control under the high TET exposure is in the range of 1.6-1.9, while the fold change was reduced to 1.3 at 10:1 ratio of *B. fragilis*:*E. coli* LPS. At the low exposure level of TET, the LPS activity change was even lower than 1 (i.e., 0.6) when *B. fragilis* was dominant (ratio: 10:1). Collectively, our results imply that the total LPS activity and the immune dysregulations caused in response to TET is highly dependent on the *B. fragilis*:*E. coli* ratio and thereby can vary upon the individual, according to their gut microbiome composition. A few previous studies have suggested that the immune response has relied on the ratio between *Bacteroidetes*-to-*E. coli* LPS (d'Hennezel et al., 2017;

Vatanen et al., 2016). Furthermore, the production of an antagonistic form of lipopolysaccharide (LPS) *Bacteroides dorei* has been reported in a recent study, even though the mechanism is yet to be explored (Vatanen et al., 2016). The ratio of *B. fragilis*:*E. coli* in the gut can greatly vary between individuals, based on a number of other reasons, such as diet, age, disease, and geological locations. For instance, the relative abundance of *E. coli* is low compared to that of *B. fragilis* in the gut microbiome of Russian infants, while the relative abundance of *B. fragilis* increased over *E. coli* with age. In contrast, the relative abundance of *B. fragilis* is higher than *E. coli* in Finnish and Estonian infants, without significant temporal variation (Vatanen et al., 2016). Thus, we can expect a personalized response from the host immune system to the gut microbiome exposure of TET.

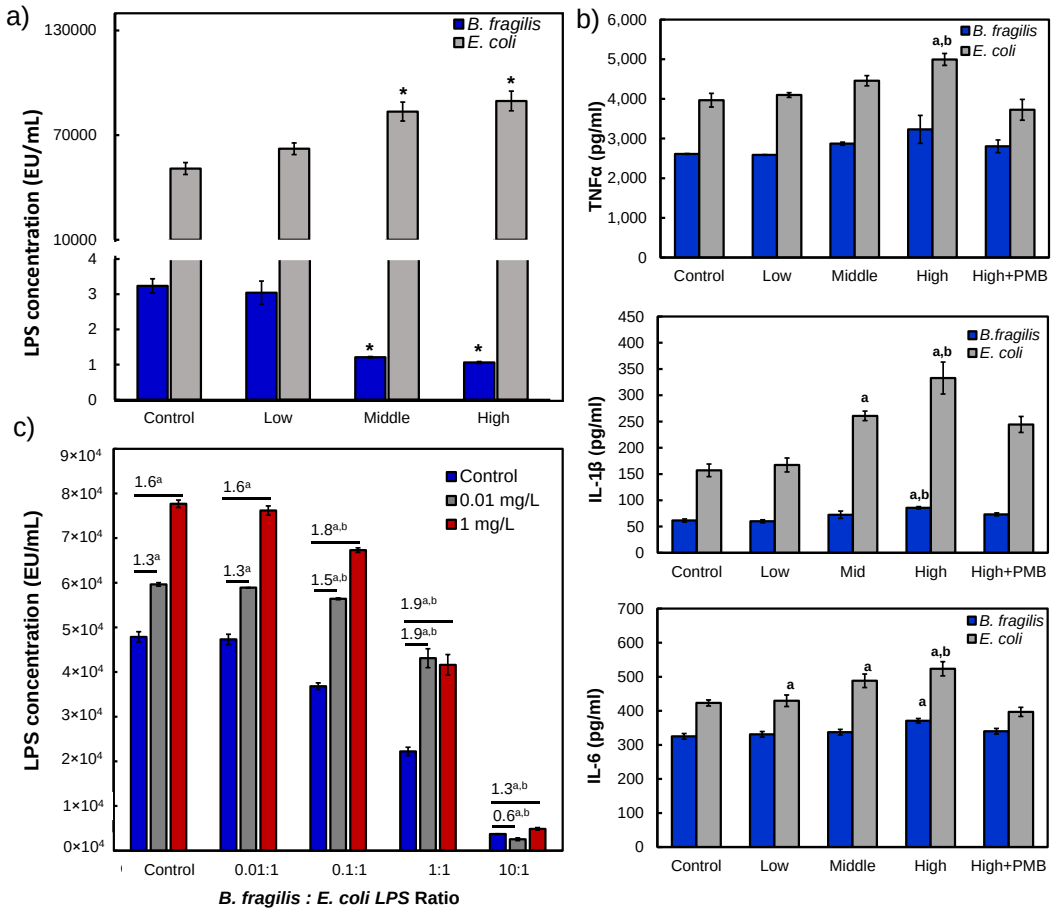

Figure 6.5. Immunogenicity of the secretome from different bacterial strains under TET exposure

a) secretome LPS concentration of *E. coli* and *B. fragilis* under TET exposure. ("*" indicates the statistical significance (p-value ≤ 0.05) with no TET treatment); b) cytokine production by the secretome of *B. fragilis and E. coli* treated with different

levels of TET. ("a" and "b" indicate the statistical significance (p-value ≤ 0.05) compared to the control and the PMB treated secretome; respectively); and c) inhibition of *E. coli* LPS at different ratios of *B. fragilis*:*E. coli* LPS under TET exposure. ("a" and "b" indicate the statistical significance (p-value ≤ 0.05) compared to the control with no *B. fragilis* and to the control with no TET at the same ratio of *B. fragilis*:*E. coli* LPS; respectively).

6.5. Short Summary

This study explored the contribution of low MW metabolites and immunoregulatory compounds (i.e., LPS) in the gut microbiome secretome affected by TET exposure to the host weight gain and related complications using an *in vitro* liver cell model. The results indicated the involvement of low MW metabolites on the liver lipid accumulation probably by AHR mediated mechanism through tryptophan and indole derivatives, which act as AHR agonists. In addition, the involvement of elevated BCAAs also can be speculated. However, future studies are warranted to elucidate the underline mechanism for TET-induced liver fat accumulation. In contrast, TET exposure did not affect the LPS release from *in vitro* gut microbiome, possibly ruling out the contribution of TET affected LPS release to host obesity. However, some further investigation can be made on the dependence of TET affected gut microbiome LPS secretion and immune response on the gut microbiome with different community structures by involving the complex interaction between LPS from different bacteria.

Chapter 7. Conclusions and Recommendations

7.1 Conclusions

The first section of the thesis investigated the toxic effects of long-term TET exposure at low or environmentally relevant levels on zebrafish. The low or environmentally relevant levels of TET could increase the zebrafish body weight with hepatic lipid accumulation when the exposure starts from the juvenile period. Induced expression of genes related to hepatic lipid metabolism and the altered hepatic metabolites, which probably can be linked with lipid accumulation, was also observed. In addition, TET exposure could increase the community diversity and some known obesogenic factors such as Firmicutes/ Bacteroidetes ratio in the zebrafish gut microbiome. On the whole, a possible link between increased zebrafish body weight gain and the TET mediated dysbiosis of gut microbiota can be speculated.

The study next investigated the TET-induced metabolic dysregulations in three model gut bacteria including *B. fragilis*, *C. sporogenes*, and *E. coli*, which represent several types of the most abundant bacterial genera in the gut. The study found a species-specific, concentration-dependent metabolic response of model gut bacteria towards TET. Notably, *B. fragilis* was highly sensitive to TET exposure, while TET generated the lowest metabolic response in *C. sporogenes*. Overall, this finding suggests the possible incidence of metabolic consequences by altered Firmicutes to Bacteroides ratio, which can be linked to the increased host body weight gain. Furthermore, TET exposure resulted in dysregulations in several metabolic pathways, known to be related to several host diseases, such as weight gain and diabetes in model bacterial strains. In addition, dysregulation of nucleotide, amino acid, vitamin, and FA metabolism at dietary dose emphasizes the risk of facing alterations in the gut microbiome of non-antibiotic users.

Furthermore, the *in vitro* study aimed to understand the response of the gut microbiome at the fed and fasted states towards TET exposure revealed a significant alteration in the gut microbiome metabolome at the fed state in a TET dose-dependent manner. Important gut microbial metabolites with host health implications including

tryptophan and indole derivatives, tyrosine and phenyl derivatives, and vitamins were significantly altered at the fed state under the clinical dose of TET. Interestingly, some of these metabolites were still responsive under the dietary dose of TET at the fed state. In contrast, both nutrients as well as the gut microbial metabolites were less responsive at the fasted state compared to the significant, apparent alterations at the fed state. The majority of responsive nutrients and metabolites have been known to modulate host health, and thus a significant, feeding state-dependent impact of TET exposure on the host health can be expected.

Lastly, the metabolic and immunological contribution of TET altered gut microbiome on increased host body weight gain and related complications was tentatively investigated. The contribution of low MW metabolites on the liver lipid accumulation probably by AHR mediated mechanism through tryptophan and indole derivatives which act as AHR ligands can be postulated. In addition, the involvement of elevated BCAAs in liver lipid accumulation also can be speculated. The result of immune response and LPS activity revealed that TET could not significantly affect the gut microbiome LPS production. However, the impact of TET on LPS release was observed to be highly bacteria-dependent and varied with the ratio of *B. fragilis:E. coli*, which can be different for each individual. Therefore, it is likely that the risk of TET exposure from either sub-pharmaceutical or dietary exposure depends on the gut bacterial composition.

In sum, the major conclusions and contributions of this study were:

(i) revealing the long-term exposure to low or environmentally relevant levels of TET could increase the zebrafish body weight gain with hepatic lipid accumulation and gut microbiome alteration (i.e., increased diversity and increased obesogenic factors) when the exposure starts from the juvenile period.

(ii) revealing the species-specific, concentration-dependent metabolic dysregulations induced by TET in model gut bacteria, which represent several types of the most abundant bacterial genera in the gut microbiome.

(iii) revealing the higher impact of TET exposure on gut microbiome secretome metabolome in a TET dose-dependent manner under the fed state compared to

that in the fasted state, altering important gut microbial metabolites with host health implications.

(iv) revealing the contribution of low MW metabolites to the liver lipid accumulation probably by AHR mediated mechanism through tryptophan and indole derivatives which act as AHR agonists and/or through a mechanism involved with elevated BCAAs.

(v) revealing no change in gut microbiome LPS secretion upon TET exposure, possibly ruling out the contribution of TET affected LPS release to the host body weight gain.

7.2 Recommendations

There are a number of knowledge gaps related to TET exposure of aquatic organisms and gut microbiome mediated toxicity are addressed by our findings and would benefit from further research:

The host effects such as increased body weight gain and liver lipid accumulation with the altered gut microbiome are revealed upon long-term TET exposure of juvenile zebrafish. However, an apparent influence of the gut microbiome on the observed host effects cannot be elucidated. Future studies can be conducted to understand the contribution of the gut microbiome to the TET-induced host effects (i.e., using germ-free zebrafish models and fecal transplantation).

The metabolic alterations induced by TET exposure only on three model bacteria were investigated in this study. However, the actual gut microbiome is a more complex system with thousands of different bacterial species with different characteristics. Thus, a higher number of model bacterial strains that cover the majority of the gut microbial community members can be considered in future studies to analyze the metabolic response. Also, high throughput metabolomics sample preparation and profiling methods can be considered for improved efficiency.

The impact of the feeding state on the gut microbiome metabolic alterations induced by TET was revealed in this study. However, only two feeding states, which represent the fed and fasted states, were considered in this study, where the fed state conditions

were achieved by supplying extra nutrients by adding additional growth media. Even though the growth media used, mGAM is suitable for culturing gut bacteria, the real nutrients provided by food intake may differ from it. Thus, the nutrients supplied by different food mixtures can be considered in future studies. Furthermore, the effect of more specific nutrition statuses such as high-fat, high-protein, or fiber-rich conditions on the impact of TET on gut microbiota can be further investigated.

The study used the *in vitro* liver cell model revealed the contribution of TET altered low MW weight metabolites on liver lipid accumulation through a few different possible mechanisms. However, future studies are warranted to elucidate the underline mechanism for TET-induced liver fat accumulation. In addition, the contribution of TET affected LPS release by gut microbiome to increased host body weight gain can be possibly ruled out due to unaffected gut microbiome LPS release by TET exposure. Further investigation can be made on the dependence of TET affected gut microbiome LPS secretion and immune response on the gut microbiome with different community structures by involving the complex interaction between LPS from different bacteria. Gut microbial communities established from the fecal samples from a large cohort with different gut microbiome composition (difference in age, gender, and diet can be considered when selecting donors) can be used for the investigation. Lastly, the TET's effect on other pathways in microbe-involved obesity can be further investigated.

References

Aalipour, F., Mirlohi, M., Jalali, M., and Azadbakht, L. (2015). Dietary exposure to tetracycline residues through milk consumption in Iran. Journal of Environmental Health Science and Engineering, **13**(1), 80.

Agwuh, K. N., and MacGowan, A. (2006). Pharmacokinetics and pharmacodynamics of the tetracyclines including glycylcyclines. Journal of Antimicrobial Chemotherapy, **58**(2), 256–265.

Almeida, A. R., Alves, M., Domingues, I., and Henriques, I. (2019). The impact of antibiotic exposure in water and zebrafish gut microbiomes: A 16S rRNA gene-based metagenomic analysis. Ecotoxicology and Environmental Safety, **186:** 109771.

Anderson, M. J. (2001). A new method for non-parametric multivariate analysis of variance. Austral Ecology, **26**, 32–46.

Andriamihaja, M., Lan, A., Beaumont, M., Audebert, M., Wong, X., Yamada, K., Yin, Y., Tomé, D., Carrasco-pozo, C., Gotteland, M., Kong, X., and Blachier, F. (2015). The deleterious metabolic and genotoxic effects of the bacterial metabolite p-cresol on colonic epithelial cells. Free Radical Biology and Medicine, **85**, 219–227.

Antunes, L. C. M., Han, J., Ferreira, R. B. R., Lolić, P., Borchers, C. H., and Finlay, B. B. (2011). Effect of antibiotic treatment on the intestinal metabolome. Antimicrobial Agents and Chemotherapy, **55**(4), 1494–1503.

Arikan, O. A., Rice, C., and Codling, E. (2008). Occurrence of antibiotics and hormones in a major agricultural watershed. Desalination, **226**, 121–133.

Arumugam, M., Raes, J., Pelletier, E., Paslier, D. Le, Yamada, T., Mende, D. R., Fernandes, G. R., Tap, J., Bruls, T., Batto, J., Bertalan, M., Borruel, N., Consortium, M., Weissenbach, J., Ehrlich, S. D., and Bork, P. (2011). Enterotypes of the human gut microbiome. Nature, **473**(7346), 174–180.

Bäckhed, F., Ley, R. E., Sonnenburg, J. L., Peterson, D. A., and Gordon, J. I. (2005). Host-bacterial mutualism in the human intestine. Science, **307**(5717), 1915–1920.

Barouei, J., Bendiks, Z., Martinic, A., Mishchuk, D., Heeney, D., Hsieh, Y. H., Kieffer, D., Zaragoza, J., Martin, R., Slupsky, C., and Marco, M. L. (2017). Microbiota, metabolome, and immune alterations in obese mice fed a high-fat diet containing type 2 resistant starch. Molecular Nutrition and Food Research, **61**(11).

Behr, C., Kamp, H., Fabian, E., Krennrich, G., Mellert, W., Peter, E., Strauss, V., Walk, T., Rietjens, I. M. C. M., and van Ravenzwaay, B. (2017). Gut microbiome-related metabolic changes in plasma of antibiotic-treated rats. Archives of Toxicology, **91**(10), 3439–3454.

Behr, C., Sperber, S., Jiang, X., Strauss, V., Kamp, H., Walk, T., Herold, M., and Beekmann, K. (2018). Microbiome-related metabolite changes in gut tissue, cecum content and feces of rats treated with antibiotics. Toxicology and Applied Pharmacology, **355**, 198–210.

Belenky, P., Ye, J. D., Porter, C. B. M., Cohen, N. R., Michael, A., Ferrante, T., Jain, S., Korry, B. J., Schwarz, E. G., Walker, G. C., and Collins, J. J. (2015). Bactericidal antibiotics induce toxic metabolic perturbations that lead to cellular damage. Cell Reports, **13**(5), 968-980.

Besten, G. den, Eunen, K. van, Groen, A. K., Venema, K., and Dirk-Jan Reijngoud, B. M. B. (2013). The role of short-chain fatty acids in the interplay between diet, gut microbiota, and host energy metabolism. Journal of Lipid Research, **54**(9), 2325–2340.

Beyer, B. A., Fang, M., Sadrian, B., J Rafael Montenegro-Burke, W. C. P., Kok, B. P. C. C., Saez, E., Kondo, T., Siuzdak, G., Lairson, L. L., Montenegro-Burke, J. R., Plaisted, W. C., Kok, B. P. C. C., Saez, E., Kondo, T., Siuzdak, G., and Lairson, L. L. (2018). Metabolomics-based discovery of a metabolite that enhances oligodendrocyte maturation. Nature Chemical Biology, **14**(1), 22–28.

Bilandžić, N., Kolanović, B. S., Varenina, I., Scortichini, G., Annunziata, L., Brstilo, M., and Rudan, N. (2011). Veterinary drug residues determination in raw milk in Croatia. Food Control, **22**(12), 1941–1948.

Bittinger, M. A., Nguyen, L. P., and Bradfield, C. A. (2003). Aspartate aminotransferase generates proagonists of the aryl hydrocarbon receptor. Molecular Pharmacology, **64**(3), 550–556.

Borghi, A. A., and Palma, M. S. A. (2014). Tetracycline: Production, waste treatment and environmental impact assessment. Brazilian Journal of Pharmaceutical Sciences, **50**(1), 25–40.

Boxall, A. B. A., Kolpin, D. W., Halling-Sorensen, B., and Tolls, J. (2003). Are veterinary medicines causing environmental risks? Environmental Science and Technology, **37**(15), 286A-294A.

Bu, Q., Wang, B., Huang, J., Deng, S., and Yu, G. (2013). Pharmaceuticals and personal care products in the aquatic environment in China: A review. Journal of Hazardous Materials, **262**, 189–211.

Carman, R. J., Simon, M. A., Petzold, H. E., Wimmer, R. F., Batra, M. R., Fernández, A. H., Miller, M. A., and Bartholomew, M. (2005). Antibiotics in the human food chain: Establishing no effect levels of tetracycline, neomycin, and erythromycin using a chemostat model of the human colonic microflora. Regulatory Toxicology and Pharmacology, **43**(2), 168–180.

Cervenka, I., Agudelo, L. Z., and Ruas, J. L. (2017). Kynurenines: Tryptophan's metabolites in exercise, inflammation, and mental health. Science, **357**(6349): eaaf9794.

Cháfer-Pericás, C., Maquieira, Á., Puchades, R., Miralles, J., and Moreno, A. (2011). Multiresidue determination of antibiotics in feed and fish samples for food safety evaluation. Comparison of immunoassay vs LC-MS-MS. Food Control, **22**(6), 993–999.

Chen, S., Hoene, M., Li, J., Li, Y., Zhao, X., Häring, H. U., Schleicher, E. D., Weigert, C., Xu, G., and Lehmann, R. (2013). Simultaneous extraction of metabolome and lipidome with methyl tert-butyl ether from a single small tissue sample for ultra-high performance liquid chromatography/mass spectrometry. Journal of Chromatography A, **1298**, 9–16.

Chen, X., and Devaraj, S. (2018). Gut microbiome in obesity, metabolic syndrome, and diabetes. Current Diabetes Reports, **18**(12): 129

Chen, Y., Jiang, X., Xiao, K., Shen, N., Zeng, R. J., and Zhou, Y. (2017). Enhanced volatile fatty acids (VFAs) production in a thermophilic fermenter with stepwise pH increase - Investigation on dissolved organic matter transformation and microbial community shift. Water Research, **112**, 261–268.

Cheng, L., and Snell, J. F. (1961). Effects of tetracyclines, some of their derivatives, and chloramphenicol on accumulation of glutamic acid in *Escherichia coli*. Journal of Bacteriology, **83(**4), 711–719.

Cho, I., Yamanishi, S., Cox, L., Methé, B. A., Zavadil, J., Gao, Z., Mahana, D., Raju, K., Teitler, I., Li, H., Alexander, V., Li, K., Gao, Z., Mahana, D., Raju, K., Teitler, I., Li, H., Alekseyenko, A. V., and Blaser, M. J. (2012). Antibiotics in early life alter the murine colonic microbiome and adiposity. Nature, **488**(7413), 621–626.

Chong, J., Liu, P., Zhou, G., & Xia, J. (2020). Using MicrobiomeAnalyst for comprehensive statistical, functional, and meta-analysis of microbiome data. Nature Protocols, **15**(3), 799-821.

Chopra, I., and Roberts, M. (2001). Tetracycline antibiotics: mode of action, applications, molecular biology, and epidemiology of bacterial resistance. Microbiology and Molecular Biology Reviews, **65**(2), 232–260.

Claus, S. P., Guillou, H., and Ellero-simatos, S. (2016). The gut microbiota: A major player in the toxicity of environmental pollutants? Biofilms and Microbiomes, **2**: 16003.

Conlon, M. A., and Bird, A. R. (2015). The impact of diet and lifestyle on gut microbiota and human health. Nutrients, **7**(1), 17–44.

Corrêa-Oliveira, R., Fachi, J. L., Vieira, A., Sato, F. T., and Vinolo, M. A. R. (2016). Regulation of immune cell function by short-chain fatty acids. Clinical and Translational Immunology, **5**(4): e73.

Cox, L. M., and Blaser, M. J. (2013). Pathways in microbe-induced obesity. Cell Metabolism, **17**(6), 883–894.

Cox, L. M., Yamanishi, S., Sohn, J., Alekseyenko, A. V., Leung, J. M., Cho, I., Kim, S. G., Li, H., Gao, Z., Mahana, D., Zárate Rodriguez, J. G., Rogers, A. B., Robine, N., Loke, P., and Blaser, M. J. (2014). Altering the intestinal microbiota during a critical developmental window has lasting metabolic consequences. Cell, **158**(4), 705–721.

d'Hennezel, E., Abubucker, S., Murphy, L. O., and Cullen, T. W. (2017). Total Lipopolysaccharide from the Human Gut Microbiome Silences Toll-Like Receptor Signaling. Host-Microbe Biology, **2**(6): e00046-17.

De Filippo, C., Cavalieri, D., Di Paola, M., Ramazzotti, M., Poullet, J. B., Massart, S., Collini, S., Pieraccini, G., Lionetti, P., Filippo, C. De, Cavalieri, D., Di, M., Ramazzotti, M., and Baptiste, J. (2010). Impact of diet in shaping gut microbiota revealed by a comparative study in children from Europe and rural Africa. Proceedings of the National Academy of Sciences, **107**(33), 14691–14696.

Dehhaghi, M., Kazemi Shariat Panahi, H., and Guillemin, G. J. (2019). Microorganisms, tryptophan metabolism, and kynurenine pathway: a complex interconnected loop influencing human health status. International Journal of Tryptophan Research, **12**: 1178646919852996.

Dekaboruah, E., Vasant, M., Dixita, S., Anil, C., and Verma, K. (2020). Human microbiome: An academic update on human body site specific surveillance and its possible role. Archives of Microbiology, **202**(8), 2147–2167.

Deng, W. J., Li, N., and Ying, G. G. (2018). Antibiotic distribution, risk assessment, and microbial diversity in river water and sediment in Hong Kong. Environmental Geochemistry and Health, **40**(5), 2191-2203.

Dethlefsen, L., and Relman, D. A. (2011). Incomplete recovery and individualized responses of the human distal gut microbiota to repeated antibiotic perturbation. Proceedings of the National Academy of Sciences, **108**(Supplement 1), 4554–4561.

Devillard, E., McIntosh, F. M., Duncan, S. H., and Wallace, R. J. (2007). Metabolism of linoleic acid by human gut bacteria: Different routes for biosynthesis of conjugated linoleic acid. Journal of Bacteriology, **189**(6), 2566–2570.

Dodd, D., Spitzer, M. H., Treuren, W. Van, Merrill, B. D., Hryckowian, A. J., Fischbach, M. A., Sonnenburg, J. L., Higginbottom, S. K., Le, A., Cowan, T. M., and Garry, P. (2017). A gut bacterial pathway metabolizes aromatic amino acids into nine circulating metabolites. Nature, **551**(7682), 648–652.

Dong, W., Macaulay, L. J., Kwok, K. W., Hinton, D. E., Ferguson, P. L., and Stapleton, H. M. (2014). The PBDE metabolite 6-OH-BDE 47 affects melanin pigmentation and THRβ mRNA expression in the eye of zebrafish embryos. Endocrine Disruptors, **2**(1), 139–148.

Donia, M. S., and Fischbach, M. A. (2016). Small Molecules from the Human Microbiota. Science, **349**(6246): 1254766.

Duncan, S. H., Hold, G. L., Harmsen, H. J. M., Stewart, C. S., and Flint, H. J. (2002). Growth requirements and fermentation products of *Fusobacterium prausnitzii*, and a proposal to reclassify it as *Faecalibacterium prausnitzii* gen. nov., comb. nov. International Journal of Systematic and Evolutionary Microbiology, **52**(6), 2141–2146.

Eagle, H., and Saz, A. K. (1954). Antibiotics. Annual Review of Microbiology, **9**, 173–226.

Eckburg, P., Bik, E. M., Bernstein, C. N., Purdom4, E., Dethlefsen, L., Sargent, M., Gill5, S. R., Nelson, K. E., and Relman, D. A. (2010). Diversity of the human intestinal microbial flora. Science, **308**(5728), 1635–1638.

Elshorbagy, A. K., Nijpels, G., Valdivia-Garcia, M., Stehouwer, C. D. A., Ocke, M., Refsum, H., and Dekker, J. M. (2013). S-adenosylmethionine is associated with fat mass and truncal adiposity in older adults. The Journal of Nutrition, **143**(12), 1982–1988.

Esteves, A., Knoll-Gellida, A., Canclini, L., Silvarrey, M. C., André, M., and Babin, P. J. (2016). Fatty acid binding proteins have the potential to channel dietary fatty acids into enterocyte nuclei. Journal of Lipid Research, **57**(2), 219–232.

Evans, M. E., and Pollack, M. (1993). Effect of antibiotic class and concentration on the release of lipopolysaccharide from *Escherichia coli*. The Journal of Infectious Diseases, **167**(6), 1336–1343.

Fabbrini, E., Sullivan, S., and Klein, S. (2010). Obesity and nonalcoholic fatty liver disease: biochemical, metabolic and clinical implications. Hepatology, **51**(2), 679–689.

Fang, M., Ivanisevic, J., Benton, H. P., Johnson, C. H., Patti, G. J., Hoang, L. T., Uritboonthai, W., Kurczy, M. E., and Siuzdak, G. (2015). Thermal degradation of small molecules: A global metabolomic investigation. Analytical Chemistry, **87**(21), 10935–10941.

Fayolle, F., Privitera, G., and Sebald, M. (1980). Tetracycline transport in *Bacteroides fragilis*. Antimicrobial Agents and Chemotherapy, **18**(4), 502–505.

Federici, E., Prete, R., Lazzi, C., Pellegrini, N., Moretti, M., Corsetti, A., and Cenci, G. (2017). Bacterial composition, genotoxicity, and cytotoxicity of fecal samples from individuals consuming omnivorous or vegetarian diets. Frontiers in Microbiology, **8**: 300.

Finlay, A. C., Hobby, G. L., P, S. Y., Regna, P. P., Routien, J. B., Seeley, D. B., Shull, M., Sobin, B. A., Solomons, I. A., Vinson, J. W., and Kane, J. H. (1950). Terramycin, a new antibiotic. Science, **111**(2874): 85.

Food and Drug Administration. (2017). Summary report on antimicrobials sold or distributed for use in food-producing animals.

Francino, M. P. (2016). Antibiotics and the human gut microbiome: Dysbioses and accumulation of resistances. Frontiers in Microbiology, **6**: 1543.

Fujisaka, S., Ussar, S., Clish, C., Devkota, S., Dreyfuss, J. M., Sakaguchi, M., Soto, M., Konishi, M., Softic, S., Altindis, E., Li, N., Gerber, G., Bry, L., and Kahn, C. R. (2016). Antibiotic effects on gut microbiota and metabolism are host dependent. Journal of Clinical Investigation, **126**(12), 4430–4443.

Gao, J., Xu, K., Liu, H., Liu, G., Bai, M., Peng, C., Li, T., and Yin, Y. (2018). Impact of the gut microbiota on intestinal immunity mediated by tryptophan metabolism. Frontiers in Cellular and Infection Microbiology, **8**: 13.

Gill, S., Pop, M., DeBoy, R., and Eckburg, P. (2006). Metagenomic analysis of the human distal gut microbiome. Science, **312**(5778), 1355–1359.

Goodman, Z. D. (2014). The impact of obesity on liver histology. Clinics in Liver Disease, 18(1), 33–40.

Grill, J. P., Schneider, F., Crociani, J., and Ballongue, J. (1995). Purification and characterization of conjugated bile salt hydrolase from *Bifidobacterium longum* BB536. Applied and Environmental Microbiology, **61**(7), 2577–2582.

Gulkowska, A., Leung, H. W., So, M. K., Taniyasu, S., Yamashita, N., Yeung, L. W. Y., Richardson, B. J., Lei, A. P., Giesy, J. P., and Lam, P. K. S. (2008). Removal of antibiotics from wastewater by sewage treatment facilities in Hong Kong and Shenzhen, China. Water Research, **42**(1–2), 395–403.

Halfvarson, J., Brislawn, C. J., Lamendella, R., Vázquez-Baeza, Y., Walters, W. A., Bramer, L. M., D'Amato, M., Bonfiglio, F., McDonald, D., Gonzalez, A., Mcclure,

E. E., Dunklebarger, M. F., Knight, R., & Jansson, J. K. (2017). Dynamics of the human gut microbiome in inflammatory bowel disease. Nature Microbiology, **2**: 17004.

Hasan, T., Allen, M., and Cooperman, B. S. (1985). Anhydrotetracycline is a major product of tetracycline photolysis. Journal of Organic Chemistry, **50**(10), 1755–1757.

Hash, J. H., Wisshnick, M., and Miller, P. A. (1964). On the mode of action of the tetracycline antibiotics in *Staphylococcus aureus*. The Journal of Biological Chemistry, **239**(6), 2070–2078.

He, F., Wu, C., Li, P., Li, N., Zhang, D., Zhu, Q., Ren, W., and Peng, Y. (2018). Functions and signaling pathways of amino acids in intestinal inflammation. BioMed Research International, **2018**: 9171905.

He, J., Hu, B., Shi, X., Weidert, E. R., Lu, P., Xu, M., Huang, M., Kelley, E. E., and Xiea, W. (2013). Activation of the aryl hydrocarbon receptor sensitizes mice to nonalcoholic steatohepatitis by deactivating mitochondrial sirtuin. Molecular and Cellular Biology, **33**(10), 2047–2055.

He, L., Prodhan, M. A. I., Yuan, F., Yin, X., Lorkiewicz, P. K., Wei, X., Feng, W., McClain, C., and Zhang, X. (2018). Simultaneous quantification of straight-chain and branched-chain short chain fatty acids by gas chromatography mass spectrometry. Journal of Chromatography B, **1092**, 359–367.

Hendrikx, T., and Schnabl, B. (2019). Indoles: Metabolites produced by intestinal bacteria capable of controlling liver disease manifestation. Journal of Internal Medicine, **286**(1), 32–40.

Hernández, E., Bargiela, R., Diez, M. S., Friedrichs, A., Pérez-Cobas, A. E., Gosalbes, M. J., Knecht, H., Martínez-Martínez, M., Seifert, J., Bergen, M. von, Artacho, A., Ruiz, A., Campoy, C., Latorre, A., Ott, S. J., Moya, A., Suárez, A., DosSantos, V. A. P. M., and Ferrer, M. (2013). Functional consequences of

microbial shifts in the human gastrointestinal tract linked to antibiotic treatment and obesity. Gut Microbes, **4**(4), 306–315.

Hoerr, V., Duggan, G. E., Zbytnuik, L., Poon, K. K. H., Große, C., Neugebauer, U., Methling, K., Löffler, B., and Vogel, H. J. (2016). Characterization and prediction of the mechanism of action of antibiotics through NMR metabolomics. BMC Microbiology, **16**: 82.

Hooshmand, B., Mangialasche, F., Kalpouzos, G. G., Solomon, A., Kåreholt, I., Smith, A. D., Refsum, H., Wang, R., Mühlmann, M., Ertl-Wagner, B., Laukka, E. J., Bäckman, L., Fratiglioni, L., and Kivipelto, M. (2016). Association of Vitamin B_{12}, folate, and sulfur amino acids with brain magnetic resonance imaging measures in older adults a longitudinal population-based study. JAMA Psychiatry, **73**(6), 606–613.

Huang, J. J., Hu, H. Y., Lu, S. Q., Li, Y., Tang, F., Lu, Y., and Wei, B. (2012). Monitoring and evaluation of antibiotic-resistant bacteria at a municipal wastewater treatment plant in China. Environment International, **42**, 31–36.

Hubbard, T. D., Murray, I. A., and Perdew, G. H. (2015). Indole and tryptophan metabolism: Endogenous and dietary routes to Ah receptor activation. Drug Metabolism and Disposition, **43**(10), 1522–1535.

Ivanisevic, J., Stauch, K. L., Petrascheck, M., Benton, H. P., Epstein, A. A., Fang, M., Gorantla, S., Tran, M., Hoang, L., Kurczy, M. E., Boska, M. D., Gendelman, H. E., Fox, H. S., and Siuzdak, G. (2016). Metabolic drift in the aging brain. Aging, **8**(5), 1000–1020.

Javid, A., Mesdaghinia, A., Nasseri, S., Mahvi, A. H., Alimohammadi, M., and Gharibi, H. (2016). Assessment of tetracycline contamination in surface and groundwater resources proximal to animal farming houses in Tehran, Iran. Journal of Environmental Health Science and Engineering, **14**(1): 4.

Jia, J., Cheng, M., Xue, X., Guan, Y., and Wang, Z. (2020). Characterization of tetracycline effects on microbial community, antibiotic resistance genes and

antibiotic resistance of *Aeromonas spp*. in gut of goldfish *Carassius auratus* Linnaeus. Ecotoxicology and Environmental Safety, **191**: 110182.

Jia, W., Xie, G., and Jia, W. (2018). Bile acid–microbiota crosstalk in gastrointestinal inflammation and carcinogenesis. Nature Reviews Gastroenterology & Hepatology, **15**(2), 111–128.

Jin, U., Lee, S., Sridharan, G., Lee, K., Davidson, L. A., Jayaraman, A., Chapkin, R. S., Alaniz, R., and Safe, S. (2014). Microbiome-derived tryptophan metabolites and their aryl hydrocarbon receptor-dependent agonist and antagonist activities. Molecular Pharmacology, **85**(5), 777–788.

Jin, Y., Wu, Y., Zeng, Z., Jin, C., Wu, S., Wang, Y., and Fu, Z. (2016). Exposure to oral antibiotics induces gut microbiota dysbiosis associated with lipid metabolism dysfunction and low-grade inflammation in mice. Toxicological Sciences, **154**(1), 140–152.

Jones-Dias, D., Carvalho, A. S., Moura, I. B., Manageiro, V., Igrejas, G., Caniça, M., and Matthiesen, R. (2017). Quantitative proteome analysis of an antibiotic resistant *Escherichia coli* exposed to tetracycline reveals multiple affected metabolic and peptidoglycan processes. Journal of Proteomics, **156**, 20–28.

Jung, J. Y., Ahn, Y., Khare, S., Gokulan, K., Pineiro, S. A., and Carl E. Cerniglia. (2018). An in vitro study to assess the impact of tetracycline on the human intestinal microbiome. Anaerobe, **49**, 85–94.

Kaur, H., Bose, C., Mande, S. S., and Mason, S. (2019). Tryptophan metabolism by gut microbiome and gut-brain-axis: An *in silico* analysis. Frontiers in Neuroscience, **13**: 365.

Keerthisinghe, T. P., Wang, F., Wang, M., Yang, Q., Li, J., Yang, J., Xi, L., Dong, W., and Fang, M. (2020). Long-term exposure to TET increases body weight of juvenile zebrafish as indicated in host metabolism and gut microbiome. Environment International, **139**: 105705.

Keerthisinghe, T. P., Wang, M., Zhang, Y., Dong, W., and Fang, M. (2019). Low-dose tetracycline exposure alters gut bacterial metabolism and host-immune response: "Personalized" effect? Environment International, **131**: 104989.

Kind, T., Liu, K. H., Lee, D. Y., Defelice, B., Meissen, J. K., and Fiehn, O. (2013). LipidBlast in silico tandem mass spectrometry database for lipid identification. Nature Methods, **10**(8), 755–758.

Koh, A., Molinaro, A., Nieuwdorp, M., Khan, M. T., Schmidt, C., Wu, H., Carreras, A., Jeong, H., Olofsson, L. E., and Bergh, P. (2018). Microbially produced imidazole propionate impairs insulin signaling through mTORC1. Cell, **175**(4), 947–961.

Kohout, M., Kohoutova, B., and Heimberg, M. (1971). The regulation of hepatic triglyceride metabolism by free fatty acids. Journal of Biological Chemistry, **246**(16), 5067–5074.

Kolpin, D. W., Furlong, E. T., Meyer, M. T., Thurman, E. M., Zaugg, S. D., Barber, L. B., and Buxton, H. T. (2002). Pharmaceuticals, hormones, and other organic wastewater contaminants in U.S. streams, 1999-2000: A national reconnaissance. Environmental Science and Technology, **36**(6), 1202–1211.

Kostic, A. D., Gevers, D., Knip, M., Xavier, R. J., La, H., Oikarinen, S., Harmsen, H. J. M., Goffau, M. C. De, Welling, G., Alahuhta, K., Korhonen, T., and Virtanen, S. M. (2015). The dynamics of the human infant gut microbiome in development and in progression toward type 1 diabetes. Cell Host and Microbe, **17**(2), 260–273.

Krishnan, S., Ding, Y., Saedi, N., Alaniz, R. C., Jayaraman, A., Lee, K., Krishnan, S., Ding, Y., Saedi, N., Choi, M., Sridharan, G. V, and Sherr, D. H. (2018). Gut microbiota-derived tryptophan metabolites modulate inflammatory response in hepatocytes and macrophages. Cell Reports, **23**(4), 1099–1111.

KüHne, M., Ihnen, D., Möller, G., and Agthe, O. (2001). Stability of tetracycline in water and liquid manure. Journal of Veterinary Medicine Series A, **47**(6), 379–384.

Kümmerer, K. (2003). Promoting resistance by the emission of antibiotics from hospitals and households into effluent. Clinical Microbiology and Infection, **9**(12), 1203–1214.

Langille, M. G. I., Zaneveld, J., Caporaso, J. G., McDonald, D., Knights, D., Reyes, J. A., Clemente, J. C., Burkepile, D. E., Thurber, R. L. V., Knight, R., Beiko, R. G., and Huttenhower, C. (2013). Predictive functional profiling of microbial communities using 16S rRNA marker gene sequences. Nature Biotechnology, **31**(9), 814–821.

Laprairie, R. B., Denovan-Wright, E. M., and Wright, J. M. (2017). Differential regulation of the duplicated fabp7, fabp10 and fabp11 genes of zebrafish by peroxisome proliferator activated receptors. Comparative Biochemistry and Physiology Part - B: Biochemistry and Molecular Biology, **213**, 81–90.

Li, J., Dong, T., Keerthisinghe, T. P., Chen, H., Li, M., Chu, W., Yang, J., Hu, Z., Allen, S., Dong, W., and Fang, M. (2020). Long-term oxytetracycline exposure potentially alters brain thyroid hormone and serotonin homeostasis in zebrafish. Journal of Hazardous Materials, **399**: 123061.

Li, M., Wang, B., Zhang, M., Rantalainen, M., Wang, S., Zhou, H., Zhang, Y., Shen, J., Pang, X., Zhang, M., Wei, H., Chen, Y., Lu, H., Zuo, J., Su, M., Qiu, Y., Jia, W., Xiao, C., Smith, L.M., Yang, S., Holmes, E., Tang, H., Zhao, G., Nicholson, J.K., Li, L., Zhao, L. (2008). Symbiotic gut microbes modulate human metabolic phenotypes. Proceedings of the National Academy of Sciences, **105**(6), 2117–2122.

Licht, T. R., and Bahl, M. I. (2019). Impact of the gut microbiota on chemical risk assessment. Current Opinion in Toxicology, **15**, 109–113.

Lin, X., Kang, L., Li, H., and Peng, X. (2014). Fluctuation of multiple metabolic pathways is required for *Escherichia coli* in response to chlortetracycline stress. Molecular BioSystems, **10**(4), 901–908.

Liou, A. P., Paziuk, M., Luevano, J.-M., Machinen, S., Turnbaugh, P. J., and Kaplan, L. M. (2013). Conserved Shifts in the Gut Microbiota Due to Gastric Bypass Reduce Host Weight and Adiposity. Science Translational Medicine, **5**(178): 178ra41.

Liu, Y., Hou, Y., Wang, G., Zheng, X., and Hao, H. (2020). Gut microbial metabolites of aromatic amino acids as signals in host – microbe interplay. Trends in Endocrinology and Metabolism, **31**(11), 818–834.

Looft, T., Johnson, T. A., Allen, H. K., Bayles, D. O., Alt, D. P., Stedtfeld, R. D., Sul, W. J., Stedtfeld, T. M., Chai, B., Cole, J. R., Hashsham, S. A., Tiedje, J. M., and Stanton, T. B. (2012). In-feed antibiotic effects on the swine intestinal microbiome. Proceedings of the National Academy of Sciences, **109**(5), 1691–1696.

Magnúsdóttir, S., Ravcheev, D., De Crécy-Lagard, V., and Thiele, I. (2015). Systematic genome assessment of B-vitamin biosynthesis suggests co-operation among gut microbes. Frontiers in Genetics, **6**: 148.

Maier, L., Pruteanu, M., Kuhn, M., Zeller, G., Telzerow, A., Anderson, E., Brochado, A. R., Fernandez, K. C., and Dose, H. (2018). Extensive impact of non-antibiotic drugs on human gut bacteria. Nature, **555**(7698), 623–628.

Mao, H., Lv, Z., Sun, H., Li, R., Zhai, B., Wang, Z., Awasthi, M. K., Wang, Q., and Zhou, L. (2018). Improvement of biochar and bacterial powder addition on gaseous emission and bacterial community in pig manure compost. Bioresource Technology, **258**, 195–202.

Marciano, J. J., Sá, F. De, Fiol, D., Cristina, A., Tardelli, M., Marques, M. C., Santana, L. L., Del Fiol, F. de S., Ferreira, A. C. M. T., Marques, M. C., and Santana, L. L. (2017). Changes in weight and body fat after use of tetracycline and *Lactobacillus gasseri* in rats. Brazilian Journal of Pharmaceutical Sciences, **53**(1): e16059.

Matsumoto, M., Ooga, T., Kibe, R., Aiba, Y., Koga, Y., and Benno, Y. (2017). Colonic absorption of low-molecular-weight metabolites influenced by the intestinal microbiome: A pilot study. PLoS One, **12**(1): e0169207.

Maurice, C. F., Haiser, H. J., and Turnbaugh, P. J. (2013). Xenobiotics shape the physiology and gene expression of the active human gut microbiome. Cell, **152**(1), 39–50.

Mcgarr, S. E., Ridlon, J. M., and Hylemon, P. B. (2005). Diet, Anaerobic Bacterial Metabolism, and Colon Cancer. Journal of Clinical Gastroenterology, **39**(2), 98–109.

McMurry, L., and Levy, S. B. (1978). Two transport systems for tetracycline in sensitive Escherichia coli: critical role for an initial rapid uptake system insensitive to energy inhibitors. Antimicrobial Agents and Chemotherapy, **14**(2), 201–209.

Mcvay Jr, L. V. (1952). Studies on the concentration and bacterial effect of aureomycin in different portions of the intestinal tract. Journal of Clinical Investigation, **31**(1), 27–31.

Mensink, R. P. (2005). Metabolic and health effects of isomeric fatty acids. Current Opinion in Lipidology, **16**(1), 27–30.

Metcalf, J. L., Xu, Z. Z., Weiss, S., Lax, S., Van Treuren, W., Hyde, E. R., Song, S. J., Amir, A., Larsen, P., Sangwan, N., Haarmann, D., Humphrey, G. C., Ackermann, G., Thompson, L. R., Lauber, C., Bibat, A., Nicholas, C., Gebert, M. J., Petrosino, J. F., Reed, S.C., Gilbert, J.A., Lynne, A.M., Bucheli, S.R., Carter, D.O., Knight, R. (2016). Microbial community assembly and metabolic function during mammalian corpse decomposition. Science, **351**(6269), 158–162.

Meyer, T. W., and Hostetter, T. H. (2012). Uremic solutes from colon microbes. Kidney International, **81**(10), 949–954.

Migliore, L., Rotini, A., and Thaller, M. C. (2013). Low doses of tetracycline trigger the *E. coli* growth: A case of hormetic response. Dose-Response, **11**(4), 550–557.

Miller, G. H. (1969). Inhibition of cell division protein synthesis and nucleic acid synthesis in Escherichia coli w by tetracycline antibiotics. Ph.D. Thesis. Medical College of Virginia, Richmond, Virginia.

Modi, S. R., Collins, J. J., and Relman, D. A. (2014). Antibiotics and the gut microbiota. Journal of Clinical Investigation, **124**(10), 4212–4218.

Montenegro-Burke, J. R., Woldstad, C. J., Fang, M., Bade, A. N., McMillan, J. E., Edagwa, B., Boska, M. D., Gendelman, H. E., and Siuzdak, G. (2019). Nanoformulated antiretroviral therapy attenuates brain metabolic oxidative stress. Molecular Neurobiology, **56**(4), 2896–2907.

Morowitz, M. J., Carlisle, E. M., and Alverdy, J. C. (2011). Contributions of intestinal bacteria to nutrition and metabolism in the critically III. Surgical Clinics of North America, **91**(4), 771–785.

Morrison, D. J., and Preston, T. (2016). Formation of short chain fatty acids by the gut microbiota and their impact on human metabolism. Gut Microbes, **7**(3), 189–200.

Nelson, M. L., and Levy, S. B. (2011). The history of the tetracyclines. Annals of the New York Academy of Sciences, **1241**(1), 17–32.

Ng, K. M., Tropini, C., Xavier, K. B., Sonnenburg, J. L., Tropini, C., Frankel, M. R., Treuren, W. Van, Ng, K. M., Laughlin, C. T. O., Merrill, B. D., Yu, F. B., Pruss, K. M., Oliveira, R. A., Sonnenburg, J. L., and Huang, K. C. (2019). Recovery of the gut microbiota after antibiotics depends on host diet, community context, and environmental reservoirs. Cell Host and Microbe, **26**(5), 650–665.

Nunes, B., Antunes, S. C., Gomes, R., Campos, J. C., Braga, M. R., Ramos, A. S., and Correia, A. T. (2015). Acute effects of tetracycline exposure in the freshwater fish gambusia holbrooki : antioxidant effects , neurotoxicity and histological alterations. Archives of Environmental Contamination and Toxicology, **68**(2), 371–381.

Pallister, T., Jackson, M. A., Martin, T. C., Zierer, J., Jennings, A., Mohney, R. P., Macgregor, A., Steves, C. J., Cassidy, A., Spector, T. D., and Menni, C. (2017). Hippurate as a metabolomic marker of gut microbiome diversity: Modulation by diet and relationship to metabolic syndrome. Scientific Reports, **7**: 13670.

Pedersen, H. K., Gudmundsdottir, V., Nielsen, H. B., Hyotylainen, T., Nielsen, T., Jensen, B. A. H., Forslund, K., Hildebrand, F., Prifti, E., Falony, G., Chatelier, E. Le, Levenez, F., Doré, J., Mattila, I., Plichta, D. R., Pöhö, P., Hellgren, L. I., Arumugam, M., Sunagawa, S., Vieira-Silva, S., Jørgensen, T., Holm, J.B., Trošt, K., Consortium, M., Kristiansen, K., Brix, S., Raes, J., Wang, J., Hansen, T., Bork, P., Brunak, S., Oresic, M., Ehrlich, S.D., Pedersen, O. (2016). Human gut microbes impact host serum metabolome and insulin sensitivity. Nature, **535**(7612), 376–381.

Pena, A., Paulo, M., Silva, L. J. G., Seifrtová, M., Lino, C. M., and Solich, P. (2010). Tetracycline antibiotics in hospital and municipal wastewaters: A pilot study in Portugal. Analytical and Bioanalytical Chemistry, **396**(8), 2929–2936.

Peng, B., Liu, M., Han, Y., Wanjaya, E. R., and Fang, M. (2019). Competitive biotransformation among phenolic xenobiotic mixtures: underestimated risks for toxicity assessment. Environmental Science and Technology, **53**(20), 12081–12090.

Pérez-cobas, A. E., Gosalbes, M. J., Friedrichs, A., Knecht, H., Artacho, A., Eismann, K., Otto, W., Rojo, D., Bargiela, R., Bergen, M. Von, Neulinger, S. C., Däumer, C., Heinsen, F., Latorre, A., Barbas, C., Seifert, J., Martins, V., Ott, S. J., Ferrer, M., and Moya, A. (2013). Gut microbiota disturbance during antibiotic therapy: A multi-omic approach. Gut, **62**(11), 1591–1601.

Peters, A., Krumbholz, P., Ja, E., Rothemund, S., Gaudl, A., Ceglarek, U., and Sta, C. (2019). Metabolites of lactic acid bacteria present in fermented foods are highly potent agonists of human hydroxycarboxylic acid receptor 3. PLoS Genetics, **15**(5): e1008145.

Pi, Y., Gao, K., Peng, Y., Mu, C. L., and Zhu, W. Y. (2019). Antibiotic-induced alterations of the gut microbiota and microbial fermentation in protein parallel the changes in host nitrogen metabolism of growing pigs. Animal, **13**(2), 262–272.

Pizarro, C., Arenzana-Rámila, I., Pérez-Del-Notario, N., Pérez-Matute, P., and González-Sáiz, J. M. (2013). Plasma lipidomic profiling method based on ultrasound extraction and liquid chromatography mass spectrometry. Analytical Chemistry, **85**(24), 12085–12092.

Qu, J., Ko, C.-W., Tso, P., and Bhargava, A. (2019). Apolipoprotein A-IV: A multifunctional protein involved in protection against atherosclerosis and diabetes. Cells, **8**: 319.

Raetz, C. R. H., and Whitfield, C. (2002). Lipopolysaccharide endotoxins. Annual Review of Biochemistry, **71**, 635–700.

Ridlon, J., Kang, D., Hylemon, P., and Bajaj, J. (2014). Bile acids and the Gut Microbiome. Current Opinion in Gastroenterology, **30**(3), 332–338.

Ridlon, J. M., Kang, D.-J., and Hylemon, P. B. (2006). Bile salt biotransformations by human intestinal bacteria. Journal of Lipid Research, **47**(2), 241–259.

Risérus, U., Vessby, B., Ärnlöv, J., and Basu, S. (2004). Effects of cis-9, trans-11 conjugated linoleic acid supplementation on insulin sensitivity, lipid peroxidation, and proinflammatory markers in obese men. American Journal of Clinical Nutrition, **80**(2), 279–283.

Roberts, M. C. (2003). Tetracycline therapy: Update. Clinical Infectious Diseases, **36**(4), 462–467.

Roca-Saavedra, P., Rodriguez, J. A., Lamas, A., Miranda, J. M., Nebot, C., Cardelle-Cobas, A., Franco, C. M., and Cepeda, A. (2018). Low-dosage antibiotic intake can disturb gut microbiota in mice. CyTA - Journal of Food, **16**(1), 672–678.

Round, J. L., and Mazmanian, S. K. (2009). The gut microbiota shapes intestinal immune responses during health and disease. Nature Reviews Immunology, **9**(5), 313–323.

Saito, Y., Sato, T., Nomoto, K., and Tsuji, H. (2018). Identification of phenol- and p -cresol-producing intestinal bacteria by using media supplemented with tyrosine and its metabolites. FEMS Microbiology Ecology, **94**(9): fiy125.

Sarmah, A. K., Meyer, M. T., and Boxall, A. B. A. (2006). A global perspective on the use, sales, exposure pathways, occurrence, fate and effects of veterinary antibiotics (VAs) in the environment. Chemosphere, **65**(5), 725–759.

Sayin, S. I., Wahlström, A., Felin, J., Jäntti, S., Marschall, H. U., Bamberg, K., Angelin, B., Hyötyläinen, T., Orešič, M., and Bäckhed, F. (2013). Gut microbiota regulates bile acid metabolism by reducing the levels of tauro-beta-muricholic acid, a naturally occurring FXR antagonist. Cell Metabolism, **17**(2), 225–235.

Scheperjans, F., Aho, V., Pereira, P. A. B., Koskinen, K., Paulin, L., Pekkonen, E., Haapaniemi, E., Kaakkola, S., Eerola-Rautio, J., Pohja, M., Kinnunen, E., Murros, K., and Auvinen, P. (2015). Gut microbiota are related to Parkinson's disease and clinical phenotype. Movement Disorders, **30**(3), 350–358.

Schmidt, T. S. B., Raes, J., and Bork, P. (2018). The human gut microbiome: From association to modulation. Cell, **172**(6), 1198–1215.

Schnappinger, D., and Hillen, W. (1996). Tetracyclines: Antibiotic action, uptake, and resistance mechanisms. Archives of Microbiology, **165**(6), 359–369.

Shiba, T., Kawakami, K., Sasaki, T., Makino, I., Kato, I., Kobayashi, T., Uchida, K., and Kaneko, K. (2014). Effects of intestinal bacteria-derived p -cresyl sulfate on Th1-type immune response *in vivo* and *in vitro*. Toxicology and Applied Pharmacology, **274**(2), 191–199.

Srinivasan, V., Maestroni, G. J. M., Cardinali, D. P., Esquifino, A. I., Perumal, P., and Miller, S. C. (2005). Melatonin, immune function and aging. Immunity and Ageing, **2**: 17

Stellwag, E. J., and Hylemon, P. B. (1976). Purification and characterization of bile salt hydrolase from *Bacteroides fragilis* subsp. *fragilis*. Biochimica et Biophysica Acta, **452**(1), 165–176.

Suzuki, S., and Hoa, P. T. P. (2012). Distribution of quinolones, sulfonamides, tetracyclines in aquatic environment and antibiotic resistance in Indochina. Frontiers in Microbiology, **3**: 67.

Takamine, F., and Imamura, T. (1995). Isolation and characterization of bile acid 7-dehydroxylating bacteria from human feces. Microbiology and Immunology, **39**(1), 11–18.

Tan, B., Huang, B., Wang, J., Guang, G. P., Yang, C. B., and Y.Yin. (2017). Aromatic amino acids alleviate intestinal inflammation in piglets through calcium-sensing receptor activation. Journal of Animal Science, **95**(Supplement 4), 201–202.

Taylor, A. A., Marcus, I. M., Guysi, R. L., and Walker, S. L. (2015). Metal oxide nanoparticles induce minimal phenotypic changes in a model colon gut microbiota. Environmental Engineering Science, **32**(7), 602–612.

The Human Microbiome Project Consortium. (2012). Structure, function and diversity of the healthy human microbiome. Nature, **486**(7402), 207–214.

Thuny, F., Richet, H., Casalta, J. P., Angelakis, E., Habib, G., and Raoult, D. (2010). Vancomycin treatment of infective endocarditis is linked with recently acquired obesity. PLoS One, **5**(2): e9074.

Tong, L., Huang, S., Wang, Y., Liu, H., and Li, M. (2014). Occurrence of antibiotics in the aquatic environment of Jianghan Plain, central China. Science of the Total Environment, **497–498**, 180–187.

Tong, L., Wang, L., Yao, S., Jin, L., Yang, J., Zhang, Y., Ning, G., and Zhang, Z. (2019). PPARγ attenuates hepatic steatosis through autophagy-mediated fatty acid oxidation. Cell Death and Disease, **10**: 197.

Topping, D. L., and Clifton, P. M. (2001). Short-chain fatty acids and human colonic function: Roles of resistant starch and nonstarch polysaccharides. Physiological Reviews, **81**(3), 1031–1064.

Townsend, S., Caubilla Barron, J., Loc-Carrillo, C., and Forsythe, S. (2007). The presence of endotoxin in powdered infant formula milk and the influence of endotoxin and *Enterobacter sakazakii* on bacterial translocation in the infant rat. Food Microbiology, **24**(1), 67–74.

Tso, S., Qi, X., Gui, W., Chuang, J. L., Morlock, L. K., Wallace, A. L., Ahmed, K., Laxman, S., Campeau, P. M., Lee, B. H., Hutson, S. M., Tu, B. P., Williams, N. S., Tambar, U. K., Wynn, R. M., and Chuang, D. T. (2013). Structure-based design and mechanisms of allosteric inhibitors for mitochondrial branched-chain α -ketoacid

dehydrogenase kinase. Proceedings of the National Academy of Sciences, **110**(24), 9728–9733.

Tsugawa, H., Cajka, T., Kind, T., Ma, Y., Higgins, B., Ikeda, K., Kanazawa, M., VanderGheynst, J., Fiehn, O., and Arita, M. (2015). Data independent MS/MS deconvolution for comprehensive metabolome analysis. Nature Methods, **12**(6), 523–526.

Turnbaugh, P. J., Ley, R. E., Mahowald, M. A., Magrini, V., Mardis, E. R., and Gordon, J. I. (2006). An obesity-associated gut microbiome with increased capacity for energy harvest. Nature, **444**(7122), 1027–1031.

Uno, K., Katagiri, H., Yamada, T., Ishigaki, Y., Ogihara, T., Imai, J., Hasegawa, Y., Gao, J., Kaneko, K., Iwasaki, H., Ishihara, H., Sasano, H., Inukai, K., Mizuguchi, H., Asano, T., Shiota, M., Nakazato, M., and Oka, Y. (2006). Neuronal pathway from the liver modulates energy expenditure and systemic insulin sensitivity. Science, **312**(5780), 1656–1659.

Upadhyay, V., Poroyko, V., Kim, T., Devkota, S., Fu, S., Liu, D., Tumanov, A. V., Koroleva, E. P., Deng, L., Nagler, C., Chang, E., Tang, H., and Fu, Y.-X. (2013). Lymphotoxin regulates commensal responses to enable diet- induced obesity. Nature Immunology, **13**(10), 947–953.

van den Berg, E. H., Flores-Guerrero, J. L., Gruppen, E. G., de Borst, M. H., Wolak-Dinsmore, J., Connelly, M. A., Bakker, S. J. L., and Dullaart, R. P. F. (2019). Non-alcoholic fatty liver disease and risk of incident type 2 diabetes: Role of circulating branched-chain amino acids. Nutrients, **11**(3): 705.

Vatanen, T., Kostic, A. D., D'Hennezel, E., Siljander, H., Franzosa, E. A., Yassour, M., Kolde, R., Vlamakis, H., Arthur, T. D., Hämäläinen, A. M., Peet, A., Tillmann, V., Uibo, R., Mokurov, S., Dorshakova, N., Ilonen, J., Virtanen, S. M., Szabo, S. J., Porter, J. A., … Xavier, R. J. (2016). Variation in microbiome LPS immunogenicity contributes to autoimmunity in humans. Cell, **165**(4), 842–853.

Velmurugan, G. (2018). Gut microbiota in toxicological risk assessment of drugs and chemicals: The need of hour. Gut Microbes, **9**(5), 465–468.

Vernocchi, P., Del Chierico, F., and Putignani, L. (2016). Gut microbiota profiling: Metabolomics based approach to unravel compounds affecting human health. Frontiers in Microbiology, **7**: 1144.

Vijay-kumar, M., Aitken, J. D., Carvalho, F. A., Cullender, T. C., Mwangi, S., Srinivasan, S., Sitaraman, S. V, Knight, R., Ley, R. E., and Gewirtz, A. T. (2010). Metabolic Syndrome and Altered Gut Microbiota in Mice Lacking Toll-Like Receptor 5. Science, **328**(5975), 228–231.

Vragović, N., Bažulić, D., and Njari, B. (2011). Risk assessment of streptomycin and tetracycline residues in meat and milk on Croatian market. Food and Chemical Toxicology, **49**(2), 352–355.

Wahlström, A., Sayin, S. I., Marschall, H., and Ba, F. (2016). Intestinal crosstalk between bile acids and microbiota and its impact on host metabolism. Cell Metabolism, **24**(1), 41–50.

Wang, Zeneng, Klipfell, E., Bennett, B. J., Koeth, R., Levison, B. S., Dugar, B., Feldstein, A. E., Britt, E. B., Fu, X., Chung, Y. M., Wu, Y., Schauer, P., Smith, J. D., Allayee, H., Tang, W. H. W., Didonato, J. A., Lusis, A. J., and Hazen, S. L. (2011). Gut flora metabolism of phosphatidylcholine promotes cardiovascular disease. Nature, **472**(7341), 57–65.

Wang, Zhuozhong, Cui, B., Zhang, F., Yang, Y., Shen, X., Li, Z., Zhao, W., Zhang, Y., Deng, K., Rong, Z., Yang, K., Yu, X., Li, K., Han, P., and Zhu, Z. (2019). Development of a correlative strategy to discover colorectal tumor tissue derived metabolite biomarkers in plasma using untargeted metabolomics. Analytical Chemistry, **91**(3), 2401−2408.

Warth, B., Spangler, S., Fang, M., Johnson, C. H., Forsberg, E. M., Granados, A., Martin, R. L., Domingo-almenara, X., Huan, T., Rinehart, D., Montenegro-burke, J. R., Hilmers, B., Aisporna, A., Hoang, L. T., Uritboonthai, W., Benton, H. P.,

Richardson, S. D., Williams, A. J., and Siuzdak, G. (2017). Exposome-scale investigations guided by global metabolomics, pathway analysis, and cognitive computing. Analytical Chemistry, **89**(21), 11505–11513.

Wells, J. E., Berr, F., Thomas, L. A., Dowling, R. H., and Hylemon, P. B. (2000). Isolation and characterization of cholic acid 7α-dehydroxylating fecal bacteria from cholesterol gallstone patients. Journal of Hepatology, **32**(1), 4–10.

Wikoff, W. R., Anfora, A. T., Liu, J., Schultz, P. G., Lesley, S. A., Peters, E. C., and Siuzdak, G. (2009). Metabolomics analysis reveals large effects of gut microflora on mammalian blood metabolites. Proceedings of the National Academy of Sciences, **106**(10), 3698–3703.

Wilmanski, T., Rappaport, N., Earls, J. C., Magis, A. T., Manor, O., Lovejoy, J., Omenn, G. S., Hood, L., Gibbons, S. M., and Price, N. D. (2019). Blood metabolome predicts gut microbiome α-diversity in humans. Nature Biotechnology, **37**, 1217–1228.

Winckler, C., and Grafe, A. (2000). Use of veterinary drugs in intensive animal production. Journal of Soils and Sediments, **1**: 66

Xu, C.-X., Wang, C., Zhang, Z.-M., Jaeger, C. D., Krager, S. L., Bottum, K. M., Liu, J., Liao, D.-F., and Tischkau, S. A. (2016). Aryl hydrocarbon receptor deficiency protects mice from diet-induced adiposity and metabolic disorders through increased energy expenditure. International Journal of Obesity, **39**(8), 1300–1309.

Yang, S., Cha, J., and Carlson, K. (2005). Simultaneous extraction and analysis of 11 tetracycline and sulfonamide antibiotics in influent and effluent domestic wastewater by solid-phase extraction and liquid chromatography-electrospray ionization tandem mass spectrometry. Journal of Chromatography A, **1097**(1–2), 40–53.

Yoo, D. K., and Lee, S.-H. (2016). Effect of lipopolysaccharide (LPS) exposure on the reproductive organs of immature female rats. Development and Reproduction, **20**(2), 113–121.

Young, W. B., and Tuttle, J. G. (1952). Achromycin-A new form of aureomycin. American Journal of Medicine, **16**(4), 612–613.

Yu, X., Wu, Y., Deng, M., Liu, Y., Wang, S., He, X., Allaire-leung, M., Wan, J., Zou, Y., Yang, C., and Tu, W. (2019). Tetracycline antibiotics as PI3K inhibitors in the Nrf2-mediated regulation of antioxidative stress in zebrafish larvae. Chemosphere, **226**, 696–703.

Zampieri, M., Szappanos, B., Buchieri, M. V., Trauner, A., Piazza, I., Picotti, P., Gagneux, S., Borrell, S., Gicquel, B., Lelievre, J., Papp, B., and Sauer, U. (2018). High-throughput metabolomic analysis predicts mode of action of uncharacterized antimicrobial compounds. Science Translational Medicine, **10**(429): eaal3973.

Zampieri, M., Zimmermann, M., Claassen, M., and Sauer, U. (2017). Nontargeted metabolomics reveals the multilevel response to antibiotic perturbations. Cell Reports, **19**(6), 1214–1228.

Zelante, T., Iannitti, R. G., Cunha, C., Luca, A. De, Giovannini, G., Pieraccini, G., Zecchi, R., Angelo, C. D., Massi-benedetti, C., Fallarino, F., Carvalho, A., Puccetti, P., and Romani, L. (2013). Tryptophan catabolites from microbiota engage aryl hydrocarbon receptor and balance. Immunity, **39**(2), 372–385.

Zhang, L. S., and Davies, S. S. (2016). Microbial metabolism of dietary components to bioactive metabolites: Opportunities for new therapeutic interventions. Genome Medicine, **8**(1), 46.

Zhang, Q., Cheng, J., and Xin, Q. (2015). Effects of tetracycline on developmental toxicity and molecular responses in zebrafish (*Danio rerio*) embryos. Ecotoxicology, **24**, 707–719.

Zhang, Y., Keerthisinghe, T. P., Han, Y., Liu, M., Wanjaya, E. R., and Fang, M. (2018). “Cocktail” of xenobiotics at human relevant levels reshapes the gut bacterial

metabolome in a species-specific manner. Environmental Science and Technology, **52**(19), 11402–11410.

Zhang, Y., Liu, M., Peng, B., Jia, S., Koh, D., Wang, Y., Cheng, H. S., Tan, N. S., Warth, B., Chen, D., and Fang, M. (2020). Impact of mixture effects between emerging organic contaminants on cytotoxicity: A systems biological understanding of synergism between tris (1,3-dichloro-2-propyl) phosphate and triphenyl phosphate. Environmental Science and Technology, **54**(17), 10722–10734.

Appendix A

Text A1

Metabolite profiling and quality control

The profiling of metabolites was conducted using HPLC system (Agilent Technologies) coupled to a 6550 Q-TOF (Agilent Technologies, Singapore), according to our previous studies (Beyer et al., 2018; Fang et al., 2015). Hydrophilic interaction chromatography (HILIC) with a Luna aminopropyl column (pore size: 3 μm, 150 mm Length ×10 mm I.D., Phenomenex, Torrance, California) was used for metabolite profiling and the electrospray ionization (ESI) in both positive and negative mode was used for mass spectrometry (MS) analysis which has shown a good coverage of polar metabolites (Ivanisevic et al., 2013). The mobile phase was composed of A= 20 mM ammonium acetate and 40 mM ammonium hydroxide in 95% water and 5% acetonitrile, and B= 95% acetonitrile and 5% water.

To correct the mass, retention time, and response drift, a mix of metabolites was prepared by pooling all treated and control samples and were run after every six samples. A pooled mixture of treated and control samples was run using a method which was modified from our previous study for data-dependent acquisition (DDA) auto-MS/MS and targeted MS/MS of selected precursors (Warth et al., 2017).

Metabolite identification and metabolic pathway analysis

The processing of metabolome data was carried out using XCMS online web platform (http://xcmsonline.scripps.edu). The first screening was based on the significant features with p-value ≤ 0.05, |fold change| > 1.2, and intensity >10 000 ion counts. All those features were manually checked to minimize the false positive hits. MS/MS fragment match, accurate mass match, and in-house retention time match are the methods used for metabolite identification (Zhang et al., 2018). Open source platforms KEGG (http://www.genome.jp/kegg/) and Metaboanalyst (http://www.metaboanalyst.ca) were incorporated for further pathway analysis. The heatmap analysis was conducted using R software (http://www.R-project.org.).

Lipidomic profiling and identification

Lipidomics profiling was performed in accordance with a previous study (Pizarro et al., 2013). Briefly, profiling of lipids was conducted using a reversed-phase HPLC system (Agilent Technologies) coupled to a 6550 Q-TOF (Agilent Technologies, Singapore). Reversed-phase C18 Zorbax Eclipse Plus column RRHD (pore size: 1.8 μm, 50 mm Length ×2.1 mm I.D.) was used for the lipidomics profiling and the electro spray ionization (ESI) in positive mode was used for mass spectrometry analysis. The mobile phase was composed of A= 10 mM ammonium in acetate in 40% water and 60% acetonitrile, and B= 10 mM ammonium acetate in 90% isopropanol and 10% acetonitrile. The data processing was carried out in a similar way to metabolomics analysis (see **Section 3.3.5** in the main text) using XCMS online web platform. In addition, MS-DIAL (V. 2.84) software program with built-in LipidBlast database was incorporated for the lipid annotation (Kind et al., 2013; Tsugawa et al., 2015).

Text A2

Bacterial strains and cultivation conditions

The bacterial strains in this study included *Escherichia coli* K12-MG1655, *Bacteroides fragilis* ATCC25285, and *Clostridium sporogenes* ATCC15579. These three model bacteria are commonly found inhabiting the human gastrointestinal tract as commensal bacteria. *Clostridium spp*. and *Bacteroides spp*. are two of the most abundant genera in cecal content, accounting for >80% while the relative abundance of *E. coli* was reported between 3% and 29% in the gastrointestinal tract (Eckburg et al., 2010). Moreover, the three strains cover Gram-positive and negative bacteria for a better understanding of the effect of TET on each type. The bacterial cultures were stored in -80^{o}C in reinforced clostridial medium (RCM) (Oxide, Thermo Scientific Microbiology, Singapore) containing 25% glycerol. All bacteria were revived in RCM in anaerobic growth incubator at 37^{o}C for overnight before the following experiment. Anaerobic conditions were obtained by flushing the anaerobic tube-sealed medium with O_2-free nitrogen gas for 20 min, and all experiments were carried out in anaerobic chamber.

TET treatment of model bacteria

TET hydrochloride was purchased from Sigma-Aldrich (Singapore), and the stock solution was prepared at 100 mg/mL in high-performance liquid chromatography (HPLC) grade DMSO, diluted in the anaerobic RCM medium to the respective concentrations with vehicle (DMSO) concentration being lower than 0.1% (v/v). Control samples were prepared by diluting DMSO in anaerobic RCM medium to 0.1% (v/v).

The inhibition of TET on model bacteria was tested using dose-response assay. Briefly, each bacterium was inoculated from an overnight culture in fresh medium at 1% (v/v) %. A serial dilution of TET was prepared and added into the bacterial cultures, with three replicates for each dose concentration. Bacterial growth was monitored by reading optical density at 600 nm with a spectrophotometer (DR1900, HACH, Southeast Asia). The four-parameter logistic curve fitting was used to predict the inhibitory concentration (IC) (Huang et al., 2012).

For metabolomics study, each model bacteria were treated with TET at three different dose concentrations (**Table B7**). The high dose was IC_{90}, the concentration at which 90% growth of bacteria is inhibited compared to control, for each model strain used. The middle concentration is IC_{50}, the concentration at which 50% growth of bacteria is inhibited compared to control. The low dose is 0.01 ppm, which was selected to simulate the TET concentrations occurring in the gut via indirect means such as the consumption of poultry and dairy products containing TET (Aalipour et al., 2015; Cháfer-Pericás et al., 2011), The exposure concentration in the gut was predicted with a model used previously in our study (Zhang et al., 2018).

Briefly, 1% (v/v) of overnight revived bacterial culture was inoculated and allowed to grow until the late exponential phase before the TET treatment. All bacterial cultures and controls were prepared in triplicate with a final volume of 20 mL and were cultivated in an incubating shaker under anaerobic conditions at 37 °C for 24 h before cell harvesting. After incubation, the cell pellets and the secretome was separated by centrifugation at 8,000 rpm for 3 min for metabolomics and immunological studies, respectively. The cell pellets were then rapidly washed by ice-cooled phosphate buffered saline (PBS) to remove the growth medium residues. Thereafter, the cell pellets were proceeded to metabolite extraction, and secretome was stored at -40 °C until analysis. Optical density measurement was also conducted upon harvest for future normalization.

Metabolite extraction and profiling

After harvesting, the cell lysis was performed by 3 cycles of homogenization for 1 min at 30 Hz, snap-freeze, thaw and ice-water sonication. The homogenization was assisted with glass beads (0.5 mm). The lysates were centrifuged at 20,000 g for 15 min at 4 °C, and then the extract was dried by speed-vacuum evaporation (CentriVap Benchtop Centrifugal Vacuum Concentrator, Labconco, U.S.A.) at 10 °C followed by reconstitution in acetonitrile/HPLC water at the volume ratio of 1:1 to a normalized volume by bacteria culture optical density.

The profiling of metabolites was conducted using HPLC system (Agilent Technologies) coupled to a 6550 Q-TOF (Agilent Technologies, Singapore) according to our previous study (Zhang et al., 2018). Hydrophilic interaction

chromatography (HILIC) with a Luna aminopropyl column (pore size: 3 μm, 150 mm Length ×10 mm I.D., Phenomenex, Torrance, California) was used for metabolite profiling and the electro spray ionization (ESI) in negative mode was used for mass spectrometry (MS) analysis which has shown a good coverage of polar metabolites (Ivanisevic et al., 2013). The mobile phase was composed of A= 20 mM ammonium acetate and 40 mM ammonium hydroxide in 95% water and 5% acetonitrile, and B= 95% acetonitrile and 5% water.

To correct the mass, retention time, and response drift, a mix of metabolites was prepared by pooling all treated and control samples of each bacteria and were run after every six samples. Variation of the three biological replicates for both control and treated samples was manually checked with a standard deviation of most features being less than 15%. A pooled mixture of treated and control samples of each bacteria was run with method from our previous study, which was modified for data-dependent acquisition (DDA) auto-MS/MS and targeted MS/MS of selected precursors (Zhang et al., 2018).

Metabolites and metabolic pathway analysis

The metabolome data processing was carried out using XCMS online web platform (http://xcmsonline.scripps.edu). The first screening was based on the significant features with *p*-value ≤0.05, |fold change| > 1.5, and intensity >10 000 ion counts. All those features were manually checked to minimize the false positive hits. MS/MS fragment match, accurate mass match, and in-house retention time match are the methods used for metabolite identification. Open source platforms KEGG (http://www.genome.jp/kegg/) and Metaboanalyst (http://www.metaboanalyst.ca) were incorporated for further pathway analysis. Overlapped features across different dose levels and model bacteria were aligned by m/z and retention time. Statistical analysis, including non-metric multi-dimensional analysis and heatmap analysis, was conducted by PAST (https://folk.uio.no/ohammer/past/) and R software (http://www.R-project.org.). Further normalization of the data was carried out when needed using a previously published method when necessary (Wang et al., 2013).

Derivatization and GC-MS analysis of SCFA

For derivatization, 100 mM PFBBr in acetone, 0.5M phosphate buffer (PBS, pH 7), and a sample of 1ml were mixed at a ratio of 14:2:5 (v/v/v) with the spiked internal standard in a glass tube. Then the sample was vortex mixed and incubated in a water bath at 60 °C for 1.5 h. The sample was then cooled down and vortexed for 3 minutes after adding 1.5 mL of hexane to the mixture. The hexane phase was then dried, reconstituted in toluene and analyzed using Agilent 7890B GC system coupled with 5977A mass selective detector (MSD).

HP-5ms (30 m × 250 µm, i.d., with 0.25 µm film thickness, model No. HP 190915-433) obtained from Agilent Technologies J&W (Santa Clara, CA, USA) were used for SCFA separation. The flow rate of helium was set at 1.5 mL/min. The temperatures of inlet, ion source and transfer line were all set to 220 °C. The column temperature was programmed as follows: the initial temperature of 70 °C for 5 min, then ramped to 135 °C at a rate of 5°C/min and then to 300 °C at a rate of 100 °C/min and then maintained at 300 °C for 5 min. Splitless mode with 2 µL injection volume was used with solvent delay time was set to 8.5 min. The energy of electron ionization (EI) was set to 70 eV and the mass spectral data were collected in the single ion monitoring (SIM) mode (L. He et al., 2018).

Text A3

Establishment *in vitro* gut microbial community.

In-vitro gut microbiome was established and maintained in a compact chemostat system (Winpact model FS-05) under controlled conditions. Modified Gifu anaerobic broth (mGAM) purchased from HyServe GmbH & Co.KG, Germany was used as the growth media and fecal matter from one healthy donor who had not been received antibiotics for more than 8 months prior to sampling was used as the reactor inoculum in accordance with a few previous studies (Liu et al., 2018; Maier et al., 2018; Taylor et al., 2015). Before inoculation, the whole reactor chamber with the medium was autoclaved for sterilization. Then the outlet for gas collection was open and the medium inside was flushed with N_2 through the N_2 purge inlet connected with a 0.22 μm gas filter for at least an hour. The fresh fecal sample from one healthy donor was transferred to anaerobic chamber within 1 hr. Approximately 20 g sample was mixed with growth media and settled for 5 min to remove large particles. Then the supernatant was transferred to the pre-reduced reactor medium for inoculation. The N_2 purging continued for several hours after inoculation. Then the N_2 purge inlet was closed, and the gas collection outlet was connected with an empty gas bag to collect any gas production. To maintain the anaerobic condition of the influent, the medium bottle was immediately connected with a N_2 gas bag while the medium inside was still hot after being autoclaved. The effluent bottle was also autoclaved and flushed with N_2 through a filtered inlet. After N_2 flushing, another empty gas bag was then connected to avoid oxygen leakage to the system. The chemostat was run with a working volume of 2 L and a residence time of 2.8 days at 37 °C. The pH was maintained at 7.0 by adding 2M NaOH solution controlled with a built-in pH probe inside the reactor chamber. The gut reactor was sampled three times a week for routine monitoring of OD_{600}, chemical oxygen demand (COD), and SCFA measurement. The community analysis for the *in vitro* gut microbiome was conducted after one month of operation when the nutrient profiles were stable.

DNA extraction and 16s rRNA gene sequence analysis.

DNA was extracted from the fecal inoculum, stable reactor culture, and the reactor culture incubated under fed and fasted states for the microbial community analysis

using QIAamp® Fast DNA stool mini kit (QIAGEN) according to the manufacturer' s protocol. The sequencing and analysis were carried out at the NovogeneAIT Genomics, Singapore. Briefly, the sequencing of 16S rRNA genes was conducted using IonS5^{TM}XL sequencing platform.

The raw sequence data were then processed to obtain effective reads using QIIME2 (V2019.4.0, https://docs.qiime2.org/2020.11/about/). The chimera sequences were detected and removed using UCHIME algorithm (UCHIME Algorithm, http://www.drive5.com/usearch/manual/uchime_algo.html) by comparing with the reference database (Gold database, http://drive5.com/uchime/uchime_download.html). We have collected a total of 274,700 sequences, and 271 amplicon sequence variants (ASVs) were identified by performing sequence analysis by DADA2 package (V2019.04.1, https://docs.qiime2.org/2020.11/plugins/available/dada2/denoise-single/). Species annotation was conducted using pre-Trained Naive Bayes classifier (https://docs.qiime2.org/2020.11/tutorials/feature-classifier/) and the SSUrRNA database of Silva_132_99% (pre-Trained classifier in QIIME2, https://www.arb-silva.de/no_cache/download/archive/release_132/) was the database used.

Further filtration, rarefaction, and normalization were performed using the online platform, MicrobiomeAnalyst (https://www.microbiomeanalyst.ca/) (Chong et al., 2020). The filtration was carried out to remove the features containing all zeros, or appearing in only one sample, and with low abundance and low variance. Subsequently, the data were rarefied to minimum library size and normalized using the total sum scaling (TSS) normalization method.

Dose selection for TET treatment

TET exposure of the *in-vitro* gut microbiome was conducted under two different feed states at three different dose levels (**Table B9).** The highest dose was to represent the TET level that occurs in the colon after the TET intake at the therapeutic dose. 173.2 µM was estimated as the intestinal concentration of TET with a single daily dose of 519.85 µM (Maier et al., 2018). Then, considering 77-88% absorption of TET and assuming the total absorption is occurring in the small intestine, ~10 mg/L is reaching the column after each intake (Agwuh and MacGowan, 2006). Assuming a single daily dose 10 mg/L was selected as the highest dose of exposure and the lowest dose was

to represent the human relevant dietary exposure concentration of TET occurring in the colon via the consumption of poultry and dairy products containing TET residues (Aalipour et al., 2015; Cháfer-Pericás et al., 2011), which was roughly predicted with a previously used model (Zhang et al., 2018). As a result, the low dose at 0.01 mg/L was selected to simulate the dietary level TET concentrations. In addition, one intermediate level, 1 mg/L was used to observe the dose-responsiveness of TET's effect on the colonic microbiota.

Sequence Accession Number

The 16S rRNA gene sequence datasets used in this study were deposited in GenBank under the following accession numbers: fecal inoculum (SAMN17795873), *in vitro* gut microbiome (SAMN17795874), fasted states gut microbiome (SAMN17795875), and fed state gut microbiome (SAMN17795876).

Metabolite profiling and quality control

The profiling of the metabolites was conducted using an HPLC system (Agilent Technologies, Singapore) coupled to a 6550 Q-TOF (Agilent Technologies, Singapore), in accordance with our previous studies (Beyer et al., 2018; Fang et al., 2015; Keerthisinghe et al., 2019). To have better metabolite coverage, two different separation methods were deployed. A Waters ACQUITY UPLC BEH Amide (3 µm, 2.1 × 100 mm) in negative electro spray ionization (ESI) mode (HILIC-ESI (-)) was used for better separation of polar metabolites and an Atlantis T3 column (3 µm, 2.1 × 100 mm) in both ESI (+) and ESI (-) modes (RP-ESI (±)) was used for hydrophobic metabolites. Both profiling methods were slightly modified from a previous study (Wang et al., 2019). For HILIC-ESI (-) method, the injection volume was 5 µL and the mobile phase was composed of A= 25 mM ammonium acetate and 25 mM ammonium hydroxide in 95% water and 5% acetonitrile and B=95% acetonitrile and 5% water. Flow rate was 0.25 mL/min and the column temperature were 30 °C. For RP-ESI (+) method, the injection volume was 5 µL. The mobile phase A was 0.1% formic acid in water and mobile phase B was 0.1% formic acid in acetonitrile. The linear gradient was set as follows: 0~1 min: 1% B; 1~8 min: 1% B to 100% B; 8~10 min: 100% B; 10~10.5 min: 100% B to 1% B; 10.5 ~ 12.5 min: 1% B. Flow rate is 0.5 mL/min and column temperature is 25 °C. Other parameters were set as follows: gas temperature: 225°C; gas flow: 14 L/min; sheath gas temperature: 275°C; sheath

gas flow: 11 L/min; nozzle voltage: 1000 V; nebulizer pressure: 35 psig; capillary voltage: 3500V and -3500V for positive and negative mode; nozzle voltage: 1000 V; fragmentor: 175 V, collision energy: 0 V and scan rate: 1 spectra/second. To correct the mass, retention time and response drift, a mix of metabolites was prepared by pooling all treated and control cell samples. QC samples were analyzed every six injections of biological samples and a blank sample (acetonitrile: water, 1:1, v:v) to correct the mass, retention time and response drift. Data-dependent acquisition (DDA) auto-MS/MS and targeted MS/MS of selected precursors were run with QC sample to confirm the identity of the metabolites.

Gut microbial product and nutrient identification and differentiation.

The nutrients supplied to the gut microbial community through mGAM and the produced metabolites specific to our *in-vitro* gut microbiome were differentiated by comparing the relative levels of metabolic features in the gut microbiome secretome compared to the blank medium without microorganisms. The metabolites with significantly high levels in the blank medium compared to gut microbiome secretome have been considered as supplied nutrients (**Table B10).** In addition, the features with no significant change were also considered as nutrients since they were obviously available in the media, and we did not have enough evidence to prove that they were produced by the *in vitro* gut microbiome system. In contrast, a metabolite has been considered as a product that specific to our *in vitro* gut microbiome system when its level is significantly higher in the gut bacterial secretome compared to that in the blank media.

Appendix A: References

- Aalipour, F., Mirlohi, M., Jalali, M., and Azadbakht, L. (2015). Dietary exposure to tetracycline residues through milk consumption in Iran. Journal of Environmental Health Science and Engineering, **13**(1), 80.

- Agwuh, K. N., and MacGowan, A. (2006). Pharmacokinetics and pharmacodynamics of the tetracyclines including glycylcyclines. Journal of Antimicrobial Chemotherapy, **58**(2), 256–265.

- Beyer, B. A., Fang, M., Sadrian, B., J Rafael Montenegro-Burke, W. C. P., Kok, B. P. C. C., Saez, E., Kondo, T., Siuzdak, G., Lairson, L. L., Montenegro-Burke, J. R., Plaisted, W. C., Kok, B. P. C. C., Saez, E., Kondo, T., Siuzdak, G., and Lairson, L. L. (2018). Metabolomics-based discovery of a metabolite that enhances oligodendrocyte maturation. Nature Chemical Biology, **14**(1), 22–28.

- Cháfer-Pericás, C., Maquieira, Á., Puchades, R., Miralles, J., and Moreno, A. (2011). Multiresidue determination of antibiotics in feed and fish samples for food

safety evaluation. Comparison of immunoassay vs LC-MS-MS. Food Control, **22**(6), 993–999.

- Chong, J., Liu, P., Zhou, G., & Xia, J. (2020). Using MicrobiomeAnalyst for comprehensive statistical, functional, and meta-analysis of microbiome data. Nature Protocols, 15(3), 799-821.

- Eckburg, P., Bik, E. M., Bernstein, C. N., Purdom4, E., Dethlefsen, L., Sargent, M., Gill5, S. R., Nelson, K. E., and Relman, D. A. (2010). Diversity of the human intestinal microbial flora. Science, **308**(5728)), 1635–1638.

- Fang, M., Ivanisevic, J., Benton, H. P., Johnson, C. H., Patti, G. J., Hoang, L. T., Uritboonthai, W., Kurczy, M. E., and Siuzdak, G. (2015). Thermal degradation of small molecules: a global metabolomic investigation. Analytical Chemistry, **87**(21), 10935–10941.

- He, L., Prodhan, M. A. I., Yuan, F., Yin, X., Lorkiewicz, P. K., Wei, X., Feng, W., McClain, C., and Zhang, X. (2018). Simultaneous quantification of straight-chain and branched-chain short chain fatty acids by gas chromatography mass spectrometry. Journal of Chromatography B, **1092**, 359–367.

- Huang, J. J., Hu, H. Y., Lu, S. Q., Li, Y., Tang, F., Lu, Y., and Wei, B. (2012). Monitoring and evaluation of antibiotic-resistant bacteria at a municipal wastewater treatment plant in China. Environment International, **42**, 31–36.

- Ivanisevic, J., Zhu, Z. J., Plate, L., Tautenhahn, R., Chen, S., O'Brien, P. J., Johnson, C. H., Marletta, M. A., Patti, G. J., and Siuzdak, G. (2013). Toward 'Omic scale metabolite profiling: A dual separation-mass spectrometry approach for coverage of lipid and central carbon metabolism. Analytical Chemistry, **85**(14), 6876–6884.

- Javid, A., Mesdaghinia, A., Nasseri, S., Mahvi, A. H., Alimohammadi, M., and Gharibi, H. (2016). Assessment of tetracycline contamination in surface and groundwater resources proximal to animal farming houses in Tehran, Iran. Journal of Environmental Health Science and Engineering, **14**(1): 4.

- Kind, T., Liu, K. H., Lee, D. Y., Defelice, B., Meissen, J. K., and Fiehn, O. (2013). LipidBlast in silico tandem mass spectrometry database for lipid identification. Nature Methods, **10**(8), 755–758.

- Liu, Y., Hou, Y., Wang, G., Zheng, X., and Hao, H. (2020). Gut microbial metabolites of aromatic amino acids as signals in host – microbe interplay. Trends in Endocrinology and Metabolism, **31**(11), 818–834.

- Maier, L., Pruteanu, M., Kuhn, M., Zeller, G., Telzerow, A., Anderson, E., Brochado, A. R., Fernandez, K. C., and Dose, H. (2018). Extensive impact of non-antibiotic drugs on human gut bacteria. Nature, **555**(7698), 623–628.

- Taylor, A. A., Marcus, I. M., Guysi, R. L., and Walker, S. L. (2015). Metal oxide nanoparticles induce minimal phenotypic changes in a model colon gut microbiota. Environmental Engineering Science, **32**(7), 602–612.

- Pizarro, C., Arenzana-Rámila, I., Pérez-Del-Notario, N., Pérez-Matute, P., and González-Sáiz, J. M. (2013). Plasma lipidomic profiling method based on ultrasound extraction and liquid chromatography mass spectrometry. Analytical Chemistry, **85**(24), 12085–12092.

- Tsugawa, H., Cajka, T., Kind, T., Ma, Y., Higgins, B., Ikeda, K., Kanazawa, M., VanderGheynst, J., Fiehn, O., and Arita, M. (2015). Data independent MS/MS deconvolution for comprehensive metabolome analysis. Nature Methods, **12**(6), 523–526.

- Wang, S. Y., Kuo, C. H., and Tseng, Y. J. (2013). Batch normalizer: A fast total abundance regression calibration method to simultaneously adjust batch and injection order effects in liquid chromatography/time-of-flight mass spectrometry-based metabolomics data and comparison with current calibration methods. Analytical Chemistry, **85**(2), 1037–1046.

- Wang, Zhuozhong, Cui, B., Zhang, F., Yang, Y., Shen, X., Li, Z., Zhao, W., Zhang, Y., Deng, K., Rong, Z., Yang, K., Yu, X., Li, K., Han, P., and Zhu, Z. (2019). Development of a correlative strategy to discover colorectal tumor tissue derived

metabolite biomarkers in plasma using untargeted metabolomics. Analytical Chemistry, **91**(3), 2401−2408.

- Warth, B., Spangler, S., Fang, M., Johnson, C. H., Forsberg, E. M., Granados, A., Martin, R. L., Domingo-almenara, X., Huan, T., Rinehart, D., Montenegro-burke, J. R., Hilmers, B., Aisporna, A., Hoang, L. T., Uritboonthai, W., Benton, H. P., Richardson, S. D., Williams, A. J., and Siuzdak, G. (2017). Exposome-scale investigations guided by global metabolomics, pathway analysis, and cognitive computing. Analytical Chemistry, **89**(21), 11505–11513.

- Zhang, Y., Keerthisinghe, T. P., Han, Y., Liu, M., Wanjaya, E. R., and Fang, M. (2018). "Cocktail" of xenobiotics at human relevant levels reshapes the gut bacterial metabolome in a species-specific manner. Environmental Science and Technology, **52**(19), 11402–11410.

Appendix B

Table B1. Survey of TET levels in aquatic environments

Location	**Sample Matrix**	**Range** (μg/L)	**Reference**
Hong Kong	STPs influent	0.096 - 1.30	(Gulkowska et al., 2008)
Portugal	Hospital effluents	42.2 - 158	(Pena et al., 2010)
USA	WWTPs	n.d. - 0.2	(Yang et al., 2005)
China	River water	n.d. - 0.32	(Bu et al., 2013)
USA	River water	.005	(Arikan et al., 2008)
Iran	Animal wastewater	0.28 - 0.54.	(Javid et al., 2016)
China	Animal farm effluents	10.3	(Suzuki and Hoa, 2012)
USA	Water streams	n.d. - 0.11	(Kolpin et al., 2002)
China	Surface water	n.d. - 0.14	(Tong et al., 2014)
China	Ground water	n.d. - 0.12	(Tong et al., 2014)

n.d.: non-detection; WWTPs: wastewater treatment plants; STP: sewage treatment plants

Table B2. Primers used for quantitative real-time PCR

Gene	Primer sequences (5′–3′)
Ppar-αb	F: CTGCGGGACATCTCTCAGTC
	R: GAG AGG TGG AGG TGA ACT CG
Fabp2	F: CT ATTCTCTGGC AGACGGCAC
	R: TCT TGG CCT CGA CTC CAT CA
Fabp11a	F: CGAGAACG GCAAACTTGTGC
	R: CAC ATA TGT CCT GAC AGC C
Apoa4b.1	F: GCCTTTGTGGCATT CACAG
	R: CTT GAC CCA GTT GAG ACT C
Dgat2	F: GATCGA CCTGGGTGAG AGAC
	R: TTC CCT GAA CAT GGG CAA GC
C/Ebpα	F: AACGGAGCGAGCTTGACTT
	R: AAATCATGCCCATTAGCTGC
18s	F: CCTGCGGCTTAATTTGACTC
	R: GACAAATCGCTCCACCAACT

Fw: forward; Rev: reverse.

Table B3. Identified glycerolipids and respective fold changes at two TET exposure levels

Lipid subclass	**Lipid name**	**m/z**	**Adduct**	**1 µg/L TET**			**100 µg/L TET**		
				FC	***p*-value**	***q*-value**	**FC**	***p*-value**	***q*-value**
DAG	DAG 15:0	348.262	[M+NH4]+	1.22	0.66	0.93	1.04	0.88	0.91
DAG	DAG 16:0	362.325	[M+NH4]+	2.32	0.05	0.93	0.42	0.14	0.8
DAG	DAG 18:3	384.272	[M+NH4]+	0.87	0.57	0.93	3.15	0.24	0.8
DAG	DAG 18:3	384.281	[M+NH4]+	1.4	0.48	0.93	9.77	0.26	0.8
DAG	DAG 32:3	580.494	[M+NH4]+	0.95	0.83	0.93	1.15	0.56	0.8
DAG	DAG 34:1	612.556	[M+NH4]+	0.99	0.96	0.98	0.96	0.88	0.91
DAG	DAG 36:1	640.587	[M+NH4]+	1.01	0.97	0.98	1.04	0.85	0.91
DAG	DAG 36:2	638.571	[M+NH4]+	1.24	0.41	0.93	1.35	0.41	0.8
DAG	DAG 36:3	636.555	[M+NH4]+	0.89	0.75	0.93	0.93	0.88	0.91

DAG	DAG 36:3	636.556	[M+NH4]+	1.54	0.15	0.93	1.71	0.2	0.8
DAG	DAG 36:4	634.54	[M+NH4]+	1.53	0.08	0.93	1.89	0.08	0.8
DAG	DAG 36:8	626.492	[M+NH4]+	1.59	0.34	0.93	2.94	0.36	0.8
DAG	DAG 44:12	730.542	[M+NH4]+	1.22	0.71	0.93	1.3	0.6	0.8
DAG	DAG 46:5	772.68	[M+NH4]+	1.39	0.47	0.93	1.48	0.21	0.8
DAG	DAG 48:7	796.681	[M+NH4]+	0.87	0.81	0.93	0.91	0.81	0.91
DGDG	DGDG 34:2	934.64	[M+NH4]+	1.1	0.82	0.93	1.02	0.95	0.95
DGTS	DGTS 15:0	474.345	[M+H]+	1.67	0.16	0.93	0.68	0.36	0.8
DGTS	DGTS 15:1	472.333	[M+H]+	1.38	0.31	0.93	6.05	0.31	0.8
DGTS	DGTS 16:0	488.358	[M+H]+	0.87	0.83	0.93	19.86	0.34	0.8
DGTS	DGTS 19:2	526.377	[M+H]+	1.86	0.31	0.93	1.54	0.58	0.8
DGTS	DGTS 19:3	524.37	[M+H]+	1.51	0.33	0.93	1.36	0.62	0.8
DGTS	DGTS 21:2	554.405	[M+H]+	1.38	0.58	0.93	1.05	0.86	0.91
DGTS	DGTS 29:1	668.544	[M+H]+	2.02	0.07	0.93	2.11	0.48	0.8
DGTS	DGTS 42:1	850.747	[M+H]+	0.3	0.16	0.93	0.82	0.74	0.91
DGTS	DGTS 43:0	866.772	[M+H]+	0.18	0.09	0.93	0.65	0.47	0.8
DGTS	DGTS 43:1	864.762	[M+H]+	0.57	0.12	0.93	0.86	0.62	0.8
DGTS	DGTS 43:2	862.747	[M+H]+	0.82	0.39	0.93	1.12	0.59	0.8

DGTS	DGTS 44:2	876.762	[M+H]+	0.8	0.53	0.93	0.92	0.8	0.91
DGTS	DGTS 44:3	874.748	[M+H]+	0.93	0.78	0.93	1.15	0.58	0.8
DGTS	DGTS 45:1	892.794	[M+H]+	0.81	0.65	0.93	0.78	0.49	0.8
DGTS	DGTS 45:2	890.777	[M+H]+	0.58	0.12	0.93	0.82	0.54	0.8
DGTS	DGTS 45:3	888.763	[M+H]+	1.2	0.58	0.93	1.62	0.15	0.8
DGTS	DGTS 46:4	901.77	[M+H]+	0.27	0.35	0.93	0.45	0.47	0.8
DGTS	DGTS 46:5	898.755	[M+H]+	1.57	0.53	0.93	1.24	0.4	0.8
DGTS	DGTS 47:3	916.79	[M+H]+	0.67	0.25	0.93	0.61	0.22	0.8
DGTS	DGTS 47:4	914.775	[M+H]+	0.8	0.37	0.93	1.32	0.31	0.8
DGTS	LDGTS 14:1	444.332	[M+H]+	0.93	0.9	0.96	17.02	0.34	0.8
DGTS	LDGTS 15:1	458.351	[M+H]+	1.2	0.67	0.93	0.81	0.71	0.9
DGTS	LDGTS 17:2	484.366	[M+H]+	1.56	0.14	0.93	1.43	0.3	0.8
MAG	MAG 13:0	306.262	[M+NH4]+	2.29	0.06	0.93	0.38	0.15	0.8
MAG	MAG 15:0	334.293	[M+NH4]+	2.34	0.03	0.93	0.51	0.23	0.8
MAG	MAG 19:0	390.356	[M+NH4]+	2.14	0.06	0.93	0.33	0.1	0.8
MAG	MAG 19:1	388.342	[M+NH4]+	1.11	0.69	0.93	1.15	0.58	0.8
MAG	MAG 21:0	418.387	[M+NH4]+	2.61	0.04	0.93	0.29	0.1	0.8

MAG	MAG 26:4	480.393	[M+NH4]+	0.62	0.73	0.93	1.16	0.89	0.91
MGDG	MGDG 22:2	604.422	[M+NH4]+	2.06	0.19	0.93	2.4	0.29	0.8
MGDG	MGDG 7:0	398.203	[M+NH4]+	1.17	0.43	0.93	0.71	0.21	0.8
SQDG	SQDG 40:1	922.689	[M+NH4]+	1.08	0.95	0.98	1.89	0.5	0.8
TAG	TAG 36:1	659.525	[M+Na]+	1.23	0.37	0.93	1.57	0.13	0.35
TAG	TAG 36:2	657.505	[M+Na]+	1.22	0.67	0.93	1.31	0.67	0.77
TAG	TAG 36:3	655.492	[M+Na]+	1.44	0.23	0.93	1.39	0.37	0.52
TAG	TAG 37:7	656.496	[M+NH4]+	4.14	0.02	0.93	4.06	0.15	0.38
TAG	TAG 41:1	724.636	[M+NH4]+	0.86	0.55	0.93	0.75	0.22	0.38
TAG	TAG 42:0	740.676	[M+NH4]+	1.07	0.83	0.93	1.27	0.48	0.6
TAG	TAG 42:4	732.614	[M+NH4]+	1	0.99	0.99	1.16	0.26	0.42
TAG	TAG 43:0	754.692	[M+NH4]+	1.42	0.47	0.93	1.25	0.71	0.78
TAG	TAG 43:1	752.675	[M+NH4]+	1.16	0.68	0.93	1.45	0.28	0.44

TAG	TAG 44:0	768.707	[M+NH4]+	0.98	0.93	0.97	1.09	0.75	0.8
TAG	TAG 44:1	766.689	[M+NH4]+	1.25	0.47	0.93	1.36	0.36	0.52
TAG	TAG 45:1	780.705	[M+NH4]+	1.21	0.49	0.93	1.34	0.33	0.51
TAG	TAG 45:1	785.662	[M+Na]+	1.03	0.91	0.96	1.11	0.73	0.79
TAG	TAG 45:2	778.69	[M+NH4]+	1.2	0.59	0.93	1.28	0.37	0.52
TAG	TAG 46:2	792.707	[M+NH4]+	1.24	0.58	0.93	1.39	0.36	0.52
TAG	TAG 46:2	797.663	[M+Na]+	1.12	0.75	0.93	1.31	0.49	0.61
TAG	TAG 46:3	790.691	[M+NH4]+	1.19	0.67	0.93	1.75	0.16	0.38
TAG	TAG 47:2	806.723	[M+NH4]+	1.12	0.68	0.93	1.19	0.47	0.6
TAG	TAG 47:4	801.694	[M+NH4]+	0.82	0.33	0.93	0.77	0.15	0.38
TAG	TAG 47:5	800.682	[M+NH4]+	0.97	0.94	0.97	1	1	1
TAG	TAG 47:9	792.606	[M+NH4]+	0.72	0.56	0.93	1.47	0.62	0.73

TAG	TAG 48:3	818.724	[M+NH4]+	1.13	0.7	0.93	1.47	0.2	0.38
TAG	TAG 48:3	823.678	[M+Na]+	1.05	0.87	0.96	1.26	0.45	0.6
TAG	TAG 48:5	814.697	[M+NH4]+	0.94	0.75	0.93	0.8	0.41	0.57
TAG	TAG 49:3	832.739	[M+NH4]+	1.11	0.7	0.93	1.32	0.22	0.38
TAG	TAG 49:4	830.729	[M+NH4]+	0.85	0.42	0.93	0.79	0.2	0.38
TAG	TAG 50:0	857.741	[M+Na]+	1.36	0.41	0.93	1.64	0.02	0.19
TAG	TAG 50:4	844.744	[M+NH4]+	0.82	0.34	0.93	0.78	0.19	0.38
TAG	TAG 50:4	849.694	[M+Na]+	1.06	0.81	0.93	1.35	0.19	0.38
TAG	TAG 50:5	842.729	[M+NH4]+	0.91	0.55	0.93	0.8	0.26	0.42
TAG	TAG 50:5	847.678	[M+Na]+	1.34	0.46	0.93	1.68	0.08	0.27
TAG	TAG 50:6	840.713	[M+NH4]+	0.99	0.9	0.96	0.9	0.53	0.64
TAG	TAG 51:4	858.76	[M+NH4]+	0.79	0.29	0.93	0.87	0.45	0.6
TAG	TAG 51:6	854.73	[M+NH4]+	0.97	0.67	0.93	0.84	0.18	0.38

TAG	TAG 51:7	852.714	[M+NH4]+	1.04	0.86	0.96	0.96	0.85	0.89
TAG	TAG 52:4	872.772	[M+NH4]+	1.07	0.62	0.93	1.33	0.05	0.23
TAG	TAG 52:5	870.755	[M+NH4]+	1.16	0.59	0.93	1.65	0.03	0.19
TAG	TAG 52:6	868.74	[M+NH4]+	1.34	0.45	0.93	1.93	0.02	0.19
TAG	TAG 52:6	868.745	[M+NH4]+	1.01	0.91	0.96	0.99	0.9	0.93
TAG	TAG 52:7	866.729	[M+NH4]+	1.03	0.72	0.93	1.04	0.69	0.77
TAG	TAG 53:0	899.79	[M+Na]+	1.12	0.5	0.93	1.52	0.03	0.19
TAG	TAG 53:1	897.774	[M+Na]+	1.15	0.54	0.93	1.75	0.01	0.19
TAG	TAG 53:10	874.698	[M+NH4]+	1.29	0.48	0.93	1.69	0.03	0.19
TAG	TAG 53:3	893.748	[M+Na]+	1.07	0.77	0.93	1.28	0.19	0.38
TAG	TAG 53:4	886.786	[M+Na]+	1.15	0.41	0.93	1.45	0.04	0.21
TAG	TAG 53:6	882.754	[M+NH4]+	1.09	0.75	0.93	1.87	0.02	0.19
TAG	TAG 53:7	880.746	[M+NH4]+	1.03	0.7	0.93	1.08	0.68	0.77

TAG	TAG 53:7	880.755	[M+NH4]+	0.92	0.63	0.93	1.64	0.06	0.23
TAG	TAG 53:8	878.73	[M+NH4]+	0.98	0.78	0.93	0.99	0.93	0.94
TAG	TAG 53:9	876.713	[M+NH4]+	1.09	0.73	0.93	1.37	0.06	0.23
TAG	TAG 54:6	901.726	[M+Na]+	1.1	0.64	0.93	1.42	0.04	0.21
TAG	TAG 54:6	896.771	[M+NH4]+	1.17	0.52	0.93	1.74	0.03	0.19
TAG	TAG 54:6	897.779	[M+NH4]+	0.99	0.89	0.96	1.14	0.12	0.34
TAG	TAG 54:7	894.755	[M+NH4]+	1.3	0.47	0.93	2	0.05	0.23
TAG	TAG 54:7	899.711	[M+Na]+	1.27	0.5	0.93	1.71	0.06	0.23
TAG	TAG 55:10	902.729	[M+NH4]+	1.08	0.69	0.93	1.5	0.03	0.19
TAG	TAG 55:3	916.815	[M+NH4]+	1.06	0.62	0.93	1.33	0.03	0.19
TAG	TAG 55:7	908.777	[M+NH4]+	1.09	0.3	0.93	1.11	0.24	0.41
TAG	TAG 55:8	906.761	[M+NH4]+	1.08	0.25	0.93	1.12	0.11	0.33
TAG	TAG 55:8	911.733	[M+Na]+	0.78	0.35	0.93	1.68	0.1	0.31

TAG	TAG 56:12	917.668	[M+Na]+	0.8	0.64	0.93	1.23	0.6	0.72
TAG	TAG 56:8	920.771	[M+NH4]+	1.18	0.63	0.93	2.18	0.09	0.29
TAG	TAG 56:9	918.772	[M+NH4]+	1.09	0.75	0.93	1.67	0.01	0.19
TAG	TAG 57:10	930.76	[M+NH4]+	1.16	0.49	0.93	1.42	0.22	0.38
TAG	TAG 57:10	930.774	[M+NH4]+	0.83	0.65	0.93	1.56	0.2	0.38
TAG	TAG 58:10	944.77	[M+NH4]+	1.39	0.48	0.93	2.5	0.17	0.38
TAG	TAG 58:6	957.787	[M+Na]+	0.84	0.62	0.93	1.43	0.47	0.6
TAG	TAG 62:3	1019.951	[M+Na]+	1.04	0.8	0.93	0.66	0.08	0.27

FC: Fold Change by compare metabolic expression level at TET exposure vs. non-treated control

Table B4. Identified glycerophospholipids and respective fold changes at two TET exposure levels

Lipid subclass	Lipid name	m/z	Adduct	1 µg/L TET			100 µg/L TET		
				FC	*p*-value	q-value	FC	*p*-value	q-value
LPC	LPC 11:0	426.248	[M+H]+	0.86	0.56	0.99	0.99	0.97	0.99
LPC	LPC 12:0	440.263	[M+H]+	0.93	0.83	0.99	0.95	0.84	0.99
LPC	LPC 20:4	544.341	[M+H]+	1.79	0.34	0.99	1.44	0.42	0.99
LPC	LPC 22:3	574.385	[M+H]+	1.93	0.47	0.99	1.02	0.98	0.99
LPE	LPE 16:2	450.248	[M+H]+	1.28	0.38	0.99	1.17	0.5	0.99
LPE	LPE 16:3	448.255	[M+H]+	1.01	0.99	0.99	1.8	0.14	0.99
LPE	LPE 18:0	482.325	[M+H]+	1.58	0.26	0.99	1.54	0.48	0.99
LPE	LPE 18:4	474.265	[M+H]+	1.59	0.18	0.99	0.28	0.04	0.99
LPE	LPE 20:3	504.307	[M+H]+	1.68	0.35	0.99	1.47	0.63	0.99
PC	PC 16:0e	496.34	[M+H]+	2.71	0.23	0.99	2.17	0.33	0.99
PC	PC 16:1e	494.317	[M+H]+	1.31	0.45	0.99	6.37	0.31	0.99
PC	PC 17:0e	510.356	[M+H]+	2.4	0.23	0.99	1.69	0.51	0.99
PC	PC 17:1e	508.331	[M+H]+	0.7	0.74	0.99	0.22	0.28	0.99
PC	PC 18:0e	524.371	[M+H]+	1.65	0.3	0.99	1.4	0.58	0.99
PC	PC 18:1e	522.355	[M+H]+	2.09	0.33	0.99	1.24	0.63	0.99
PC	PC 18:1e	522.356	[M+H]+	2.52	0.34	0.99	1.73	0.28	0.99
PC	PC 18:2e	520.332	[M+H]+	1.57	0.03	0.99	1.25	0.25	0.99
PC	PC 19:0e	538.387	[M+H]+	2.39	0.14	0.99	1.83	0.43	0.99
PC	PC 19:2e	534.354	[M+H]+	2.48	0.22	0.99	1.36	0.67	0.99
PC	PC 20:0e	552.402	[M+H]+	1.66	0.22	0.99	1.3	0.54	0.99
PC	PC 20:0e	552.403	[M+H]+	2.53	0.07	0.99	1.68	0.42	0.99
PC	PC 20:2e	548.361	[M+H]+	1.95	0.5	0.99	1.35	0.75	0.99
PC	PC 20:5	556.303	[M+H]+	0.98	0.89	0.99	1.29	0.45	0.99

PC	PC 21:3e	560.378	[M+H]+	0.99	0.95	0.99	3.02	0.27	0.99
PC	PC 22:0e	580.437	[M+H]+	1.06	0.75	0.99	1.21	0.32	0.99
PC	PC 26:2e	632.468	[M+H]+	1.31	0.37	0.99	1.23	0.52	0.99
PC	PC 26:4e	628.439	[M+H]+	1.4	0.52	0.99	1.13	0.83	0.99
PC	PC 29:0	692.527	[M+H]+	0.68	0.52	0.99	0.58	0.48	0.99
PC	PC 30:0	706.539	[M+H]+	0.95	0.84	0.99	0.69	0.3	0.99
PC	PC 31:0	720.555	[M+H]+	0.91	0.71	0.99	0.74	0.42	0.99
PC	PC 32:0	734.571	[M+H]+	0.83	0.48	0.99	0.72	0.33	0.99
PC	PC 32:1	732.554	[M+H]+	1.39	0.48	0.99	1.06	0.85	0.99
PC	PC 33:0	748.586	[M+H]+	0.91	0.7	0.99	0.75	0.4	0.99
PC	PC 33:1	746.569	[M+H]+	1.09	0.85	0.99	0.83	0.74	0.99
PC	PC 34:0	762.602	[M+H]+	0.75	0.28	0.99	0.7	0.31	0.99
PC	PC 34:0e	748.62	[M+H]+	0.7	0.52	0.99	0.68	0.34	0.99
PC	PC 34:1	760.586	[M+H]+	1.1	0.81	0.99	0.99	0.98	0.99
PC	PC 34:2	758.569	[M+H]+	0.97	0.96	0.99	0.81	0.72	0.99
PC	PC 34:3	756.552	[M+H]+	1.27	0.44	0.99	1.05	0.91	0.99
PC	PC 35:1	774.602	[M+H]+	1.31	0.5	0.99	1.02	0.97	0.99
PC	PC 35:2	772.587	[M+H]+	1.33	0.67	0.99	0.71	0.54	0.99
PC	PC 36:1	788.617	[M+H]+	1.04	0.92	0.99	0.92	0.84	0.99
PC	PC 36:2	786.602	[M+H]+	1.01	0.99	0.99	0.68	0.55	0.99
PC	PC 38:3e	798.649	[M+H]+	1.02	0.98	0.99	0.98	0.97	0.99
PC	PC 38:6	806.57	[M+H]+	1.1	0.87	0.99	0.85	0.77	0.99
PC	PC 40:3e	826.678	[M+H]+	0.93	0.84	0.99	0.99	0.99	0.99
PC	PC 40:6	834.601	[M+H]+	1.12	0.85	0.99	0.77	0.66	0.99
PC	PC 40:6e	820.615	[M+H]+	1.27	0.62	0.99	0.99	0.99	0.99
PC	PC 40:7	832.585	[M+H]+	1.3	0.74	0.99	0.49	0.34	0.99
PC	PC 41:3e	840.687	[M+H]+	1.6	0.61	0.99	0.98	0.98	0.99
PC	PC 43:3	882.696	[M+H]+	0.65	0.57	0.99	0.97	0.97	0.99

PC	PC 45:3e	896.741	[M+H]+	0.99	0.98	0.99	1.6	0.22	0.99
PC	PC 45:6e	890.702	[M+H]+	1.14	0.91	0.99	1.48	0.69	0.99
PC	PC 47:3	938.752	[M+H]+	1.16	0.69	0.99	2.19	0.13	0.99
PC	PC 48:9e	926.713	[M+H]+	1.46	0.74	0.99	3.21	0.28	0.99
PE	PE 16:0e	454.294	[M+H]+	2.66	0.18	0.99	2.05	0.23	0.99
PE	PE 16:1	466.246	[M+H]+	0.85	0.71	0.99	0.75	0.54	0.99
PE	PE 20:4	516.274	[M+H]+	0.82	0.44	0.99	0.84	0.4	0.99
PE	PE 21:3e	518.323	[M+H]+	2.3	0.39	0.99	1.73	0.57	0.99
PE	PE 21:5e	514.307	[M+H]+	1.01	0.99	0.99	1.17	0.81	0.99
PE	PE 22:3e	532.334	[M+H]+	1.53	0.21	0.99	1.02	0.98	0.99
PE	PE 23:3e	546.353	[M+H]+	1.59	0.45	0.99	1.27	0.74	0.99
PE	PE 32:0	692.523	[M+H]+	0.8	0.48	0.99	0.74	0.5	0.99
PE	PE 33:0	706.543	[M+H]+	1.3	0.53	0.99	1.65	0.52	0.99
PE	PE 33:0e	692.557	[M+H]+	1.32	0.29	0.99	1.31	0.52	0.99
PE	PE 33:1e	690.532	[M+H]+	1.76	0.47	0.99	3.2	0.3	0.99
PE	PE 34:0	720.556	[M+H]+	0.61	0.3	0.99	0.8	0.56	0.99
PE	PE 34:0e	706.572	[M+H]+	1.2	0.64	0.99	1.09	0.86	0.99
PE	PE 35:0e	720.589	[M+H]+	0.95	0.81	0.99	0.95	0.86	0.99
PE	PE 35:1e	718.573	[M+H]+	0.78	0.54	0.99	0.98	0.96	0.99
PE	PE 35:2e	716.564	[M+H]+	1.22	0.11	0.99	1.18	0.58	0.99
PE	PE 35:3	728.522	[M+H]+	1.04	0.9	0.99	0.61	0.31	0.99
PE	PE 36:3	742.54	[M+H]+	0.84	0.68	0.99	0.58	0.34	0.99
PE	PE 37:1e	746.604	[M+H]+	1.24	0.68	0.99	3.01	0.08	0.99
PE	PE 37:2e	744.586	[M+H]+	1.7	0.57	0.99	1.85	0.5	0.99
PE	PE 37:3	756.552	[M+H]+	0.79	0.41	0.99	0.66	0.26	0.99
PE	PE 37:3e	742.57	[M+H]+	0.95	0.89	0.99	0.85	0.78	0.99
PE	PE 38:3	770.573	[M+H]+	0.88	0.66	0.99	0.7	0.3	0.99
PE	PE 39:3	784.583	[M+H]+	0.76	0.3	0.99	0.81	0.51	0.99

PE	PE 40:4	796.592	[M+H]+	1.49	0.36	0.99	0.88	0.85	0.99
PE	PE 40:6	792.555	[M+H]+	1.92	0.4	0.99	1.41	0.59	0.99
PE	PE 41:4	810.599	[M+H]+	1.12	0.73	0.99	1.12	0.79	0.99
PE	PE 43:5e	822.643	[M+H]+	0.91	0.73	0.99	1	0.99	0.99
PE	PE 43:6e	820.625	[M+H]+	1.58	0.46	0.99	3.2	0.34	0.99
PE	PE 44:5e	836.659	[M+H]+	0.89	0.65	0.99	0.88	0.66	0.99
PE	PE 44:6e	834.653	[M+H]+	1.23	0.85	0.99	0.26	0.5	0.99
PE	PE 45:5e	850.675	[M+H]+	0.74	0.41	0.99	0.96	0.91	0.99
PE	PE 45:6e	848.659	[M+H]+	0.98	0.94	0.99	1.06	0.9	0.99
PE	PE 46:5e	864.69	[M+H]+	0.76	0.27	0.99	0.87	0.61	0.99
PE	PE 46:6e	862.674	[M+H]+	0.92	0.8	0.99	0.92	0.8	0.99
PE	PE 47:5e	877.7	[M+H]+	0.77	0.59	0.99	1.03	0.95	0.99
PE	PE 48:4e	894.725	[M+H]+	0.84	0.48	0.99	1.5	0.19	0.99
PG	PG 18:1	542.328	M+NH4]+	2.42	0.28	0.99	1.98	0.09	0.99
PG	PG 43:1	892.711	M+NH4]+	1.03	0.92	0.99	1.79	0.03	0.99
PG	PG 45:1	920.741	M+NH4]+	0.86	0.71	0.99	1.4	0.37	0.99
PS	PS 26:5	642.336	[M+H]+	1.42	0.24	0.99	1.33	0.32	0.99
PS	PS 48:10	940.599	[M+H]+	0.96	0.94	0.99	1.01	0.99	0.99

FC: Fold Change by compare metabolic expression level at TET exposure vs. non-treated control

Table B5. Identified sphingolipids and respective fold changes at two TET exposure levels

Lipid subclass	Lipid name	m/z	Adduct	1 µg/L TET			100 µg/L TET		
				FC	p-value	q-value	FC	p-value	q-value
Cer	Cer-NDS d0:0	596.598	[M+H]+	1.39	0.11	0.99	0.85	0.53	0.95
Cer	Cer-NDS d0:0	624.628	[M+H]+	1.56	0.05	0.99	0.83	0.49	0.95
Cer	Cer-NDS d28:0	456.441	[M+H]+	1.08	0.86	0.99	1.04	0.92	0.95
Cer	Cer-NDS d30:0	484.473	[M+H]+	1.07	0.87	0.99	1.29	0.51	0.95
Cer	Cer-NDS d31:0	498.487	[M+H]+	1.33	0.22	0.99	1.55	0.1	0.95
Cer	Cer-NDS d32:0	511.51	[M+H]+	0.95	0.81	0.99	0.87	0.54	0.95
Cer	Cer-NDS d33:0	526.52	[M+H]+	0.66	0.07	0.99	0.93	0.73	0.95
Cer	Cer-NDS d34:0	540.536	[M+H]+	1.12	0.72	0.99	1.24	0.46	0.95
Cer	Cer-NDS d35:1	552.535	[M+H]+	0.98	0.95	0.99	0.99	0.98	0.95
Cer	Cer-NDS d35:1	552.554	[M+H]+	0.85	0.88	0.99	0.82	0.85	0.95
Cer	Cer-NDS d36:0	568.567	[M+H]+	1.18	0.55	0.99	1.1	0.74	0.95
Cer	Cer-NDS d37:0	582.582	[M+H]+	1.02	0.91	0.99	1.03	0.85	0.95
Cer	Cer-NDS d38:2	592.567	[M+H]+	1.22	0.64	0.99	1.33	0.45	0.95

Cer	Cer-NDS d39:1	608.595	[M+H]+	1.14	0.48	0.99	1.1	0.72	0.95
Cer	Cer-NDS d41:1	636.629	[M+H]+	0.96	0.75	0.99	0.96	0.79	0.95
Cer	Cer-NDS d41:2	634.613	[M+H]+	1.17	0.49	0.99	1.25	0.44	0.95
Cer	Cer-NDS d42:1	650.644	[M+H]+	0.88	0.5	0.99	0.94	0.69	0.95
Cer	Cer-NDS d42:2	648.628	[M+H]+	0.92	0.63	0.99	0.94	0.79	0.95
Cer	Cer-NDS d43:2	662.644	[M+H]+	0.93	0.68	0.99	0.83	0.27	0.95
Cer	Cer-NDS d44:1	678.675	[M+H]+	0.79	0.34	0.99	0.74	0.19	0.95
Cer	Cer-NDS d44:2	676.66	[M+H]+	0.93	0.72	0.99	0.82	0.33	0.95
Cer	Cer-NS d36:4	560.503	[M+H]+	0.69	0.59	0.99	0.75	0.77	0.95
Cer	Cer-NS d37:4	574.515	[M+H]+	0.94	0.81	0.99	0.94	0.82	0.95
Cer	Cer-NS d40:1	622.614	[M+H]+	1.24	0.51	0.99	1.23	0.43	0.95
Cer	Cer-NS d41:3	632.589	[M+H]+	0.77	0.63	0.99	1.14	0.81	0.95
Cer	Cer-NS d41:4	630.58	[M+H]+	1.08	0.73	0.99	1.14	0.65	0.95
Cer	Cer-NS d42:4	644.596	[M+H]+	0.9	0.64	0.99	1.02	0.9	0.95
Cer	Cer-NS d42:5	642.579	[M+H]+	1.16	0.68	0.99	1.02	0.95	0.95
Cer	Cer-NS d43:4	658.611	[M+H]+	0.85	0.32	0.99	1	1	0.95

Cer	Cer-NS d43:5	656.595	[M+H]+	1.13	0.57	0.99	1.34	0.39	0.95
Cer	Cer-NS d44:4	672.626	[M+H]+	0.81	0.29	0.99	0.92	0.6	0.95
Cer	Cer-NS d44:5	670.611	[M+H]+	0.9	0.62	0.99	0.96	0.85	0.95
Cer	Cer-NS d45:5	684.626	[M+H]+	0.88	0.49	0.99	0.86	0.44	0.95
Cer	Cer-NS d46:5	698.641	[M+H]+	0.85	0.43	0.99	0.83	0.3	0.95
HexCer	HexCer-NDS d34:1	700.571	[M+H]+	1.27	0.35	0.99	1.15	0.73	0.95
HexCer	HexCer-NDS d38:2	754.611	[M+H]+	0.92	0.87	0.99	1.17	0.81	0.95
HexCer	HexCer-NDS d39:2	768.629	[M+H]+	1.23	0.62	0.99	1.45	0.59	0.95
HexCer	HexCer-NDS d41:2	796.663	[M+H]+	0.8	0.53	0.99	0.82	0.53	0.95
HexCer	HexCer-NDS d43:2	824.694	[M+H]+	0.71	0.34	0.99	0.97	0.93	0.95
HexCer	HexCer-NS d30:3	640.475	[M+H]+	1.25	0.68	0.99	0.82	0.73	0.95
HexCer	HexCer-NS d34:2	698.555	[M+H]+	1.53	0.08	0.99	1.3	0.48	0.95
HexCer	HexCer-NS d37:3	738.58	[M+H]+	0.91	0.81	0.99	0.74	0.56	0.95
HexCer	HexCer-NS d38:2	754.614	[M+H]+	0.95	0.92	0.99	1.66	0.56	0.95
HexCer	HexCer-NS d40:2	782.649	[M+H]+	0.91	0.71	0.99	0.96	0.91	0.95
HexCer	HexCer-NS d40:3	780.63	[M+H]+	1.19	0.6	0.99	1.25	0.61	0.95

HexCer	HexCer-NS d40:3	780.633	[M+H]+	1.17	0.47	0.99	1.24	0.39	0.95
HexCer	HexCer-NS d41:3	794.646	[M+H]+	3.36	0.19	0.99	2.32	0.44	0.95
HexCer	HexCer-NS d42:3	808.664	[M+H]+	0.98	0.94	0.99	0.97	0.94	0.95
HexCer	HexCer-NS d42:4	806.646	[M+H]+	0.66	0.5	0.99	1.26	0.61	0.95
HexCer	HexCer-NS d44:4	834.678	[M+H]+	0.78	0.41	0.99	0.78	0.47	0.95
HexCer	HexCer-NS d44:5	832.664	[M+H]+	0.98	0.97	0.99	1.23	0.56	0.95
HexCer	HexCer-NS d46:4	862.701	[M+H]+	0.88	0.78	0.99	1.49	0.27	0.95
HexCer	HexCer-NS d47:4	876.726	[M+H]+	0.9	0.63	0.99	1.34	0.51	0.95
SM	SM d32:1	675.543	[M+H]+	1.28	0.39	0.99	0.97	0.93	0.95
SM	SM d32:3	671.476	[M+H]+	2.13	0.07	0.99	0.73	0.68	0.95
SM	SM d33:1	689.559	[M+H]+	1.51	0.2	0.99	1.17	0.68	0.95
SM	SM d34:0	705.59	[M+H]+	1.03	0.93	0.99	0.69	0.32	0.95
SM	SM d34:4	697.523	[M+H]+	1.43	0.41	0.99	0.82	0.79	0.95
SM	SM d35:1	717.59	[M+H]+	1.21	0.22	0.99	0.95	0.84	0.95
SM	SM d36:1	731.606	[M+H]+	1	0.99	0.99	0.77	0.35	0.95
SM	SM d36:4	725.556	[M+H]+	1.22	0.13	0.99	0.81	0.47	0.95

SM	SM d37:1	745.62	[M+H]+	1.07	0.71	0.99	0.82	0.48	0.95
SM	SM d37:2	742.593	[M+H]+	1.47	0.09	0.99	1.24	0.54	0.95
SM	SM d37:3	741.59	[M+H]+	1.48	0.09	0.99	1.22	0.55	0.95
SM	SM d37:4	739.567	[M+H]+	1.37	0.43	0.99	1.06	0.93	0.95
SM	SM d38:1	759.637	[M+H]+	1.06	0.79	0.99	0.83	0.54	0.95
SM	SM d39:1	773.653	[M+H]+	0.98	0.95	0.99	0.87	0.7	0.95
SM	SM d39:2	771.635	[M+H]+	1.23	0.63	0.99	1.21	0.64	0.95
SM	SM d40:1	787.668	[M+H]+	0.91	0.61	0.99	0.75	0.29	0.95
SM	SM d40:2	785.653	[M+H]+	1.31	0.21	0.99	1.08	0.79	0.95
SM	SM d40:3	783.637	[M+H]+	1.4	0.23	0.99	1.08	0.84	0.95
SM	SM d40:4	781.619	[M+H]+	0.88	0.76	0.99	0.74	0.55	0.95
SM	SM d41:1	801.684	[M+H]+	0.92	0.71	0.99	0.77	0.32	0.95
SM	SM d41:2	799.668	[M+H]+	1.24	0.5	0.99	1.09	0.78	0.95
SM	SM d41:3	797.652	[M+H]+	1.41	0.12	0.99	0.93	0.79	0.95
SM	SM d41:4	795.632	[M+H]+	1.13	0.9	0.99	0.88	0.9	0.95
SM	SM d42:2	813.684	[M+H]+	1.05	0.71	0.99	0.8	0.36	0.95

SM	SM d42:3	811.668	[M+H]+	1.31	0.16	0.99	0.91	0.68	0.95
SM	SM d42:4	809.651	[M+H]+	0.88	0.8	0.99	0.57	0.4	0.95
SM	SM d42:4	809.658	[M+H]+	0.91	0.8	0.99	0.73	0.55	0.95
SM	SM d42:5	807.635	[M+H]+	1.29	0.24	0.99	1.12	0.73	0.95
SM	SM d43:1	829.714	[M+H]+	0.81	0.36	0.99	0.72	0.25	0.95
SM	SM d43:2	827.699	[M+H]+	1.05	0.8	0.99	0.72	0.11	0.95
SM	SM d43:3	825.679	[M+H]+	1.27	0.68	0.99	0.59	0.4	0.95
SM	SM d43:4	823.663	[M+H]+	0.86	0.56	0.99	0.84	0.54	0.95
SM	SM d43:5	821.647	[M+H]+	1.37	0.64	0.99	1.73	0.44	0.95
SM	SM d44:0	845.743	[M+H]+	1.09	0.75	0.99	1.57	0.08	0.95
SM	SM d44:3	839.697	[M+H]+	1.02	0.94	0.99	0.69	0.42	0.95
SM	SM d44:5	835.666	[M+H]+	0.99	0.97	0.99	0.74	0.31	0.95
SM	SM d45:0	859.758	[M+H]+	1.2	0.53	0.99	1.47	0.08	0.95
SM	SM d45:4	851.687	[M+H]+	0.77	0.39	0.99	0.85	0.64	0.95
SM	SM d45:5	849.674	[M+H]+	1.02	0.94	0.99	0.85	0.57	0.95
SM	SM d46:0	873.775	[M+H]+	1.04	0.74	0.99	1.34	0.06	0.95

SM	SM d46:1	871.759	[M+H]+	1.17	0.55	0.99	1.67	0.03	0.95
SM	SM d47:1	885.772	[M+H]+	1.17	0.5	0.99	1.62	0.05	0.97
SM	SM d48:0	901.806	[M+H]+	1.05	0.76	0.99	1.37	0.07	0.97
SM	SM d49:2	911.797	[M+H]+	0.85	0.37	0.99	1.19	0.3	0.97
SM	SM d50:2	925.805	[M+H]+	1.08	0.7	0.99	1.69	0.18	0.97
SM	SM d50:3	923.79	[M+H]+	1.12	0.65	0.99	1.89	0.13	0.97
SM	SM d51:2	939.828	[M+H]+	0.88	0.67	0.99	1.84	0.22	0.97
SM	SM d51:3	937.819	[M+H]+	0.87	0.67	0.99	1.36	0.44	0.97
SM	SM d52:2	953.849	[M+H]+	0.99	0.99	0.99	2.1	0.38	0.97
SM	SM d52:3	951.834	[M+H]+	0.93	0.84	0.99	1.65	0.29	0.97
SM	SM d52:4	949.805	[M+H]+	1.09	0.75	0.99	2.34	0.1	0.99
SM	SM d53:4	963.835	[M+H]+	0.97	0.89	0.99	1.65	0.17	1

FC: Fold Change by compare metabolic expression level at TET exposure vs. non-treated control.

Table B6. Identified metabolites and respective fold changes at two TET exposure levels.

Metabolite	**KEGG ID**	**m/z**	**ESI mode**	**1 µg/L TET**			**100 µg/L TET**		
				FC	**p-value**	**q-value**	**FC**	**p-value**	**q-value**
16-Hydroxy hexadecanoic acid	-	290.269	ESI (+)	1.81	0.2	0.32	4.09	0	0.03
3-Dehydrosphinganine	C02934	300.289	ESI (+)	1.12	0.84	0.85	3.14	0.05	0.07
3-Phosphoglyceric acid	C00597	184.986	ESI (-)	2.33	0.38	0.97	1.64	0.43	0.98
4-Hydroxycinnamic acid	C00811	165.052	ESI (+)	0.38	0	0.13	0.6	0.05	0.07
Adenine	C00147	134.047	ESI (-)	31.5	0.13	0.86	3.6	0.09	0.98
Adenosine	C00212	266.091	ESI (-)	7.17	0.33	0.97	6.28	0.34	0.98
Alpha-Linolenic acid	C06427	277.217	ESI (-)	2.14	0.02	0.27	1.56	0.95	0.98
Aminoadipic acid	C00956	144.066	ESI (+)	2.22	0.03	0.17	1.88	0.06	0.09
AMP	C00020	346.056	ESI (-)	1.58	0.91	0.97	1.33	0.75	0.98
Beta-D-Glucose 6-phosphate	C01172	259.023	ESI (-)	1.48	0.89	0.97	1.25	0.88	0.98
Capric acid	C01571	171.14	ESI (-)	2.73	0.83	0.97	4.12	0.37	0.98
Choline	C00114	104.107	ESI (+)	1.22	0.48	0.57	1.54	0.03	0.05
Citric acid	C00158	191.02	ESI (-)	1.66	0.95	0.97	1.19	0.44	0.98
Citrulline	C00327	176.108	ESI (+)	1.58	0.33	0.41	1.03	0.97	0.97

cAMP	C00575	328.044	ESI (-)	6.32	0.34	0.97	5.63	0.34	0.98
cGMP	C00942	344.039	ESI (-)	3.11	0.42	0.97	2.16	0.57	0.98
Cytidine	C00475	242.08	ESI (-)	1.3	0.59	0.97	1.2	0.96	0.98
Cytosine	C00380	112.051	ESI (+)	2.21	0.28	0.35	2.09	0.02	0.05
D-Glutamine	C00819	145.062	ESI (-)	1.35	0.79	0.97	1.33	0.97	0.98
Diaminopimelic acid	C00666	189.088	ESI (-)	1.54	0.63	0.97	1.12	0.88	0.98
Dodecanoic acid	C02679	199.171	ESI (-)	1.28	0.86	0.97	1.26	0.9	0.98
D-Proline	C00763	114.056	ESI (-)	1.37	0.39	0.97	1.27	0.88	0.98
D-Ribose 5-phosphate	C00117	229.012	ESI (-)	2.16	0.64	0.97	1.24	0.76	0.98
D-Sedoheptulose 7-phosphate	C00281	289.033	ESI (-)	1.71	0.52	0.97	1.36	0.83	0.98
D-Xylose	C00181	149.046	ESI (-)	3.2	0.37	0.97	2.13	0.5	0.98
Ethyl dodecanoate	-	246.243	ESI (+)	2.27	0.15	0.32	3.57	0.01	0.03
FMN	C00061	455.1	ESI (-)	1.99	0.83	0.97	1.3	0.68	0.98
Fumaric acid	C00122	115.004	ESI (-)	1.54	0.17	0.91	1.17	0.46	0.98
Gaidic acid	-	253.218	ESI (-)	1.67	0.03	0.27	1.37	0.6	0.98
Gluconic acid	C00257	195.052	ESI (-)	1.17	0.56	0.97	1.29	0.24	0.98
Glyceric acid	C00258	105.019	ESI (-)	1.29	0.41	0.97	1.35	0.19	0.98
GMP	C00144	362.051	ESI (-)	1.56	0.61	0.97	1.36	0.66	0.98

Guanosine	C00387	282.085	ESI (-)	1.7	0.4	0.97	1.53	0.87	0.98
IMP	C00130	347.04	ESI (-)	1.86	0.27	0.97	1.57	0.93	0.98
Inosine	C00294	267.074	ESI (-)	1.35	0.71	0.97	1.47	0.51	0.98
Ketosphingosine	C06121	298.272	ESI (+)	0.5	0.04	0.17	0.46	0.02	0.05
L-Acetylcarnitine	C02571	204.123	ESI (+)	1.13	0.79	0.84	1.21	0.57	0.65
L-Arginine	C00062	173.103	ESI (-)	1.18	0.76	0.97	1.37	0.41	0.98
L-Aspartic acid	C00049	132.03	ESI (-)	1.51	0.59	0.97	1.65	0.79	0.98
L-Glutamic acid	C00025	146.046	ESI (-)	1.63	1	1	1.51	0.75	0.98
L-Histidine	C00135	156.077	ESI (+)	1.78	0.05	0.22	1.78	0.01	0.03
L-Homoserine	C00263	118.051	ESI (-)	1.11	0.98	1	1.36	0.85	0.98
Linoleic acid	C01595	279.233	ESI (-)	1.92	0.02	0.27	1.65	0.86	0.98
L-Lactic acid	C00186	89.024	ESI (-)	1.53	0.16	0.87	1.36	0.02	0.98
L-Leucine	C00123	130.062	ESI (-)	1.52	0.92	0.97	1.3	0.67	0.98
L-Methionine	C00073	148.044	ESI (-)	1.69	0.93	0.97	1.64	0.99	0.99
L-Phenylalanine	C00079	164.072	ESI (-)	1.3	0.03	0.27	1.34	0.08	0.98
L-Pipecolic acid	C00408	128.072	ESI (-)	1.76	0.65	0.97	1.75	0.69	0.98
L-Proline	C00148	116.069	ESI (+)	1.06	0.85	0.85	0.93	0.83	0.88
L-Tryptophan	C00078	203.083	ESI (-)	1.49	0.09	0.64	1.55	0.11	0.98

L-Tyrosine	C00082	182.077	ESI (+)	0.61	0.01	0.13	0.63	0.05	0.07
L-Valine	C00183	116.072	ESI (-)	1.3	0.75	0.97	1.36	0.87	0.98
Malate	C00497	133.014	ESI (-)	1.4	0.19	0.93	1.21	0.28	0.98
N-Acetyl-glucosamine 1-phosphate	C04256	300.049	ESI (-)	2.21	0.44	0.97	1.52	0.38	0.98
N-Acetylhistidine	C02997	196.073	ESI (-)	2.03	0.02	0.27	1.92	0.04	0.98
N-Acetyl-L-aspartic acid	C01042	174.041	ESI (-)	1.4	0.53	0.97	1.35	0.87	0.98
NAD	C00003	662.102	ESI (-)	1.82	0.93	0.97	1.76	0.17	0.98
Niacinamide	C00153	123.055	ESI (+)	1.06	0.79	0.84	1.19	0.16	0.19
Oleic acid	C00712	281.249	ESI (-)	1.98	0.02	0.27	1.5	0.5	0.98
Palmitic acid	C00249	255.233	ESI (-)	1.43	0.21	0.96	1.17	0.79	0.98
Palmitic amide	-	256.263	ESI (+)	1.92	0.18	0.32	5.73	0.03	0.05
Pantothenic acid	C00864	218.104	ESI (-)	1.92	0.84	0.97	1.21	0.97	0.98
Pyroglutamic acid	C01879	128.035	ESI (-)	3.23	0.36	0.97	2.82	0.38	0.98
Riboflavin	C00255	375.132	ESI (-)	2.92	0.69	0.97	2.46	0.64	0.98
S-Adenosylmethionine	C00019	399.142	ESI (+)	2.82	0.07	0.22	4.13	0.01	0.03
Serine	C00065	106.05	ESI (+)	1.48	0.12	0.29	1.42	0.02	0.05
S-Methylthioadenosine	C00170	298.096	ESI (+)	2.46	0.07	0.22	3.91	0.02	0.05

Stearic acid	C01530	302.305	ESI (+)	2.37	0.15	0.32	4.14	0	0.03
Succinic acid	C00042	117.019	ESI (-)	1.62	0.61	0.97	1.14	0.71	0.98
Succinyladenosine	-	382.103	ESI (-)	2.37	0.61	0.97	1.46	0.29	0.98
Taurine	C00245	126.021	ESI (+)	1.19	0.27	0.35	1.27	0.09	0.12
Tetradecanal	-	230.245	ESI (+)	1.6	0.27	0.35	3.28	0	0.03
Thymidine	C00214	241.082	ESI (-)	1.83	0.86	0.97	2.83	0.46	0.98
trans-Cinnamic acid	C00423	149.058	ESI (+)	0.73	0.21	0.34	0.67	0.1	0.13
UDP-N-acetyl-D-galactosamine	G10611	606.074	ESI (-)	3.8	0.47	0.97	1.7	0.58	0.98
UMP	C00105	323.029	ESI (-)	3.45	0.32	0.97	1.5	0.6	0.98
Uracil	C00106	111.021	ESI (-)	1.39	0.88	0.97	1.14	0.83	0.98
Uridine	C00299	243.062	ESI (-)	1.66	0.86	0.97	1.52	0.91	0.98
Xanthine	C00385	151.026	ESI (-)	1.69	0.54	0.97	1.56	0.14	0.98

FC: Fold Change by compare metabolic expression level at TET exposure vs. non-treated control.

Table B7. Three exposure levels of TET for three model bacteria

Model bacteria		**TET concentration (mg/L)**
B. fragilis	Low	0.01
	Middle	0.08
	High	0.16
C. sporongenes	Low	0.01
	Middle	0.065
	High	0.13
E. coli	Low	0.01
	Middle	0.5
	High	7.4

Table B8. Metabolites identified across all three model bacteria, and respective fold changes at three exposure levels.

Metabolite	KEGG	m/z	*E. coli*						*B. fragilis*						*C. sporogense*					
			High		**Middle**		**Low**		**High**		**Middle**		**Low**		**High**		**Middle**		**Low**	
			FC	Sig.	FC	Sig.	FC	Sig.	FC	Sig.	FC	Sig.	FC	Sig.	FC	Sig.	FC	Sig.	FC	Sig.
2-hydroxyglucorate	**C02630**	**147.03**	0.70	0.09	0.73	0.07	0.72	0.01	0.63	0.04	0.96	0.82	0.88	0.46	0.88	0.65	0.75	0.36	0.57	0.06
2-Acetolactate	**C00900**	**131.035**	0.55	0.06	0.72	0.05	0.76	0.19	0.92	0.36	0.74	0.01	0.84	0.17	1.09	0.72	1.11	0.57	0.95	0.82
2-Methylbutyric acid	**C18319**	**101.061**	0.77	0.75	1.55	0.6	1.32	0.47	0.15	0.01	0.09	0.00	0.41	0.06	1.08	0.83	0.89	0.73	0.89	0.75
3-Furoic acid	**C01546**	**111.009**	0.41	0.01	0.6	0.00	0.8	0.19	0.78	0.37	0.60	0.02	0.74	0.13	1.35	0.39	1.38	0.36	0.93	0.90
3-Phospho-D-glycerate	**C00597**	**184.985**	0.92	0.65	1.44	0.00	1.22	0.42	1.83	0.24	0.55	0.01	1.05	0.8	1.11	0.61	1.25	0.17	0.93	0.69
4-Pyridoxic acid	**C00847**	**182.046**	0.70	0.01	0.74	0.00	1.03	0.91	0.56	0.00	0.69	0.04	0.93	0.14	1.05	0.81	0.79	0.24	0.86	0.45
5-Hydroxy-L-tryptophan	**C01017**	**219.077**	0.79	0.37	0.78	0.14	0.92	0.36	0.8	0.05	0.85	0.13	0.99	0.91	1.13	0.41	1.00	0.98	0.89	0.50
5-L-Glutamyl-L-alanine	**C03740**	**217.083**	0.43	0.00	0.65	0.00	0.93	0.65	0.94	0.39	0.78	0.07	0.91	0.22	0.84	0.29	0.76	0.13	1.00	1.00
Adenine	**C00147**	**134.047**	0.80	0.47	0.86	0.41	1.44	0.12	1.46	0.04	1.27	0.12	1.24	0.27	0.90	0.64	0.63	0.05	0.69	0.10
Acetoacetyl-CoA	**C00332**	**424.977**	2.72	0.05	1.46	0.15	0.90	0.70	0.78	0.06	0.55	0.02	0.87	0.45	0.72	0.02	0.65	0.01	0.68	0.02
Acetyl-CoA	**C00024**	**403.556**	1.05	0.77	1.27	0.09	1.24	0.23	0.49	0.00	0.75	0.13	1.02	0.92	0.97	0.86	0.79	0.22	0.85	0.40
Adenosine	**C00212**	**266.089**	0.67	0.28	1.27	0.37	1.97	0.09	1.73	0.00	1.72	0.04	1.25	0.4	0.98	0.91	1.10	0.68	1.17	0.59
ADP	**C00008**	**426.022**	0.56	0.04	1.02	0.9	1.11	0.5	1.04	0.89	0.46	0.01	0.79	0.29	0.54	0.00	0.63	0.00	0.75	0.01
AMP	**C00020**	**346.056**	0.61	0.03	0.76	0.05	1.15	0.74	2.05	0.02	2.96	0.03	1.32	0.39	0.83	0.52	1.08	0.69	1.07	0.80
Arabitol	**C00532**	**151.061**	0.34	0.01	0.46	0.01	0.37	0.00	1.64	0.15	1.09	0.79	0.83	0.67	1.05	0.78	1.01	0.95	0.88	0.48

Arginine	**C00062**	**173.104**	0.36	0.10	0.9	0.8	0.58	0.14	2.82	0.00	3.16	0.00	2.49	0.02	0.92	0.68	0.87	0.53	0.77	0.27
Aspartic acid	**C00049**	**132.030**	0.54	0.01	0.74	0.03	0.83	0.1	0.83	0.00	0.61	0.00	0.67	0.00	0.66	0.17	0.37	0.01	0.59	0.07
ATP	**C00002**	**505.988**	1.05	0.82	1.72	0.00	1.09	0.94	0.46	0.00	0.09	0.00	0.52	0.04	0.79	0.08	0.49	0.00	0.61	0.01
Beta-D-Glucose 6-phosphate	**C01172**	**259.022**	1.22	0.14	0.99	0.92	1.02	0.86	1.22	0.00	0.87	0.22	0.92	0.66	0.89	0.63	0.89	0.61	0.77	0.29
Butyryl-CoA	**C00136**	**417.570**	ND	ND	ND	ND	ND	ND	0.51	0.00	0.39	0.00	0.67	0.10	0.67	0.11	0.57	0.01	0.66	0.02
cAMP	**C00575**	**328.045**	0.71	0.13	0.79	0.08	0.99	0.82	1.03	0.00	0.82	0.31	0.94	0.79	1.05	0.87	1.12	0.61	0.76	0.48
Capric acid	**C01571**	**171.139**	1.23	0.7	1.15	0.73	1.04	0.96	0.57	0.00	1.07	0.83	0.83	0.64	0.59	0.00	0.8	0.08	1.08	0.68
CDP	**C00112**	**402.010**	2.45	0.07	2.32	0.00	1.49	0.18	1.3	0.00	0.15	0.01	0.36	0.04	0.67	0.00	0.72	0.11	0.63	0.00
cGMP	**C00942**	**344.040**	0.60	0.03	0.71	0.01	0.93	0.66	0.72	0.00	0.62	0.01	0.78	0.22	1.13	0.6	1.18	0.41	0.9	0.73
cis-Aconitate	**C00417**	**173.008**	1.03	0.95	1.14	0.76	2.54	0.19	4.19	0.00	4.12	0.00	2.63	0.15	0.88	0.53	0.9	0.58	0.83	0.46
Citric acid	**C00158**	**191.020**	0.43	0.01	0.6	0.00	0.81	0.21	0.85	0.00	0.59	0.04	0.73	0.14	1.35	0.38	1.38	0.36	0.91	0.85
CMP	**C00055**	**322.044**	0.65	0.15	0.61	0.06	0.84	0.49	1.65	0.00	1.16	0.42	1.02	0.93	0.80	0.46	0.91	0.67	0.85	0.57
Cytidine	**C00475**	**242.078**	0.89	0.63	1.18	0.49	1.71	0.09	0.76	0.00	0.55	0.00	0.59	0.02	0.76	0.65	0.81	0.67	0.58	0.33
Mannitol	**C00392**	**181.072**	0.59	0.02	0.9	0.22	1.03	1.00	1.51	0.00	1.89	0.02	1.26	0.56	0.92	0.66	0.74	0.02	0.92	0.50
Deoxyuridine	**C00526**	**227.068**	1.74	0.33	1.62	0.33	1.01	0.84	1.30	0.00	1.56	0.07	1.58	0.12	1.01	0.98	1.14	0.71	1.16	0.72
Glutamine	**C00819**	**145.062**	0.68	0.05	0.69	0.02	0.78	0.27	1.01	0.00	0.76	0.35	0.66	0.17	1.15	0.89	2.22	0.29	2.08	0.59
Dihydrothymine	**C00906**	**127.051**	0.80	0.44	0.75	0.06	0.89	0.38	0.61	0.00	0.77	0.03	0.9	0.30	1.16	0.70	0.71	0.32	0.78	0.50
Dihydrouracil	**C00429**	**113.034**	0.96	0.88	0.88	0.68	1.58	0.42	0.73	0.00	0.69	0.00	0.77	0.05	0.63	0.37	0.70	0.39	1.29	0.33
Homoserine	**C00263**	**118.051**	0.77	0.49	0.67	0.13	0.95	0.76	3.43	0.00	38.25	0.12	15.25	0.20	0.99	0.99	0.31	0.38	0.6	0.66
Phenylalanine	**C00079**	**164.072**	0.49	0.26	0.86	0.74	0.29	0.03	0.85	0.00	1.20	0.11	1.12	0.22	0.96	0.75	0.94	0.55	1.36	0.44

dTMP	**C00364**	**321.050**	2.10	0.00	0.92	0.71	0.74	0.26	0.67	0.00	1.23	0.48	1.06	0.84	1.00	0.99	1.06	0.52	0.99	0.93
Epiandrosterone	**C07635**	**289.217**	ND	ND	ND	ND	ND	ND	0.25	0.00	0.62	0.00	0.53	0.00	0.65	0.07	0.53	0.01	0.84	0.36
Erythrulose	**C02045**	**119.035**	5.40	0.08	0.72	0.24	0.88	0.54	1.19	0.00	0.77	0.12	0.96	0.85	0.82	0.49	1.22	0.6	1.82	0.08
FAD	**C00016**	**784.149**	1.04	0.85	1.06	0.59	1.25	0.16	1.44	0.00	1.42	0.07	1.18	0.27	0.72	0.00	0.88	0.08	0.95	0.35
FMN	**C00061**	**455.095**	0.82	0.63	0.88	0.69	1.33	0.24	2.25	0.00	1.60	0.01	1.31	0.04	0.78	0.02	0.95	0.64	0.93	0.28
Fumarate	**C00122**	**115.003**	0.47	0.07	0.71	0.08	0.43	0.01	0.87	0.00	0.93	0.48	1.01	0.91	1.34	0.33	1.04	0.87	0.78	0.48
Gaidic acid	-	**253.217**	1.46	0.58	1.47	0.34	0.9	0.96	1.34	0.00	3.64	0.11	0.68	0.49	0.54	0.02	0.86	0.39	1.03	0.88
D-Gluconic acid	**C00257**	**195.051**	1.02	0.91	0.92	0.63	0.94	0.25	1.30	0.00	0.89	0.59	0.89	0.52	0.95	0.72	1.22	0.30	1.08	0.74
Glutamate	**C00025**	**146.046**	1.01	0.94	0.79	0.07	0.89	0.32	1.16	0.00	0.84	0.29	0.90	0.42	1.01	0.95	0.89	0.29	0.75	0.11
Oxidized Glutathione	**C00127**	**611.144**	1.06	0.80	1.13	0.41	1.16	0.57	0.66	0.00	0.45	0.00	0.77	0.33	1.28	0.37	1.14	0.50	0.85	0.56
Glycerol-2-phosphate	**C02979**	**171.006**	0.61	0.00	1.00	0.94	0.74	0.00	1.96	0.00	1.29	0.23	1.27	0.07	0.96	0.62	0.92	0.27	1.06	0.40
GMP	**C00144**	**362.050**	0.59	0.17	0.67	0.11	0.71	0.18	1.75	0.00	0.87	0.44	0.84	0.43	0.99	0.97	1.04	0.91	1.03	0.90
Guanosine	**C00387**	**282.084**	0.33	0.00	0.66	0.01	1.11	0.56	0.96	0.00	1.05	0.84	0.77	0.28	1.31	0.67	1.50	0.37	1.89	0.25
Histidine	**C00135**	**154.062**	0.81	0.43	0.75	0.05	0.76	0.12	1.92	0.00	1.48	0.27	1.21	0.49	0.86	0.58	0.57	0.01	0.74	0.11
IMP	**C00130**	**347.032**	0.56	0.50	1.43	0.39	3.68	0.03	3.19	0.00	1.51	0.20	1.43	0.05	0.81	0.21	0.89	0.30	0.92	0.50
Inosine	**C00294**	**267.073**	0.34	0.00	0.44	0.00	0.73	0.11	1.15	0.00	0.76	0.28	0.81	0.48	0.92	0.93	0.97	0.97	1.19	0.82
Nicotinic acid	**C00253**	**122.033**	2.21	0.11	1.02	0.93	0.95	0.74	0.36	0.00	0.50	0.20	0.46	0.09	0.06	0.02	0.17	0.01	0.53	0.13
Lactic acid	**C00186**	**89.024**	0.62	0.00	0.77	0.03	1.02	0.75	1.83	0.00	0.94	0.70	1.35	0.34	1.27	0.19	1.11	0.57	0.79	0.27
Lauric acid	**C02679**	**199.170**	1.80	0.3	1.53	0.23	1.45	0.33	1.03	0.00	1.27	0.31	0.76	0.32	0.52	0.06	0.70	0.18	0.85	0.57
L-Leucine	**C00123**	**130.101**	0.66	0.54	0.72	0.49	0.93	0.99	1.48	0.00	0.97	0.92	1.35	0.19	1.13	0.53	1.08	0.69	0.96	0.83

Linoleic acid	**C01595**	**279.233**	2.47	0.40	2.12	0.26	0.40	0.87	1.97	0.00	1.27	0.32	0.80	0.26	0.78	0.08	0.86	0.19	0.93	0.59
LPG 14:0	-	**455.244**	3.57	0.23	2.11	0.01	1.77	0.20	0.47	0.00	0.49	0.00	0.84	0.39	1.16	0.39	1.08	0.65	0.75	0.16
LPG 15:1	-	**467.286**	0.89	0.56	1.28	0.13	1.13	0.83	0.14	0.00	0.22	0.00	0.53	0.00	0.43	0.01	0.62	0.03	0.86	0.37
Lumichrome	**C01727**	**241.073**	0.83	0.37	0.74	0.18	1.00	0.81	1.06	0.00	1.43	0.01	1.49	0.05	0.89	0.66	0.94	0.82	0.94	0.81
Lysine	**C00047**	**145.999**	0.67	0.15	0.73	0.08	0.96	0.66	1.01	0.00	1.46	0.21	1.23	0.07	1.03	0.97	0.59	0.5	0.84	0.81
Malic acid	**C00711**	**133.014**	0.90	0.71	0.73	0.19	0.66	0.12	0.87	0.00	0.97	0.77	1.03	0.73	1.05	0.69	1.03	0.83	0.89	0.31
Methionine	**C00073**	**148.044**	0.16	0.24	1.27	0.83	0.61	0.70	1.67	0.00	1.53	0.45	1.69	0.49	0.85	0.64	0.71	0.14	0.9	0.7
Myristic acid	**C06424**	**227.201**	1.55	0.16	1.36	0.20	4.86	0.22	2.65	0.00	2.24	0.14	0.78	0.34	0.48	0.01	1.00	0.98	1.12	0.5
N-Acetyl-alpha-D-glucosamine 1-phosphate	**C04256**	**300.049**	0.83	0.36	0.93	0.75	1.01	0.69	1.59	0.00	2.41	0.10	1.11	0.78	0.90	0.45	1.44	0.01	1.23	0.11
N-Acetyl-L-aspartate	**C01042**	**174.041**	0.57	0.00	0.70	0.01	0.83	0.01	1.32	0.00	1.72	0.02	1.11	0.72	1.08	0.75	1.23	0.33	0.82	0.44
N-Acetylleucine	**C02710**	**172.098**	0.54	0.37	1.11	0.85	1.02	0.90	0.21	0.00	0.44	0.00	0.87	0.12	1.01	0.97	0.90	0.50	0.97	0.84
NAD	**C00003**	**662.101**	0.83	0.53	1.30	0.04	1.30	0.29	1.36	0.00	1.23	0.11	1.12	0.11	0.83	0.36	0.75	0.08	0.90	0.45
NADH	**C00004**	**664.117**	2.03	0.20	2.24	0.00	0.53	0.28	4.37	0.00	12.01	0.03	3.07	0.05	1.40	0.27	2.36	0.00	1.32	0.12
NADP	**C00006**	**742.067**	0.92	0.63	1.20	0.09	1.17	0.26	1.43	0.00	0.43	0.01	0.76	0.22	0.89	0.11	0.83	0.01	0.78	0.0
NADPH	**C00005**	**744.084**	ND	ND	ND	ND	ND	ND	3.24	0.00	3.23	0.01	1.72	0.06	1.21	0.25	1.43	0.01	1.11	0.38
Oleic acid	**C00712**	**281.249**	1.29	0.58	1.86	0.10	1.15	0.56	1.25	0.00	0.97	0.88	0.64	0.06	0.68	0.06	0.79	0.18	0.97	0.87
O-Phospho-L-threonine	-	**198.023**	0.60	0.49	0.73	0.55	0.98	0.92	0.68	0.00	0.67	0.05	0.81	0.28	0.58	0.01	0.66	0.01	0.91	0.41
PA(10:0/10:0)	-	**479.285**	0.99	0.98	0.94	0.85	3.62	0.01	0.08	0.00	0.16	0.00	0.34	0.02	0.54	0.01	0.76	0.06	0.90	0.43
Palmitic acid	**C00249**	**255.233**	0.55	0.44	2.50	0.07	1.25	0.49	1.71	0.00	1.41	0.28	0.71	0.19	0.76	0.06	0.94	0.61	1.04	0.71

PE (15:0-15:0)	-	**662.475**	0.93	0.91	20.03	0.04	8.17	0.22	2.04	0.00	1.85	0.00	1.63	0.00	1.11	0.53	0.90	0.48	0.97	0.85
PE (14:1e/14:1)	-	**616.435**	ND	ND	ND	ND	ND	ND	1.25	0.00	0.8	0.04	1.02	0.78	0.99	0.91	1.00	0.95	0.84	0.00
PE(14:0/0:0)	-	**424.246**	0.78	0.11	1.07	0.60	0.98	0.28	0.36	0.00	0.37	0.00	0.67	0.00	0.96	0.78	1.15	0.30	0.92	0.54
Penth othenic acid	**C00864**	**218.103**	0.51	0.00	0.81	0.13	0.88	0.10	1.9	0.00	1.40	0.21	1.28	0.13	0.54	0.21	0.69	0.38	0.85	0.73
PG (16:0-16:4)	-	**713.439**	ND	ND	ND	ND	ND	ND	0.17	0.00	0.35	0.03	1.09	0.77	0.95	0.93	1.83	0.23	1.44	0.54
PG(16:0/0:0)	-	**483.272**	0.85	0.77	1.77	0.18	1.08	0.89	0.31	0.00	0.41	0.00	0.94	0.67	1.26	0.26	0.96	0.83	0.64	0.09
PG(18:0/0:0)	-	**511.301**	1.57	0.31	0.59	0.38	0.75	0.50	0.18	0.00	0.43	0.02	1.01	0.96	0.65	0.25	0.75	0.35	0.89	0.72
Phosphatidyl-L-serine	**C02737**	**384.105**	0.37	0.01	0.58	0.04	0.43	0.01	0.27	0.00	0.32	0.00	0.55	0.02	1.19	0.11	1.16	0.06	1.08	0.48
L-Pipecolic acid	**C00408**	**128.072**	0.33	0.40	1.22	0.84	0.61	0.72	0.41	0.00	0.54	0.00	0.64	0.00	0.69	0.13	0.54	0.01	0.72	0.12
Pyroglutamic acid	**C01879**	**128.035**	0.57	0.00	0.76	0.01	0.78	0.01	1.31	0.00	0.98	0.86	0.95	0.55	0.99	0.94	0.89	0.43	0.87	0.38
Riboflavin	**C00255**	**375.131**	0.68	0.25	0.69	0.08	0.81	0.44	1.58	0.00	1.52	0.07	1.17	0.29	1.00	0.99	1.12	0.46	0.98	0.92
Ribose-1-phosphate	**C00620**	**229.012**	0.68	0.04	0.95	0.66	1.05	0.55	3.02	0.00	1.63	0.08	1.41	0.15	0.93	0.69	1.36	0.01	1.34	0.03
Sarcosine	**C00213**	**88.040**	0.55	0.00	0.72	0.00	0.87	0.05	0.93	0.00	1.72	0.02	0.82	0.96	0.70	0.76	0.43	0.42	0.75	0.73
Sedoheptulose 7-phosphate	**C00281**	**289.033**	1.91	0.00	1.35	0.01	0.93	0.47	2.36	0.00	1.06	0.63	0.86	0.19	0.80	0.01	0.92	0.28	1.16	0.05
Serine	**C00065**	**104.035**	0.60	0.01	0.63	0.00	0.78	0.07	2.04	0.00	1.17	0.44	1.11	0.30	0.79	0.48	0.46	0.01	0.70	0.12
Sorbitol 6- phosphate	**C00644**	**261.038**	0.88	0.48	0.77	0.06	0.63	0.02	2.20	0.00	2.58	0.07	1.52	0.30	0.64	0.01	1.13	0.12	1.07	0.62
Succinic acid	**C00042**	**117.019**	0.72	0.00	0.79	0.00	0.93	0.16	1.28	0.00	0.94	0.39	1.06	0.57	1.15	0.55	1.06	0.79	0.92	0.74
Succinoadenosine	-	**382.100**	0.56	0.00	0.65	0.02	0.68	0.02	0.29	0.00	0.32	0.00	0.59	0.04	1.22	0.07	1.17	0.04	1.09	0.42
Thiamin diphosphate	**C00068**	**424.033**	0.39	0.03	1.07	0.83	0.91	0.23	1.72	0.00	3.63	0.05	1.61	0.42	0.71	0.26	1.10	0.76	0.99	0.97
Thymidine	**C00214**	**241.082**	1.65	0.32	0.84	0.55	1.03	0.59	1.65	0.00	2.36	0.04	1.94	0.11	1.25	0.63	0.97	0.92	1.07	0.86

Tryptophan	**C00078**	**203.083**	0.14	0.23	1.31	0.82	0.92	0.91	0.45	0.00	1.60	0.20	1.11	0.81	0.60	0.21	0.79	0.41	1.16	0.63
Tyrosine	**C00082**	**180.067**	0.79	0.27	0.78	0.08	0.88	0.46	1.17	0.00	6.83	0.04	7.04	0.33	1.11	0.91	0.36	0.25	0.65	0.57
UDP	**C00015**	**402.995**	1.32	0.44	0.69	0.16	0.76	0.29	1.55	0.00	1.66	0.05	1.00	0.99	1.65	0.32	1.03	0.96	0.68	0.46
UDP-D-galactose	**C00052**	**565.047**	2.44	0.00	1.33	0.06	1.33	0.18	1.72	0.00	0.75	0.19	0.92	0.63	1.15	0.44	0.92	0.62	0.81	0.25
UDP-D-Xylose	**C00190**	**149.046**	ND	ND	ND	ND	ND	ND	2.05	0.00	1.24	0.06	1.10	0.28	1.22	0.06	1.03	0.71	0.97	0.75
UDP-N-acetyl-D-galactosamine	**C00203**	**606.269**	0.66	0.04	0.74	0.01	0.88	0.34	0.97	0.00	0.75	0.19	0.87	0.45	0.96	0.79	0.73	0.15	0.67	0.04
UMP	**C00105**	**323.028**	0.55	0.02	0.65	0.01	0.73	0.05	1.7	0.00	1.42	0.01	1.11	0.39	1.00	0.98	1.11	0.54	0.93	0.72
Uracil	**C00106**	**111.020**	0.59	0.01	0.72	0.01	0.89	0.29	1.15	0.00	0.91	0.24	0.98	0.80	1.16	0.20	1.06	0.56	0.93	0.63
Uridine	**C00299**	**243.062**	0.72	0.27	1.15	0.40	1.26	0.22	1.96	0.00	1.78	0.06	1.19	0.39	1.41	0.11	1.35	0.13	1.14	0.49
UTP	**C00075**	**482.961**	2.16	0.06	1.44	0.05	1.00	0.74	0.84	0.00	0.42	0.00	0.63	0.01	0.86	0.69	0.48	0.12	0.68	0.38
Xanthine	**C00385**	**151.026**	0.60	0.00	0.71	0.00	0.93	0.64	1.31	0.00	0.91	0.41	0.93	0.25	1.02	0.84	1.00	0.98	0.98	0.84
Xanthurenic acid	**C02470**	**204.033**	0.38	0.03	0.69	0.13	0.56	0.05	0.68	0.00	0.63	0.02	1.00	0.99	0.87	0.11	0.78	0.06	0.81	0.03
L-α-Hydroxyisovaleric acid	-	**117.055**	ND	ND	ND	ND	ND	ND	0.15	0.00	0.12	0.00	0.36	0.01	0.74	0.26	0.73	0.18	0.84	0.45

FC: Fold Change by compare metabolic expression level at TET exposure vs. non-treated control

Sig.: Statistical significance given by *p*-value for the fold change

ND: not detected

Table B9. Exposure conditions and TET concentrations

Feed condition		TET concentration (mg/L)
Fed state	Therapeutic dose	10
	Intermediate dose	1
	Dietary dose	0.01
	Control	0
Fasted state	Therapeutic dose	10
	Intermediate dose	1
	Dietary dose	0.01
	Control	0

Table B10. Gut microbial product and nutrient identification. An asterisk indicates the statistical significance (p-value ≤0.05) between blank media and the gut microbiome secretome.

Metabolite category	Metabolite Name	KEGG ID	m/z	Detection mode	Microbiome secretome	Blank media	*p*-value	Nutrient /microbial product
Amino acids	Gamma-Aminobutyric acid	C00334	102.056	HILIC-ESI (-)	High*	Low	0	Microbial product
Amino acids	2-Aminoisobutyric acid	C03665	102.056	HILIC-ESI (-)	High*	Low	0.01	Microbial product
Amino acids	2-Hydroxybutyric acid	C05984	103.04	HILIC-ESI (-)	High*	Low	0	Microbial product
Amino acids	Serine	C00065	104.036	HILIC-ESI (-)	Low	High*	0	Nutrient
Amino acids	p-Cresol	C01468	107.051	RP-ESI (-)	High*	Low	0	Microbial product
Amino acids	Proline	C00148	114.056	HILIC-ESI (-)	Low	High*	0	Nutrient
Amino acids	Valine	C00183	116.072	HILIC-ESI (-)	Low	High*	0	Nutrient
Amino acids	5-Aminopentanoic acid	C00431	116.073	HILIC-ESI (-)	High*	Low	0	Microbial product
Amino acids	L-α-Hydroxyisovaleric acid	-	117.056	HILIC-ESI (-)	High*	Low	0	Microbial product
Amino acids	Threonine	C00188	118.051	HILIC-ESI (-)	Low	High*	0	Nutrient
Amino acids	Phenylethylamine	C05332	122.097	RP-ESI (+)	High*	Low	0	Microbial product
Amino acids	Taurine	C00245	124.008	HILIC-ESI (-)	High*	Low	0	Microbial product
Amino acids	Pyroglutamic acid	C01879	128.035	HILIC-ESI (-)	Low	High*	0	Nutrient
Amino acids	N-Acetyl-L-alanine	-	130.051	HILIC-ESI (-)	High*	Low	0	Microbial product
Amino acids	Indole-3-carbinol	-	130.066	RP-ESI (+)	High*	Low	0	Microbial product

Amino acids	Leucine	C00123	130.088	HILIC-ESI (-)	Low	High*	0	Nutrient
Amino acids	Asparagine	C00152	131.043	HILIC-ESI (-)	Low	High*	0	Nutrient
Amino acids	Ornithine	C00077	131.082	HILIC-ESI (-)	Low	High*	0	Nutrient
Amino acids	Aspartic acid	C00049	132.031	HILIC-ESI (-)	Low	High*	0	Nutrient
Amino acids	3-Methylindole	C08313	132.08	RP-ESI (+)	Low	High*	0	Nutrient
Amino acids	Indoxyl	C05658	134.06	RP-ESI (+)	High*	Low	0	Microbial product
Amino acids	4-Aminomethylindole	-	144.067	HILIC-ESI (-)	High*	Low	0	Microbial product
Amino acids	N-Propionylalanine	-	144.067	HILIC-ESI (-)	High*	Low	0	Microbial product
Amino acids	Methylglutaric acid	-	145.051	HILIC-ESI (-)	High*	Low	0	Microbial product
Amino acids	Glutamine	C00064	145.061	HILIC-ESI (-)	Low	High*	0	Nutrient
Amino acids	Lysine	C00047	145.098	HILIC-ESI (-)	Low	High*	0	Nutrient
Amino acids	Glutamic acid	C00025	146.046	HILIC-ESI (-)	Low	High*	0	Nutrient
Amino acids	Indole-3-aldehyde	C08493	146.06	RP-ESI (+)	High*	Low	0	Microbial product
Amino acids	4-Guanidinobutanoic acid	C01035	146.092	RP-ESI (+)	High*	Low	0	Microbial product
Amino acids	Methionine	C00073	148.044	HILIC-ESI (-)	Low	High*	0	Nutrient
Amino acids	Cinnamic acid	C00423	149.06	RP-ESI (+)	High	Low	0.1	Microbial product
Amino acids	Hydrocinnamic acid	C05629	149.061	RP-ESI (-)	High*	Low	0	Microbial product
Amino acids	4-Hydroxyphenylacetic acid	C00642	151.04	HILIC-ESI (-)	High*	Low	0	Microbial product
Amino acids	N-methyl-L-glutamic Acid	C01046	160.062	HILIC-ESI (-)	Low	High*	0	Nutrient
Amino acids	Tryptamine	C00398	161.107	RP-ESI (+)	High*	Low	0	Microbial product

Amino acids	Indole-3-carboxylic acid	C19837	162.057	RP-ESI (+)	High*	Low	0	Microbial product
Amino acids	Phenylalanine	C00079	164.072	HILIC-ESI (-)	Low	High*	0	Nutrient
Amino acids	Coumaric acid	C05838	165.051	RP-ESI (+)	Low	High*	0	Nutrient
Amino acids	Phenyllactic acid	C01479	165.056	RP-ESI (-)	High*	Low	0	Microbial product
Amino acids	4-Methoxyphenylacetic acid		165.056	RP-ESI (-)	High*	Low	0	Microbial product
Amino acids	3-Phenoxypropionic acid	-	165.056	HILIC-ESI (-)	High*	Low	0	Microbial product
Amino acids	Vanillylmandelic acid	C05584	165.056	RP-ESI (-)	High*	Low	0	Microbial product
Amino acids	Cysteic acid	C00506	167.997	HILIC-ESI (-)	High*	Low	0	Microbial product
Amino acids	N-Acetylornithine	C00437	173.093	HILIC-ESI (-)	Low	High*	0	Nutrient
Amino acids	Arginine	C00062	173.105	HILIC-ESI (-)	Low	High*	0	Nutrient
Amino acids	N-Acetyl-L-aspartic acid	C01042	174.041	HILIC-ESI (-)	Low	High*	0	Nutrient
Amino acids	Citrulline	C00327	174.089	HILIC-ESI (-)	Low	High*	0	Nutrient
Amino acids	N-Acetylleucine	C02710	174.114	RP-ESI (+)	High*	Low	0	Microbial product
Amino acids	Indoleacetic acid	C00954	176.072	RP-ESI (+)	High*	Low	0	Microbial product
Amino acids	N-Formyl-L-methionine	C03145	176.073	HILIC-ESI (-)	Low	High	0.41	Nutrient
Amino acids	Serotonin	C00780	177.102	RP-ESI (+)	High*	Low	0.01	Microbial product
Amino acids	Tyrosine	C00082	182.079	RP-ESI (+)	Low	High*	0	Nutrient
Amino acids	Kynurenic acid	C01717	188.036	HILIC-ESI (-)	High*	Low	0	Microbial product
Amino acids	N-Acetylglutamic acid	C00624	188.068	HILIC-ESI (-)	Low	High*	0	Nutrient
Amino acids	p-Cresol sulfate	-	189.022	RP-ESI (+)	High*	Low	0	Microbial product

Amino acids	Indole-3-propionic acid	-	190.086	RP-ESI (+)	High*	Low	0	Microbial product
Amino acids	Tryptophan	C00078	203.083	HILIC-ESI (-)	Low	High*	0	Nutrient
Amino acids	Xanthurenic acid	C02470	206.048	HILIC-ESI (-)	High*	Low	0.02	Microbial product
Amino acids	Indolelactic acid	C02043	206.081	RP-ESI (+)	High*	Low	0	Microbial product
Amino acids	N-Acetyl-L-phenylalanine	C03519	206.082	HILIC-ESI (-)	Low	High*	0.01	Nutrient
Amino acids	L-Kynurenine	C00328	207.078	HILIC-ESI (-)	High*	Low	0	Microbial product
Amino acids	Formyl-5-hydroxykynurenamine	C05647	209.092	RP-ESI (+)	High*	Low	0	Microbial product
Amino acids	O-Succinyl-L-homoserine	C01118	218.067	HILIC-ESI (-)	High*	Low	0	Microbial product
Amino acids	5-Hydroxy-L-tryptophan	C00643	221.092	RP-ESI (+)	High*	Low	0	Microbial product
Amino acids	Porphobilinogen	C00931	225.088	HILIC-ESI (-)	High*	Low	0	Microbial product
Amino acids	5-Methoxytryptophan	NA	233.094	HILIC-ESI (-)	Low	High	0.11	Nutrient
Amino acids	Saccharopine	C00449	275.125	HILIC-ESI (-)	Low	High*	0	Nutrient
Amino acids	Indole-3-acetyl-L-valine	-	275.139	RP-ESI (+)	High*	Low	0	Microbial product
Carbon and energy sources	Maleic acid	C00122	115.004	HILIC-ESI (-)	Low	High*	0	Nutrient
Carbon and energy sources	Succinic acid	C00042	117.019	HILIC-ESI (-)	Low	High*	0	Nutrient
Carbon and energy sources	Malic acid	C03668	133.014	HILIC-ESI (-)	Low	High*	0	Nutrient
Carbon and energy sources	2-Hydroxyglutarate	C02630	147.03	HILIC-ESI (-)	Low	High*	0.01	Nutrient
Carbon and energy sources	D-Galactose	C00984	179.055	HILIC-ESI (-)	Low	High*	0	Nutrient
Carbon and energy sources	Citric acid	C00158	191.02	HILIC-ESI (-)	Low	High*	0	Nutrient
Carbon and energy sources	Glucosamine 6-phosphate	C00352	258.039	HILIC-ESI (-)	Low	High*	0	Nutrient

Carbon and energy sources	Glucose 6-phosphate	C00092	259.023	HILIC-ESI (-)	Low	High*	0	Nutrient
Lipids and fatty acids	Malonic acid	C04025	103.004	HILIC-ESI (-)	High*	Low	0	Microbial product
Lipids and fatty acids	Choline	C00114	104.107	RP-ESI (+)	Low	High*	0	Nutrient
Lipids and fatty acids	Glutaric acid	C00489	131.035	HILIC-ESI (-)	Low	High*	0	Nutrient
Lipids and fatty acids	Leucininc acid	-	131.071	HILIC-ESI (-)	High*	Low	0	Microbial product
Lipids and fatty acids	Glycerophosphate	C00093	171.005	HILIC-ESI (-)	Low	High*	0	Nutrient
Lipids and fatty acids	Sphinganine	C00836	302.305	RP-ESI (+)	High*	Low	0	Microbial product
Lipids and fatty acids	Lithocholic acid	C03990	377.308	RP-ESI (+)	Low	High	0.75	Nutrient
Lipids and fatty acids	Chenodeoxycholic acid	C02528	391.285	RP-ESI (-)	High*	Low	0	Microbial product
Lipids and fatty acids	Cholic acid	C00695	407.28	RP-ESI (-)	High*	Low	0	Microbial product
Lipids and fatty acids	Glycocholic acid	C01921	466.315	RP-ESI (+)	Low	High*	0	Nutrient
Lipids and fatty acids	Acetic acid	C00033		GC-FID	High*	Low	0.01	Microbial product
Lipids and fatty acids	Propionic acid	C00163		GC-FID	High*	Low	0	Microbial product
Lipids and fatty acids	Isobutyric acid	C02632		GC-FID	High*	Low	0	Microbial product
Lipids and fatty acids	Butyric acid	C00246		GC-FID	High*	Low	0	Microbial product
Nucleotides	Uracil	C00106	111.02	HILIC-ESI (-)	Low	High*	0	Nutrient
Nucleotides	Purine	C15587	119.035	HILIC-ESI (-)	High*	Low	0.02	Microbial product
Nucleotides	Hypoxanthine	C00262	135.03	HILIC-ESI (-)	Low	High*	0	Nutrient
Nucleotides	Xanthine	C00385	151.027	HILIC-ESI (-)	Low	High*	0	Nutrient
Nucleotides	Orotic acid	C00295	155.007	HILIC-ESI (-)	Low	High*	0	Nutrient

Nucleotides	Deoxyuridine	C00526	227.068	HILIC-ESI (-)	High*	Low	0	Microbial product
Nucleotides	Thymidine	C00214	241.084	HILIC-ESI (-)	High	Low	0.12	Microbial product
Nucleotides	Cytidine	C02961	242.085	HILIC-ESI (-)	Low	High	0.37	Nutrient
Nucleotides	Uridine	C00299	243.063	HILIC-ESI (-)	Low	High*	0	Nutrient
Nucleotides	Inosine	C00294	267.075	HILIC-ESI (-)	Low	High*	0	Nutrient
Nucleotides	Guanosine	C00387	284.098	RP-ESI (+)	Low	High*	0	Nutrient
Vitamins	Nicotinic acid	C00253	122.025	HILIC-ESI (-)	High*	Low	0	Microbial product
Vitamins	Niacinamide	C00153	123.056	RP-ESI (+)	High*	Low	0	Microbial product
Vitamins	p-Aminobenzoic acid	C00568	138.055	RP-ESI (+)	High*	Low	0	Microbial product
Vitamins	Pyridoxamine	C00534	169.097	RP-ESI (+)	High*	Low	0	Microbial product
Vitamins	Ascorbic acid	C01041	175.025	HILIC-ESI (-)	High*	Low	0	Microbial product
Vitamins	4-Pyridoxic acid	C00847	182.047	HILIC-ESI (-)	High*	Low	0.01	Microbial product
Vitamins	Pantothenic acid	C00864	220.118	RP-ESI (+)	High*	Low	0	Microbial product
Vitamins	Biotin	C00120	245.095	RP-ESI (+)	Low	High	0.49	Nutrient
Vitamins	Riboflavin	C00255	377.144	RP-ESI (+)	Low	High	0.4	Nutrient

Table B11. Identified metabolites and respective fold changes at three TET exposure levels under the fed and fasted state.

Metabolite category	Subcategory	Metabolite Name	KEGG ID	m/z	Detection mode	Fed state						Fasted state					
						10 mg/L TET		1 mg/L TET		0.01mg/L TET		10 mg/L TET		1 mg/L TET		0.01 mg/L TET	
						FC	*p*-value	FC	*p*-value	FC	*p*-value	FC	*p*-value	FC	*p*-value	FC	*p*-value
1	1.1	Indole-3-carbinol	-	130.066	RP-ESI (+)	1.2	0	1.1	0.5	0.9	0.1	1.1	0.2	1.2	0	1.1	0.1
1	1.1	Skatole	C08313	132.08	RP-ESI (+)	0.8	0	0.8	0	0.8	0	1.1	0.3	1	0.7	1	0.4
1	1.1	Indoxyl	C05658	134.06	RP-ESI (+)	0.8	0	0.8	0	0.8	0	0.9	0	0.9	0	1	0.6
1	1.1	Aminomethylindole	-	144.067	HILIC-ESI (-)	1.3	0	1	0.9	1	0.5	1.1	0.1	1	0.7	1	0.3
1	1.1	Indole-3-aldehyde	C08493	146.06	RP-ESI (+)	1.2	0	1	0.7	1	0.8	1.1	0	1	0.3	1	0.5
1	1.1	Tryptamine	C00398	161.107	RP-ESI (+)	0.9	0	0.9	0	1	0.8	1	0.6	1	0.6	1	0.4
1	1.1	Indole-3-carboxylic acid	C19837	162.057	RP-ESI (+)	1.5	0	1.1	0.4	1	0.6	1	0.2	1.2	0.3	1	0.2
1	1.1	Indoleacetic acid	C00954	176.072	RP-ESI (+)	1	0.8	1	0.5	1	0.4	1	0.4	1	0	1	0
1	1.1	Serotonin	C00780	177.102	RP-ESI (+)	1.2	0.2	1.2	0.1	1.1	0.6	1.2	0.5	1.1	0.7	1.4	0.2
1	1.1	Kynurenic acid	C01717	188.036	HILIC-ESI (-)	0.9	0	0.8	0	0.9	0	1.1	0.1	1	0.2	1.1	0.1

1	1.1	Indole-3-propionic acid	-	190.086	RP-ESI (+)	1.1	0	1.1	0	1	0.4	1	0.6	1	0.4	1	1
1	1.1	Tryptophan	C00078	203.083	HILIC-ESI (-)	3.5	0	2.8	0	1.3	0.2	1.1	0.7	1	1	0.7	0.1
1	1.1	Xanthurenic acid	C02470	206.048	RP-ESI (+)	0.3	0	0.2	0	0.4	0	1.6	0	1.7	0	1	0.9
1	1.1	Indolelactic acid	C02043	206.081	RP-ESI (+)	5.4	0	3.6	0	1.2	0.2	1.6	0	1.3	0	1.1	0.3
1	1.1	L-Kynurenine	C00328	207.078	HILIC-ESI (-)	1	0.6	0.9	0	1	0	1.1	0.1	1	0.2	1	0.2
1	1.1	Formyl-5-hydroxykynurenamine	C05647	209.092	RP-ESI (+)	1.2	0.1	1	0.1	1.2	0.2	0.9	0.5	0.9	0.4	0.9	0.3
1	1.1	Hydroxy-L-tryptophan	C00643	221.092	RP-ESI (+)	1.4	0	1.3	0	1.3	0	1.6	0	1.5	0	1	0.1
1	1.1	5-Methoxytryptophan	NA	233.094	HILIC-ESI (-)	1.1	0.3	0.8	0.1	0.9	0.1	1.2	0.4	0.9	0.5	0.8	0.2
1	1.1	Indole-3-acetyl-L-valine	-	275.139	RP-ESI (+)	3.1	0	2.4	0	1.1	0	1.2	0	1.2	0	1	0.2
1	1.2	p-Cresol	C01468	107.051	RP-ESI (-)	1.1	0	1.1	0.2	0.9	0.1	1	0.4	1	1	1	0.8
1	1.2	Phenylethylamine	C05332	122.097	RP-ESI (+)	1.1	0.1	1	0.4	1	0.9	1	0.3	1	0.6	1	0.5
1	1.2	Cinnamic acid	C00423	149.06	RP-ESI (+)	1.2	0.2	1	0.9	1	0.9	1	1	0.9	0.6	1	1
1	1.2	Hydrocinnamic acid	C05629	149.061	RP-ESI (-)	1.3	0	1.1	0	1	0.6	1	0.1	1	0.4	1	0.1

1	1.2	4-Hydroxyphenylacetic acid	C00642	151.04	HILIC-ESI (-)	45.6	0	31.5	0	1.3	0	1.8	0	1.7	0	1	0.6
1	1.2	Phenylalanine	C00079	164.072	HILIC-ESI (-)	3.9	0	2.7	0	1	0.9	1	0.9	0.9	0.6	0.9	0.7
1	1.2	Coumaric acid	C05838	165.051	RP-ESI (+)	0.7	0	0.9	0.2	0.9	0.4	1	0.5	0.8	0.3	0.9	0.1
1	1.2	3-Phenoxypropionic acid	-	165.056	HILIC-ESI (-)	1.6	0	1.3	0	1	0.5	1.2	0	1.1	0.3	1	0.7
1	1.2	4-Methoxyphenylacetic acid		165.056	RP-ESI (-)	1.2	0	1.1	0	1	0.1	1	0.4	1	0.7	1	0.5
1	1.2	Vanillylmandelic acid	C05584	165.056	RP-ESI (-)	1.8	0	1.5	0	1	0.5	1.1	0	1.1	0	1	0.1
1	1.2	Phenyllactic acid	C01479	165.056	RP-ESI (-)	3	0	2.1	0	1.2	0.2	1.2	0.1	1.1	0.2	1.1	0.4
1	1.2	Tyrosine	C00082	182.079	RP-ESI (+)	1.4	0	1.3	0.1	1.1	0.5	1	0.3	1.2	0.2	1	0.7
1	1.2	p-Cresol sulfate	-	189.022	RP-ESI (+)	1.2	0	1.1	0.1	1	0.9	1	0.7	1	0.7	1	0.6
1	1.3	N-Acetyl-L-phenylalanine	C03519	206.082	HILIC-ESI (-)	2.8	0	1.4	0.3	1	1	1.3	0	1.1	0.1	1	0.5
1	1.3	Gamma-Aminobutyric acid	C00334	102.056	HILIC-ESI (-)	1.1	0.6	0.8	0.3	0.9	0.4	1.1	0.5	1	0.9	1	0.9
1	1.3	2-Aminoisobutyric acid	C03665	102.056	HILIC-ESI (-)	27.8	0	19.3	0	1.2	0	1.1	0.6	1	0.9	1	1

1	1.3	2-Hydroxybutyric acid	C05984	103.04	HILIC-ESI (-)	5.5	0	5.1	0	1.4	0.1	1.2	0.1	1	0.6	1	0.6
1	1.3	Serine	C00065	104.036	HILIC-ESI (-)	2	0	1.7	0.1	0.9	0.8	1.1	0.8	1.2	0.7	1.1	0.9
1	1.3	Proline	C00148	114.056	HILIC-ESI (-)	112.9	0	59.8	0	1.7	0.3	1.2	0.3	1.2	0.4	1	0.8
1	1.3	Valine	C00183	116.072	HILIC-ESI (-)	13	0	22.1	0	1	0.8	1.1	0.6	1	0.9	1	0.8
1	1.3	5-Aminopentanoic acid	C00431	116.073	HILIC-ESI (-)	1.1	0	1	0.6	1	0.7	1.1	0	1	0.1	1	0.1
1	1.3	L-α-Hydroxyisovaleric acid	-	117.056	HILIC-ESI (-)	1.6	0.1	1.6	0.1	0.9	0.4	1.1	0.7	1	0.8	1	0.8
1	1.3	Threonine	C00188	118.051	HILIC-ESI (-)	2.9	0	2.3	0	1.1	0.7	1.9	0.3	0.4	0.3	0.5	0.4
1	1.3	Taurine	C00245	124.008	HILIC-ESI (-)	1.1	0	1	0.4	1	0.1	1.1	0	1	0.5	1	0.2
1	1.3	Pyroglutamic acid	C01879	128.035	HILIC-ESI (-)	0.9	0.8	1	0.9	1.1	0.1	1	0.9	0.7	0.2	0.9	0.6
1	1.3	N-Acetyl-L-alanine	-	130.051	HILIC-ESI (-)	1.5	0	1.5	0	1.2	0.1	1.2	0	1.1	0.2	1.1	0.2
1	1.3	Leucine	C00123	130.088	HILIC-ESI (-)	15.6	0	9.9	0	0.9	0.4	1.2	0.4	1.1	0.5	1.2	0.3
1	1.3	Glutaric acid	C00489	131.035	HILIC-ESI (-)	0.7	0.3	0.8	0.7	0.7	0.4	1.2	0.1	1.2	0.1	1.1	0.4
1	1.3	Asparagine	C00152	131.043	HILIC-ESI (-)	1.3	0.2	1.1	0.6	1.1	0.8	1.1	0	1.1	0.1	1.1	0.1
1	1.3	Ornithine	C00077	131.082	HILIC-ESI (-)	28.2	0	24	0	1.1	0.6	1.1	0.5	1	1	1.1	0.8
1	1.3	Aspartic acid	C00049	132.031	HILIC-ESI (-)	31.2	0	9.8	0	1.2	0.8	1.3	0.4	1	0.8	1.1	0.7

1	1.3	N-Propionylalanine	-	144.067	HILIC-ESI (-)	3.5	0	2.8	0	1.5	0.2	1.2	0.1	1.1	0.3	1.1	0
1	1.3	Methylglutaric acid	-	145.051	HILIC-ESI (-)	0.8	0	0.8	0	1.1	0.3	1.1	0.1	1	0.4	1	0.2
1	1.3	Glutamine	C00064	145.061	HILIC-ESI (-)	1.7	0	1.3	0	1	0.5	1.3	0	1.2	0	1	0.6
1	1.3	Lysine	C00047	145.098	HILIC-ESI (-)	0.8	0.5	0.9	0.7	0.8	0.4	0.8	0.4	0.7	0	0.7	0.1
1	1.3	Glutamic acid	C00025	146.046	HILIC-ESI (-)	31.9	0	0.7	0	0.9	0.6	0.9	0	0.9	0.1	1.1	0.3
1	1.3	4-Guanidinobutanoic acid	C01035	146.092	RP-ESI (+)	1.1	0.7	1	0.9	1.4	0.3	1	0.7	1.2	0.2	0.9	0.4
1	1.3	2-Hydroxyglutarate	C02630	147.03	HILIC-ESI (-)	9.5	0	0.9	0.7	0.7	0.4	1.5	0	1.1	0.5	1.1	0.7
1	1.3	Methionine	C00073	148.044	HILIC-ESI (-)	79.8	0	33.1	0	1	0.8	0.9	0.6	0.8	0.2	0.9	0.5
1	1.3	N-methyl-L-glutamic Acid	C01046	160.062	HILIC-ESI (-)	1.7	0	1.3	0	1	0.3	1.2	0.2	1.1	0.5	1	0.7
1	1.3	Cysteic acid	C00506	167.997	HILIC-ESI (-)	1.2	0.3	0.9	0.5	0.9	0.4	1.2	0.3	1.2	0.4	1.1	0.5
1	1.3	N-Acetylornithine	C00437	173.093	HILIC-ESI (-)	16.7	0	15	0	1.2	0.5	1.1	0.5	1.1	0.4	1.1	0.6
1	1.3	Arginine	C00062	173.105	HILIC-ESI (-)	2.7	0	2	0	1.2	0.2	1.2	0.1	1.1	0.1	1.1	0.4
1	1.3	N-Acetyl-L-aspartic acid	C01042	174.041	HILIC-ESI (-)	2.1	0	0.9	0.7	0.8	0.4	1.2	0	1.1	0.1	1.1	0.4
1	1.3	Citrulline	C00327	174.089	HILIC-ESI (-)	31.6	0	26.2	0	1.1	0.5	1	0.8	1.1	0.8	1	0.9
1	1.3	N-Acetylleucine	C02710	174.114	RP-ESI (+)	1.1	0	0.7	0.2	0.9	0	1	0.2	1	0	1	0.1

1	1.3	N-Formyl-L-methionine	C03145	176.073	HILIC-ESI (-)	0.7	0	0.5	0	1	0.7	1	1	1.1	0.2	1.1	0
1	1.3	N-Acetylglutamic acid	C00624	188.068	HILIC-ESI (-)	1.5	0.1	1	0.9	0.8	0.5	1.1	0.8	0.9	0.8	1.1	0.8
1	1.3	O-Succinyl-L-homoserine	C01118	218.067	HILIC-ESI (-)	1.9	0	1.3	0.2	1	0.8	1.2	0.3	1.2	0.2	1	0.9
1	1.3	Porphobilinogen	C00931	225.088	HILIC-ESI (-)	1.1	0.1	1	0.4	1	0.9	1.1	0.1	1.1	0.4	1.1	0.3
1	1.3	Saccharopine	C00449	275.125	HILIC-ESI (-)	7.2	0	1.1	0.3	1.1	0.6	1.1	0.2	1.1	0	1	0.5
2	2.1	Maleic acid	C00122	115.004	HILIC-ESI (-)	1.8	0.2	1.5	0.4	0.9	0.7	0.9	0.6	1.3	0.2	1.1	0.8
2	2.1	Succinic acid	C00042	117.019	HILIC-ESI (-)	1	1	0.7	0.4	0.7	0.3	1	0.6	1.1	0.2	1	0.7
2	2.1	Malic acid	C03668	133.014	HILIC-ESI (-)	2	0.1	1.2	0.6	1.3	0.3	1.3	0.1	1	0.8	1	1
2	2.1	D-Galactose	C00984	179.055	HILIC-ESI (-)	10.6	0	3.1	0	1.8	0	1.2	0.6	0.9	0.8	0.9	0.6
2	2.1	Citric acid	C00158	191.02	HILIC-ESI (-)	1.7	0	0.9	0.3	0.9	0.1	1.1	0.2	0.9	0.4	1	0.8
2	2.1	Glucosamine 6-phosphate	C00352	258.039	HILIC-ESI (-)	8.7	0	1.1	0.8	1.2	0.6	1.2	0.7	0.5	0.3	0.8	0.7
2	2.1	Glucose 6-phosphate	C00092	259.023	HILIC-ESI (-)	3	0	1.5	0	1.4	0.1	1.1	0.3	0.9	0.1	0.9	0.1
3	3.1	Lithocholic acid	C03990	377.308	RP-ESI (+)	1	1	2.7	0.3	0.5	0.2	0.4	0.4	0.3	0.4	0.7	0.8

3	3.1	Chenodeoxycholic acid	C02528	391.285	RP-ESI (-)	1	0.4	1	0.8	1	0.6	0.9	0	0.9	0	1	0.7
3	3.1	Cholic acid	C00695	407.28	RP-ESI (-)	1.1	0	0.9	0.2	1	0	1	0.5	1	0.9	1	0.9
3	3.1	Glycocholic acid	C01921	466.315	RP-ESI (+)	0.6	0	0.8	0	0.9	0.2	1.1	0.2	1	0.8	1	0.5
3	3.2	Acetic acid	C00033	0	GC-FID	1	0.6	1.1	0.1	1	0.9	1	1	1	0.7	1	0.6
3	3.2	Propionic acid	C00163	0	GC-FID	1.3	0	1.1	0	1	0.4	1	0.2	1	0.6	1	0.3
3	3.2	Isobutyric acid	C02632	0	GC-FID	1.1	0	1	0.6	1	0	1.1	0.1	1	0.5	1	0.4
3	3.2	Butyric acid	C00246	0	GC-FID	1.1	0.1	1.1	0.1	1	0.6	1.1	0.1	1	0.8	1	0.6
3	3.3	Malonic acid	C04025	103.004	HILIC-ESI (-)	0.8	0.6	0.8	0.5	0.8	0.4	1.1	0.5	1.1	0.5	1	0.9
3	3.3	Choline	C00114	104.107	RP-ESI (+)	1	0.7	3.6	0.2	0.8	0.3	1	0.8	0.9	0.8	0.9	0.9
3	3.3	Leucininc acid	-	131.071	HILIC-ESI (-)	2	0	1.5	0.1	0.9	0	1.1	0.1	1	0.4	1	0.6
3	3.3	Glycerophosphate	C00093	171.005	HILIC-ESI (-)	1.3	0.1	1.3	0.2	1	0.9	1.1	0.5	0.8	0.2	1.1	0.5
3	3.3	Sphinganine	C00836	302.305	RP-ESI (+)	1.7	0	1.2	0	0.9	0	1	0.5	0.9	0.2	1	0.7
4	4.1	Uracil	C00106	111.02	HILIC-ESI (-)	1.7	0	1.5	0	1.2	0.1	2.6	0	1.9	0	1.2	0.1
4	4.1	Purine	C15587	119.035	HILIC-ESI (-)	1.8	0	1.5	0	0.9	0.6	1.2	0.6	1.1	0.8	1.1	0.7
4	4.1	Hypoxanthine	C00262	135.03	HILIC-ESI (-)	0.8	0.7	0.3	0.1	0.8	0.4	0.7	0.5	0.7	0.4	0.2	0
4	4.1	Xanthine	C00385	151.027	HILIC-ESI (-)	4.6	0	6.2	0	1.1	0.1	1.3	0	1.3	0	1.1	0.4

4	4.1	Orotic acid	C00295	155.007	HILIC-ESI (-)	1.2	0.3	0.7	0.2	0.9	0.4	1	0.9	0.9	0.4	1	0.9
4	4.1	Deoxyuridine	C00526	227.068	HILIC-ESI (-)	1	0.9	0.9	0.1	1	0.4	1.1	0.4	1	0.9	1	0.9
4	4.1	Thymidine	C00214	241.084	HILIC-ESI (-)	1.2	0.1	1	0.8	1.1	0.5	1.1	0.1	1.1	0.1	1	0.6
4	4.1	Cytidine	C02961	242.085	HILIC-ESI (-)	1.4	0	1.2	0.1	1.1	0.6	1.1	0.1	1.1	0.4	1	0.7
4	4.1	Uridine	C00299	243.063	HILIC-ESI (-)	1.5	0	0.9	0.6	1	0.7	1.2	0	1.1	0.1	1	0.4
4	4.1	Inosine	C00294	267.075	HILIC-ESI (-)	0.5	0.1	0.6	0	0.8	0.3	1.1	0	1	0.2	1	0.1
4	4.1	Guanosine	C00387	284.098	RP-ESI (+)	1.9	0.1	1.4	0.2	1.2	0.4	1.3	0	1.4	0	1.1	0.4
5	5.1	Nicotinic acid	C00253	122.025	HILIC-ESI (-)	0.9	0	0.8	0	1	0.2	1.1	0.1	1	0.8	1	0.2
5	5.1	Niacinamide	C00153	123.056	RP-ESI (+)	0.7	0.2	0.7	0.3	1.2	0.4	1.1	0.2	1.1	0.2	1	0.7
5	5.1	p-Aminobenzoic acid	C00534	138.055	RP-ESI (+)	1	0	1	0.6	1	0.3	1	0.2	1	0.7	1	0.8
5	5.1	Pyridoxamine	C01041	169.097	RP-ESI (+)	1.3	0	1.1	0	1	0.2	1	0.3	1	0.4	1	0.8
5	5.1	Ascorbic acid	C00847	175.025	HILIC-ESI (-)	0.9	0.7	0.8	0.1	0.9	0.6	1.1	0.7	1.1	0.5	1	0.9
5	5.1	4-Pyridoxic acid	C00864	182.047	HILIC-ESI (-)	0.8	0	0.7	0	0.9	0.1	1.1	0.4	1	0.7	1	0.6
5	5.1	Pantothenic acid	C00120	220.118	RP-ESI (+)	0.7	0	0.8	0	0.9	0.3	1.1	0.2	1.1	0.1	1.1	0.2
5	5.1	Biotin	C00255	245.095	RP-ESI (+)	1.1	0	1	0.1	1	0.1	1	0.8	1	0.3	1.1	0.6
5	5.1	Riboflavin	C05584	377.144	RP-ESI (+)	1.3	0	1	0.9	1	0.7	1	0.8	1	0.9	1	0.5

FC: abundance ratios of metabolites in the bacterial secretome from each TET treatment to their respective TET free controls. Metabolite categories 1, 2, 3, 4, and 5 stands for Amino acids, carbon and energy sources, lipids and fatty acids, nucleotides, and vitamins; respectively.

Subcategories 1.1, 1.2, 1.3, 2.1, 3.1, 3.2, 3.3, 4.1, and 5.1 stands for tryptophan and indole derivatives, tyrosine and phenyl derivatives, other amino acids, carbon and energy sources, bile acids, SCFAs, other lipids and fatty acids, nucleotides, and vitamins.

Table B12. Identified glycerolipids and respective fold changes in the HepG2 cells exposed to TET 10mg/L treated gut microbiome secretome

Lipid subclass	Lipid name	m/z	Adduct	10 mg/L TET treated secretome	
				FC	p value
DAG	DAG 19:2	400.303	[M+NH4]+	1.01	0.83
DAG	DAG 20:1	416.337	[M+NH4]+	1.04	0.52
DAG	DAG 21:0	208.168	[M+NH4]+	1.18	0.04
DAG	DAG 24:0	474.415	[M+NH4]+	1.04	0.51
DAG	DAG 24:5	464.333	[M+NH4]+	1.04	0.43
DAG	DAG 24:6	418.321	[M+NH4]+	1.03	0.91
DAG	DAG 26:3	496.4	[M+NH4]+	1.09	0.31
DAG	DAG 27:0	510.469	[M+NH4]+	1.52	0.07
DAG	DAG 27:3	510.416	[M+NH4]+	1.04	0.73
DAG	DAG 28:1	511.44	[M+H]+	1.46	0.03
DAG	DAG 28:1;O	527.434	[M+H]+	0.19	0.04
DAG	DAG 28:4	522.416	[M+NH4]+	1.03	0.7
DAG	DAG 29:3	538.457	[M+NH4]+	1.08	0.57
DAG	DAG 30:4	550.447	[M+NH4]+	0.96	0.62
DAG	DAG 31:0	572.522	[M+NH4]+	1.11	0.49
DAG	DAG 31:0	572.538	[M+NH4]+	1.27	0.05
DAG	DAG 32:1	549.485	[M+H]+	1.41	0.02
DAG	DAG 32:4	578.478	[M+NH4]+	1.11	0.1
DAG	DAG 32:7	572.425	[M+NH4]+	1.07	0.56

DAG	DAG 33:0	600.509	[M+NH4]+	1.12	0.19
DAG	DAG 34:1	627.521	[M+H]+	1.28	0.03
DAG	DAG 34:4	606.512	[M+NH4]+	1.26	0.1
DAG	DAG 36:2	638.572	[M+NH4]+	0.73	0.01
DAG	DAG 36:2	621.547	[M+H]+	0.59	0.05
DAG	DAG 36:5	632.523	[M+NH4]+	0.99	0.95
DAG	DAG 36:5	632.525	[M+NH4]+	1.3	0.09
DAG	DAG 37:4	648.562	[M+NH4]+	0.93	0.66
DAG	DAG 37:4	631.53	[M+H]+	0.49	0.02
DAG	DAG 37:5	629.511	[M+H]+	0.58	0
DAG	DAG 38:5	660.555	[M+NH4]+	0.61	0
DAG	DAG 38:5	643.526	[M+H]+	0.76	0.05
DAG	DAG 38:6	641.51	[M+H]+	0.62	0.01
DAG	DAG 39:5	657.542	[M+H]+	0.1	0
DAG	DAG 4:0	194.097	[M+NH4]+	1.04	0.63
DAG	DAG 40:4	689.596	[M+NH4]+	0.48	0.01
DAG	DAG 40:5	688.587	[M+NH4]+	0.47	0.01
DAG	DAG 40:7	667.526	[M+H]+	0.52	0
DAG	DAG 42:7	695.558	[M+H]+	0.47	0
DAG	DAG 42:8	710.58	[M+NH4]+	0.79	0.08
DAG	DAG 43:5;O2	745.592	[M+H]+	1.58	0.02
DAG	DAG 44:5	744.648	[M+NH4]+	1.12	0.39
DAG	DAG 46:0	782.758	[M+NH4]+	0.99	0.94
DAG	DAG 46:1	780.742	[M+NH4]+	0.95	0.52

DAG	DAG 46:5	772.68	[M+NH4]+	1.09	0.38
DAG	DAG 47:5	786.698	[M+NH4]+	1.1	0.67
DAG	DAG 48:12	769.576	[M+H]+	1.17	0.02
DAG	DAG 48:2	806.758	[M+NH4]+	1	0.99
DAG	DAG 48:5	800.711	[M+NH4]+	1.11	0.24
DAG	DAG 49:4	816.748	[M+NH4]+	0.97	0.83
DAG	DAG 50:5	828.742	[M+NH4]+	1.08	0.4
DAG	DAG O-28:3	493.417	[M+H]+	0.81	0.02
DAG	DAG O-35:3	591.532	[M+H]+	1.5	0.03
DAG	DAG O-36:3	605.549	[M+H]+	1.26	0.02
DAG	DAG O-36:4	603.534	[M+H]+	1.81	0
DAG	DAG O-36:6	599.502	[M+H]+	2.05	0
DAG	DAG O-37:5	615.533	[M+H]+	3.57	0
DAG	DAG O-38:4	631.564	[M+H]+	1.97	0
DAG	DAG O-38:6	627.534	[M+H]+	1.41	0.01
DAG	DAG O-38:7	625.517	[M+H]+	2.02	0
DAG	DAG O-40:7	653.548	[M+H]+	1.81	0
DAG	DAG O-40:8	651.533	[M+H]+	1.81	0.02
DAG	DAG O-52:13	809.646	[M+H]+	0.35	0.03
MAG	MAG 17:0	362.325	[M+NH4]+	1.04	0.48
MAG	MAG 18:1	374.306	[M+NH4]+	1.31	0.01
MAG	MAG 18:2	372.31	[M+NH4]+	1.06	0.42
MAG	MAG 19:1	388.342	[M+NH4]+	1.02	0.68
MAG	MAG 20:5	394.292	[M+NH4]+	1.02	0.81

MAG	MAG 25:0	457.42	[M+H]+	1.19	0.04
MAG	MAG 26:0	461.355	[M+H]+	2.14	0
MAG	MAG 28:1	497.449	[M+H]+	1.26	0.04
MAG	MAG 32:2	551.499	[M+H]+	1.39	0.04
MAG	MAG 34:2	579.523	[M+H]+	1.36	0.05
MAG	MAG 34:4	575.502	[M+H]+	1.94	0
MAG	MAG O-18:2	341.304	[M+H]+	1.28	0.01
MAG	MAG O-18:3	339.289	[M+H]+	1.46	0.01
MAG	MAG O-33:2	551.538	[M+H]+	0.69	0.03
TAG	TAG 36:1	669.542	[M+H]+	0.5	0.01
TAG	TAG 36:1	654.552	[M+NH4]+	3.62	0
TAG	TAG 36:3	650.535	[M+NH4]+	1.01	0.86
TAG	TAG 36:7	647.418	[M+Na]+	1.01	0.96
TAG	TAG 37:1	673.542	[M+Na]+	0.92	0.41
TAG	TAG 37:1	673.541	[M+Na]+	0.92	0.41
TAG	TAG 37:7	661.436	[M+Na]+	1.05	0.71
TAG	TAG 38:3	678.673	[M+NH4]+	1.04	0.72
TAG	TAG 38:5	679.508	[M+Na]+	1.36	0.03
TAG	TAG 39:4	705.524	[M+H]+	1.24	0.05
TAG	TAG 40:4	704.577	[M+NH4]+	1.28	0.14
TAG	TAG 40:9	699.471	[M+Na]+	0.97	0.88
TAG	TAG 41:4	718.593	[M+NH4]+	1.1	0.21
TAG	TAG 41:8	715.488	[M+Na]+	1.17	0.29
TAG	TAG 42:0	740.674	[M+NH4]+	0.87	0.2

TAG	TAG 42:1	738.659	[M+NH4]+	0.86	0.38
TAG	TAG 42:2	736.644	[M+NH4]+	0.92	0.3
TAG	TAG 42:2	736.645	[M+NH4]+	0.98	0.87
TAG	TAG 43:0	754.69	[M+NH4]+	0.53	0.02
TAG	TAG 44:0	768.706	[M+NH4]+	0.92	0.33
TAG	TAG 44:1	771.645	[M+Na]+	0.88	0.31
TAG	TAG 44:1	766.69	[M+NH4]+	0.95	0.58
TAG	TAG 44:10	748.539	[M+NH4]+	1.12	0.56
TAG	TAG 44:4	760.643	[M+NH4]+	1.03	0.82
TAG	TAG 44:9	755.538	[M+Na]+	1.44	0.05
TAG	TAG 44:9	755.519	[M+Na]+	1.04	0.58
TAG	TAG 45:0	782.721	[M+NH4]+	0.81	0.06
TAG	TAG 45:1	780.706	[M+NH4]+	0.85	0.12
TAG	TAG 46:0	796.738	[M+NH4]+	0.82	0.04
TAG	TAG 46:0	801.692	[M+Na]+	0.91	0.35
TAG	TAG 46:1	799.677	[M+Na]+	0.92	0.4
TAG	TAG 46:1	794.723	[M+NH4]+	0.94	0.48
TAG	TAG 46:1	801.516	[M+Na]+	1.17	0.04
TAG	TAG 46:10	776.543	[M+NH4]+	0.97	0.88
TAG	TAG 46:2	797.661	[M+Na]+	0.94	0.58
TAG	TAG 46:2	792.669	[M+NH4]+	1.02	0.84
TAG	TAG 46:4	788.676	[M+NH4]+	1.07	0.56
TAG	TAG 46:4	788.674	[M+NH4]+	1.04	0.67
TAG	TAG 46:9	778.589	[M+NH4]+	1.06	0.57

TAG	TAG 47:1	813.691	[M+Na]+	0.8	0.07
TAG	TAG 47:1	808.737	[M+NH4]+	0.84	0.09
TAG	TAG 47:10	790.602	[M+NH4]+	1.66	0.08
TAG	TAG 47:2	806.721	[M+NH4]+	0.87	0.25
TAG	TAG 47:9	792.604	[M+NH4]+	0.95	0.65
TAG	TAG 48:1	822.753	[M+NH4]+	0.96	0.57
TAG	TAG 48:2	820.738	[M+NH4]+	0.97	0.78
TAG	TAG 48:2	826.696	[M+Na]+	0.95	0.53
TAG	TAG 48:2	825.692	[M+Na]+	0.96	0.65
TAG	TAG 48:3	823.677	[M+Na]+	0.94	0.63
TAG	TAG 48:3	818.722	[M+NH4]+	1.01	0.92
TAG	TAG 48:3	819.725	[M+NH4]+	1	1
TAG	TAG 48:4	816.705	[M+NH4]+	1.08	0.42
TAG	TAG 49:1	836.768	[M+NH4]+	0.88	0.18
TAG	TAG 49:10	818.633	[M+NH4]+	1.37	0.09
TAG	TAG 49:11	816.619	[M+NH4]+	1.34	0.12
TAG	TAG 49:3	832.736	[M+NH4]+	0.9	0.37
TAG	TAG 49:5	828.712	[M+NH4]+	0.94	0.43
TAG	TAG 50:2	848.769	[M+NH4]+	1.01	0.89
TAG	TAG 50:3	851.708	[M+Na]+	0.99	0.93
TAG	TAG 50:3	846.753	[M+NH4]+	1.01	0.92
TAG	TAG 50:4	845.74	[M+NH4]+	1.07	0.46
TAG	TAG 51:3	860.768	[M+NH4]+	0.93	0.41
TAG	TAG 51:3	865.723	[M+Na]+	0.9	0.34

TAG	TAG 51:4	858.753	[M+NH4]+	1	1
TAG	TAG 51:5	856.743	[M+NH4]+	0.9	0.1
TAG	TAG 51:6	854.732	[M+NH4]+	0.99	0.93
TAG	TAG 51:7	852.713	[M+NH4]+	1	0.97
TAG	TAG 52:3	874.784	[M+NH4]+	1.01	0.87
TAG	TAG 52:4	872.768	[M+NH4]+	1	0.99
TAG	TAG 52:4	877.723	[M+Na]+	0.98	0.9
TAG	TAG 52:5	870.752	[M+NH4]+	0.96	0.67
TAG	TAG 52:5	870.752	[M+NH4]+	0.96	0.67
TAG	TAG 52:6	868.75	[M+NH4]+	0.91	0.3
TAG	TAG 52:6	868.736	[M+NH4]+	0.9	0.27
TAG	TAG 53:13	868.67	[M+NH4]+	1.02	0.82
TAG	TAG 53:8	878.732	[M+NH4]+	1.04	0.76
TAG	TAG 54:5	898.783	[M+NH4]+	0.96	0.65
TAG	TAG 54:6	901.723	[M+Na]+	0.95	0.81
TAG	TAG 54:6	896.768	[M+NH4]+	0.96	0.63
TAG	TAG 54:7	899.705	[M+Na]+	0.84	0.34
TAG	TAG 54:7	894.751	[M+NH4]+	0.92	0.41
TAG	TAG 55:5	912.798	[M+NH4]+	0.86	0.3
TAG	TAG 55:6	910.783	[M+NH4]+	0.73	0.27
TAG	TAG 55:7	908.767	[M+NH4]+	0.63	0.09
TAG	TAG 56:6	924.799	[M+NH4]+	0.94	0.55
TAG	TAG 56:7	927.738	[M+Na]+	0.97	0.79
TAG	TAG 56:7	922.784	[M+NH4]+	0.97	0.76

TAG	TAG 56:8	920.768	[M+NH4]+	0.96	0.69
TAG	TAG 57:1	953.855	[M+Na]+	2.64	0
TAG	TAG 58:8	948.799	[M+NH4]+	0.94	0.56
TAG	TAG 64:19	1110.725	[M+Na]+	1.33	0.02

Table B13. **Identified glycerophospolipids and respective fold changes in the HepG2 cells exposed to TET 10mg/L treated gut microbiome secretome**

Lipid subclass	Lipid name	m/z	Adduct	10 mg/L TET treated secretome	
				FC	p value
PE	PE 29:4	642.406	[M+H]+	1.01	0.7
PE	PE 31:0	678.505	[M+H]+	1.26	0.07
PE	PE 31:0e	664.525	[M+H]+	1.35	0.15
PE	PE 32:0	692.521	[M+H]+	1.06	0.69
PE	PE 32:0e	678.542	[M+H]+	1.15	0.43
PE	PE 33:0	706.537	[M+H]+	1.14	0.18
PE	PE 33:0e	692.558	[M+H]+	1.13	0.22
PE	PE 33:1	704.521	[M+H]+	1.23	0.05
PE	PE 33:1e	690.541	[M+H]+	1.12	0.22
PE	PE 33:2e	688.524	[M+H]+	1.57	0.33
PE	PE 34:0	720.553	[M+H]+	0.98	0.82
PE	PE 34:0e	706.572	[M+H]+	0.97	0.78
PE	PE 34:1	718.537	[M+H]+	1.19	0.32
PE	PE 34:8	704.435	[M+H]+	1.09	0.65
PE	PE 35:0e	720.586	[M+H]+	0.89	0.56
PE	PE 35:1	732.553	[M+H]+	1.32	0.06
PE	PE 35:1e	718.574	[M+H]+	1.28	0.09
PE	PE 35:2	730.537	[M+H]+	1.18	0.05
PE	PE 36:0	748.583	[M+H]+	0.99	0.95

PE	PE 36:0e	734.599	[M+H]+	0.91	0.64
PE	PE 36:1	746.569	[M+H]+	1.13	0.28
PE	PE 36:1e	732.587	[M+H]+	1.2	0.22
PE	PE 36:2	744.552	[M+H]+	1.1	0.33
PE	PE 36:2e	730.591	[M+H]+	2.9	0.07
PE	PE 36:9e	716.473	[M+H]+	1.07	0.4
PE	PE 37:0	762.598	[M+H]+	1	0.98
PE	PE 37:0e	748.619	[M+H]+	0.89	0.27
PE	PE 37:1e	746.605	[M+H]+	1.22	0.12
PE	PE 37:2	758.568	[M+H]+	1.38	0
PE	PE 37:2e	744.588	[M+H]+	1.17	0.2
PE	PE 37:3	756.552	[M+H]+	1.24	0.07
PE	PE 37:3e	742.571	[M+H]+	1.19	0.12
PE	PE 37:4	754.535	[M+H]+	1.43	0.05
PE	PE 38:1	774.599	[M+H]+	1.06	0.63
PE	PE 38:2	772.524	[M+H]+	1.1	0.28
PE	PE 38:2e	758.598	[M+H]+	1.13	0.29
PE	PE 38:3	770.567	[M+H]+	1.09	0.4
PE	PE 39:1e	774.634	[M+H]+	1.03	0.8
PE	PE 39:2e	772.619	[M+H]+	1.2	0.17
PE	PE 39:3	784.584	[M+H]+	1.13	0.13
PE	PE 39:3e	770.601	[M+H]+	1	0.99
PE	PE 39:4	782.566	[M+H]+	1.26	0.11
PE	PE 39:4e	768.588	[M+H]+	1.27	0.08

PE	PE 39:5	780.55	[M+H]+	1.26	0.05
PE	PE 40:1	802.63	[M+H]+	0.91	0.55
PE	PE 40:2	800.615	[M+H]+	1.08	0.51
PE	PE 40:3	798.597	[M+H]+	1.12	0.3
PE	PE 40:6	792.558	[M+H]+	1.47	0.37
PE	PE 40:6	791.544	[M+H]+	1.24	0.01
PE	PE 41:2	814.63	[M+H]+	1.18	0.35
PE	PE 41:3	812.613	[M+H]+	1.12	0.34
PE	PE 41:4	810.597	[M+H]+	1.09	0.75
PE	PE 41:5	808.584	[M+H]+	1.12	0.11
PE	PE 41:5	808.581	[M+H]+	1.21	0.08
PE	PE 41:5e	794.604	[M+H]+	1.2	0.1
PE	PE 41:6	806.568	[M+H]+	1.16	0.4
PE	PE 41:6e	792.587	[M+H]+	1.08	0.52
PE	PE 41:7	804.549	[M+H]+	1.36	0.09
PE	PE 42:5	822.599	[M+H]+	1.03	0.86
PE	PE 42:7	818.568	[M+H]+	1.13	0.53
PE	PE 43:5	836.614	[M+H]+	1.17	0.44
PE	PE 43:5e	822.631	[M+H]+	1.17	0.4
PE	PE 43:6	834.599	[M+H]+	1.05	0.68
PE	PE 43:6e	820.622	[M+H]+	1.17	0.18
PE	PE 43:7	832.583	[M+H]+	1.1	0.19
PE	PE 43:8	830.567	[M+H]+	1.31	0.13
PE	PE 45:6	862.63	[M+H]+	0.98	0.89

PE	PE 46:10	868.589	[M+H]+	4.02	0.04
PE	PE 52:6	960.738	[M+H]+	1.04	0.67
PC	PC 17:0e	510.355	[M+H]+	1.05	0.5
PC	PC 24:0e	608.472	[M+H]+	1.08	0.09
PC	PC 25:0	636.459	[M+H]+	1.04	0.37
PC	PC 32:0	734.569	[M+H]+	1.03	0.76
PC	PC 32:0	734.56	[M+H]+	1.3	0
PC	PC 33:0	748.572	[M+H]+	1.16	0.34
PC	PC 33:1	746.563	[M+H]+	0.7	0.03
PC	PC 34:1	760.575	[M+H]+	1.19	0.08
PC	PC 34:8e	732.494	[M+H]+	1.04	0.79
PC	PC 36:1	788.615	[M+H]+	1.06	0.55
PC	PC 36:2	786.65	[M+H]+	1.18	0.45
PC	PC 39:1e	816.691	[M+H]+	1.04	0.83
PC	PC 40:3	840.652	[M+H]+	1.02	0.9
PC	PC 40:4	838.629	[M+H]+	1.08	0.5
PC	PC 42:10	854.572	[M+H]+	1.46	0.03
PC	PC 42:11	852.558	[M+H]+	2.53	0
PC	PC 42:7	860.613	[M+H]+	1.13	0.47
PC	PC 44:0e	888.783	[M+H]+	1.05	0.68
PC	PC 44:10	882.604	[M+H]+	1.29	0.02
PC	PC 44:11	880.589	[M+H]+	1.95	0
PC	PC 44:9	884.611	[M+H]+	1.82	0.01
PC	PC 48:1	956.802	[M+H]+	0.93	0.64

PC	PC 48:2	954.785	[M+H]+	0.91	0.53
PC	PC 48:3e	938.798	[M+H]+	1.2	0.54
PC	PC 52:6	1002.801	[M+H]+	1.01	0.87
PG	PG 40:5	825.556	[M+H]+	2.37	0.03
PG	PG 43:0	877.697	[M+H]+	1.83	0.04
PG	PG 43:5;O	883.599	[M+H]+	7.38	0
PA	PA 52:11	907.608	[M+H]+	2.87	0.02
PA	PA 50:10	881.593	[M+H]+	1.93	0
PA	PA 50:9	883.608	[M+H]+	1.32	0.03
PA	PA 49:12	863.563	[M+H]+	2.01	0
PI	PI 38:5	885.545	[M+H]+	1.85	0
PI	PI O-36:7	839.513	[M+H]+	1.68	0.04
PI	PI 38:4	887.562	[M+H]+	1.51	0.01
PI	PI 40:7	909.544	[M+H]+	1.34	0
PI	PG 45:10	885.547	[M+H]+	5.76	0.01
PI	PI 36:4	859.528	[M+H]+	3.51	0.03
PS	PS 47:8	930.603	[M+H]+	2.59	0
PS	PS 44:9	886.548	[M+H]+	2.05	0
PS	PS 45:8	902.573	[M+H]+	1.99	0
PS	PS 47:7	932.62	[M+H]+	1.94	0.01
PS	PS 45:7	904.59	[M+H]+	1.41	0
PS	PS 42:5	866.581	[M+H]+	1.39	0.03
PS	PS 35:3	771.514	[M+H]+	1.16	0.53
PS	PS 38:6	808.52	[M+H]+	1	0.99

PS	PS 41:6	850.556	[M+H]+	0.98	0.9
PS	PS 41:7	848.55	[M+H]+	0.98	0.92
PS	PS 43:6	878.576	[M+H]+	1.07	0.33

Table B14 Identified sphingolipids and respective fold changes in the HepG2 cells exposed to TET 10mg/L treated gut microbiome secretome

Lipid subclass	Lipid name	m/z	Adduct	10 mg/L TET treated secretome	
				FC	p value
Cer	Cer 29:0;O3	486.449	[M+H]+	1.57	0.01
Cer	Cer 36:2;O2	564.542	[M+H]+	0.83	0.03
Cer	Cer 36:4;O2	560.501	[M+H]+	0.84	0
Cer	Cer 40:0;O5	672.614	[M+H]+	0.81	0.02
Cer	Cer 42:4;O2	644.593	[M+H]+	0.82	0.03
Cer	Cer 43:4;O4	690.602	[M+H]+	0.47	0
Cer	Cer-NDS d26:0	428.409	[M+H]+	1.02	0.61
Cer	Cer-NDS d28:0	456.44	[M+H]+	1.04	0.52
Cer	Cer-NDS d31:0	498.496	[M+H]+	1.09	0.16
Cer	Cer-NDS d42:1	650.643	[M+H]+	0.88	0.29
Cer	Cer-NDS d46:1	706.705	[M+H]+	1	0.99
Cer	Cer-NDS d48:1	734.736	[M+H]+	1.01	0.8
Cer	Cer-NS d26:4	422.345	[M+H]+	1.34	0.21
Cer	Cer-NS d27:1	440.409	[M+H]+	1.02	0.75
Cer	Cer-NS d29:4	462.388	[M+H]+	1.12	0.35
Cer	Cer-NS d30:4	476.408	[M+H]+	1.06	0.31
Cer	Cer-NS d31:4	490.422	[M+H]+	0.98	0.73
Cer	Cer-NS d34:1	538.519	[M+H]+	0.91	0.5
Cer	Cer-NS d35:4	552.534	[M+H]+	1.06	0.4
Cer	Cer-NS d39:1	608.596	[M+H]+	1	0.97

Cer	Cer-NS d40:1	622.604	[M+H]+	0.97	0.81
Cer	Cer-NS d42:1	650.643	[M+H]+	1.03	0.73
Cer	Cer-NS d42:2	648.626	[M+H]+	0.86	0.16
Cer	Cer-NS d44:5	670.609	[M+H]+	0.88	0.15
Cer	Cer-NS d52:4	796.773	[M+H]+	0.77	0.08
Cer	HexCer-NDS d49:1	910.813	[M+H]+	0.89	0.1
Cer	HexCer-NDS d51:2	936.831	[M+H]+	0.94	0.47
Cer	HexCer-NS d30:4	638.462	[M+H]+	1.25	0.16
Cer	HexCer-NS d34:1	700.573	[M+H]+	1.21	0.31
Cer	HexCer-NS d38:3	752.601	[M+H]+	1.15	0.53
Cer	HexCer-NS d40:1	784.665	[M+H]+	0.72	0.05
Cer	HexCer-NS d42:1	812.695	[M+H]+	0.84	0.29
Cer	HexCer-NS d47:1	882.776	[M+H]+	0.95	0.44
Cer	HexCer-NS d48:1	896.799	[M+H]+	0.91	0.57
Cer	HexCer-NS d48:4	890.742	[M+H]+	1.07	0.51
Cer	HexCer-NS d49:2	908.8	[M+H]+	0.95	0.57

Cer	HexCer-NS d50:4	919.776	[M+H]+	1.02	0.81
Cer	HexCer-NS d52:4	946.799	[M+H]+	0.98	0.82
Cer	HexCer-NS d53:5	958.817	[M+H]+	0.9	0.66
SM	SM 29:0	683.498	[M+H]+	0.6	0.01
SM	SM 36:4	757.555	[M+H]+	1.29	0.04
SM	SM d26:0	592.46	[M+H]+	0.99	0.95
SM	SM d32:1	675.542	[M+H]+	1.41	0.05
SM	SM d33:1	689.557	[M+H]+	1.46	0.07
SM	SM d34:0	705.58	[M+H]+	1.29	0.13
SM	SM d34:1	703.574	[M+H]+	1.27	0.14
SM	SM d34:2	701.558	[M+H]+	1.41	0.04
SM	SM d35:1	717.589	[M+H]+	1.11	0.22
SM	SM d35:1	717.526	[M+H]+	1.2	0.04
SM	SM d36:1	731.604	[M+H]+	0.98	0.81
SM	SM d38:1	759.633	[M+H]+	0.91	0.5
SM	SM d40:0	789.677	[M+H]+	1.02	0.79
SM	SM d40:1	787.667	[M+H]+	0.87	0.27
SM	SM d40:2	785.651	[M+H]+	1.12	0.43
SM	SM d41:1	801.682	[M+H]+	0.87	0.29
SM	SM d42:1	815.698	[M+H]+	0.96	0.74
SM	SM d42:2	813.683	[M+H]+	0.98	0.87
SM	SM d42:3	811.667	[M+H]+	1.17	0.23

SM	SM d46:0	873.771	[M+H]+	1.01	0.94
SM	SM d46:1	871.755	[M+H]+	0.95	0.62
SM	SM d48:0	901.802	[M+H]+	1	0.99
SM	SM d50:1	927.818	[M+H]+	0.95	0.61
SM	SM d50:2	925.803	[M+H]+	0.97	0.76
SM	SM d52:2	953.835	[M+H]+	1.23	0.01
SM	SM d52:3	951.819	[M+H]+	0.96	0.72

Appendix C

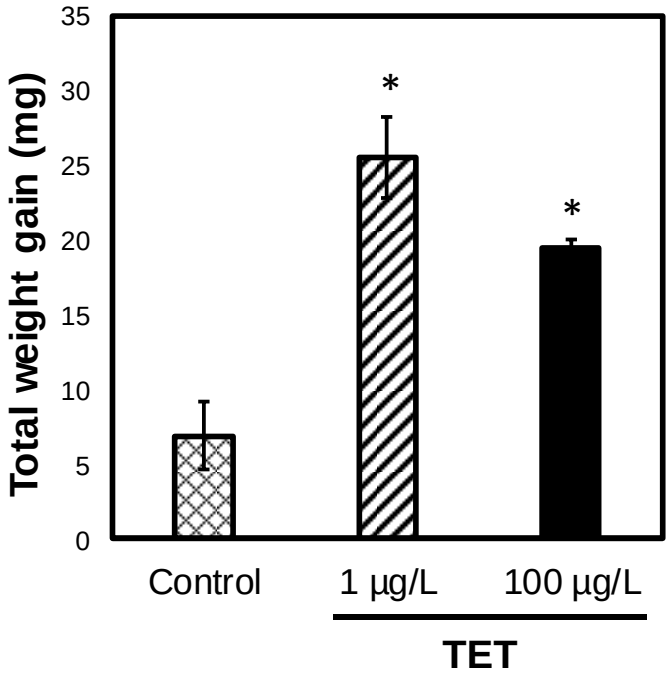

Figure C1. Total weight gain during the exposure period. "*" indicates statistical significance (*p-value* ≤0.05) between TET treated and control groups.

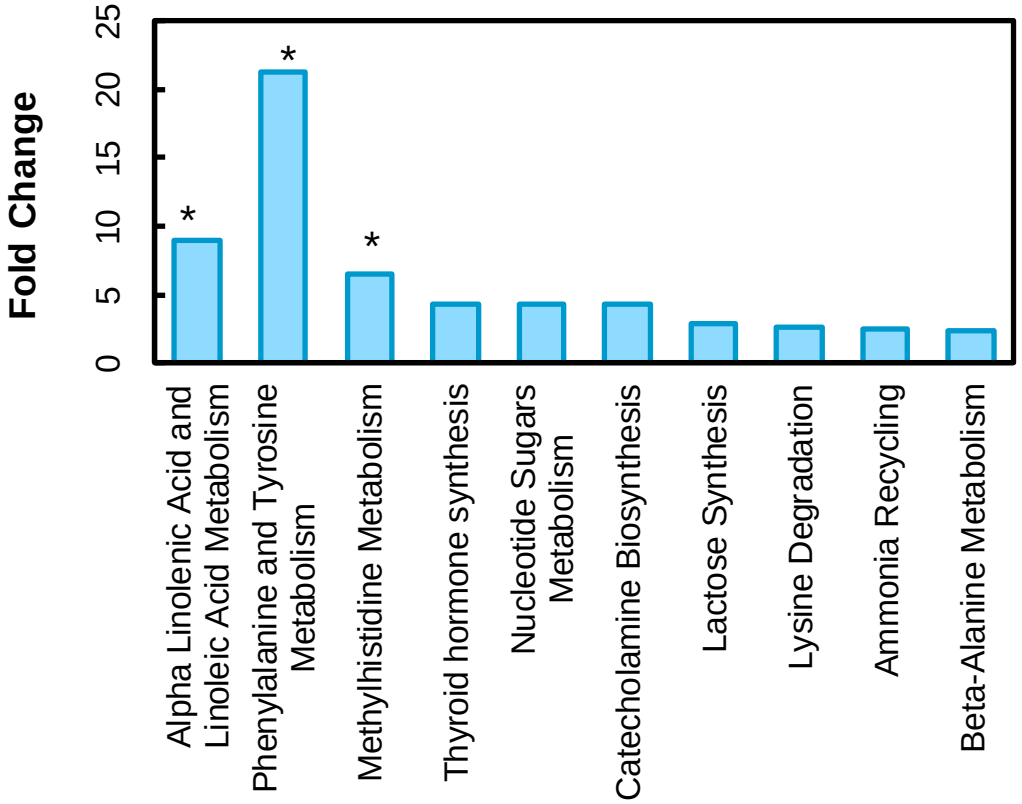

Figure C2. Enrichment analysis of significant metabolic pathways at 1 µg/L. "*" indicates statistical significance (*p-value* ≤0.05) between TET treated and control groups.

Figure C3. Classic Venn diagram summarizing the number of shared and distinct OTUs in the gut microbial communities of control, 1 µg/L, and 100 µg/L TET treated zebrafish

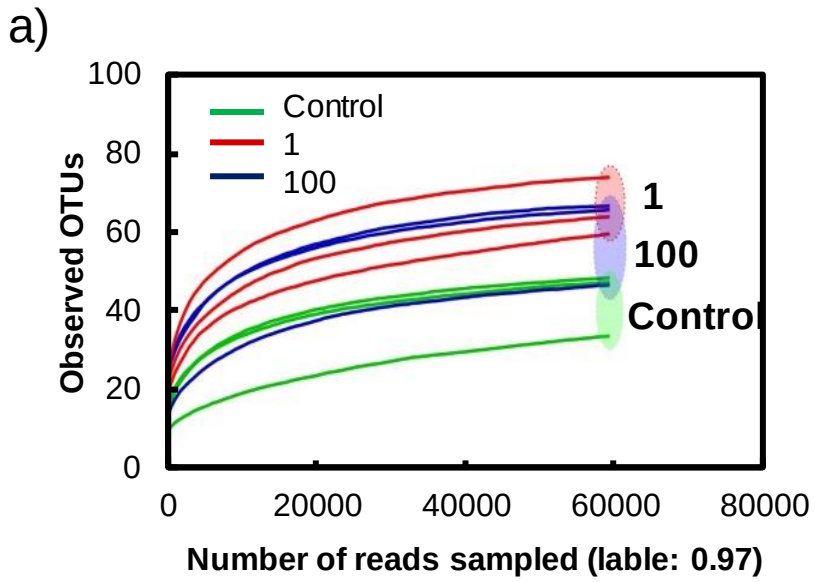

Figure C4. Rarefaction curves of control and TET treated zebrafish gut microbial communities

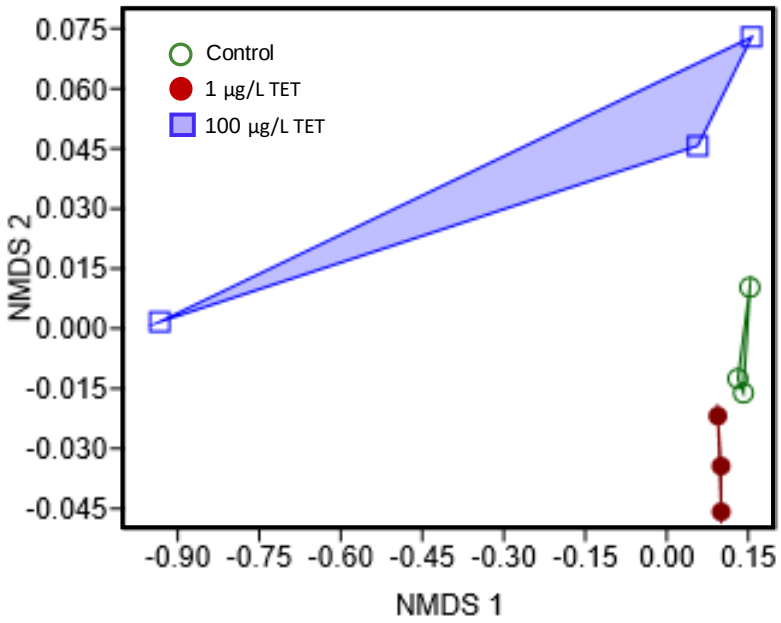

Figure C5. Non-metric multidimensional scaling (NMDS) ordination of control, 1 µg/L, and 100 µg/L TET treated zebrafish. The NMDS plot was generated based on OTU composition data using the Bray-Curtis distance metrics.

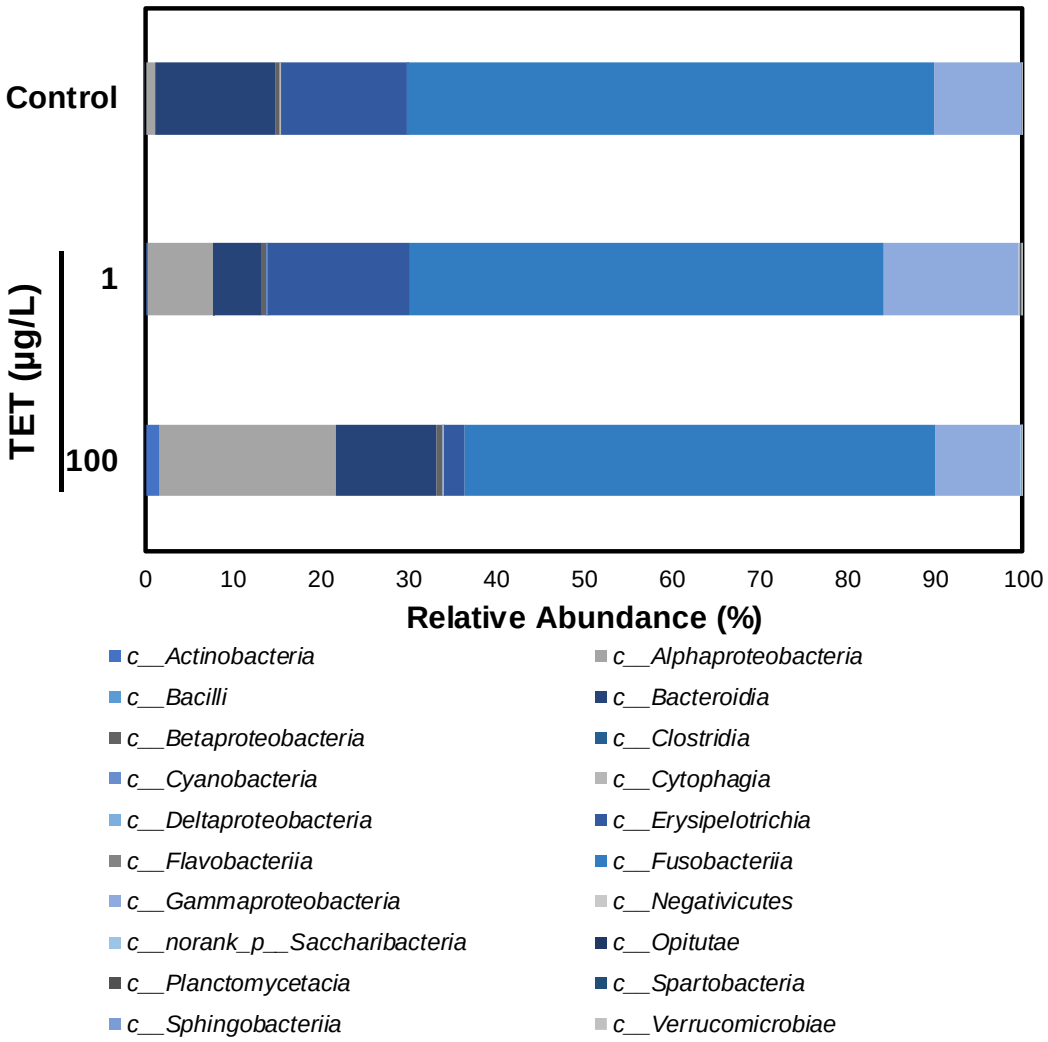

Figure C6. Bar graph representation of the class level relative abundance in the gut microbiomes of zebrafish exposed to 0 (control), 1, and 100 µg/L of TET.

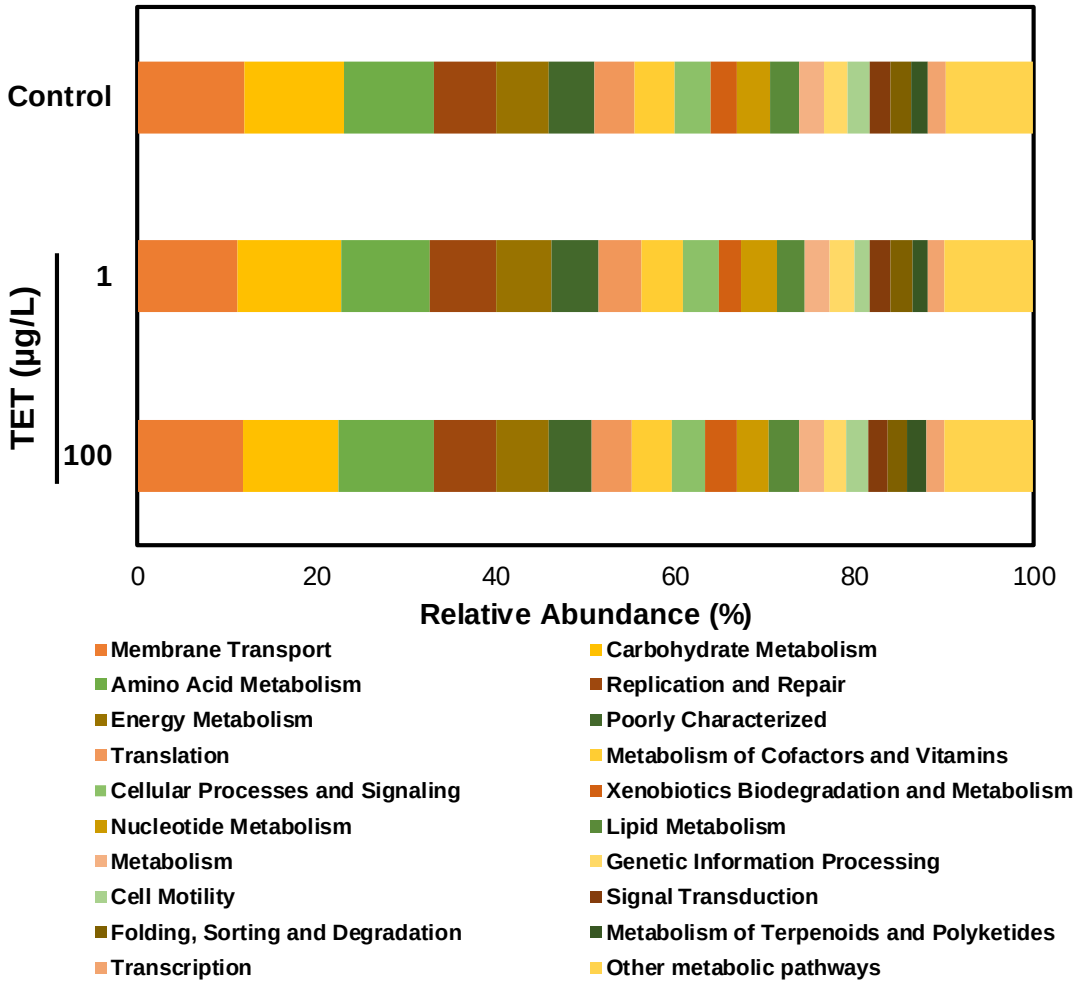

Figure C7. Bar graph representation of the predicted metabolic pathway level relative abundance in the gut microbiomes of zebrafish exposed to 0 (control), 1, and 100 µg/L of TET.

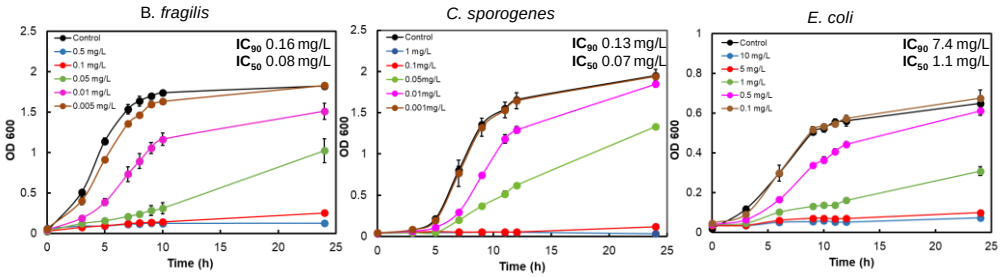

Figure C8. Growth curves of each of the three model bacteria, *B. fragilis*, *C. sporogenes*, and *E. coli* under the exposure of different levels of TET. Bacterial growth was observed via optical density at 600 nm (OD_{600}) for 24 hours. The IC values are predicated based on the 4-parameter logistic model.

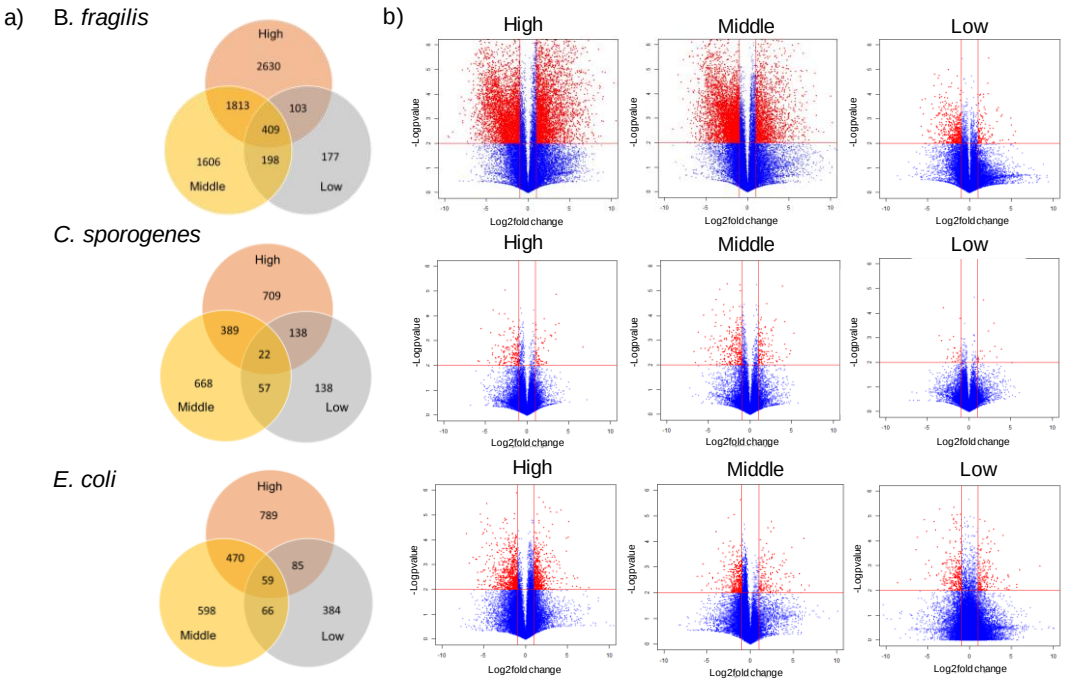

Figure C9. Dysregulated feature numbers in three model strains under three levels of TET exposure. (a) Classic Venn diagram summarizing the number of shared and distinct features; and (b)The volcano plot graphically representing the significantly up/down regulated features.

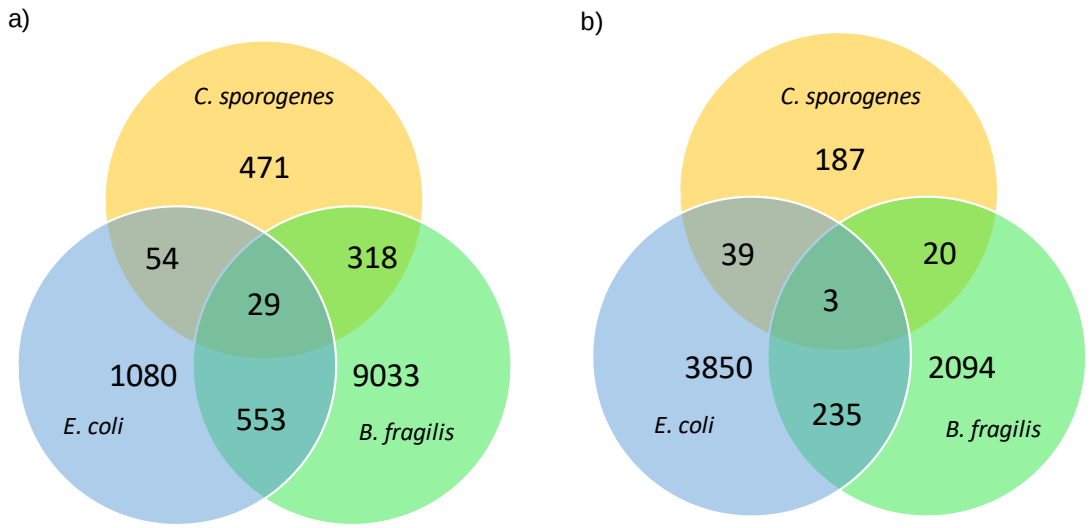

Figure C10. Classic Venn diagram summarizing the number of shared and distinct features in each model bacteria with (a) middle and (b) low level of TET exposure.

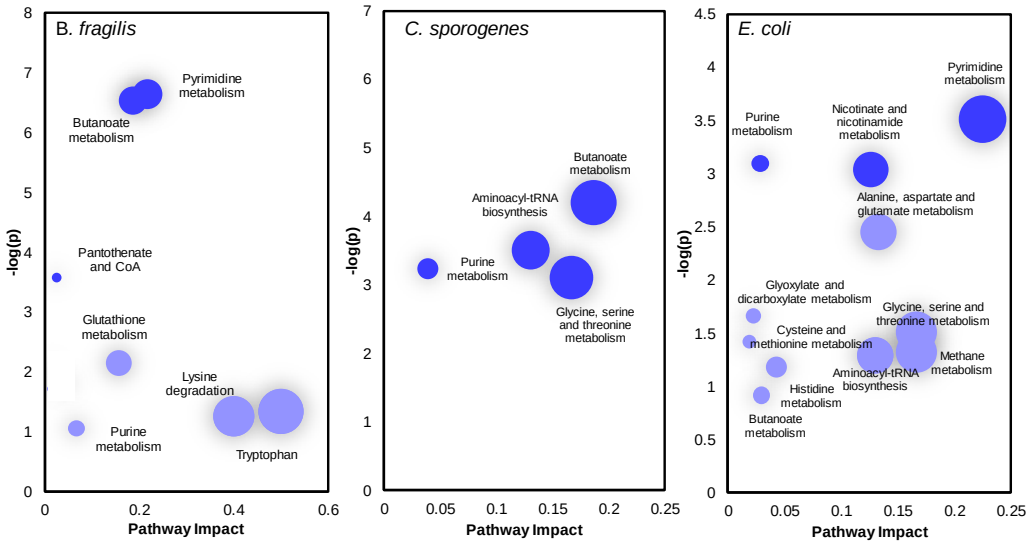

Figure C11. **Pathway impact analysis of significant metabolic pathways in model bacteria under the middle level of TET exposure**. The data analysis was conducted by the open source platform MetaboAnalyst. The size of the bubble implies the pathway impact and the color intensity indicates the significance of the impact (*p*-value <0.05).

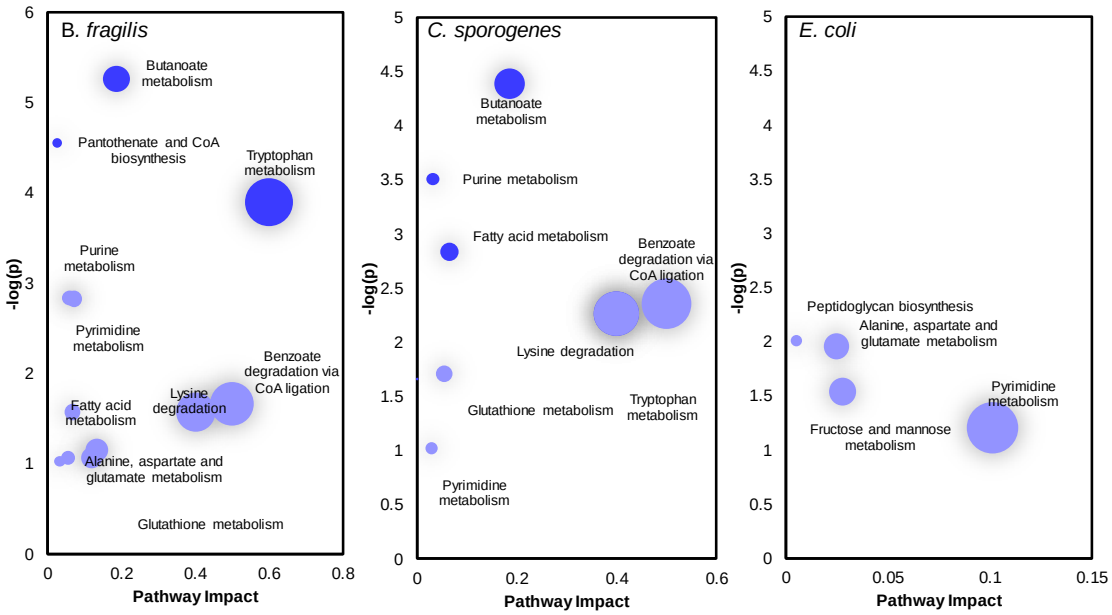

Figure C12. Pathway impact analysis of significant metabolic pathways in model bacteria under the low level of TET exposure. The data analysis was conducted by the open source platform MetaboAnalyst. The size of the bubble implies the pathway impact and the color intensity indicates the significance of the impact (*p*-value ≤0.05).

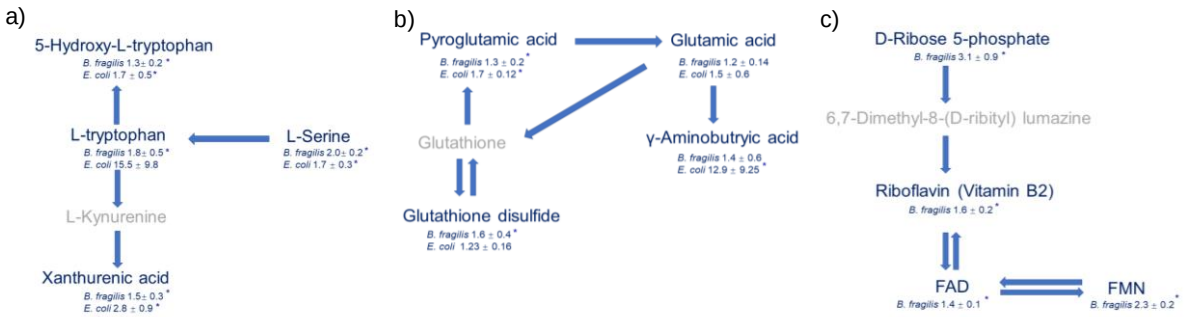

Figure C13. Examples of identified metabolic pathways in model bacteria under high level of TET exposure. (a) Metabolites related to riboflavin metabolism in *B. fragilis*, (b) Metabolites involved in tryptophan metabolism in *B. fragilis* and *E. coli*; and (c) Metabolites involved in glutathione metabolism in *B. fragilis* and *E. coli* (* represents statistical significance of p-value ≤ 0.05 in either up/down-regulation).

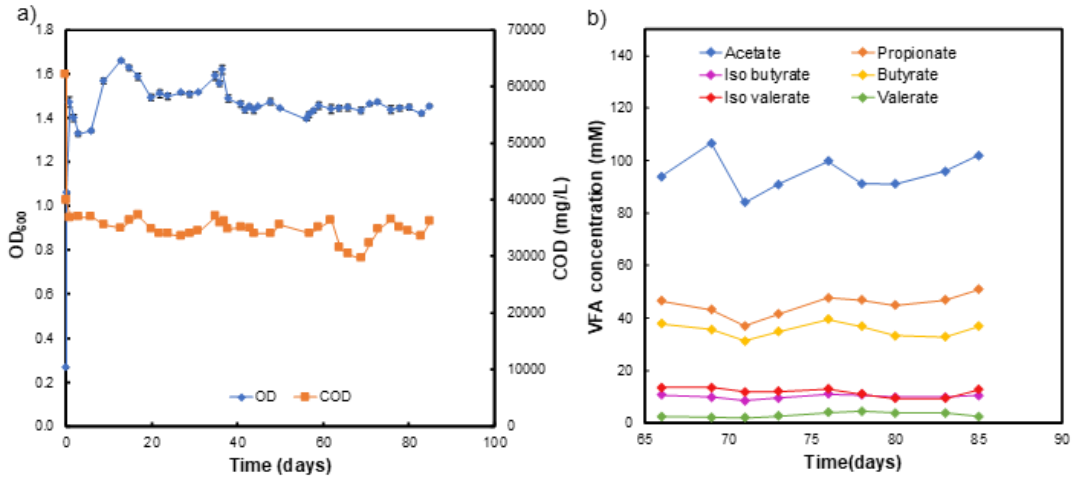

Figure C14. Reactor parameter monitoring. a) OD_{600} and COD profile and b) SCFA monitoring of gut reactor.

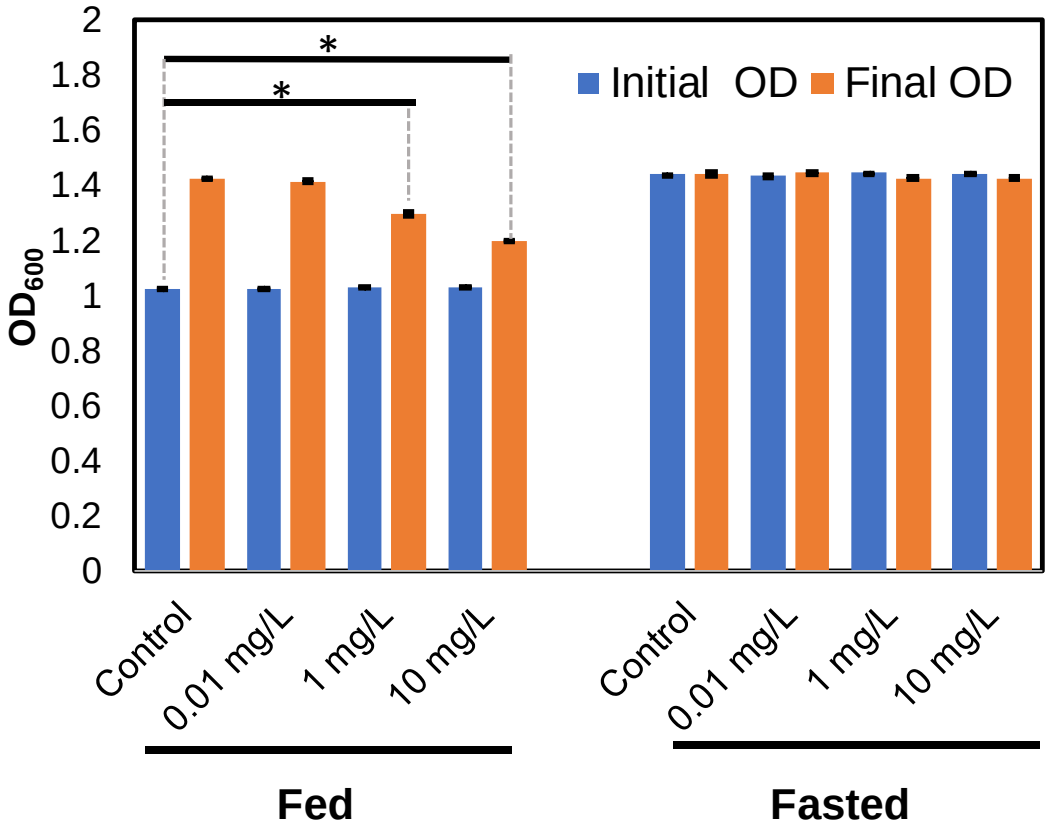

Figure C15. Growth of *in vitro* gut microbial community under TET exposure at the fed and fasted states. Bacterial growth was observed via optical density at 600 nm (OD_{600}) after 24 hours of incubation. "*" indicates the statistical significance (*p*-value ≤ 0.05).

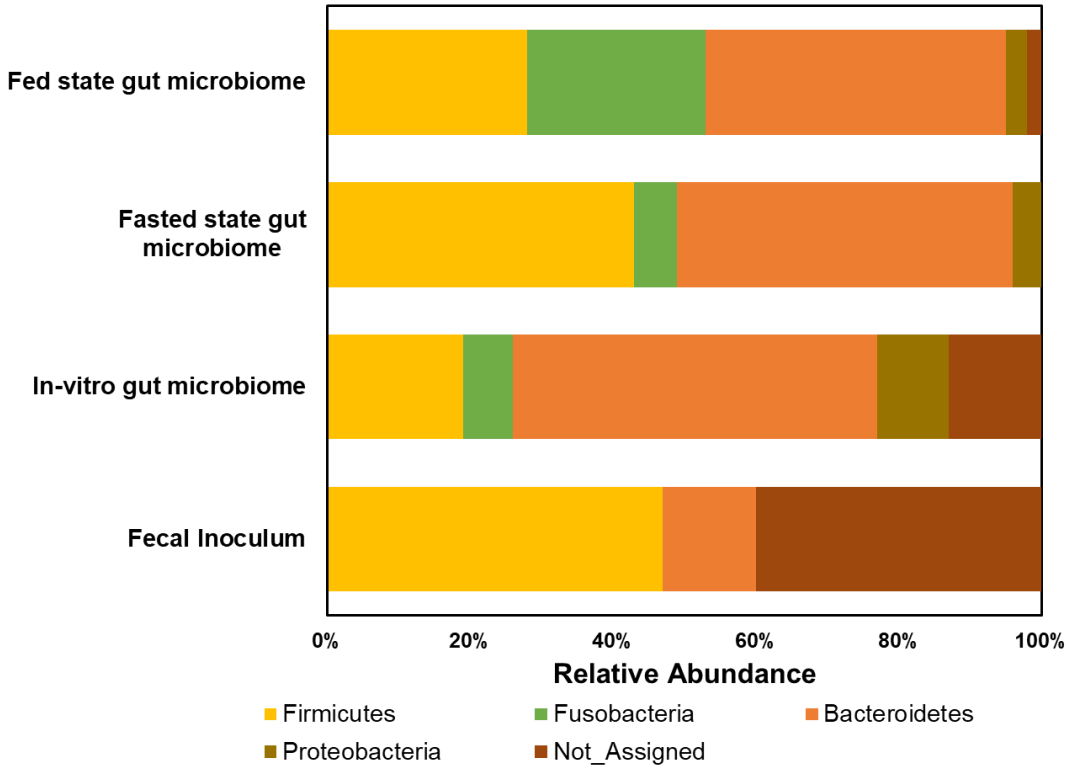

Figure C16. Bar graph representation of phylum level relative abundance fecal inoculum, stable *in vitro* gut microbiome, *in vitro* gut microbiome maintained at the fed and fasted states for 24 hours.

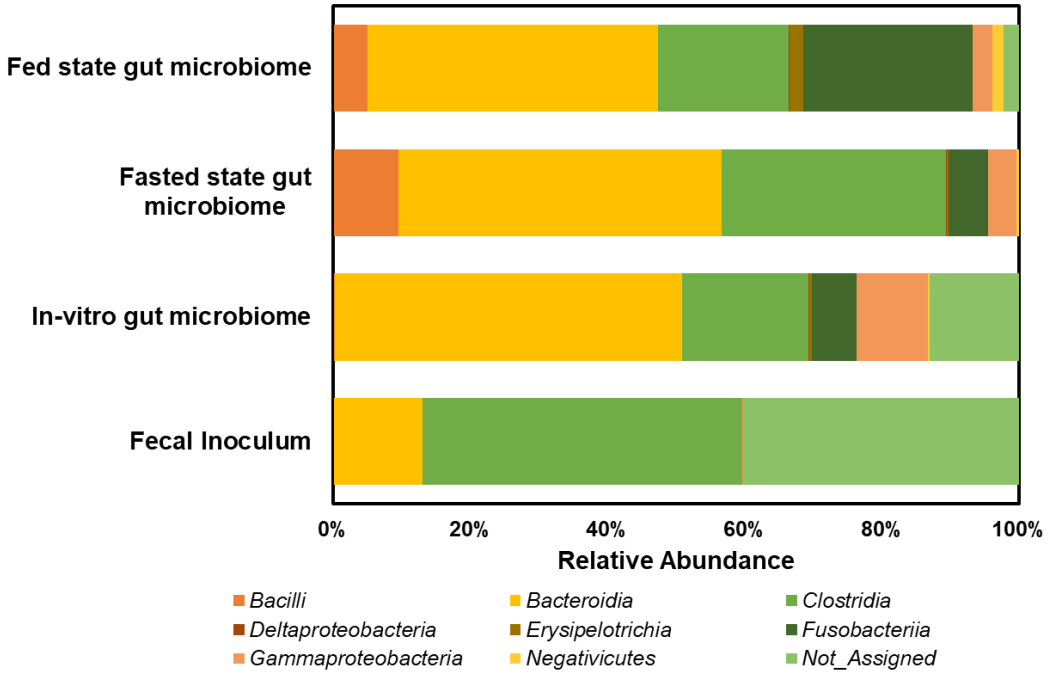

Figure C17. Bar graph representation of class level relative abundance fecal inoculum, stable *in vitro* gut microbiome, *in vitro* gut microbiome maintained at the fed and fasted states for 24 hours.

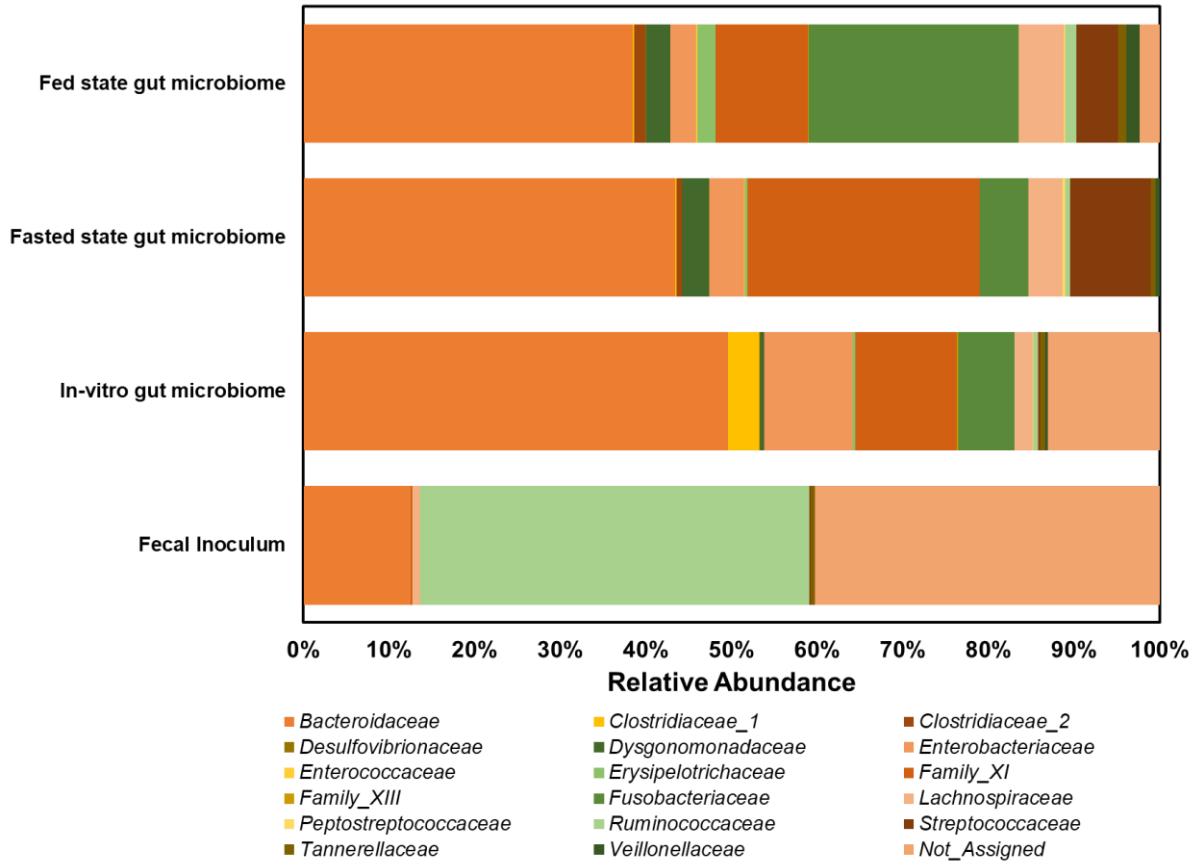

Figure C18. Bar graph representation of family level relative abundance fecal inoculum, stable in vitro gut microbiome, in vitro gut microbiome maintained at the fed and fasted states for 24 hours.

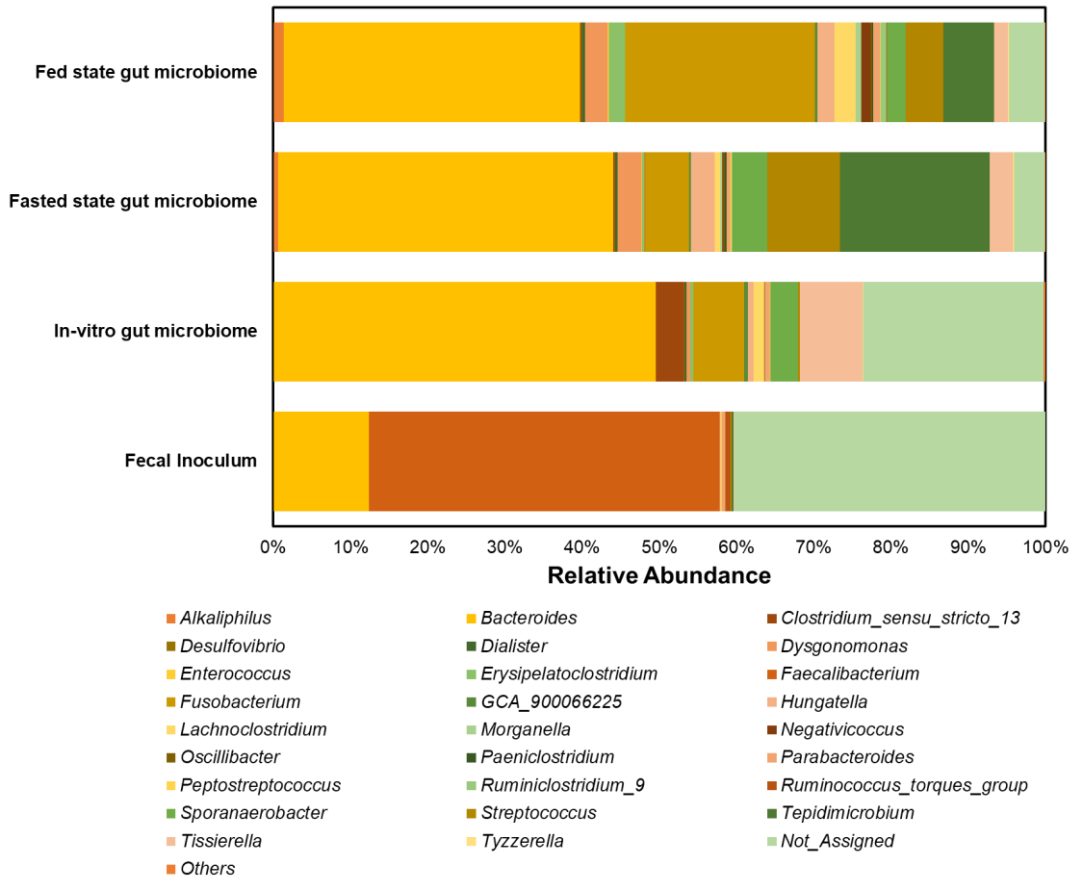

Figure C19. Bar graph representation of genus level relative abundance fecal inoculum, stable *in vitro* gut microbiome, *in vitro* gut microbiome maintained at the fed and fasted states for 24 hours.

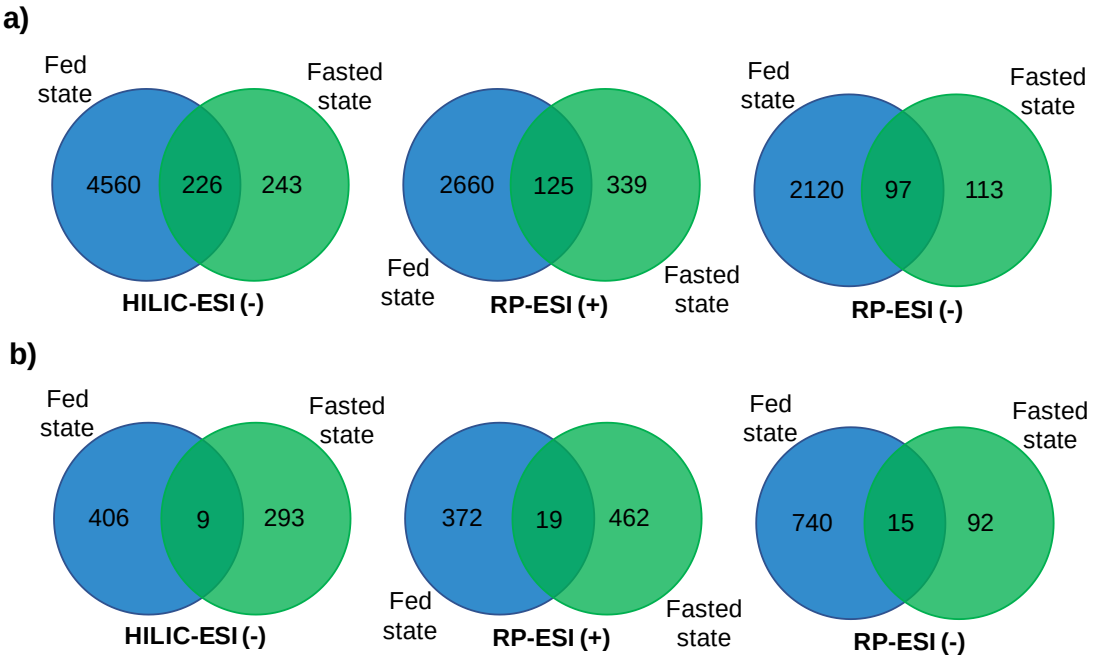

Figure C20. classic Venn diagram summarizing the number of shared and distinct features in the fed and fasted states observed in HILIC-ESI (-), RP-ESI (+), and RP-ESI (-) profiling method at a) 1 and b) 0.01 mg/L TET.

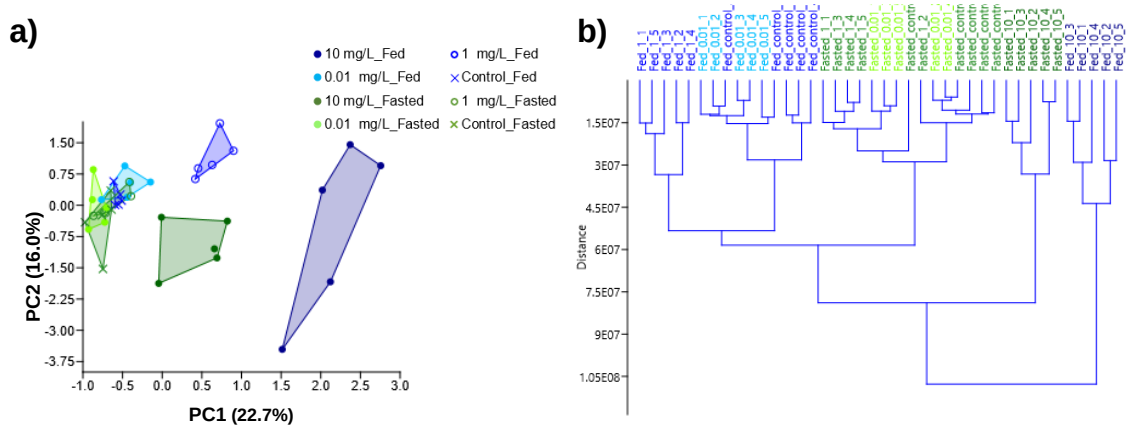

Figure C21. a) Principle Component Analysis (PCA) and b) hierarchical clustering of metabolic features in the gut microbiome secretome under TET exposure at the fed and fasted states detected under RP-ESI (+) profiling method.

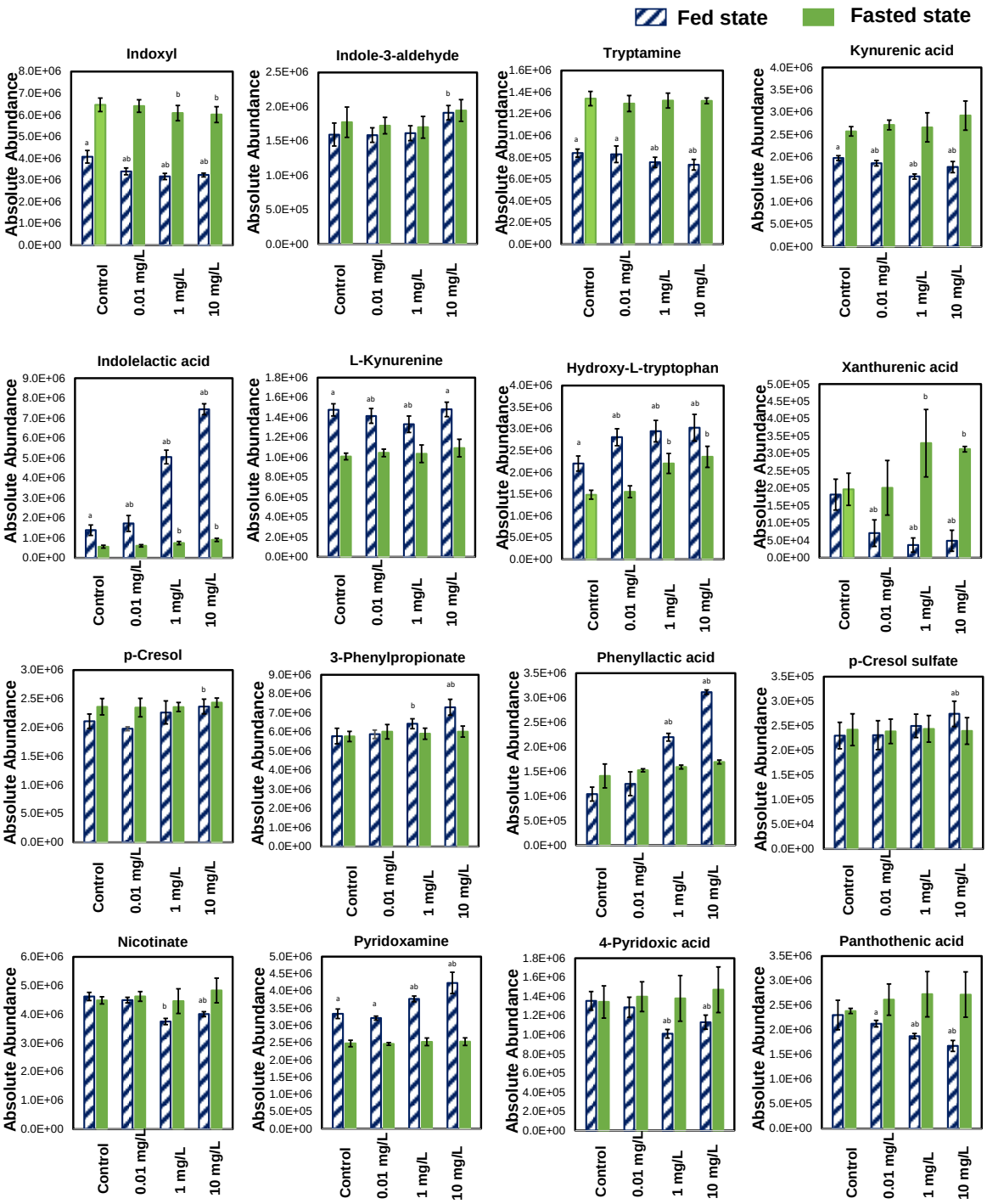

Figure C22. Absolute abundance of few representative metabolic features under TET exposure at the fed and fasted states. Data presented as the mean ± SD of five replicates. 'a' indicates the statistical significance (p-value ≤ 0.05) with the fasted group at same TET dose and 'b' indicates the statistical significance (p-value ≤ 0.05) with the control group in the same feeding state.